UNIVERSITAT DE BARCELONA

Avaluació dels efectes lipidòmics i fenotípics d'estressants ambientals sobre cultius cel·lulars mitjançant mètodes bioanalítics i quimiomètrics

Núria Dalmau Solà

AVALUACIÓ DELS EFECTES LIPIDÒMICS I FENOTÍPICS D'ESTRESSANTS AMBIENTALS SOBRE CULTIUS CEL·LULARS MITJANÇANT MÈTODES BIOANALÍTICS I QUIMIOMÈTRICS

Núria Dalmau Solà

UNIVERSITAT DE BARCELONA

CSIC
CONSEJO SUPERIOR DE INVESTIGACIONES CIENTÍFICAS

UNIVERSITAT DE BARCELONA

AVALUACIÓ DELS EFECTES LIPIDÒMICS I FENOTÍPICS D'ESTRESSANTS AMBIENTALS SOBRE CULTIUS CEL·LULARS MITJANÇANT MÈTODES BIOANALÍTICS I QUIMIOMÈTRICS

Núria Dalmau Solà

AVALUACIÓ DELS EFECTES LIPIDÒMICS I FENOTÍPICS D'ESTRESSANTS AMBIENTALS SOBRE CULTIUS CEL·LULARS MITJANÇANT MÈTODES BIOANALÍTICS I QUIMIOMÈTRICS

Núria Dalmau Solà

FACULTAT DE QUÍMICA

DEPARTAMENT D'ENGINYERIA QUÍMICA I QUÍMICA ANALÍTICA

Programa de Doctorat:

Química Analítica i Medi Ambient

Avaluació dels efectes lipidòmics i fenotípics d'estressants ambientals sobre cultius cel·lulars mitjançant mètodes bioanalítics i quimiomètrics

---

Memòria presentada per

Núria Dalmau Solà

Per optar al grau de Doctora per la Universitat de Barcelona

Directors:

Dr. Romà Tauler Ferré

Dra. Carmen Bedia Girbés

Departament de Química Ambiental

Institut de Diagnosi Ambiental i Estudis de l'Aigua (IDAEA)

Consejo Superior de Investigaciones Científicas (CSIC)

Tutora:

Dra. Anna de Juan Capdevila

Departament d'Enginyeria Química i Química Analítica

Universitat de Barcelona (UB)

El Dr. **Romà Tauler Ferré**, professor d'investigació del Departament de Química Ambiental de l'Institut de Diagnosi Ambiental i Estudis de l'Aigua adscrit al Consejo Superior de Investigaciones Científicas, i la **Dra. Carmen Bedia Girbés**, investigadora post-doctoral del mateix Departament,

FAN CONSTAR,

Que la present memòria titulada; "**Avaluació dels efectes lipidòmics i fenotípics d'estressants ambientals sobre cultius cel·lulars mitjançant mètodes bioanalítics i quimiomètrics**", ha estat realitzada sota la nostra direcció per la Sra. **Núria Dalmau Solà** i que tots els resultats presentats són fruits de les experiències realitzades per la citada doctoranda en el Departament de Química Ambiental de l'Institut de Diagnosi Ambiental i Estudis de l'Aigua adscrit al Consejo Superior de Investigaciones Científicas.

I per tal de que així consti expedeixen el present certificat.

Barcelona, Setembre de 2019

Dr. Romà Tauler Ferré

Dra. Carmen Bedia Girbés

Als meus pares i germanes, i a l'Alan;

AGRAÏMENTS

Arribat el final d'aquesta etapa voldria agrair a tots els qui han format part i ho han fet possible. No voldria deixar-me ningú, però si és així perdoneu-me.

Primer de tot, agrair als meus directors, el Dr. Romà Tauler i la Dra. Carmen Bedia, l'oportunitat de poder realitzar aquesta Tesi doctoral en aquest gran grup i dins un gran projecte. Romà, gràcies per la teva dedicació, per fer-me un lloc en aquest grup i per compartir els teus coneixements quimiomètrics i científics. A tu Carma, moltíssimes gràcies per obrir-me les portes al món de la investigació i dels cultius cel·lulars. Per ensenyar-m'ho tot sobre la biologia cel·lular, i sobre el món dels lípids, i per estar en tot moment al meu costat. També, agrair a la meva tutora de Tesi, la Dra. Anna de Juan, per la seva ajuda i dedicació durant aquest temps.

Agrair a tots i cadascun dels integrants del projecte CHEMAGEB. Primer, al Dr. Joaquim Jaumot que també ha contribuït activament en aquesta Tesi, ja que va participar en el tractament quimiomètric de les dades analítiques en les primeres publicacions. Als altres postdocs del grup: el Cristian (company de rajola per un temps) i l'Igor. Els que van començar com a doctorands i els vam veure arribar a doctors: la Mireia, el Xin i l'Stefan. Als futurs doctors del grup: Marc i Miriam, molta sort i a totes les persones que han anat passant pel grup: Celia, Yahya, Aline, Amrita, Alejandro, Masha i alguns que hem dec deixar. Per últim, als meus nens, el meu suport i el millor d'aquesta gran família, sense vosaltres la Tesi no hauria estat el mateix: Eva, Meritxell, Elba, Elena, Francesc i Víctor. Gràcies per tot CHEMAGEB!

Agrair l'oportunitat de realitzar una estada al CRCT de Toulouse al Dr. Thierry Levade i a la Dra. Nathalie Andrieu-Abadie, *merci pour tout*. Encara que l'idioma va ser una barrera, tots els doctorands van acollir-me com una més (Thibault, Patricie, Justine, Fatima, Caroline *et* Élie). Mencionar también a Luís que nos conocimos en una ciudad extraña para los dos y sobrevivimos a ello.

Gràcies a les meves amigues: Elsa, Andrea, Helena i Francina (encara que estiguis lluny) per entendre que no sempre estic disponible i animar-me en aquest últim esprint. Gràcies també, als meus companys dels Laboratoris ERN perquè han estat al dia de

tots els meus progressos d'escriptura de la Tesi des del dia que hi vaig entrar. Teniu tots pastetes assegurades: Marta, Miguel, Maribel, Anna, Irene i Francisco; i als ex-companys: Cristina, Mireies i Natalia. Ara ja no tindré que escriure per les tardes.

Per acabar, agrair als qui també han patit aquesta Tesi amb mi des del principi i des de sempre, la meva família. Als meus pares, per animar-me a seguir sempre endavant i créixer com a persona; i als *tuppers* de la mama que eren l'enveja del lab. A les meves germanes perquè ho són tot per mi i també han viscut aquest camí amb mi. Especial menció a la meva germana petita, l'Helena, l'autora d'aquesta portada i d'alguns dibuixos que fan més aclaridora i atractiva aquesta Tesi, una gran artista! A tu, Alan, per animar-me sempre, per venir fins a Toulouse, per estar colze a colze amb mi en aquesta última i estressant etapa, i per fer-me sentir important.

GRÀCIES!

ÍNDEX

RESUM

Les ciències òmiques proporcionen una visió holística de la fisiologia cel·lular i del funcionament dels sistemes biològics i estan presents en tots els camps d'estudi de la biologia molecular. La lipidòmica és una subdisciplina de la metabolòmica, la qual a la seva vegada és una de les branques principals de l'òmica. En el camp ambiental, els estudis òmics tenen la finalitat d'avaluar les alteracions que els organismes poden patir com a conseqüència de l'exposició a diferents factors presents en el medi, com poden ser els compostos químics contaminants (per exemple els pesticides), i que en el seu conjunt donen lloc al que avui en dia s'anomena l'exposòmica.

Els estudis lipidòmics duts a terme en aquesta Tesi s'han realitzat seguint una anàlisi no dirigida emprant la cromatografia de líquids acoblada a l'espectrometria de masses (LC-MS). Aquesta és una de les tècniques analítiques més potents que ha estat àmpliament emprada gràcies a la seva capacitat d'anàlisi dels metabòlits i lípids dels diversos sistemes biològics. L'aproximació òmica no dirigida porta associada l'anàlisi multivariant de dades, donat el gran volum de dades que s'acostumen a generar. En aquests estudis és necessària la compressió de les dades sense pèrdua d'informació espectral i resolució, i una identificació simultània de l'elevat nombre de compostos químics presents en les mostres. Per tot això, els conjunts de dades LC-MS necessiten ser processats adequadament a partir de mètodes d'anàlisi multivariant de dades i de mètodes quimiomètrics.

En aquest sentit, s'ha realitzat la validació d'una nova metodologia pel tractament de dades de LC-MS d'estudis òmics no dirigits. Aquesta nova metodologia es denomina ROIMCR i està basada en l'acoblament d'un mètode de compressió i filtració de les dades, sense pèrdua de resolució espectral, com és el mètode de selecció de les Regions d'interès (ROI), amb el mètode de resolució multivariant de corbes per mínims quadrats alternats (MCR-ALS). A partir de l'anàlisi d'una mescla sintètica de diferents lípids i de mostres de cultius cel·lulars que els contenien es va realitzar la validació del mètode ROIMCR, prèviament desenvolupat en el nostre grup d'investigació.

En aquesta Tesi a més, s'han estudiat els efectes de diferents estressants ambientals sobre diversos models cel·lulars. En un primer bloc es van determinar els efectes de tres disruptors endocrins (Aroclor 1254, Clorpirifòs i Aldrin) en el fenotip i el lipidoma de les cèl·lules de càncer de pròstata DU145. Es va comprovar que l'exposició cel·lular a l'Aroclor i el Clorpirifòs indueix un fenotip maligne amb mecanismes similars en ambdós casos. Aquests resultats van ser diferents als observats en les cèl·lules exposades a Aldrin, que presentaven un fenotip de transició epitelial mesenquimal (EMT. Posteriorment, es va aprofundir en l'estudi lipidòmic de la inducció de la EMT en les cèl·lules DU145 mitjançant la citoquina TNFα. En l'estudi lipidòmic no dirigit de la inducció de EMT es va poder detectar i confirmar un increment significatiu de triacilglicèrids (TAGs), que també s'havia detectat en l'exposició crònica als diferents disruptors endocrins estudiats.

En l'altre bloc d'exposòmica d'aquesta Tesi, s'ha realitzat l'estudi lipidòmic no dirigit dels efectes de la radiació solar UV de forma aguda i crònica en els melanòcits i queratinòcits primaris humans. Aquest tipus de cèl·lules es troba present en l'epidermis, una de les capes de la pell humana que té com a funció principal protegir el cos humà de les agressions ambientals externes, entre els quals destaca la radiació solar. Ambdós models cel·lulars de l'epidermis varen presentar patrons fenotípics i una composició de lípids diferents a la irradiació UV, ja que cadascun adopta una estratègia diferent de supervivència. En el cas dels melanòcits, els canvis s'aprecien en les irradiacions agudes, donant lloc a pseudòpodes. Per contra, amb el pas de les irradiacions (irradiació crònica) tendeixen a adquirir els valors de les mostres control. D'altra banda, els queratinòcits presenten les modificacions de forma més progressiva, fent-se més significatives amb l'augment del nombre d'irradiacions UV, mostrant la inducció de la diferenciació cel·lular cap a corneòcits.

En conjunt, aquesta Tesi pretén aportar i contribuir al desenvolupament de les eines de recerca de la lipidòmica analítica no dirigida en estudis exposòmics on s'avaluen els efectes produïts pels estressants ambientals sobre cultius cel·lulars, com a organisme biològic model.

ABREVIATURES I ACRÒNIMS

ALS	Mínims quadrats alternats, *alternating least squares*
aSMase	Esfingomielinasa ácida, *acid sphingomyelinase*
BPA	Bisfenol A, *bisphenol A*
Cer	Ceramida, *ceramide*
CPS	Clorpirifòs, chlorpyriphos
CWT	C*ontinuos wavelet transform*
DAG	Diacilglicerol, diacylglycerol
DNA	Àcid desoxiribonucleic, *deoxyribonucleic acid*
DE	Disruptors endocrins, *endocrine disruptors (ED)*
EMT	Transició epitelial mesenquimal, *epithelial mesenquimal transition*
ESI	Ionització per electrosprai, *electrospray ionization*
FITC	Isotiocianat de fluoresceïna, fluorescein isothiocyanate
FN	Falsos negatius, *false negative*
FP	Falsos positius, *false positive*
GC	Cromatografia de gasos, *gas chromatography*
GC-MS	Cromatografia de gasos acoblada a l'espectrometria de masses, *gas chromatography coupled to mass spectrometry*
GL	Glicerolípids, *glycerolipids*
GluCer	Glucosilceramida, *glucosylceramide*
GP	Glicerofosfolípids, *glycerophosholipids*
HMDB	*Human Metabolome Database*
HPLC	Cromatografia de líquids d'alta eficàcia, *high performance liquid chromatography*
ILCNC	International Lipid Classification and Nomenclature Committee
IUPAC	International Union of Pure and Applied Chemistry
LacCer	Lactocilceramida, *lactosylceramide*
LC	Cromatografia de líquids, *liquid chromatography*
LC-MS	Cromatografia de líquids acoblada a l'espectrometria de masses, *liquid chromatography coupled to mass spectrometry*

Lof	Manca d'ajust, *lack of fit*
LV	Variable latent, *latent variable*
m/z	Relació de massa i càrrega, *mass-to-charge ratio*
MAG	Monoacilglicerol, *monoacylglycerol*
MCR-ALS	Resolució multivariant de corbes per mínims quadrats alternats, *multivariate curve resolution alternating least squares*
MED	Dosis mínima eritemal, *minimum erythemal dose*
MMP	Metal·loproteïnases, *metalloproteinase*
mRNA	Àcid ribonucleic missatger, *Messenger ribonucleic acid*
MS	Espectrometria de masses, *mass spectrometry*
OPLS-DA	Anàlisi discriminant de projeccions ortogonals multidireccionals a estructures latents, *two-way orthogonal projections to latent structures- discriminant analysis*
PA	Àcid fosfatídic, *phosphatidic acid*
PBDE	Bifenilèster polibromat, *polibromate biphenylester*
PC	Fosfatidilcolina, *phosphatidylcholine*
PCA	Anàlisi per component principals, *principal component analysis*
PCB	Bifenil policlorat, *polychlorinated biphenyl*
PE	Fosfatidiletanolamina, *phosphatidylethanolamine*
PFC	Compost perfluorat, *perfluorinated compound*
PG	Fosfatidilglicerol, *phosphatidylglycerol*
PI	Fosfatidilinositol, *phosphatidylinositol*
PKC	Proteïna kinasa C, *protein kinase C*
PLS	Regressió per mínims quadrats parcials, *partial least squares regression*
PLS-DA	Anàlisi discriminant per mínims quadrats parcials, *partial least squares-discriminant analysis*
POPs	Contaminants orgànics persistents, *persistent organic pollutants*
ppm	Parts per milió, *parts per million*
PS	Fosfatidilserina, *phosphatidylserine*
PCR	Reacció en cadena de la polimerasa, *polymerase chain reaction*

qRT-PCR	Reacció en cadena de la polimerasa quantitativa en temps real, *quantitative polymerase chain reaction at real time*
QqQ	Triple quadrupol, *triple quadrupole*
Q-ToF	Quadrupol-temps de vol, *quadrupole-time-of-flight*
q/r	Càrrega/radi, *charge/radius*
ROS	Espècies reactives d'oxigen, *reactive oxygen species*
RNA	Àcid ribonucleic, *ribonucleic acid*
RNA-seq	Seqüència de RNA, *RNA sequencing*
RMN	Espectroscòpia de ressonància magnètica nuclear, *nuclear magnetic resonance*
ROI	Cerca de les regions d'interès, *regions of interest*
ROIMCR	Combinació de Regions d'interès amb la resolució Multivariant per corbes per mínims quadrats alternats
rRNA	Àcid ribonucleic ribosòmic*, ribosomal ribonucleic acid*
S1P	Esfingosina-1-fosfat, *sphingosine-1-phosphate*
SIMPLISMA	SIMPL*e-to-use Interactive Self-Modeling Analysis*
SL	Esfingolípids, *sphingolipids*
SM	Esfingomielina, *sphingomyeline*
s/n	Relació senyal /soroll, *signal to noise ratio*
SPH	Esfinganina, *sphinganine*
SVD	Descomposició en valors singulars, *singular value decomposition*
TAG	Triacilglicèrids, *triacylglycerols*
TBT	Tributilestany, *tributylin*
TIC	Cromatograma total d'ions, *total ion chromatogram*
TNFα	*Tumor necrosis factor alpha*
ToF	Temps de vol, *time-of-flight*
tRNA	Àcid ribonucleic de transferència, *transfer ribonucleic acid*
UE	Unió europea, *European union*
UHPLC	Cromatografia de líquids d'ultra alta eficàcia, *ultra performance liquid chromatography*
UV	Ultravioleta

UV-vis	Ultravioleta visible, *ultraviolet-visible*
VIP	Importància de la variable en la projecció, *variable importance in projection*
VN	Veritables negatius, *true negative*
VP	Veritables positius, *true positive*
WB	*Western blot*

NOTACIÓ

La notació matemàtica utilitzada en aquesta Tesi correspon a l'acceptada per la comunitat científica. Les lletres minúscules cursives (per exemple, *x*) indiqueu escalars. Les lletres minúscules en negreta (per exemple, **x**) indiquen vectors. Les lletres majúscules en negreta (per exemple, **X**) indiquen matrius. La transposició d'una matriu s'indica amb una "T" com a superíndex (per exemple, $\mathbf{X}^{\mathbf{T}}$).

Capítol 1.
Objectius i estructura de la Tesi

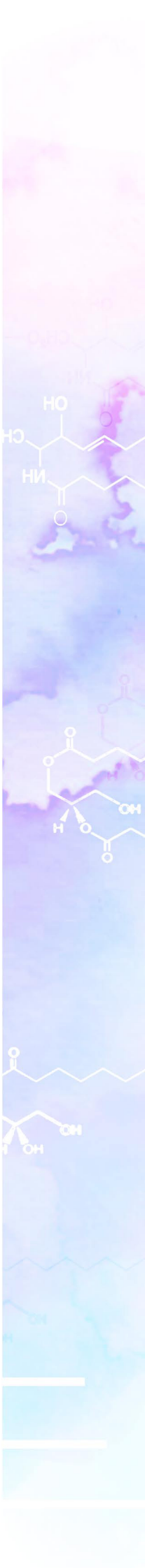

1.1. Objectius

L'objectiu principal d'aquesta Tesi és la realització d'estudis exposòmics de caire lipidòmic en cultius de cèl·lules mitjançant el tractament quimiomètric no dirigit de les dades generades. Aquestes anàlisis pretenen extreure el màxim d'informació per tal de descobrir la participació dels diferents lípids i el seu comportament en la resposta de les cèl·lules enfront els diferents estímuls generats. De manera més precisa, en aquesta Tesi es proposen els següents objectius específics:

- Estudi dels efectes de l'exposició crònica de cèl·lules DU145 de càncer de pròstata a diferents disruptors endocrins i contaminants ambientals (Aldrin, Aroclor i Clorpirifós), mitjançant una caracterització fenotípica i lipidòmica.
- Estudi dels canvis lipídics que es produeixen durant la transició epitelial-mesenquimal (EMT) en cèl·lules de càncer de pròstata DU145, emprant un anàlisi multivariant no dirigit (MCR-ALS) sobre les dades de LC-MS.
- Estudi dels canvis lipidòmics i fenotípics que es produeixen en cultius primaris de melanòcits i queratinòcits exposats de forma aguda i crònica a radiació solar simulada.
- Validació de la metodologia ROIMCR desenvolupada en el grup de recerca per l'anàlisi multivariant de dades LC-MS.

Aquesta Tesi s'ha realitzat en el marc del projecte europeu CHEMAGEB (*CHEMometric and High-throughput Omics Analytical Methods for Assessment of Global Change Effects on Environmental and Biological Systems*). L'objectiu principal d'aquest projecte ha estat el desenvolupament de nous mètodes analítics i quimiomètrics per avaluar els efectes del canvi climàtic i la pol·lució en diferents organismes model representatius dels ecosistemes; mitjançant una aproximació òmica (metabolòmica, transcriptòmica o genòmica). Dins d'aquest projecte, aquesta Tesi s'ha centrat en els estudis lipidòmics no dirigits en diversos cultius cel·lulars humans, utilitzant com a metodologia analítica la cromatografia de líquids acoblada a l'espectrometria de masses.

1.2. Estructura de la Tesi

La present memòria està estructurada en sis capítols que es descriuen a continuació.
En el **primer capítol** es presenten els objectius que han motivat la realització d'aquesta Tesi, es detalla l'estructura i la relació dels treballs científics de la present memòria.

En el **segon capítol** es fa una introducció sobre els lípids, les diferents tècniques òmiques i les metodologies experimentals d'anàlisi dirigides i no dirigides que s'utilitzen. A continuació, es detallen els mètodes quimiomètrics que s'han emprat en el tractament de les dades LC-MS obtingudes de l'anàlisi lipidòmica no dirigida. Seguidament, es descriu el terme d'exposòmica i els diferents estressants ambientals aplicats al llarg d'aquesta Tesi. Per últim, es menciona el treball amb cultius cel·lulars i l'avaluació dels efectes estressants mitjançant tècniques de biologia cel·lular i molecular.

En el **tercer capítol** es presenten els resultats i la discussió de la validació de la metodologia ROIMCR per al tractament de dades no dirigides obtingudes mitjançant LC-MS. En aquest treball es van emprar diferents concentracions d'una mescla de lípids coneguts, els quals van ser també incorporats a una mostra real procedent de l'extracció de lípids de cèl·lules A375 (melanoma), per tal de posar a prova la metodologia ROIMCR en diferents graus de complexitat.

En el **quart capítol** es mostren els resultats de l'aplicació d'una estratègia d'anàlisi no dirigida dels perfils lipídics LC-MS de cèl·lules de càncer de pròstata exposades de forma crònica a diferents disruptors endocrins (Aldrin, Aroclor i Clorpirifós). En aquest capítol també es presenten els resultats de la transició epitelial messenquimal (EMT) induïda en les cèl·lules de càncer de pròstata DU145. En ambdues publicacions, es recullen els resultats obtinguts de l'anàlisi conjunta per MCR-ALS de les dades LC-MS de mostres de cultius cel·lulars, la selecció i identificació dels lípids, la concentració dels quals canvia més en relació a les condicions estressants aplicades, i la interpretació biològica dels fenòmens relacionats amb els canvis lipídics observats.

En el **cinquè capítol** es presenten els treballs dirigits a l'anàlisi lipidòmica no dirigida centrada en dos models de cèl·lules de l'epidermis humana (melanòcits i queratinòcits

primaris) exposats a la radiació UV de forma aguda i crònica. Les dades LC-MS van ser processades seguint la metodologia ROIMCR i es van realitzar diverses proves biològiques per corroborar els resultats obtinguts. També es va realitzar una interpretació biològica dels resultats obtinguts, per tal de determinar aquelles rutes lipídiques més afectades.

Finalment, en el **sisè capítol** es recullen les conclusions generals més importants de la present Tesi.

1.3. Relació dels treballs científics presents en la memòria

A continuació es detallen totes les publicacions de la present Tesi:

Article 1. ***Validation of the Regions of Interest Multivariate Curve Resolution (ROIMCR) procedure for untargeted LC-MS lipidomic analysis***

Autors: Núria Dalmau, Carmen Bedia i Romà Tauler

Revista: Analytica Chimica Acta (2018) 1025, 80-91

Article 2. ***Phenotypic malignant changes and untargeted lipidomic analysis of long-term exposed prostate cancer cells to endocrine disruptors***

Autors: Carmen Bedia, Núria Dalmau, Joaquim Jaumot i Romà Tauler

Revista: Environmental Research (2015) 140, 18-31

Grau de participació: Realització de tota la part experimental. Cultius cel·lulars i tots els assaigs biològics.

Article 3. ***Epithelial-to-mesenchymal transition involves triacylglycerol accumulation in DU145 prostate cancer cells***

Autors: Núria Dalmau, Joaquim Jaumot, Romà Tauler i Carmen Bedia

Revista: Molecular BioSystems (2015) 11, 397-406

Article 4. ***Untargeted lipidomic analysis of primary human epidermal melanocytes acutely and chronically exposed to UV radiation***

Autors: Núria Dalmau, Nathalie Andrieu-Abadie, Romà Tauler i Carmen Bedia

Revista: Molecular Omics (2018) 14(3), 170-180

Article 5. ***Phenotypic and lipidomic characterization of primary human epidermal keratinocytes exposed to simulated solar UV radiation***

Autors: Núria Dalmau, Nathalie Andrieu-Abadie, Romà Tauler i Carmen Bedia

Revista: Journal of Dermatological Science (2018) 92(1), 97-105

Capítol 2.
Introducció

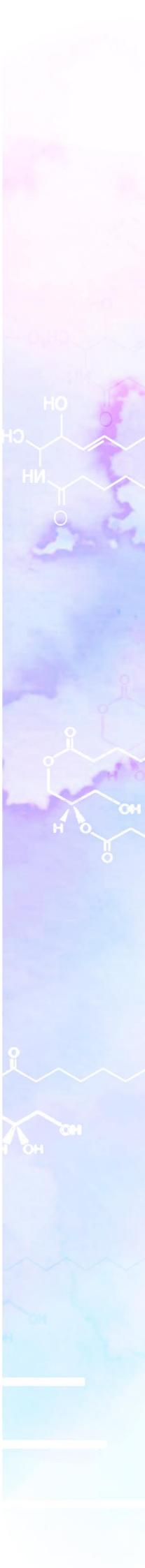

2.1. Lípids

Els lípids són biomolècules hidrofòbiques o amfifíliques d'origen natural que tenen tasques úniques i específiques en l'organització i funcionament de les cèl·lules. D'una banda són components estructurals de les diferents membranes cel·lulars, el que els confereix un paper clau tant en el manteniment de la seva fluïdesa com en els intercanvis que s'hi produeixen (transport de nutrients, excreció de residus, etc.). D'altra banda, els lípids estenen la seva funcionalitat a altres àmbits com la senyalització cel·lular, les accions endocrines i l'emmagatzematge d'energia.[1-2] Els lípids són biomolècules que s'inclouen dins del grup dels metabòlits i poden ser classificats en vuit grups: àcids grassos, glicerolípids (GL), glicerofosfolípids (GP), esfingolípids (SL), sacarolípids, policètids, esterols i terpens o isoprenoides (veure Figura 1). Aquesta classificació va ser publicada l'any 2009 pel International Lipid Classification and Nomenclature Committe (ILCNC)[3] i és vàlida per mamífers, plantes, bacteris i fongs.

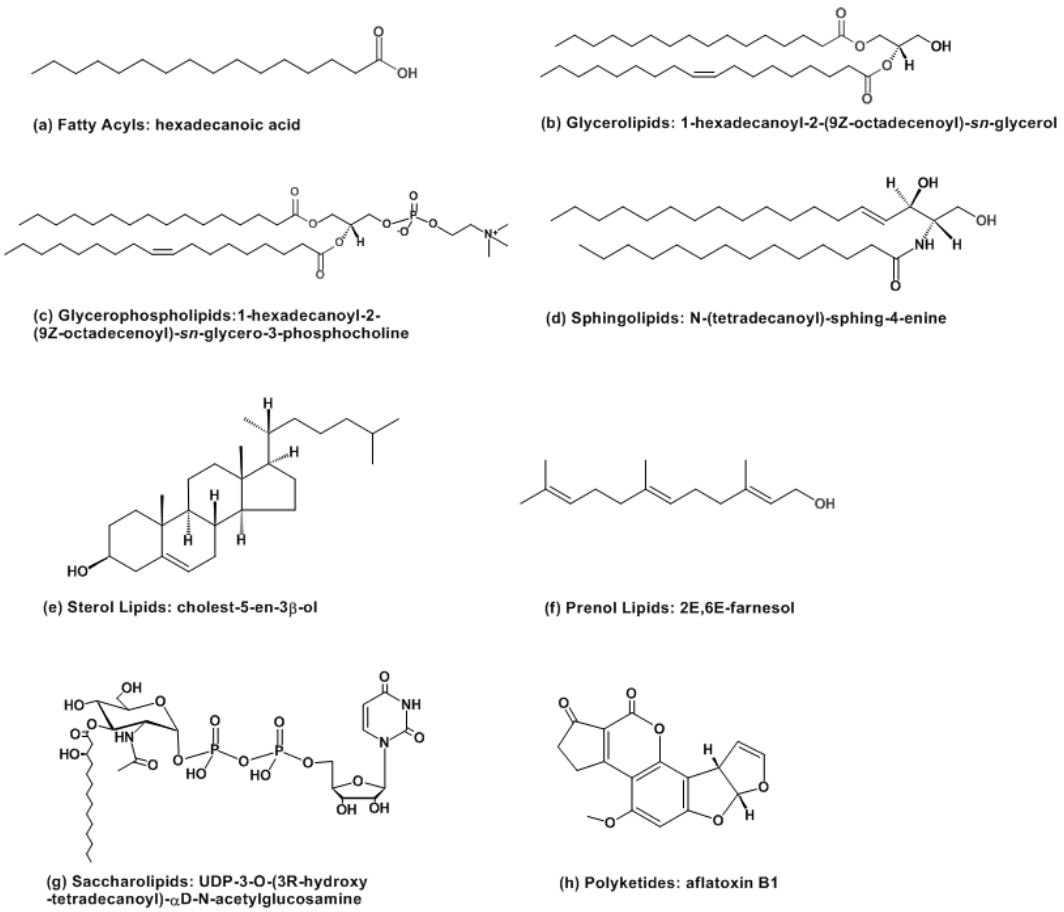

Figura 1. Classificació dels lípids en els 8 grups descrits per la IUPAC (Figura extreta de https://www.lipidmaps.org/data/classification/lipid_cns.html).

La importància dels estudis lipídics es deu al paper essencial que juguen en un gran nombre de malalties com desordres cardiovasculars[4], càncer[5], malalties neurodegeneratives[6], obesitat[7] o diabetis[8]. Una revisió de Sunshine *et al.* l'any 2017 feia referència al recent interès dels lípids com a reguladors de la senyalització cel·lular, ja que les membranes lipídiques poden interactuar directament associant-se amb receptors o missatgers secundaris.[9]

Entre totes les famílies de lípids, els treballs realitzats en aquesta Tesi han fet especial èmfasi en l'anàlisi dels esfingolípids, els glicerolípids i els glicerofosfolípids.

Els **esfingolípids** (SLs) són una família de lípids que ha despertat molt interès científic en les darreres dècades. Els SLs tenen un pes important en la regulació i control de les funcions cel·lulars. A part de la seva contribució com components estructurals de membranes cel·lulars, també són àmpliament reconeguts com a reguladors de les funcions cel·lulars vitals.[10-11] La ceramida és la molècula central del metabolisme d'esfingolípids. Estructuralment, es tracta d'un aminodiol de cadena llarga (base esfingoide), unida per un enllaç amida a un àcid gras de longitud de cadena variable, veure Figura 2. La ceramida és un inductor de la mort cel·lular programada o apoptosi, així de com de la parada del cicle cel·lular.[12] Per aquesta raó, té un paper molt important en la regulació de la supervivència cel·lular, en la diferenciació de les cèl·lules i en les respostes inflamatòries. La ceramida pot ser generada seguint la síntesi *de novo* a partir de serina i palmitoil CoA, així com de la hidròlisi d'esfingolípids complexos presents en la membrana plasmàtica, com les esfingomielines o els glicoesfingolípids.

La ceramida és catabolitzada per l'acció de les ceramidases per alliberar l'àcid gras i l'esfingosina, la qual a la seva vegada es pot fosforil·lar per produir esfingosina 1-fosfat (S1P), un esfingolípid anti-apoptòtic, que està involucrat en la proliferació cel·lular i en la motilitat de les cèl·lules i desenvolupament vascular. L'augment de la generació de S1P activa les rutes de senyalització que intervenen en la supervivència cel·lular i transformació maligna, en la invasió o l'angiogènesi, i en tots els processos involucrats en la patogènesi del càncer. El metabolisme dels esfingolípids sovint es troba alterat en el càncer. L'exemple d'alteració més conegut es localitza en el reòstat ceramida/S1P.

Els canvis metabòlics que regulen la relació ceramida/S1P poden conduir a un desequilibri i determinar la supervivència o mort de la cèl·lula.[11, 13]

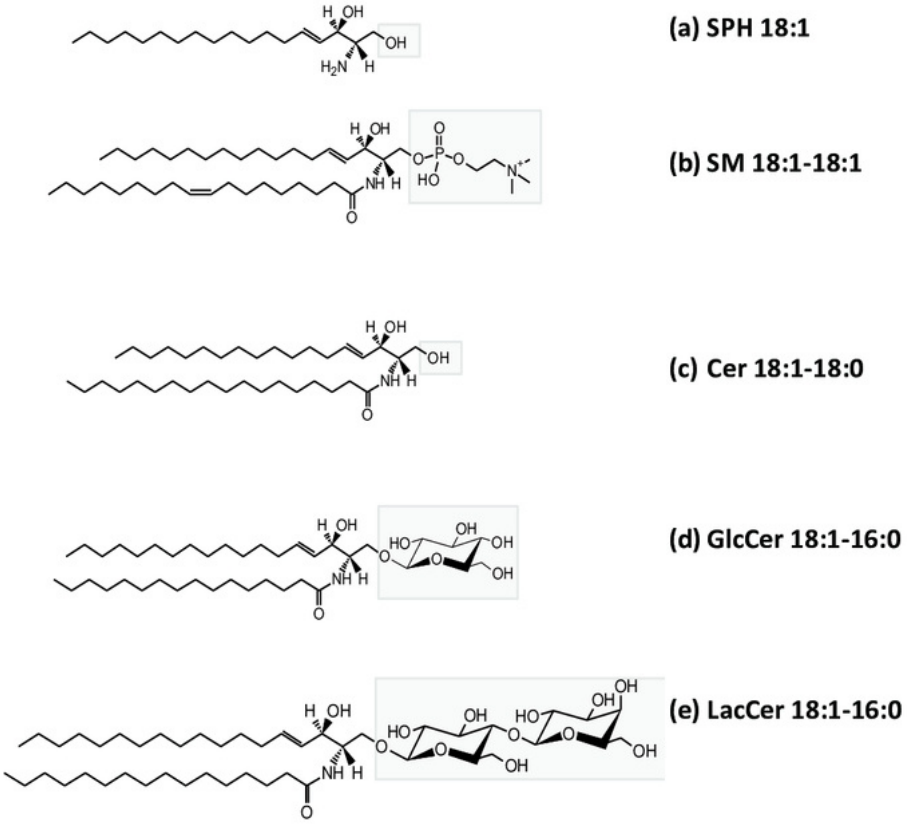

Figura 2. Esquema dels principals esfingolípids (SLs). Es poden apreciar una esfinganina (SPH), una esfingomielina (SM), una ceramida (Cer), una glucosilceramida (GluCer) i una lactocilceramida (LacCer).

D'altra banda, els glicerolípids i els glicerofosfolípids tenen una gran rellevància en la membrana biològica. Els **glicerolípids** (GLs) són un grup de lípids estructuralment heterogeni que juga un paper clau en l'estructura i funcionament de la membrana cel·lular, a més de conformar la major reserva d'energia del cos humà. Estructuralment, els GLs estan formats per un grup glicerol mono-, di- o tri-substituït per àcids grassos mitjançant un enllaç èster, donant lloc als monoacilglicèrids (MAG), diacilglicèrids (DAG) i triacilglicèrids (TAG), veure Figura 3.[14] Degut a aquesta estructura, els GLs són molècules no-polars i hidrofòbiques, és a dir que són insolubles en aigua. Per exemple, els TAGs són els lípids no polars més abundants en olis i greixos d'origen animal i vegetal. Aquests representen la major forma d'emmagatzematge de

lípids i energia a l'organisme humà. També estan presents en els fluids corporals com la sang en forma de lipoproteïnes, per tal de permetre la transferència de lípids entre teixits.[15]

El DAG, a més de ser un lípid intermedi en la síntesi de TAG, és un important segon missatger associat a la membrana cel·lular que duu a terme l'activació de proteïnes relacionades amb gran diversitat de cascades de senyalització. Una de les proteïnes més caracteritzades per la seva activació mitjançant DAG és la proteina kinasa C (PKC) que catalitza l'activació d'altres proteïnes cel·lulars específiques. Els DAG també poden ser fosforilats a la membrana per DAG kinasa per produir àcid fosfatídic (PA), un altre important missatger cel·lular.[16] En el cas dels MAG, estan relacionats amb l'estructura de la membrana i el emmagatzematge d'energia, ja que són precursors sintètics d'altres lípids més complexos. Recentment, el fet de que el 2-araquidonoïlglicerol (un MAG) s'hagi descrit com un endocannabinoid amb efectes al cervell, ha despertat l'interès per l'estudi de les funcions que altres MAG podrien tenir com a senyalitzadors cel·lulars.[17]

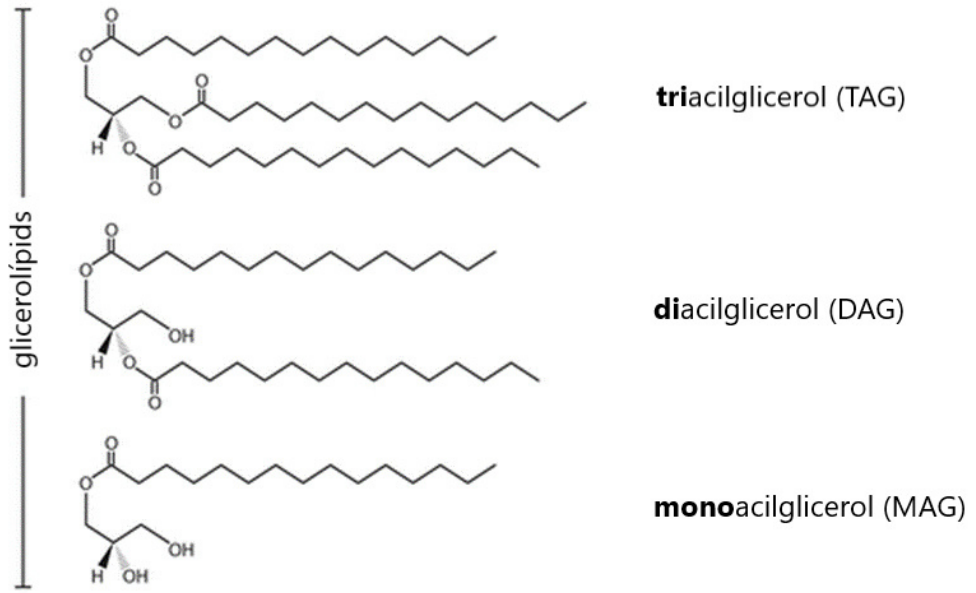

Figura 3. Esquema dels principals glicerolípids (GLs).

Els **glicerofosfolípids** (GPs) o fosfoglicèrids són lípids amb base de glicerol, derivats de l'àcid fosfatídic (PA) en el quals la regió hidrofòbica està composta per dos àcids

grassos i un alcohol polar unit en la posició C-3 del glicerol mitjançant un enllaç fosfodièster (veure Figura 4).

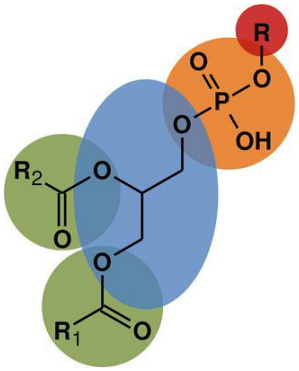

Figura 4. Estructura general dels glicerofosfolípids (GPs). Els grups que composen els GPs estan senyalats per diferents colors; el glicerol en blau, el fosfat en taronja, els àcids grassos R1 i R2 en verd i el cap polar que dona nom als diferents GPs en vermell.

Els glicerofosfolípids són grup de lípids molt abundant i de gran importància com a components de membrana, combustibles metabòlics i com a senyalitzadors moleculars. Els GPs són anomenats segons el seus grups de cap polars. Així doncs, tenim les fosfatidilcolines (PC), les fosfatidiletanolamines (PE), els fosfatidilglicerols (PG), les fosfatidilserines (PS), els fosfatidilinositols (PI) i àcid fosfatídic (PA); veure la Figura 5. Els GPs són variats i tots ells desenvolupen funcions rellevants, tot i que la més coneguda i destacable és com a component estructural de la membrana cel·lular. Degut al seu caràcter amfipàtic formen part de les bicapes lipídiques, la composició de les quals varia en funció del tipus de cèl·lula o els diferents estímuls externs. Per exemple, en els eritròcits, la part citosòlica de la membrana consisteix principalment en PE, PS i PI. En canvi, el costat exoplàsmic està format principalment per PC i esfingomielina.[18] A part de la seva funció en les membranes cel·lulars, els GPs poden actuar com a inductors de senyal i transportadors. Pel que fa a la senyalització, els GPs proporcionen els precursors de prostaglandines i leucotriens.[19] La seva distribució i el seu catabolisme específic és el que els permet dur a terme els processos de resposta biològica esmentats anteriorment. També poden actuar com a emmagatzematge de missatgers secundaris en la membrana i contribuir així a la senyalització cel·lular.[20-22]

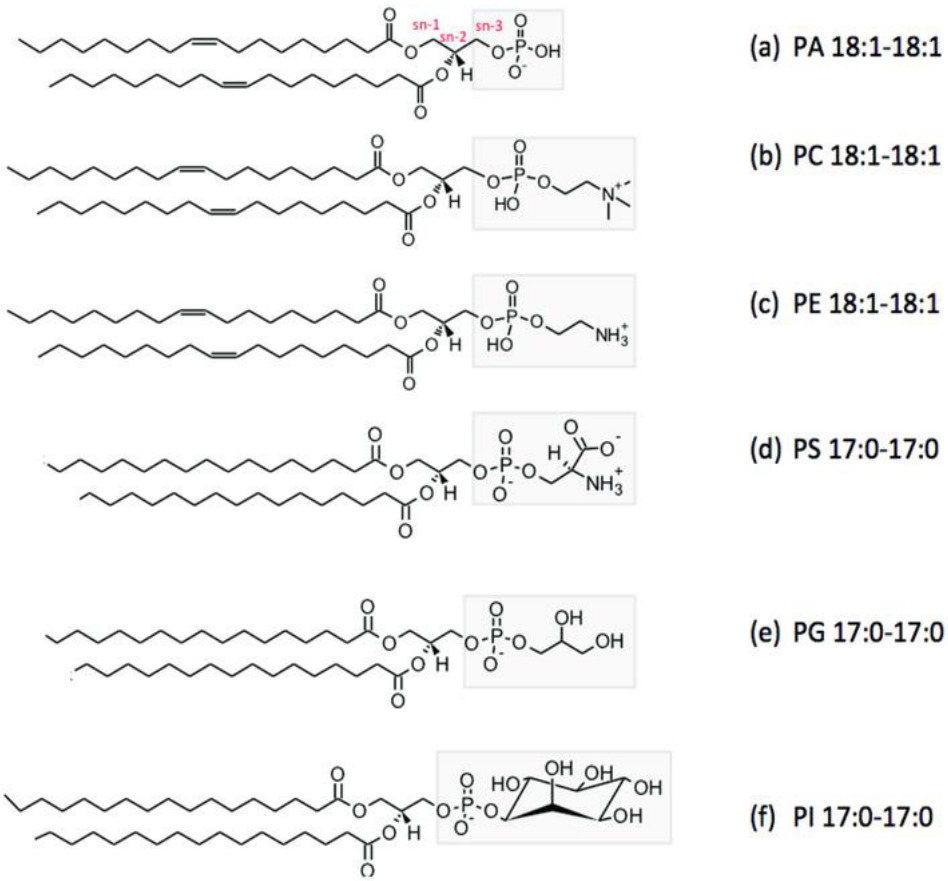

Figura 5. Exemples de molècules dels diferents tipus de glicerofosfolípids (GPs), on es poden apreciar els diferents radicals o caps polars que atorguen les propietats a cada tipus de lípid. La figura representa els grups majoritaris dins els glicerolípids com són l'àcid fosfatídic (PA), les fosfatidilcolines (PC), les fosfatidiletanolamines (PE), les fosfatidilserines (PS), els fosfatidilgrlicerols (PG) i els fosfatidilinositols (PI).

2.2. Lipidòmica

El terme "òmica", definit com a "conjunt de", és un sufix que s'afegeix a estudis de diferents àmbits per cobrir totes les tècniques que es basen en obtenir la màxima informació possible i els canvis produïts en un temps determinat i un sistema concret.[23-24] En el cas dels sistemes biològics existeixen quatre nivells principals d'estudis òmics: la genòmica que és l'àrea de coneixement que investiga la codificació del genoma; la transcriptòmica que estudia els canvis en l'expressió gènica; la proteòmica que determina l'expressió de les proteïnes i els seus canvis en les cèl·lules o teixits i, finalment; la metabolòmica, introduïda més recentment, que estudia els perfils metabòlics i els seus canvis (veure Figura 6). Les ciències òmiques són la clau per

a la interpretació i compressió dels processos biològics.[25-27] La lipidòmica és una de les ciències englobada dins la metabolòmica, ja que es considera que els lípids pertanyen al grup dels metabòlits.

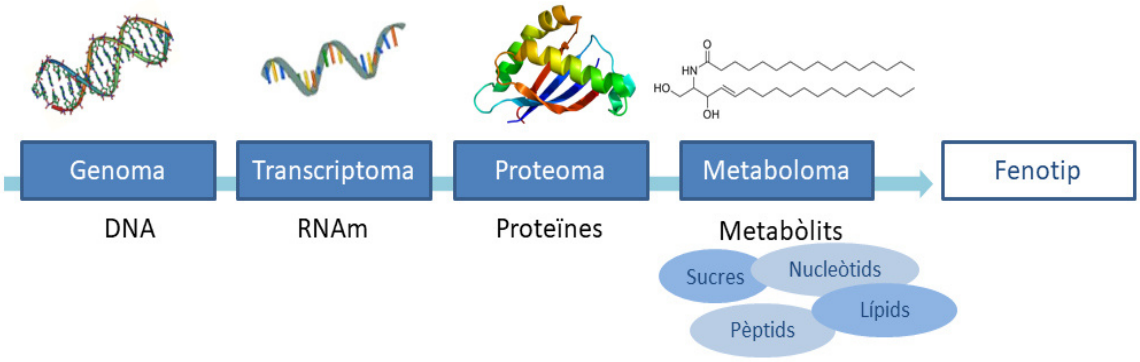

Figura 6. Representació gràfica dels quatre nivells principals d'estudis òmics.

Avui en dia, la metabolòmica i la lipidòmica són disciplines utilitzades en l'avaluació de les respostes fisiològiques associades a l'acció dels contaminants, dels seus efectes tòxics i dels desordres metabòlics produïts.[28] Aquesta importància dels darrers anys en la metabolòmica rau en el fet que descriuen el punt final de la "cascada òmica" (veure Figura 6), que relaciona la informació genètica amb el fenotip. El metabolisme d'un organisme expressa directament l'estat biològic en el que aquest es troba, el qual depèn tant del genoma com de les circumstàncies a les quals es troba exposat l'organisme.[25] Les causes que provoquen les alteracions en els sistemes biològics són diverses, entre elles l'estil de vida, l'entorn on es desenvolupa, la dieta o l'ús de fàrmacs. Els canvis o variacions no sempre es produeixen en el mateix nivell de l'escala biològica o temporal. Per tant, poder integrar tota la informació obtinguda a partir de l'estudi de la cascada òmica, es converteix en una tasca laboriosa i complexa.

Tot i que la lipidòmica és considerada una sub-disciplina de la metabolòmica, aquesta té la seva identitat pròpia. Les malalties cardiovasculars, l'obesitat i d'altres problemes associats al metabolisme són freqüentment relacionats amb els lípids, així com moltes malalties humanes, incloses el càncer i l'Alzheimer, les quals tenen també un component lipídic.[29-31] Conèixer el perfil lipídic complet del sistema biològic que s'estudia permet extreure informació sobre la relació dels lípids presents en

l'organisme i sobre la seva quantitat i comportament. Un dels objectius principals dels estudis lipidòmics és l'avaluació de les alteracions produïdes en els lípids a causa d'un determinat estrès ambiental. L'estrès pot ocasionar canvis en els diferents punts de la cascada òmica i per tant, poden ser analitzats els seus efectes en qualsevol punt, com podria ser l'estudi de la composició lipídica.

En aquesta Tesi s'han dut a terme diversos treballs de lipidòmica en models cel·lulars exposats a diferents tipus d'estrès ambiental. En un primer bloc, s'han estudiat els efectes de l'exposició crònica a diferents disruptors endocrins i la inducció de la EMT en cèl·lules de càncer de pròstata DU145. També, s'han investigat els efectes de la radiació UV a curt i llarg termini en melanòcits i queratinòcits, les principals cèl·lules de l'epidermis humana. D'altra banda, s'ha validat la nova metodologia ROIMCR pel tractament de dades òmiques i així millorar el seu processat en el cas de mesures LC-MS.

2.2.1. Anàlisi lipidòmica dirigida i no dirigida

En les diferents disciplines òmiques hi ha dues estratègies per a l'anàlisi experimental: l'anàlisi dirigida i l'anàlisi no dirigida.[32] L'anàlisi **dirigida** està focalitzada en l'estudi d'alguns metabòlits determinats d'interès i requereix de patrons de referència per l'anàlisi quantitatiu d'aquests compostos escollits.[33] Un dels principals avantatges de l'enfocament dirigit és que els mètodes d'extracció i protocols han estat optimitzats per l'anàlisi de metabòlits específics, i a més, generalment es disposa de bases de dades molt completes sobre les característiques de les molècules a estudiar.[34-35] D'altra banda, la creixent millora de les metodologies d'anàlisi disponibles, permet desenvolupar mètodes molt més sensibles i robustos per a la mesura d'un major nombre de metabòlits i de diferents mides. No obstant, el fet que l'anàlisi dirigida es centri únicament en metabòlits predeterminats pot comportar la pèrdua d'informació nova i/o rellevant per a nous descobriments.

En canvi, l'anàlisi **no dirigida** té per objectiu detectar el major nombre possible de molècules (gens, proteïnes o metabòlits) presents a la mostra, sense cap mena de filtre

i sense disposar de cap hipòtesi prèvia sobre les rutes de senyalització o metabòliques de potencial interès.[36-37] Aquesta estratègia obre la porta a la possibilitat de descobrir noves molècules que reflecteixin l'estat de les cèl·lules sota un estímul concret. Un cop s'han processat totes les dades i determinats els canvis més significatius, els estudis no dirigits poden crear noves hipòtesis al final de l'anàlisi, donant lloc a noves vies d'investigació. Els exemples més típics d'aplicacions d'anàlisi no dirigida són els estudis que s'emmarquen en la recerca de nous biomarcadors. Els biomarcadors són molècules que alerten sobre canvis específics en les cèl·lules, ja sigui en relació a malalties o a l'exposició a diferents tipus d'estrès. Aquestes molècules poden arribar a ser molt útils pel diagnòstic, pronòstic i monitorització dels diferents processos estudiats. [25, 38] Una de les grans diferències entre l'anàlisi dirigida i no dirigida és el tipus i quantitat de dades generades. L'anàlisi no dirigida obté dades més complexes ja que es registren un gran nombre de senyals per cada mostra analitzada. Això provoca que els arxius de dades generats puguin arribar a ser de l'ordre de gigabytes per mostra. Aquesta major complexitat de les dades requereix la utilització d'eines quimiomètriques adequades pel seu processament. Altres inconvenients de l'estratègia no dirigida són les dificultats de realitzar la quantificació absoluta i la identificació de totes les molècules considerades rellevants en l'estudi després de l'anàlisi.[39]

Finalment, cal destacar que les dues aproximacions poden considerar-se complementaries ja que una anàlisi no dirigida pot posar en rellevància una ruta metabòlica o senyalització concreta que pot ser estudiada més endavant de manera dirigida, per tal de corroborar aquestes hipòtesis i establir estimacions quantitatives absolutes dels efectes estudiats.[40]

Els estudis de lipidòmica tenen múltiples camps d'aplicació, des dels estudis clínics[38, 41] als ambientals[42]. En particular, aquesta Tesi s'ha centrat en l'estudi de la lipidòmica no dirigida dins el camp ambiental utilitzant cèl·lules humanes. En els estudis de lipidòmica ambiental s'avaluen els efectes que els diferents estressants presents en el medi ambient causen en els organismes model, com la radiació UV solar o els

contaminants químics ambientals presents en pesticides o subproductes de la indústria.

2.3. Tractament quimiomètric de les dades lipidòmiques

Cada mostra de l'estudi lipidòmic obtinguda mitjançant la cromatografia líquida acoblada a l'espectrometria de masses (LC-MS) proporciona una matriu de dades amb el nombre de temps de retenció a les files i el nombre de valors de *m/z* a les columnes. Cal tenir en compte que les mides d'aquestes matrius són grans, de forma que és difícil treballar amb totes les dades al mateix temps. Quan es consideren diverses mostres analitzades simultàniament, les dades obtingudes poden agrupar-se en una estructura en forma de cub amb tres direccions (*three-way data*), temps de retenció, valors de *m/z* i mostres o en una matriu de dades augmentada, on els temps de retenció de les diferents mostres es troben en les files de la matriu i el valors de *m/z* en les columnes de la matriu. Aquesta darrera estructura de dades és la que s'ha utilitzat en aquesta Tesi per l'anàlisi quimiomètrica.

A continuació es detallaran els diferents mètodes i tècniques quimiomètriques utilitzades en aquesta Tesi i posteriorment, s'especificaran i desglossaran les aproximacions emprades en els diferents treballs per a l'anàlisi de dades.

2.3.1. Anàlisi del cromatograma total d'ions (TIC)

A partir de les dades del LC-MS es poden generar els Cromatograma Total d'Ions (TIC) que per cadascuna de les mostres correspon a un cromatograma format per la suma de les intensitats de tots els valors de *m/z* de l'espectre de masses.

2.3.2. Anàlisi de components principals (PCA)

El PCA és un tipus d'anàlisi multivariant de dades basat en un model de descomposició bilineal de la matriu de dades experimentals en el producte de dues matrius ortogonals de factors, *scores* i *loadings*.[43] La seva principal utilitat és representar l'estructura multidimensional de les dades en un nombre més petit de dimensions,

generalment dos o tres, que ens permetin la representació gràfica de les fonts de variació o variança de les dades analitzades. D'aquesta manera es possibilita observar fàcilment els elements característics de l'estructura del conjunt de dades, per exemple, els grups d'objectes, els valors anòmals (*outliers*) o quines són les variables que aporten més informació. Gràficament, el mètode PCA (Figura 7) compren la descomposició de la matriu de dades (**X**) en la matriu de *scores* (**T**) que descriu les mostres a l'espai del components principals i la matriu de *loadings* (**P**) que correspon a les variables originals a l'espai dels components principals.

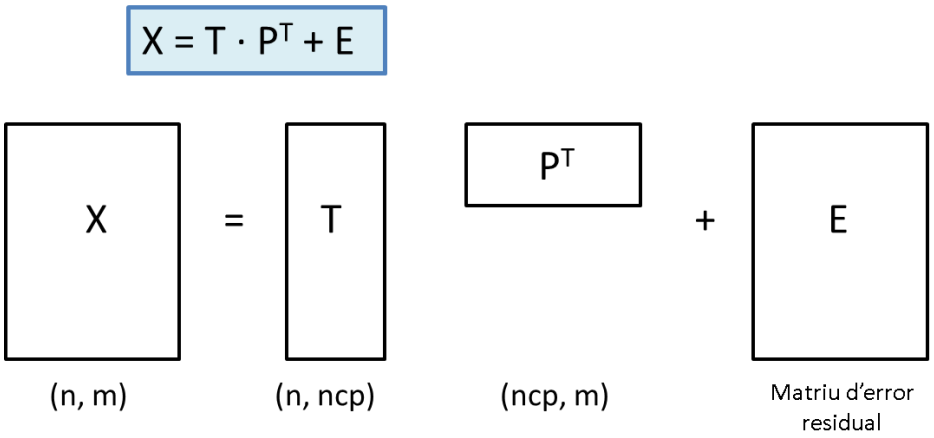

Figura 7. Equació i representació gràfica del model PCA. On **n** correspon al nombre de variables, **m** són el nombre de mostres i **ncp** són el nombre de components principals.

Els components principals són uns nous eixos ortogonals de coordenades sobre els quals es poden representar les dades experimentals (Figura 8). Dit d'una altra manera, són unes noves variables que són combinació lineal de les variables originals que descriuen de forma eficient la variació de les dades experimentals. Aquestes noves variables o components principals contenen la informació més important sobre la variació experimental de les dades, eliminen una gran part del seu soroll experimental i no repeteixen la informació superposada que pugui estar continguda en elles (són ortogonals entre si).

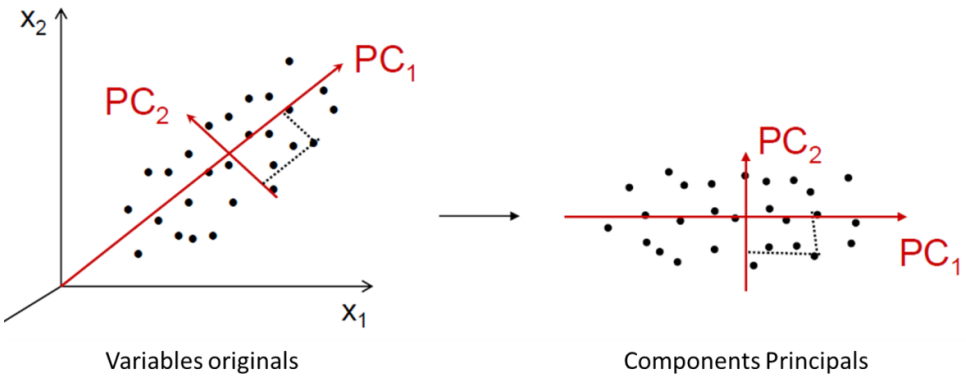

Figura 8. Representació de dades segons els Components Principals 1 i 2. El gràfic de l'esquerra representa l'esquem dels components principals (PC) segons els tres eixos (x_1, x_2 i x_3). El gràfic de la dreta representa les dades segons els eixos dels propis components PC_1 i PC_2.

Quan s'aplica PCA ens interessa, per una banda, la representació de les dades en l'espai definit pels components principals, el que es coneix amb el nom de mapa de mostres (*scores*), que permet detectar si les mostres formen i se separen en grups o classes o si hi ha algun objecte anòmal. La distància entre les mostres indica la seva similitud o diferència. Així, quan un conjunt de mostres es troben pròximes entre elles es pot dir que formen diferents grups o classes de mostres.

D'altra banda, es considera també la representació dels *loadings*, que corresponen a la descripció de les variables originals a l'espai dels components principals. Les variables més rellevants en cada component principal són les que presenten valors més alts. A partir d'aquesta representació es poden deduir les correlacions que existeixen entre les variables experimentals i la naturalesa i característiques de les fonts de variació de les dades.

2.3.3. Anàlisi discriminant de mínims quadrats parcials (PLS-DA)

Un dels objectius d'un estudi lipidòmic recau generalment en la diferenciació de les mostres en dos o més grups, que son postulats a l'inici de l'estudi, per exemple entre mostres control i mostres sotmeses a un determinat estrès ambiental. El PCA permet veure les possibles diferències entre les mostres però en el model no s'inclou aquesta informació ja que es tracta d'un anàlisi no supervisat. Quan aquesta informació sobre

la naturalesa d'un conjunt de mostres es coneix, es poden aplicar mètodes que permeten incloure aquesta informació en el model, com és el cas de l'anàlisi discriminant per mínims quadrats parcials (PLS-DA).[44]

En el PLS-DA hi ha dos blocs de dades, el bloc de dades o matriu de dades **X** que en el nostre cas, per exemple, pot correspondre als TICs mesurats sobre les diferents mostres, i el bloc de dades **Y,** que pot ser un vector o matriu de dades, on es troba la informació relativa a la pertinença de cada mostra a una determinada classe (vector o matriu de variables de classes). Quan es volen distingir les mostres que estan dins o fora d'una determinada classe es considera una sola variable **y** en forma de vector, que per cada objecte té un valor de 0 quan aquest no pertany a la classe o un valor de 1 quan sí hi pertany. En aquests casos es parla de models PLS1-DA ja que només es distingeixen la pertinença (o no) a una classe. Per contra, si es volen classificar els objectes en més classes, **Y** és una matriu de dades de pertinença a les diferents classes i es parla de models PLS2-DA.

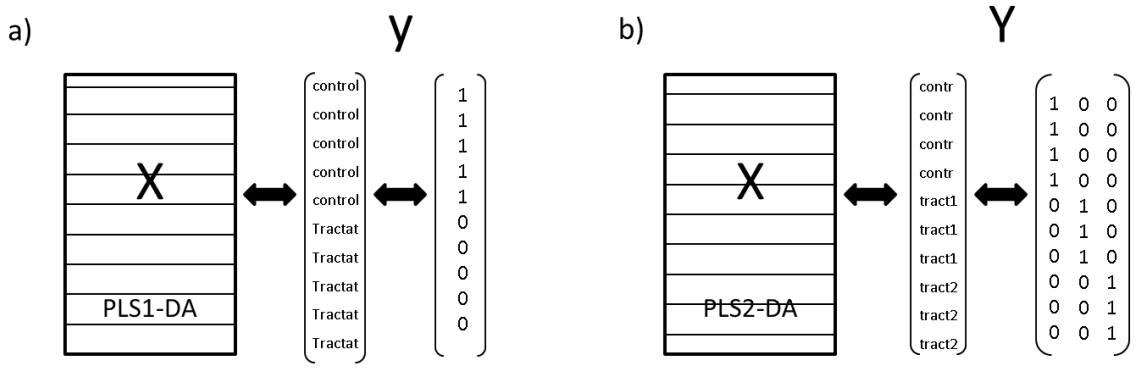

Figura 9. a) Representació del model PLS1-DA i del vector **y** codificat. b) Representació del model PLS2-DA i de la matriu **Y**.

Per exemple, en la Figura 9A es mostra la matriu **X** corresponent als TICs per totes les mostres i es relaciona amb la pertinença a mostres control o tractades, que es codifiquen en zeros i uns per a la construcció del model de discriminació entre mostres, formant un únic vector **y**. En canvi, la Figura 9B apareix també la matriu **X** referent als TICs, però la matriu **Y** mostra tres classes diferents. Això, fa que la interpretació matemàtica no sigui un únic vector, sinó una matriu amb uns i zeros en

tres columnes per poder indicar que hi ha tres classes presents. En aquesta Tesi s'ha treballat principalment amb el procediment PLS1-DA per distingir la pertinença a mostres control i a mostres tractades.

El propòsit del mètode de regressió PLSR és correlacionar les matrius **X** i **Y** amb un model bilineal emprant el nombre més petit possible de components o factors rellevants anomenats també variables latents (LV). Aquests factors es calculen de forma que inclouen les direccions de màxima covariància entre els dos blocs de dades, **X** i **Y.**[45] Aquesta relació entre els dos blocs, **X** i **Y**, queda reflectida en la matriu de pesos (**W**) que es genera durant la regressió. A partir dels vectors de pesos ($\mathbf{w_k}$) es poden calcular quines són les variables més importants en el model de predicció o projecció (*Variables Important in Projection*, VIP) per tal de facilitar la possible interpretació i selecció de les variables més importants. Aquestes variables VIP proporcionen un valor numèric per cada variable i s'ordenen d'acord a la seva importància en la projecció del model PLS. D'aquesta forma, com més gran sigui el valor VIP d'una determinada variable més important serà la variable en el model PLS. Habitualment es consideren significatives les variables amb un VIP per sobre del valor llindar de 1.[45]

Generalment, la qualitat d'un model de classificació o discriminació com el PLS-DA s'expressa utilitzant la sensibilitat i l'especificitat del model.[46] La sensibilitat mesura la probabilitat de classificar correctament una mostra que pertany a la classe (Equació 1). L'especificitat mesura la probabilitat d'assignar correctament una mostra que no pertany a la classe (Equació 2).

$$Sensibilitat = \frac{VP}{(VP+FN)} \qquad \textbf{Equació 1.}$$

$$Especificitat = \frac{VN}{(VN+FP)} \qquad \textbf{Equació 2.}$$

Els valors VP (veritables positius) indiquen el nombre de mostres que realment pertanyen al grup en que se'ls ha classificat i els VN (veritables negatius), indiquen el nombre de nostres que realment no formen part de la classe i no han estat assignades correctament. A més, els FN (falsos negatius) són el nombre de casos en que les

mostres eren d'una classe, però el model els ha disposat com que no hi pertanyen. Els FP (falsos positius) són les mostres que no s'havien classificat en la classe i el model els ha classificat a dins d'aquesta classe que no és correcta. Interessa que la sensibilitat sigui igual a 1 ja que indicaria que el model separa correctament les nostres classes. També es vol que l'especificitat sigui la més pròxima possible a 1 ja que indicarà la major probabilitat de classificar correctament una mostra que pertany a la classe.
Per tenir una idea sobre la bondat d'un model PLS-DA es pot considerar una taula de diagnòstic com la que es mostra a la Taula 2.1.

Taula 2.1. Taula de diagnòstic d'un model PLS-DA.

Pertinència a una classe segons el model	**Informació real de pertinència a una classe**	
	Positiu	Negatiu
Positiu	Nombre de veritables positius (VP)	Nombre de falsos positius (FP)
Negatiu	Nombre de falsos negatius (FN)	Nombre de veritables negatius (VN)
	VP + FN	VN + FP

Finalment, cal destacar que el model PLS-DA també es pot emprar aplicant la ortogonalitat en el model (OPLS-DA), amb l'avantatge que la interpretació dels resultats és habitualment més senzilla.[47-48] Aquesta ortogonalització s'aconsegueix rotant les matrius de *loadings* i *weights* per tal que expliquin el màxim de variància de la matriu **Y** en el primer *loading* i *weight*. Malgrat això cal destacar que la capacitat predictiva del model ortogonalitzat i sense ortogonalitzar (amb més components) és la mateixa.

2.3.4. Pre-tractament de les dades originals per interpolació i *binning* en combinació amb la divisió de finestres de temps

La interpolació i, en especial, el *binning* són procediments que poden ser emprats en la compressió de dades dels espectres *full scan* provinents de LC-MS o GC-MS. La compressió de les dades per interpolació o *binnning* s'aplica sobre els espectres de

masses enregistrats a cada temps de retenció (fila) de les dades experimentals. D'aquesta manera, els espectres originals d'alta resolució en els diferents temps de retenció, mesurats a valors diferents de *m/z* no equidistants, i es converteixen en espectres de baixa resolució, on els valors *m/z* estan separats segons el grau d'interpolació o mida de *bin* prèviament definida. En concret, en el pre-processat *binning* es sumen les lectures d'intensitat del senyal mesurat dins d'un interval espectral definit per la mida del *bin* i així formar una única mesura (suma total d'intensitats mesurades en aquest interval). Per tant, la compressió de dades amb aquestes estratègies es realitza en la dimensió espectral (eix *m/z*). Un dels inconvenients d'aquest tipus de pre-processat és la dificultat en la selecció adequada del nivell d'interpolació o mida del *bin*. Si s'escull el valor massa petit pot perjudicar en la pèrdua de forma del pic cromatogràfic i no serà detectat. D'altra banda, la tria d'un valor massa elevat pot crear múltiples co-elucions entre pics que tenen masses pròximes i s'han ajuntat, fent aleshores que els pics individuals corresponents a masses espectrals realment diferents puguin desaparèixer. Un altre desavantatge d'aquest mètode és la pèrdua de resolució espectral que es produeix en la seva aplicació, en comparació a la resolució espectral de l'espectròmetre de masses[49] o la que proporciona el mètode ROIMCR, tal com es descriu a l'apartat 2.3.6.

En la majoria d'estudis metabolòmics i lipidòmics no és suficient la reducció de la mida de les dades proporcionada pels pre-processats *binning* o d'interpolació, sinó que requereix d'algun altre procediment per poder treballar amb el gran nombre de dades generades en aquests estudis. En aquest context és quan és recomanable fer el tall del cromatograma total en diverses finestres de temps de retenció (*time windowing*), les quals poden ser analitzades de forma separada.[50-51] Si tot i això, les dades encara són massa grans per ser processades adequadament, també es poden subdividir els espectres de masses en diferents finestres o regions de l'espectre (*spectral windowing*), la qual cosa no obstant pot representar un major temps d'anàlisi de dades. Aquesta última alternativa, *spectral windowing*, no ha estat necessària aplicar-la en els nostres conjunts de dades. Aquests tipus de pre-tractaments permeten fer l'anàlisi simultània de totes les mostres experimentals (controls i tractades) ja que es

redueix significativament la mida de cada matriu augmentada de dades que es vol analitzar.

2.3.5. Resolució multivariant de corbes per mínims quadrats alternats (MCR-ALS)

El mètode MCR-ALS també és un mètode basat en el model bilineal de descomposició de les dades anàleg, en aquest cas, al de la llei de Lambert-Beer generalitzada simultàniament a moltes variables i per a múltiples mostres.[52-54] Aquest procediment és especialment útil per resoldre sistemes on el senyal segueix un model no-lineal com el de la llei de Lambert-Beer. Les principals diferències entre el mètode PCA i el MCR-ALS són que els components del MCR-ALS no són ortogonals com en PCA i que la resolució de la matriu de dades per MCR-ALS està subjecta a restriccions que proporcionen als components sentit químic i/o biològic. En canvi, els components de PCA donen solucions purament matemàtiques, que són molt útils en la determinació del nombre de fonts de variació i en la seva interpretació, però no tant en la descripció de la seva naturalesa físico-química.

En aquesta Tesi, l'objectiu és la descomposició de la matriu de dades experimentals LC-MS (**D**) en els perfils d'elució cromatogràfica (**C**) i els espectres de masses purs ($\mathbf{S^T}$) dels components (lípids) presents en les mostres analitzades (Figura 10).

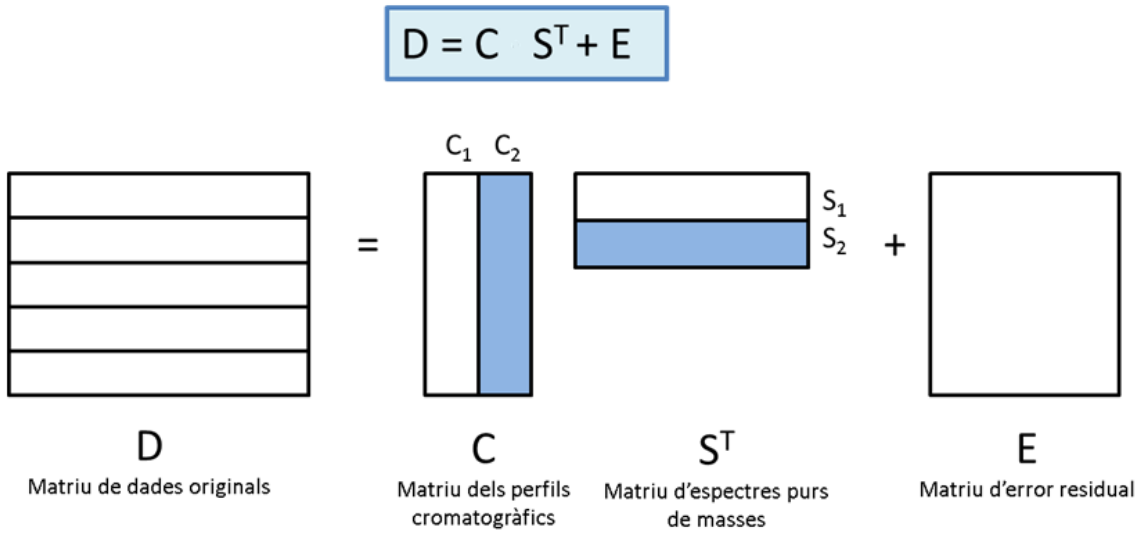

Figura 10. Equació i representació gràfica del model del mètode MCR-ALS.

Les etapes fonamentals del mètode MCR-ALS són:

I. Determinació del nombre de components .
II. Elaboració d'estimacions inicials de la matriu **C** o $\mathbf{S^T}$.
III. Càlcul i optimització de **C** o $\mathbf{S^T}$ de forma iterativa per mínims quadrats alternats sota restriccions.

La determinació del nombre de components del sistema es pot basar en el coneixement previ o es pot dur a terme amb l'ajut de mètodes quimiomètrics, com l'algorisme de descomposició en valors singulars (SVD).[55] En general, el nombre de valors singulars significatius és igual al nombre de contribucions necessàries per a descriure el conjunt de dades **D**. El següent pas és l'obtenció d'estimacions inicials dels perfils de concentracions (**C**) o bé dels espectres purs de masses ($\mathbf{S^T}$) de les contribucions químiques al sistema. Per a l'elaboració de les estimacions inicials dels espectres purs s'ha utilitzat un mètode de detecció de variables pures basat en el mètode SIMPLISMA[56] (SIMPL*e-to-use Interactive Self-Modeling Analysis*) que selecciona de forma seqüencial els espectres que es diferencien més entre ells dins el conjunt de dades originals (**D**).

Un cop feta l'estimació inicial, es fa la descomposició mitjançant un procés iteratiu basat en mínims quadrats alternats. Per tal d'aconseguir que els perfils resolts tinguin sentit químic, existeix la possibilitat d'aplicar un seguit de restriccions per adequar la forma dels perfils obtinguts a la natura de les dades analitzades. Aquestes restriccions poden ser, per exemple, no-negativitat, unimodalitat, rang local, correspondència d'espècies o trilinealitat, entre d'altres.[57] En el cas de l'anàlisi de dades de LC-MS s'aplica la restricció de la no-negativitat que consisteix en evitar la presència de valors negatius als perfils d'elució cromatogràfica o concentració i en els espectres de masses, ja que no poden presentar valors negatius de forma inherent a la mesura. A més, s'aplica una restricció de normalització fent que els espectres resolts tinguin igual intensitat màxima.

Sovint la informació continguda en un sol experiment no és suficient per a aconseguir una resolució òptima del sistema. Aquest problema es pot solucionar aportant més

informació al sistema de forma que ajudi a millorar la resolució. Per tal de fer-ho, es pot augmentar la matriu de dades **D** analitzant múltiples experiments simultàniament que aportin informació complementària. Existeixen diferents opcions quan es tracta de treballar amb una estructura multiconjunt amb matrius de dades procedents de més d'un experiment i/o mesura experimental.[58] En aquesta Tesi s'ha treballat amb l'augment de la matriu en la direcció de les columnes, veure Figura 11, que permet analitzar de forma simultània les dades LC-MS obtingudes per mostres controls i tractades.

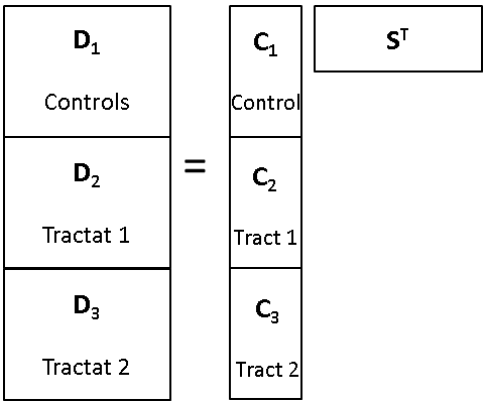

Figura 11. Resolució d'estructures multiconjunt d'una matriu augmentada en la direcció de les columnes on la direcció espectral (*m/z*) és comuna per a totes les mostres analitzades, i en canvi, la direcció cromatogràfica de temps d'elució pot ser diferent per cada mostra analitzada (no cal fer ajustament dels temps de retenció).

Un cop s'arriba a la convergència, el MCR-ALS mostra les solucions **C** i $\mathbf{S^T}$ que s'han aconseguit i uns paràmetres de qualitat per a valorar la validesa de la resolució. Entre aquests paràmetres es troba el percentatge de variància explicada (R^2), que fa referència a la proporció de variància explicada pel model (tenint en compte les matrius resoltes **C** i $\mathbf{S^T}$) respecte tota la informació que es pot trobar a la matriu **D**. El valor de R^2 es calcula de la forma següent:

$$R^2 = 100\,\frac{\sum_{i=1}^{n}\sum_{j=1}^{m} {d_{i,j}}^2 - \sum_{i=1}^{n}\sum_{j=1}^{m}(d_{i,j} - d_{i,j}^*)^2}{\sum_{i=1}^{n}\sum_{j=1}^{m} {d_{i,j}}^2}$$ **Equació 3.**

On $d_{i,j}$ és l'element de la matriu de dades originals a la fila *i* i a la columna *j* i $d^*_{i,j}$ és el mateix element, però pertanyent a la nova matriu D^* calculada amb el model bilineal obtingut amb MCR-ALS.

2.3.6. Combinació de regions d' interès amb la resolució multivariant de corbes per mínims quadrats alternats (ROIMCR)

En el Capítol 3 d'aquesta Tesi es mostra la validació del mètode ROIMCR recentment proposat per a la compressió i processat de dades LC-MS. Aquesta metodologia està basada en la combinació del mètode de selecció de les "Regions d'Interès (ROI)" i el mètode de resolució multivariant de corbes per mínims quadrats alternats (*Multivariate Curve resolution Alternating least Squares,* MCR-ALS) explicat en el punt 2.3.5. La recerca i selecció de les regions de masses amb intensitats més significatives i d'elevades densitats aconsegueix una important reducció de la mida del conjunt de dades, sense que es produeixi pèrdua de resolució espectral ni d'exactitud en la mesura de masses. La utilització d'aquest procediment permet un tractament de les dades LC-MS més àgil i acurat. En una segona fase, l'anàlisi mitjançant MCR-ALS d'aquest nou conjunt de dades ROI seleccionades, proporciona la seva resolució en els perfils d'elució cromatogràfica i espectres de masses dels components de les mostres analitzades per LC-MS.

El procediment ROIMCR s'ha implementat en l'entorn de MATLAB.[54, 59] El mètode de filtració i compressió ROI facilita el processat posterior de les dades amb MCR-ALS, agilitzant així la seva anàlisi. L'avantatge del procediment ROIMCR respecte a d'altres mètodes de pretractament i compressió de dades, com el *binning* o els *wavelets* entre d'altres, rau en el fet que la reducció de la mida de les dades es realitza sense la pèrdua de l' exactitud espectral. El procediment *binning* es va emprar en els estudis del Capítol 4 d'aquesta Tesi en combinació amb el procediment de *time windowing*, és a dir, el tall del cromatograma per finestres de temps de retenció. Per contra, el procediment ROIMCR va ser utilitzat en els estudis del Capítol 5, la qual cosa va permetre una anàlisi de dades més ràpida i òptima, sense pèrdua de resolució

espectral. La Figura 12 mostra una comparativa dels punts forts i febles del pre-processat *binning* i del ROI.

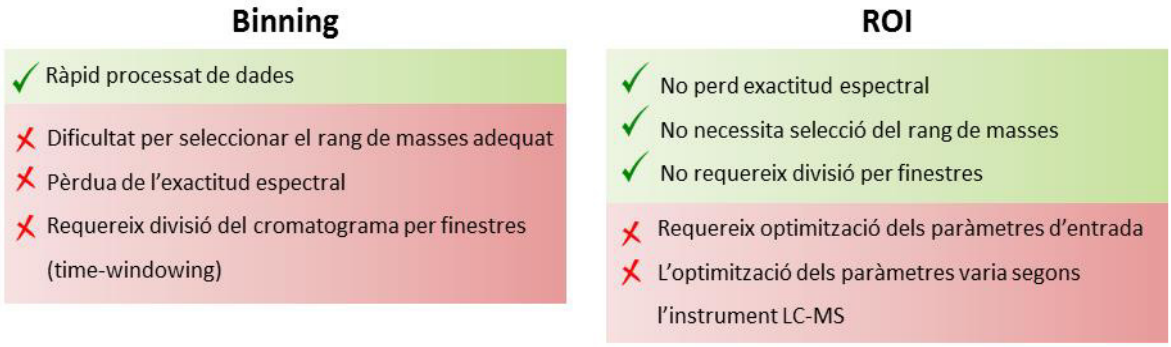

Figura 12. Avantatges i desavantatges dels mètodes de pre-processat de dades *binning* i ROI.

La compressió ROI va ser utilitzada primerament en l'algoritme de detecció de senyals anomenat centWave utilitzat en la plataforma d'anàlisi de dades XCMS.[60-61] Les diferències del nostre procediment ROIMCR respecte aquest algoritme prèviament proposat en el centWave és que en el nostre procediment no es necessària l'aplicació de la *continuous wavelet transform* (CWT) i l'ajust dels pics de LC-MS a la forma Gaussiana en la modelització i alineament dels pics cromatogràfics, degut a la utilització en el nostre cas del procediment MCR-ALS.

Per l'aplicació del procediment ROI cal l'optimització i definició de tres paràmetres que són les variables d'entrada: "threshold", "mz_error" i "minROI" els quals requereixen una optimització prèvia segons el tipus d'instrument MS emprat en les anàlisis. El primer paràmetre, el *threshold* s'utilitza per filtrar només aquelles senyals de masses, les intensitats de les quals són més elevades que el valor llindar proposat. Normalment, el valor llindar se situa entre un 0.1 – 1% del pic més intens de masses detectat. El segon paràmetre és el "mz_error" o la desviació de masses admissible de les mesures experimentals. Habitualment, s'estableix un múltiple de l'exactitud de les masses segons el espectròmetre de masses emprat en l'anàlisi. En el cas de l'equip emprat en aquesta Tesi (espectròmetre de masses ToF amb una resolució de 11,500 FWHM a una massa de 556), s'ha escollit un *mz_error* igual a 0.05 Da/e. L'últim paràmetre a optimitzar és el "minROI", que correspon al nombre mínim de parelles de

valors consecutius de *m/z* i intensitats de masses que es consideren que pertanyen al mateix ROI. Per exemple, en el nostre sistema UHPLC, el nombre mínim és de deu punts per definir un ROI; això correspondria a uns 20 segons del cromatograma (amplada de pic) necessaris per ser considerat un pic cromatogràfic. El procediment d'optimització d'aquests paràmetres ha estat descrit en una publicació prèvia del grup.[62] Es pot apreciar com el nombre de ROIs augmenta quan el valor del *threshold*, *mz_error* o nombre mínim de punts consecutius disminueix. És evident que una selecció òptima del valor llindar (*threshold*) afavoreix la qualitat de les dades i l'eliminació del soroll; tot i que un *threshold* massa elevat ocasionaria una pèrdua d'informació. A més, el paràmetre *mz_error* ha de ser establert per a cada espectròmetre de masses en particular i el "minROI" depèn fonamentalment del tipus de cromatografia emprada, ja sigui UHPLC o HPLC. La importància de l'optimització dels paràmetres d'entrada és crucial per dur a terme una bona selecció ROI.

El programa desenvolupat per a la compressió ROI genera tres variables de sortida (*outputs*). Un vector que conté els valors de *m/z* finalment seleccionats; una matriu de dades que inclou en les seves files els espectres MS a cada temps de retenció mesurat i els cromatogrames a cada mzROI en les seves columnes. Per últim, una variable MATLAB tipus cel·la que conté per a cada ROI, la informació trobada dels valors de *m/z*, dels temps de retenció, de les intensitats de masses, del nombre d'espectres i del valor de *m/z* finalment calculat pel ROI considerat. La Figura 13 mostra una representació gràfica dels *outputs* generats de la compressió ROI de dades provinents de la LC-MS.

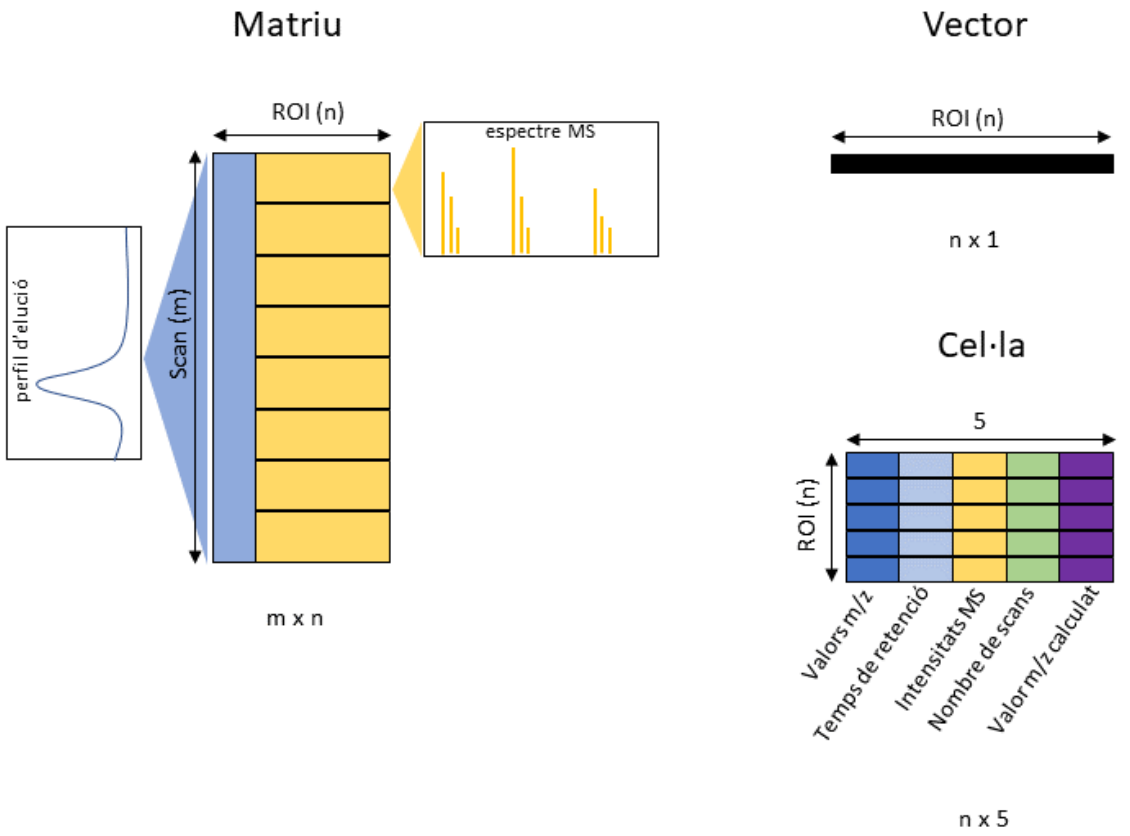

Figura 13. Representació gràfica de les variables de sortida (outputs) originades de la compressió de dades LC-MS originades per l'aplicació del procediment ROI; una matriu, un vector i una cel·la de dades. On ROI (n) és el nombre total de ROIs obtinguts. La matriu (m x ROI(n)) conté els espectres MS de tots els temps de retenció en les seves files, i els cromatogrames de cada ROI en les seves columnes. El vector generat conté la mitjana dels valors de *m/z* de cada ROI. La cel·la està formada per ROI(n) x 5 contenint la informació sobre el valors de *m/z*, els temps de retenció, les intensitats de MS i els nombres de scans de les dades incloses al mateix ROI, respectivament. Les cel·les compreses en la última columna contenen valors únics, corresponents a la mitjana dels valors m/z de cada ROI obtingut.

La Figura 14 mostra gràficament un exemple del resultat de la detecció de la regió d'interès (ROI) corresponent al lípid 1,2,3-17:0 TG. En el gràfic de l'esquerra es mostra el pic cromatogràfic corresponent a aquest lípid. Els cercles vermells indiquen les intensitats de massa dels valors *m/z* ROI seleccionats, les quals són representades en funció del temps d'elució expressats en segons. El gràfic de la dreta representa les traces de masses *m/z* (cercles negres) *vs* els temps d'elució en segons. Les traces de masses es mostren disperses al voltant d'un valor mitjà assenyalat per una línia blava i els valors a les seves desviacions estàndards (línia verda) i a dos desviacions estàndards

(línia vermella) respectivament, fet que indica una correcta distribució aleatòria dels punts dins els intervals d'acceptació. El valor de *m/z* finalment assignat a aquest ROI és el valor mitjà de la línia blava.

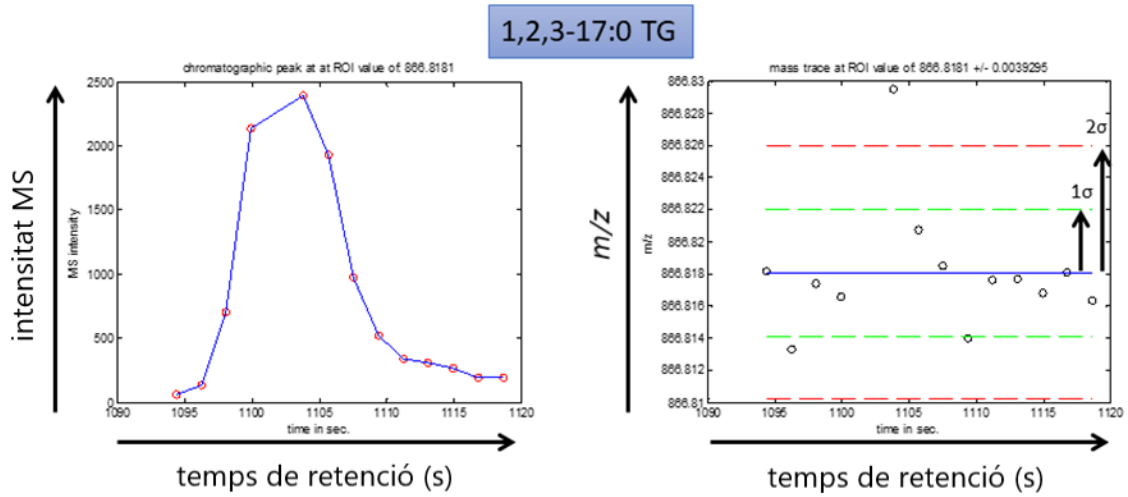

Figura 14. Representació gràfica en l'obtenció de la regió d'interès, ROI, pel lípid 1,2,3-17:0 TG. El gràfic de l'esquerra representa les intensitats de les masses en cercles vermells respecte el temps d'elució (segons). El gràfic de la dreta mostra les traces de masses *m/z* ROI respecte els temps d'elució en segons.

2.3.7. Post-anàlisi: Identificació dels lípids i interpretació biològica

A partir dels resultats obtinguts de l'anàlisi MCR-ALS es poden resoldre els perfils d'elució corresponents a les mostres dels controls i de les mostres tractades. Es poden calcular les àrees dels perfils d'elució (àrees de pic) corresponents a cada component en cadascuna a les diferents mostres. Amb aquestes àrees de pic pels diferents components a les diferents mostres, es pot fer una nova anàlisi PLS-DA i també determinar els valors dels VIPs que indiquin quins son els lípids més importants per distingir entre mostres control i tractades. Per tal de reduir la llista de potencials candidats, s'aplica un test t de Student de forma que es seleccionen aquells components la comparació de les àrees de pic de les quals donen un p-valor més baix. Finalment, per fer una interpretació biològica dels resultats, es cerquen i identifiquen els lípids candidats associats a aquests components utilitzant bases de dades en línia

com Lipid Maps[63] o HMDB (*Human Metabolome Data Base*),[64] a partir de la seva massa exacta.

2.3.8. Aproximacions emprades en l'anàlisi de les dades LC-MS generades

En el diferents treballs duts a terme dins aquesta Tesi s'han seguit tres aproximacions diferents en l'anàlisi de dades degut a l'evolució de les eines quimiomètriques pel tractament de dades òmiques dins del nostre grup de recerca.

Exploració inicial dels efectes dels tractaments a partir dels cromatogrames TIC de les dades LC-MS

Aquest primer pas consisteix en un anàlisi exploratòria dels TICs de les mostres control i tractades, veure Figura 15. Aquesta exploració inicial de dades s'ha dut a terme mitjançant l'anàlisi PCA que de forma no supervisada pot permetre observar una separació entre les mostres abans i després del tractament estudiat.

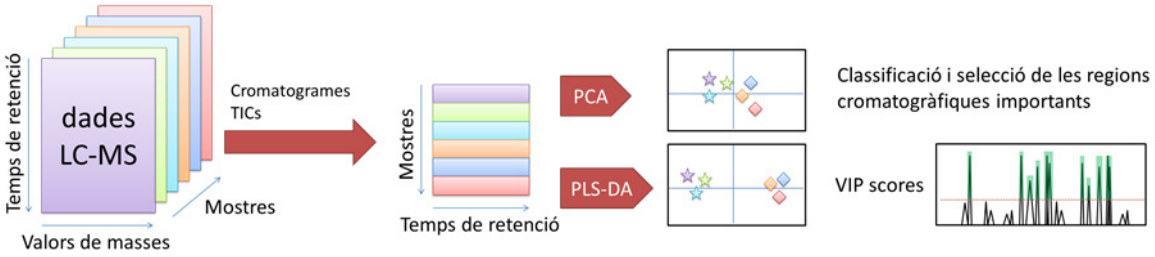

Figura 15. Flux de treball per l'exploració inicial del efectes dels tractaments.

El següent pas és l'Anàlisi Discriminant per Mínims Quadrats Parcials (PLS-DA)[44-45] que es pot considerar un mètode supervisat ja que utilitza la informació coneguda de la classe de cada mostra. Si s'observa una bona discriminació de les mostres, es procedeix a estudiar els VIP *scores* que permeten determinar quines són les regions del cromatograma més interessants en la discriminació entre mostres, i que poden emprar-se en anàlisis posteriors.

Detecció de potencials biomarcadors seguint l'estratègia del pre-tractament (*binning* + *time windowing*) i MCR-ALS

Les dades lipidòmiques LC-MS es van analitzar amb el mètode quimiomètric MCR-ALS, prèvia reducció de les dades aplicant el pre-tractament *binning* i divisió del cromatograma per finestres (*time windowing*). A la Figura 16 es mostra de forma esquematitzada els passos que es van seguir en l'aplicació d'aquest mètode i l'avaluació dels seus resultats. Aquesta estratègia ha estat portada a terme en els treballs del Capítol 4.

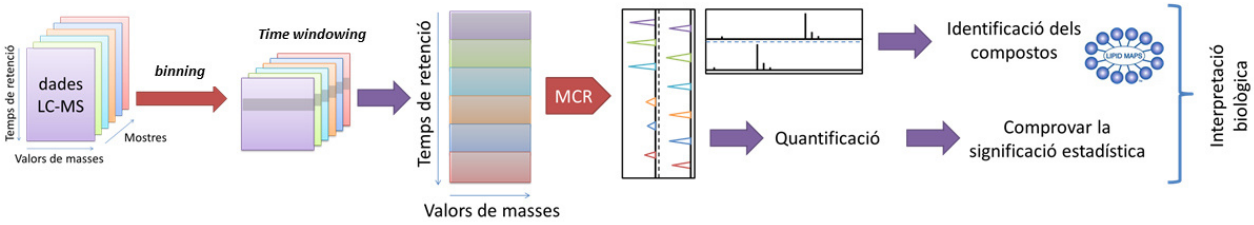

Figura 16. Flux de treball emprat en l'anàlisi de les dades LC-MS amb diferents etapes de pre-processament (*binning* i tall del cromatograma per finestres), anàlisi MCR-ALS, avaluació qualitativa i quantitativa, detecció de biomarcadors i interpretació biològica.

L'aplicació del mètode MCR-ALS permet resoldre els perfils cromatogràfics i els espectres de masses corresponents als lípids presents en les mostres analitzades. A partir d'aquests perfils, s'investiguen quins són els perfils d'elució que presenten major variació entre els grups de mostres, i els seus espectres de masses corresponents. Seguidament, s'avaluen estadísticament els potencials biomarcadors detectats. En cas d'una significació estadística positiva es procedeix a la seva identificació en una base de dades, com *Lipid Maps* o *Human Metabolome Data Base* (HMBD). Finalment, amb la llista de possibles candidats es pot fer una interpretació biològica que expliqui els canvis observats en les cèl·lules.

Detecció potencials biomarcadors seguint l'estratègia ROIMCR

Una via alternativa de pre-processat de les dades diferent del procediment descrit més amunt de la compressió de dades per "*binning*" i/o de la divisió del cromatograma per finestres (*time windowing*), és la metodologia ROIMCR explicada amb més detall en el

punt 2.3.6 i que es mostra en la Figura 17. Aquesta estratègia ha estat portada a terme en els treballs del Capítol 5.

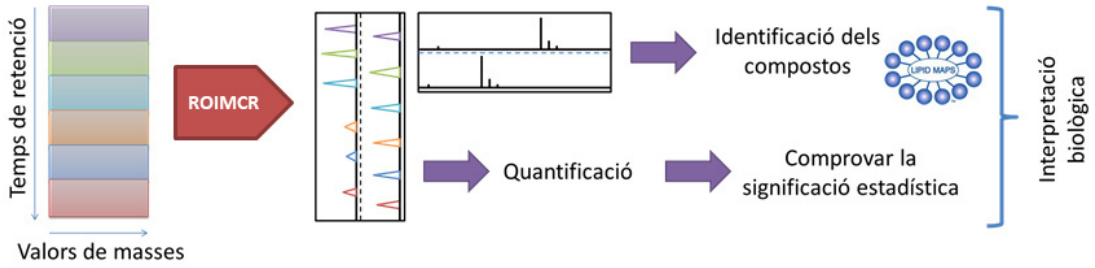

Figura 17. Flux de treball per la detecció de potencials biomarcadors seguint la metodologia ROIMCR.

2.4. Estressants ambientals en la salut, exposòmica

L'exposòmica és el terme emprat per referir-se a l'anàlisi exhaustiva de totes les exposicions ambientals que causen estrès en humans, per tal d'establir una relació amb l'etiologia de les malalties cròniques. Aquestes exposicions comprenen des de l'estil de vida, l'ambient social, la dieta o les fonts endògenes. Des del punt de vista toxicològic, les concentracions dels diferents agents químics presents en el cos humà estan directament relacionats amb l'exposició ambiental i els seus efectes adversos en teixits i òrgans. Per això, la capacitat de detectar i quantificar aquestes molècules en els fluids corporals és essencial per vincular l'exposició ambiental i les conseqüències biològiques que provoquen trastorns crònics. Els estudis epidemiològics i els experiments amb animals s'utilitzen generalment per avaluar factors que poden afectar la salut humana; especialment els efectes a l'exposició d'agents químics com a factors de risc. En aquest context, la comparació de diferents grups d'exposició en animals o humans permet descobrir possibles vincles entre factors ambientals i efectes en la salut. La metabolòmica, en aquest àmbit, serveix per identificar possibles candidats a biomarcadors a l'exposició ambiental. Seguint l'estratègia no dirigida, comentada anteriorment, es poden determinar milers de molècules simultàniament i analitzar mitjançant eines quimiomètriques quines presenten canvis com a conseqüència de l'exposició ambiental en diversos organismes model estudiats.

L'origen i tipus de mostres emprades pels estudis metabolòmics en humans i animals es variat, des de mostres d'orina[65] o plasma[66] fins saliva[67], esperma[68], biòpsies[69] o placenta[70]. Tot i això, els estudis epidemiològics ambientals en humans presenten una gran variabilitat de resultats degut a la co-exposició o les interaccions entre grups, fet que requereix analitzar una mostra gran de població per poder tenir un bon grup de mostres control respecte a mostres exposades i obtenir així resultats concloents en l'avaluació final. En altres estudis, com és el cas d'aquesta Tesi, es fan servir cultius cel·lulars com a models biològics, per així poder explorar els canvis cel·lulars que tenen lloc sota diferents exposicions ambientals en un ambient controlat.

Entre el gran nombre d'aplicacions de la metabolòmica ambiental en la salut humana destaquen les investigacions fetes sobre els efectes del tabac[71-72], la interacció amb els metalls pesants[73-74], el material particulat[75-76], els disruptors endocrins[77-78], els pesticides[79], i els contaminants orgànics persistents (POPs)[80-81] entre d'altres. Les condicions de vida, l'emplaçament geogràfic o la dieta també determinen en gran mesura la salut i els canvis en el metabolisme dels organismes.[82-83]

En aquesta Tesi s'han realitzat diversos estudis centrats en els efectes produïts pels disruptors endocrins, alguns d'ells utilitzats com a pesticides, en cèl·lules de càncer de pròstata. A més s'han estudiat els efectes de la radiació ultravioleta (UV), considerada com un factor ambiental de risc, en cultius primaris de cèl·lules de la pell. A continuació es fa una introducció sobre el treball amb cultius cel·lulars i les tècniques emprades per a l'avaluació dels diferents efectes estressants degut als factors ambientals de risc estudiats en aquesta Tesi, detallats en els següents punts.

2.4.1. Cultius cel·lulars i l'avaluació dels efectes estressants

Per realitzar els estudis en cèl·lules d'aquesta Tesi, s'han aplicat tècniques de cultius cel·lulars, per tal de preservar al màxim les seves propietats fisiològiques, bioquímiques i genètiques. El cultiu de les cèl·lules es realitza en cabines de flux laminar vertical dins de sales de cultiu cel·lular (Figura 18), el que garanteix el treball en condicions estèrils. Les cèl·lules es disposen en flascons tancats en presència de

medi de cultiu, i en el cas de la majoria de cèl·lules, aquestes s'adhereixen a la paret inferior del flascó. D'aquesta manera, les cèl·lules poden créixer i dividir-se indefinidament amb les limitacions dels nutrients presents en el medi i de l'espai físic del flascó. Es diu que un cultiu és confluent quan la superfície de cultiu del flascó està recoberta sense deixar espais. El medi de cultiu varia segons el model cel·lular emprat, així com els seus suplements, ja siguin antibiòtics per evitar les contaminacions bacterianes o sèrum boví fetal per estimular la divisió i creixement cel·lular.

El procés de creixement cel·lular s'ha d'efectuar sota condicions controlades com la temperatura, la humitat i l'atmosfera gasosa. Això s'aconsegueix mitjançant l'ús d'un incubador de cèl·lules regulat a 37°C de temperatura i 5% de CO_2, les condicions més habituals en cultius de cèl·lules humanes, però que poden variar segons la línia de treball. Quan les cèl·lules han ocupat tota la superfície del flascó, cal diluir el cultiu per mantenir les cèl·lules en vida. El nombre de dilucions d'un cultiu ha de ser controlat per tal de preservar les característiques originals de les cèl·lules al llarg del temps.

Figura 18. Cabines de flux laminar vertical dins la sala de cultiu.

Existeixen dos tipus de cultius cel·lulars, les línies cel·lulars immortalitzades i/o tumorals que es poden dividir de forma infinita i els cultius cel·lulars primaris. Aquest últim grup és menys comú ja que són cèl·lules procedents d'òrgans, teixits o fetus obtinguts a partir d'una biòpsia. Una de les característiques més rellevants dels cultius cel·lulars primaris és que permeten un nombre de divisions cel·lulars limitat. En

aquesta Tesi s'ha emprat per una banda, la línia cel·lular de càncer de pròstata DU145, disponible comercialment. Aquesta línia deriva d'una metàstasi cerebral de càncer de pròstata i té una morfologia de tipus epitelial. Per altra banda, pels estudis sobre els efectes de la radiació UV, s'han utilitzat cultius primaris de melanòcits i queratinòcits procedents de la biòpsia de pacients, proporcionats per la Dra. Corine Bertolotto (C3M, Niça, França). El manteniment d'aquests cultius primaris està detallat a les publicacions pertinents del Capítol 5.

En aquesta Tesi s'ha realitzat una sèrie d'assaigs de biologia cel·lular i molecular (veure Taula 2.2), destinats a estudiar els canvis fenotípics de les cèl·lules després d'haver estat exposades als diferents contaminants o efectes estressants comentats anteriorment. Aquests assaigs ens ajuden a saber si els diferents models cel·lulars han sofert algun canvi degut a les diverses exposicions, ja siguin agudes o cròniques. Les modificacions a detectar comprenen des de variacions en la proliferació cel·lular, la capacitat de migrar des les cèl·lules o el canvi d'expressió de gens concrets vinculats a un procés cel·lular com pot ser la inducció de la transició epitelial mesenquimal (EMT) (veure apartat 2.4.2.1).

Taula 2.2. Resum dels assaigs de biologia cel·lular i molecular emprats per l'estudi dels canvis fenotípics de les cèl·lules tractades.

Tècnica	Què és?	Ús en aquesta Tesi	Resultats esperats
Proliferació en medi líquid	Quantificació del nombre de cèl·lules vives a diferents dies i diferents concentracions, sembrades en un inici en igualtat de condicions.	Estudi comparatiu de la capacitat de proliferació en el temps.	Major creixement en les cèl·lules tractades, indicatiu d'un fenotip més agressiu.
Citometria de flux	Tècnica basada en el marcatge fluorescent de les cèl·lules (normalment amb anticossos), emprada pel recompte i classificació de cèl·lules.	Avaluació de EMT: Marcatge de la E-caderina de membrana amb un anticòs específic acoblat a fluoresceïna.	Disminució del marcatge de la E-caderina-FITC respecte les mostres no tractades.
Proliferació en medi semi-sòlid	Observació de colònies cel·lulars formades en un medi no propici pel seu creixement.	Prova de la capacitat invasiva i migratòria de cèl·lules.	Major tendència per a la formació de colònies, en cèl·lules tractades.
Assaig de migració	Avalua la capacitat de les cèl·lules de recobrir una escletxa realitzada en un cultiu confluent de cèl·lules.	Avaluació de la capacitat de migració.	Més migració en cèl·lules tractades amb contaminants.
Zimografia	Anàlisi de la presència de les metal·loproteïnases MMP-2, MMP-9, indicadors d' invasivitat, en sobrenedant de cultius, mitjançant l'electroforesi en gels de gelatina.	Prova de capacitat invasiva de les cèl·lules.	Major presència de metal·loproteïnases (més invasivitat) en les mostres tractades amb contaminants.

Tècnica	Què és?	Ús en aquesta Tesi	Resultats esperats
Immunofluorescència	Tècnica basada en el marcatge de proteïnes mitjançant anticossos específics units a grups fluoròfors.	Observació de la distribució i intensitat de la fluorescència originada pel marcatge específic de E-caderina o involucrin.	Disminució del marcatge de la E-caderina-FITC en EMT, augment de vimentin en diferenciació de queratinòcits.
Assaig enzimàtic	Mesura de l'activitat enzimàtica d'un enzim, en el nostre cas mitjançant un assaig fluorimètric.	Mesura de l'activitat de l'esfingomielinasa àcida (aSMase).	La variació de l'activitat aSMase podria explicar la causa de canvis en nivells de SM.
Quantificació de ROS	Avalua la formació d'espècies reactives d'oxigen (ROS).	Quantifica les ROS originades per una exposició ambiental.	Augment de ROS implica danys en el DNA.
qRT-PCR	Anàlisi quantitatiu de l'expressió gènica a partir de l'extracció de RNAm de les cèl·lules, mitjançant l'ús de sondes fluorescents i un termociclador dotat per detectar la fluorescència generada en la reacció en cadena de la polimerasa (PCR).	Quantificació relativa de l'expressió de diversos gens relacionats amb la EMT o la síntesi d'àcids grassos, entre controls i tractats.	Canvis d'expressió de gens causats per la inducció de EMT o exposició de contaminants.
Western Blot (WB)	Tècnica analítica emprada per detectar proteïnes específiques en l'extracte cel·lular.	Avaluació de proteïnes característiques de EMT, marcadors del cicle cel·lular i d'autofàgia.	Canvis de nivells de proteïnes a causa d'inducció de EMT, contaminants o radiació solar.

2.4.2. Els Disruptors Endocrins

Dins del grup de contaminats químics ambientals que poden ser tòxics pels organismes biològics destaquen els disruptors endocrins (DE). Els DE són molècules que per la seva naturalesa interfereixen en la síntesi, secreció, transport i unió amb receptors, i en l'acció o eliminació de les hormones naturals d'un organisme, les quals són responsables del seu desenvolupament, comportament, fertilitat i de la seva homeòstasi (metabolisme cel·lular normal).[84] Els DE es poden trobar en molts tipus de productes, entre els que destaquen els medicaments, els pesticides, les molècules utilitzades a la indústria del plàstic, els subproductes de la indústria i els productes de neteja i higiene. Alguns d'aquests DE són persistents i bioacumulables, d'altres es degraden ràpidament en el medi ambient o en el cos humà i només estan presents per un període curt de temps. L'exposició a aquest tipus de contaminants, que es produeix principalment a través del menjar i el contacte amb productes de consum diaris, ha estat relacionada amb problemes de salut, com la reducció de la fertilitat, canvis en els nivells hormonals, problemes de comportament, supressió de funcions immunitàries i diversos tipus de càncer.[85-86] Alguns dels grups de disruptors endocrins més importants són els alquilfenols, els hidrocarburs aromàtics polihalogenats com el bisfenol A (BPA), ela bifenils policlorats (PCBs), els bifenilésters polibromats (PBDEs), els metalls, els ftalats, etc. La llista detallada de disruptors endocrins es pot trobar en el següent enllaç del departament de Medi Ambient de la Comissió Europea:
http://ec.europa.eu/environment/chemicals/endocrine/strategy/substances_en.html

En el Capítol 4 d'aquesta Tesi s'avaluaran els diversos efectes de l'exposició a una sèrie de contaminants ambientals, descrits com disruptors endocrins (DE), en la progressió del càncer de pròstata. En concret s'estudiarà com l'exposició de les cèl·lules de càncer de pròstata DU145 a aquests contaminants pot influir en l'adquisició per part de les cèl·lules d'un fenotip més agressiu i com aquest pot estar relacionat amb canvis en els seus nivells lipídics. En el cas del càncer de pròstata, alguns estudis epidemiològics o centrats en models animals han suggerit una relació directa entre l'exposició a determinats DEs i el risc de desenvolupar càncer de pròstata.[87] Entre tots aquests DEs,

tres d'ells han estat escollits per a realitzar aquest treball: Aldrin, Aroclor 1254 i el Clorpirifòs (veure Taula 2.3):

- Aldrin és el nom tècnic d'una molècula organoclorada que forma part del grup de contaminants orgànics persistents (POPs). Va ser emprat com a pesticida en els camps de conreu fins el 1970 quan va ser prohibit en un gran nombre de països. Després, encara es va utilitzar per exterminar termites als EEUU, entre d'altres països. En qualsevol cas, l'Aldrin encara està present avui dia pel seu ús en el passat.[88]
- Aroclor 1254 (Aroclor) es tracta d'una mescla de 60 components representatius de bifenils policlorats (PCBs). Els PCBs són compostos lipofílics estables que s'utilitzen per diferents propòsits industrials i comercials que s'acaben bioacumulant en el mediambient i en la cadena tròfica.[89]
- Clorpirifòs (CPF) és un insecticida organofosfat cristal·lí que actua en el sistema nerviós dels insectes com un inhibidor d'acetilcolinesterasa. Tot i que ha estat descrit com moderadament tòxic per als humans, la seva exposició ha estat relacionada amb efectes neurològics, trastorns persistents en el desenvolupament i trastorns autoimmunes.[90-91]

Taula 2.3. Disruptors endocrins ambientals emprats en els estudis d'aquesta Tesi, Capítol 4.

Nom	Naturalesa	Utilització	Presència
Aldrin	Organoclorat Contaminant persistent	Insecticida Prohibit des de 1970	Bioacumulació en organismes vius
Aroclor 1254	Mescla de 60 PCBs Contaminant persistent	Aïllants, fluids hidràulics Prohibit des de 1979	Aigua, sòl i bioacumulable en organismes vius
Clorpirifòs (CPS)	Organofosfat Contaminant persistent	Insecticida	Productes agrícoles, aire

2.4.2.1. Transició epitelial mesenquimal

La transició epitelial mesenquimal (EMT) no es considera un factor exposòmic, però es va observar la seva inducció en la publicació II mitjançant un disruptor endocrí. Per això es va decidir estudiar el seu perfil lipídic paral·lelament.

La EMT és un procés essencial en múltiples funcions biològiques com el desenvolupament embrionari, la remodelació de teixits i la cicatrització de ferides (Figura 19). Recentment, s'ha demostrat que la EMT juga un paper crucial en la invasió tumoral i en la metàstasi, per exemple en el càncer de pròstata. En el procés de la EMT, les cèl·lules epitelials redueixen l'adhesió intracel·lular, adquireixen una morfologia fusiforme i augmenten les propietats migratòries i invasives, característiques de les cèl·lules mesenquimals.[92] Aquestes propietats adquirides permeten una gran mobilitat de les cèl·lules, la qual, en cèl·lules cancerígenes, es tradueix en l'expansió del tumor i en la seva metàstasi.[93] La EMT s'acompanya de canvis en els nivells de diferents proteïnes; per una banda, es produeix la pèrdua de E-caderina i β-catenina, característics de les cèl·lules epitelials, i per l'altra, es produeix l'adquisició de Vimentin o N-caderina, com a marcadors mesenquimals.[94-95] El procés d'EMT també, involucra l'expressió de molts factors de transcripció entre els que es troben Snail, Slug o Twist, associats a la progressió tumoral.[94]

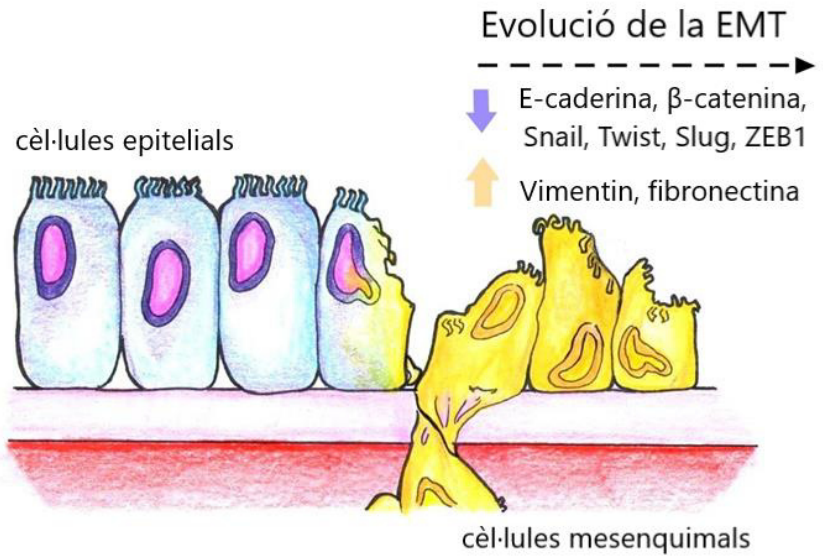

Figura 19. Representació gràfica de la Transició Epitelial Mesenquimal (EMT) en les cèl·lules.

La EMT s'ha estudiat àmpliament des del punt de vista de la genòmica, transcriptòmica i proteòmica,[96] però existeixen molt poques referències d'estudis lipídics sobre la EMT. Per això, en aquesta Tesi, a més d'avaluar els efectes de l'exposició de les cèl·lules de càncer de pròstata als contaminants, s'ha caracteritzat la EMT des del punt de vista dels lípids. Els lípids, que intervenen en diverses funcions vitals (veure apartat 2.1),

també poden estar implicats en la EMT, pel que és interessant trobar lípids biomarcadors d'aquest procés. Com a model cel·lular d'EMT, es van utilitzar cèl·lules de càncer de pròstata DU145 exposades a la citoquina inflamatòria TNFα, un reconegut inductor d'EMT utilitzat en diversos treballs de recerca.[93]

2.4.3. La radiació solar

Un altre factor ambiental de risc, però no tòxic, és la radiació solar ultravioleta (UV). La radiació UV és un dels majors factors de risc pel càncers de pell, tot i que és essencial per la vida tal i com la coneixem.[97] La radiació solar està composta d'energia radiant d'una àmplia regió de l'espectre electromagnètic que inclou la radiació UV, la visible i la radiació infraroja. A més, també hi ha radiacions de longitud d'ona més curta (ionitzant) i de longituds d'ona més llargues, corresponents a les microones i la radiofreqüència, veure la Figura 20.

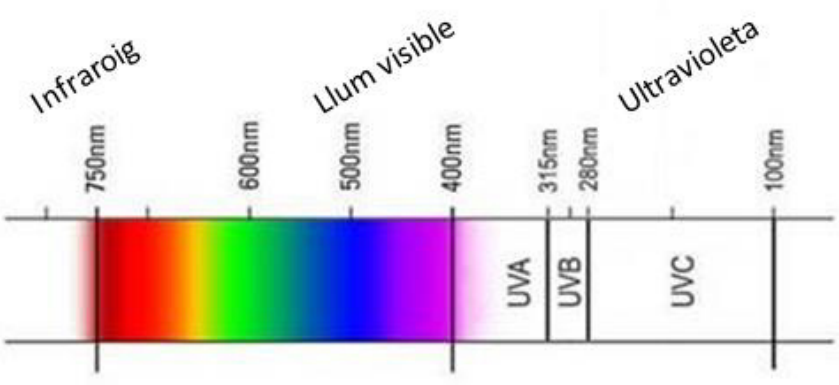

Figura 20. Espectre electromagnètic de la radiació.

La llum ultraviolada (UV) està formada per la radiació UVA de 315 a 400 nm, la radiació UVB de 285 a 315 nm i per últim la radiació UVC de 100-285 nm. La radiació UVA penetra més profundament en l'epidermis cap a la dermis i pot promoure la generació d'espècies reactives d'oxigen (ROS) i induir la carcinogènesi de la pell *in vivo*.[98] En canvi, la radiació UVB afecta més a la capa basal de l'epidermis i és responsable directe dels danys en l'ADN i dels canvis més visibles com són les cremades, el fotoenvelliment, la pèrdua d'elasticitat i to de la pell, la sequedat, la pigmentació irregular i la formació d'arrugues profundes.[99] Per últim, la radiació UVC té molta més energia que els altres dos tipus de radiació, però aquesta no penetra l'atmosfera i per

tant, no està present en la llum solar ni en el nostre estudi (pun 5). La radiació que arriba a la nostra pell està composada de mitjana per un 95% UVA i un 5% UVB; la radiació UVC i la major part de la radiació UVB és eliminada per l'ozó estratosfèric. Encara que la llum solar és la font principal de radiació UV, les làmpades i cabines de bronzejat són també fonts de radiació UV.

Les fonts de radiació UV es caracteritzen en unitats radiomètriques. Els termes de dosi s'expressen en J/m^2 i la taxa de dosis en W/m^2, les quals mesuren l'energia i la potència de la radiació respectivament. La unitat efectiva de dosi més comuna emprada en fotobiologia cutània és la dosis mínima eritemal (MED). Una MED ha estat definida com la mínima exposició a la radiació UV per produir un eritema amb marges aguts durant 24 hores després de l'exposició.[100] La radiació solar pot ser mesurada mitjançant detectors físics o químics, sovint en conjunció amb un monocromador o filtre de pas de banda per a la selecció de longitud d'ona. Els detectors físics inclouen radiòmetres, com el que s'ha emprat en els estudis d'aquesta Tesi, els quals responen a la incidència dels fotons per un efecte quàntic com la producció d'electrons. També existeixen els detectors químics que inclouen emulsions fotogràfiques, solucions actinomètriques i pel·lícules plàstiques sensibles a la radiació UV.

2.4.3.1. L' epidermis

La pell és l'òrgan amb més extensió de tot el cos i constitueix un sistema de barrera entre l'organisme i el medi que ens envolta. Per aquest motiu es tracta de l'òrgan més exposat a la radiació UV.

La pell comprèn tres regions que són, des de la superfície fins l'interior: l'epidermis, la dermis i la hipodermis.[101] A més, hi trobem els fol·licles pilo-sebacis, principalment situats entre la dermis i la hipodermis. L'**epidermis** és la part més superficial i està constituïda per varies capes (de fora cap endins): còrnia, granular, espinosa i basal (veure Figura 21). Les cèl·lules de l'epidermis són els queratinòcits, els melanòcits, les cèl·lules de Langerhans i les cèl·lules de Merkel, i es troben cohesionades per substància glucoproteïca anomenada glicocàlix.

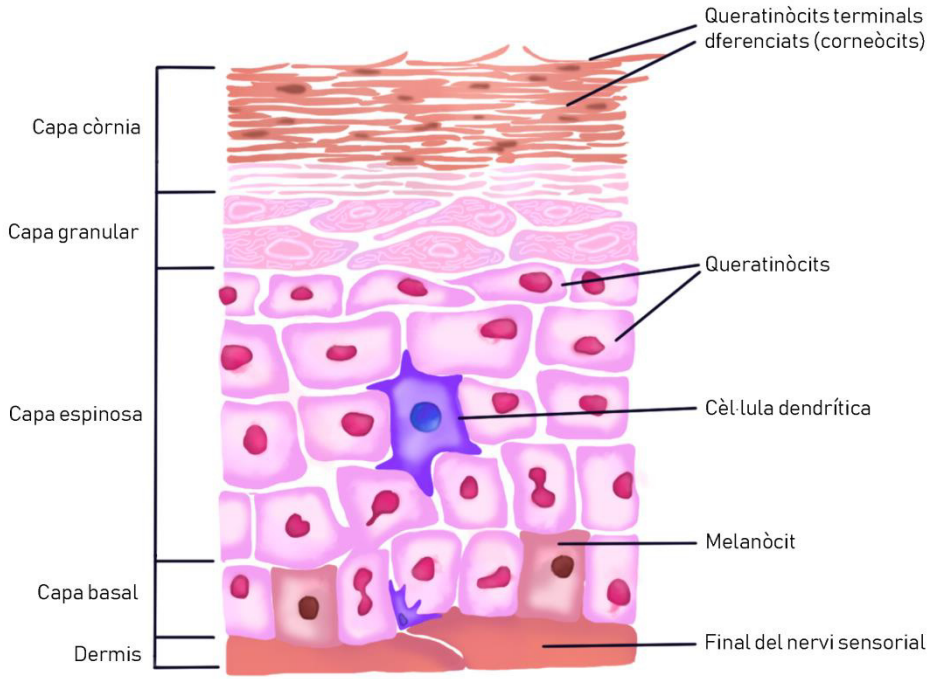

Figura 21. Representació gràfica de l'estructura de l'epidermis.

Els **queratinòcits** representen el 80% de les cèl·lules que conformen l'epidermis. Aquestes cèl·lules presenten un procés característic de diferenciació en el que perden progressivament els seus orgànuls a mesura que migren des de la capa basal de l'epidermis fins a la capa còrnia. En aquesta última capa trobem els queratinòcits terminals diferenciats, denominats corneòcits, els quals es caracteritzen per ser cèl·lules aplanades mortes que no tenen orgànuls i que es troben empaquetades amb filaments de queratina. Els corneòcits estan incrustats en una matriu extracel·lular lipídica formada principalment per ceramides, àcids grassos lliures i colesterol.[102-103] Els queratinòcits desenvolupen tres funcions: (1) la cohesió de l'epidermis, gràcies al seu citoesquelet i els seus sistemes d'unió; (2) la funció de barrera gràcies a la seva diferenciació terminal, i (3) la protecció contra la radiació lumínica, gràcies a la melanina produïda i proporcionada pels melanòcits.

El segon tipus més comú de cèl·lules en l'epidermis són els **melanòcits**. Aquests es troben intercalats entre cèl·lules de la capa basal en una relació aproximada d'un melanòcit per deu cèl·lules basals. Els melanòcits poden absorbir la radiació UV i sobreviure a un considerable estrès genotòxic.[104] La funció principal dels melanòcits és la síntesi de melanina que protegeix la pell de la radiació UV provinent de la llum solar i

atorguen a cada pell el seu color.[101] Per això, la melanina és el principal responsable de la pigmentació, tot i que també hi participen els carotenoides i la hemoglobina. Els grànuls que contenen melanina es coneixen com a melanosomes i poden variar en nombre, mida, composició i distribució. Aquests melanosomes s'exporten des dels melanòcits fins als queratinòcits adjacents mitjançant estructures allargades de la membrana plasmàtica, també anomenades projeccions dendrítiques. La formació, maduració i tràfic dels melanosomes és crucial per la pigmentació.[104] Defectes en aquest procés porten a les despigmentacions (leucodèrmies) com el vitiligo o els nevus acròmics. D'altra banda, es poden donar augments en la pigmentació (melanodèrmies), com passa en el cas dels lentígens, les taques a la pell o la dermatitis atòpica, entre d'altres.[105] El grau de producció de pigmentació varia segons el tipus de pell (color i la facilitat de coloració) i és el més útil predictor del càncer de pell en la població general. La detecció i control d'alteracions en la pell, presentació de vores irregulars, augment de mida o canvis en la coloració de lunars, nevus melanocítics o pigues poden ser una senyal d'advertència de melanoma o càncer de pell.[106]

2.5. Referències

1. Casares, D.; Escriba, P. V.; Rossello, C. A., Membrane Lipid Composition: Effect on Membrane and Organelle Structure, Function and Compartmentalization and Therapeutic Avenues. *Int J Mol Sci* **2019,** *20* (9).
2. Lordan, R.; Zabetakis, I., Invited review: The anti-inflammatory properties of dairy lipids. *J Dairy Sci* **2017,** *100* (6), 4197-4212.
3. Fahy, E.; Subramaniam, S.; Murphy, R. C.; Nishijima, M.; Raetz, C. R.; Shimizu, T.; Spener, F.; van Meer, G.; Wakelam, M. J.; Dennis, E. A., Update of the LIPID MAPS comprehensive classification system for lipids. *J Lipid Res* **2009,** *50 Suppl*, S9-14.
4. Ban, R. H.; Kamvissi, V.; Schulte, K. M.; Bornstein, S. R.; Rubino, F.; Graessler, J., Lipidomic profiling at the interface of metabolic surgery and cardiovascular disease. *Curr Atheroscler Rep* **2014,** *16* (11), 455.
5. Park, J. K.; Coffey, N. J.; Limoges, A.; Le, A., The Heterogeneity of Lipid Metabolism in Cancer. *Adv Exp Med Biol* **2018,** *1063*, 33-55.
6. Wong, M. W.; Braidy, N.; Poljak, A.; Pickford, R.; Thambisetty, M.; Sachdev, P. S., Dysregulation of lipids in Alzheimer's disease and their role as potential biomarkers. *Alzheimers Dement* **2017,** *13* (7), 810-827.
7. Smilowitz, J. T.; Zivkovic, A. M.; Wan, Y. J.; Watkins, S. M.; Nording, M. L.; Hammock, B. D.; German, J. B., Nutritional lipidomics: molecular metabolism, analytics, and diagnostics. *Mol Nutr Food Res* **2013,** *57* (8), 1319-35.
8. Markgraf, D. F.; Al-Hasani, H.; Lehr, S., Lipidomics-Reshaping the Analysis and Perception of Type 2 Diabetes. *Int J Mol Sci* **2016,** *17* (11).
9. Sunshine, H.; Iruela-Arispe, M. L., Membrane lipids and cell signaling. *Curr Opin Lipidol* **2017,** *28* (5), 408-413.

10. Hannun, Y. A.; Obeid, L. M., Sphingolipids and their metabolism in physiology and disease. *Nat Rev Mol Cell Biol* **2018,** *19* (3), 175-191.
11. Trayssac, M.; Hannun, Y. A.; Obeid, L. M., Role of sphingolipids in senescence: implication in aging and age-related diseases. *J Clin Invest* **2018,** *128* (7), 2702-2712.
12. Dadsena, S.; Hassan, D. G.; Holthuis, J. C. M., Unraveling the molecular principles by which ceramides commit cells to death. *Cell Stress* **2019,** *3* (8), 280-283.
13. Bedia, C.; Levade, T.; Codogno, P., Regulation of autophagy by sphingolipids. *Anti-cancer agents in medicinal chemistry* **2011,** *11* (9), 844-53.
14. Fahy, E.; Subramaniam, S.; Brown, H. A.; Glass, C. K.; Merrill, A. H., Jr.; Murphy, R. C.; Raetz, C. R.; Russell, D. W.; Seyama, Y.; Shaw, W.; Shimizu, T.; Spener, F.; van Meer, G.; VanNieuwenhze, M. S.; White, S. H.; Witztum, J. L.; Dennis, E. A., A comprehensive classification system for lipids. *J Lipid Res* **2005,** *46* (5), 839-61.
15. Wang, H.; Airola, M. V.; Reue, K., How lipid droplets "TAG" along: Glycerolipid synthetic enzymes and lipid storage. *Biochimica et Biophysica Acta (BBA) - Molecular and Cell Biology of Lipids* **2017,** *1862* (10, Part B), 1131-1145.
16. Eichmann, T. O.; Lass, A., DAG tales: the multiple faces of diacylglycerol--stereochemistry, metabolism, and signaling. *Cell Mol Life Sci* **2015,** *72* (20), 3931-52.
17. Poursharifi, P.; Madiraju, S. R. M.; Prentki, M., Monoacylglycerol signalling and ABHD6 in health and disease. *Diabetes Obes Metab* **2017,** *19 Suppl 1*, 76-89.
18. van Meer, G.; Voelker, D. R.; Feigenson, G. W., Membrane lipids: where they are and how they behave. *Nat Rev Mol Cell Biol* **2008,** *9* (2), 112-24.
19. Hermansson, M.; Hokynar, K.; Somerharju, P., Mechanisms of glycerophospholipid homeostasis in mammalian cells. *Prog Lipid Res* **2011,** *50* (3), 240-57.
20. Farooqui, A. A.; Horrocks, L. A.; Farooqui, T., Deacylation and reacylation of neural membrane glycerophospholipids. *J Mol Neurosci* **2000,** *14* (3), 123-35.
21. Lemke, G., Phosphatidylserine Is the Signal for TAM Receptors and Their Ligands. *Trends Biochem Sci* **2017,** *42* (9), 738-748.
22. Lo Vasco, V. R., The Phosphoinositide Signal Transduction Pathway in the Pathogenesis of Alzheimer's Disease. *Curr Alzheimer Res* **2018,** *15* (4), 355-362.
23. Nicholson, J. K.; Lindon, J. C.; Holmes, E., 'Metabonomics': understanding the metabolic responses of living systems to pathophysiological stimuli via multivariate statistical analysis of biological NMR spectroscopic data. *Xenobiotica* **1999,** *29* (11), 1181-9.
24. Barh, D.; Zambare, V.; Azevedo, V., *OMICS: Applications in Biomedical, Agricultural, and Environmental Sciences*. 1st ed.; CRC Press: 2013.
25. Monteiro, M. S.; Carvalho, M.; Bastos, M. L.; Guedes de Pinho, P., Metabolomics analysis for biomarker discovery: advances and challenges. *Curr Med Chem* **2013,** *20* (2), 257-71.
26. Patti, G. J.; Yanes, O.; Siuzdak, G., Innovation: Metabolomics: the apogee of the omics trilogy. *Nat Rev Mol Cell Biol* **2012,** *13* (4), 263-9.
27. Karahalil, B., Overview of Systems Biology and Omics Technologies. *Curr Med Chem* **2016,** *23* (37), 4221-4230.
28. Gross, R. W., The evolution of lipidomics through space and time. *Biochim Biophys Acta Mol Cell Biol Lipids* **2017,** *1862* (8), 731-739.
29. Gruber, F.; Kremslehner, C.; Narzt, M. S., The impact of recent advances in lipidomics and redox lipidomics on dermatological research. *Free Radic Biol Med* **2019**.
30. Kohno, S.; Keenan, A. L.; Ntambi, J. M.; Miyazaki, M., Lipidomic insight into cardiovascular diseases. *Biochem Biophys Res Commun* **2018,** *504* (3), 590-595.
31. Armitage, E. G.; Southam, A. D., Monitoring cancer prognosis, diagnosis and treatment efficacy using metabolomics and lipidomics. *Metabolomics* **2016,** *12*, 146.
32. Patti, G. J.; Yanes, O.; Siuzdak, G., Innovation: Metabolomics: the apogee of the omics trilogy. *Nature Reviews Molecular Cell Biology* **2012,** *13* (4), 263-269.

33. Bouhifd, M.; Hartung, T.; Hogberg, H. T.; Kleensang, A.; Zhao, L., Review: toxicometabolomics. *J Appl Toxicol* **2013,** *33* (12), 1365-83.
34. Cajka, T.; Fiehn, O., Toward Merging Untargeted and Targeted Methods in Mass Spectrometry-Based Metabolomics and Lipidomics. *Anal Chem* **2016,** *88* (1), 524-45.
35. Lu, W.; Bennett, B. D.; Rabinowitz, J. D., Analytical strategies for LC-MS-based targeted metabolomics. *J Chromatogr B Analyt Technol Biomed Life Sci* **2008,** *871* (2), 236-42.
36. Schrimpe-Rutledge, A. C.; Codreanu, S. G.; Sherrod, S. D.; McLean, J. A., Untargeted Metabolomics Strategies-Challenges and Emerging Directions. *J Am Soc Mass Spectrom* **2016,** *27* (12), 1897-1905.
37. Caldwell, G. W.; Leo, G. C., Can Untargeted Metabolomics Be Utilized in Drug Discovery/Development? *Curr Top Med Chem* **2017,** *17* (24), 2716-2739.
38. Khamis, M. M.; Adamko, D. J.; El-Aneed, A., Mass spectrometric based approaches in urine metabolomics and biomarker discovery. *Mass Spectrom Rev* **2017,** *36* (2), 115-134.
39. Cajka, T.; Smilowitz, J. T.; Fiehn, O., Validating Quantitative Untargeted Lipidomics Across Nine Liquid Chromatography-High-Resolution Mass Spectrometry Platforms. *Anal Chem* **2017,** *89* (22), 12360-12368.
40. Melnik, A. V.; da Silva, R. R.; Hyde, E. R.; Aksenov, A. A.; Vargas, F.; Bouslimani, A.; Protsyuk, I.; Jarmusch, A. K.; Tripathi, A.; Alexandrov, T.; Knight, R.; Dorrestein, P. C., Coupling Targeted and Untargeted Mass Spectrometry for Metabolome-Microbiome-Wide Association Studies of Human Fecal Samples. *Anal Chem* **2017,** *89* (14), 7549-7559.
41. Wang, M.; Wang, C.; Han, R. H.; Han, X., Novel advances in shotgun lipidomics for biology and medicine. *Prog Lipid Res* **2016,** *61*, 83-108.
42. Andra, S. S.; Austin, C.; Patel, D.; Dolios, G.; Awawda, M.; Arora, M., Trends in the application of high-resolution mass spectrometry for human biomonitoring: An analytical primer to studying the environmental chemical space of the human exposome. *Environ Int* **2017,** *100*, 32-61.
43. Bro, R.; Smilde, A. K., Principal component analysis. *Analytical Methods* **2014,** *6* (9), 2812-2831.
44. Barker, M.; Rayens, W., Partial least squares for discrimination. *Journal of Chemometrics* **2003,** *17* (3), 166-173.
45. Wold, S.; Sjöström, M.; Eriksson, L., PLS-regression: a basic tool of chemometrics. *Chemometrics and Intelligent Laboratory Systems* **2001,** *58* (2), 109-130.
46. Massart, D. L.; Buydens, L. M. C.; Vandegiste, B. G. M., *Handbook of Chemometrics and Qualimetrics*. 1st edn. ed.; Elsevier: Amsterdam, The Netherlands, 1997; Vol. 20.
47. Bylesjö, M.; Rantalainen, M.; Cloarec, O.; Nicholson, J. K.; Holmes, E.; Trygg, J., OPLS discriminant analysis: Combining the strengths of PLS-DA and SIMCA classification. *Journal of Chemometrics* **2006,** *20* (8-10), 341-351.
48. Trygg, J.; Wold, S., Orthogonal projections to latent structures (O-PLS). *Journal of Chemometrics* **2002,** *16* (3), 119-128.
49. Tautenhahn, R.; Bottcher, C.; Neumann, S., Highly sensitive feature detection for high resolution LC/MS. *BMC Bioinformatics* **2008,** *9*, 504.
50. Farres, M.; Pina, B.; Tauler, R., Chemometric evaluation of Saccharomyces cerevisiae metabolic profiles using LC-MS. *Metabolomics* **2015,** *11*, 210-224.
51. Gorrochategui, E.; Casas, J.; Porte, C.; Lacorte, S.; Tauler, R., Chemometric strategy for untargeted lipidomics: biomarker detection and identification in stressed human placental cells. *Anal Chim Acta* **2015,** *854*, 20-33.
52. De Juan, A.; Tauler, R., Chemometrics applied to unravel multicomponent processes and mixtures: Revisiting latest trends in multivariate resolution. *Analytica Chimica Acta* **2003,** *500* (1-2), 195-210.
53. Tauler, R., Multivariate curve resolution applied to second order data. *Chemometrics and Intelligent Laboratory Systems* **1995,** *30* (1), 133-146.

54. Jaumot, J.; Gargallo, R.; de Juan, A.; Tauler, R., A graphical user-friendly interface for MCR-ALS: a new tool for multivariate curve resolution in MATLAB. *Chemometrics and Intelligent Laboratory Systems* **2005,** *76* (1), 101-110.
55. Golub, G. H.; Reinsch, C., Singular value decomposition and least squares solutions. *Numerische Mathematik* **1970,** *14* (5), 403-420.
56. Windig, W.; Stephenson, D. A., Self-modeling mixture analysis of second-derivative near-infrared spectral data using the simplisma approach. *Analytical Chemistry* **1992,** *64* (22), 2735-2742.
57. Tauler, R.; Smilde, A.; Kowalski, B., Selectivity, local rank, three-way data analysis and ambiguity in multivariate curve resolution. *Journal of Chemometrics* **1995,** *9* (1), 31-58.
58. Tauler, R. M., M.; de Juan, A., Multiset Data Analysis: Extended Multivaried Curve Resolution. Elsevier: 2010; Vol. 2, pp 473-505.
59. Gorrochategui, E.; Jaumot, J.; Lacorte, S.; Tauler, R., *Data analysis strategies for targeted and untargeted LC-MS metabolomic studies: Overview and workflow*. 2016; Vol. 82.
60. Smith, C. A.; Want, E. J.; O'Maille, G.; Abagyan, R.; Siuzdak, G., XCMS: processing mass spectrometry data for metabolite profiling using nonlinear peak alignment, matching, and identification. *Anal Chem* **2006,** *78* (3), 779-87.
61. Tautenhahn, R.; Patti, G. J.; Rinehart, D.; Siuzdak, G., XCMS Online: a web-based platform to process untargeted metabolomic data. *Anal Chem* **2012,** *84* (11), 5035-9.
62. Gorrochategui, E.; Jaumot, J.; Tauler, R., ROIMCR: a powerful analysis strategy for LC-MS metabolomic datasets. *BMC Bioinformatics* **2019,** *20* (1), 256.
63. Schmelzer, K.; Fahy, E.; Subramaniam, S.; Dennis, E. A., The lipid maps initiative in lipidomics. *Methods Enzymol* **2007,** *432*, 171-83.
64. Wishart, D. S.; Tzur, D.; Knox, C.; Eisner, R.; Guo, A. C.; Young, N.; Cheng, D.; Jewell, K.; Arndt, D.; Sawhney, S.; Fung, C.; Nikolai, L.; Lewis, M.; Coutouly, M. A.; Forsythe, I.; Tang, P.; Shrivastava, S.; Jeroncic, K.; Stothard, P.; Amegbey, G.; Block, D.; Hau, D. D.; Wagner, J.; Miniaci, J.; Clements, M.; Gebremedhin, M.; Guo, N.; Zhang, Y.; Duggan, G. E.; Macinnis, G. D.; Weljie, A. M.; Dowlatabadi, R.; Bamforth, F.; Clive, D.; Greiner, R.; Li, L.; Marrie, T.; Sykes, B. D.; Vogel, H. J.; Querengesser, L., HMDB: the Human Metabolome Database. *Nucleic Acids Res* **2007,** *35* (Database issue), D521-6.
65. Yang, Q. J.; Zhao, J. R.; Hao, J.; Li, B.; Huo, Y.; Han, Y. L.; Wan, L. L.; Li, J.; Huang, J.; Lu, J.; Yang, G. J.; Guo, C., Serum and urine metabolomics study reveals a distinct diagnostic model for cancer cachexia. *J Cachexia Sarcopenia Muscle* **2018,** *9* (1), 71-85.
66. Jove, M.; Collado, R.; Quiles, J. L.; Ramirez-Tortosa, M. C.; Sol, J.; Ruiz-Sanjuan, M.; Fernandez, M.; de la Torre Cabrera, C.; Ramirez-Tortosa, C.; Granados-Principal, S.; Sanchez-Rovira, P.; Pamplona, R., A plasma metabolomic signature discloses human breast cancer. *Oncotarget* **2017,** *8* (12), 19522-19533.
67. Yilmaz, A.; Geddes, T.; Han, B.; Bahado-Singh, R. O.; Wilson, G. D.; Imam, K.; Maddens, M.; Graham, S. F., Diagnostic Biomarkers of Alzheimer's Disease as Identified in Saliva using 1H NMR-Based Metabolomics. *J Alzheimers Dis* **2017,** *58* (2), 355-359.
68. Zhao, K.; Zhang, J.; Xu, Z.; Xu, Y.; Xu, A.; Chen, W.; Miao, C.; Liu, S.; Wang, Z.; Jia, R., Metabolomic Profiling of Human Spermatozoa in Idiopathic Asthenozoospermia Patients Using Gas Chromatography-Mass Spectrometry. *Biomed Res Int* **2018,** *2018*, 8327506.
69. Farrokhi Yekta, R.; Rezaie Tavirani, M.; Arefi Oskouie, A.; Mohajeri-Tehrani, M. R.; Soroush, A. R., The metabolomics and lipidomics window into thyroid cancer research. *Biomarkers* **2017,** *22* (7), 595-603.
70. Chatgilialoglu, A.; Rossi, M.; Alviano, F.; Poggi, P.; Zannini, C.; Marchionni, C.; Ricci, F.; Tazzari, P. L.; Taglioli, V.; Calder, P. C.; Bonsi, L., Restored in vivo-like membrane lipidomics positively influence in vitro features of cultured mesenchymal stromal/stem cells derived from human placenta. *Stem Cell Res Ther* **2017,** *8* (1), 31.

71. Jones, D. P.; Walker, D. I.; Uppal, K.; Rohrbeck, P.; Mallon, C. T.; Go, Y. M., Metabolic Pathways and Networks Associated With Tobacco Use in Military Personnel. *J Occup Environ Med* **2016,** *58* (8 Suppl 1), S111-6.
72. Vulimiri, S. V.; Misra, M.; Hamm, J. T.; Mitchell, M.; Berger, A., Effects of mainstream cigarette smoke on the global metabolome of human lung epithelial cells. *Chem Res Toxicol* **2009,** *22* (3), 492-503.
73. Dudka, I.; Kossowska, B.; Senhadri, H.; Latajka, R.; Hajek, J.; Andrzejak, R.; Antonowicz-Juchniewicz, J.; Gancarz, R., Metabonomic analysis of serum of workers occupationally exposed to arsenic, cadmium and lead for biomarker research: a preliminary study. *Environ Int* **2014,** *68*, 71-81.
74. Ellis, J. K.; Athersuch, T. J.; Thomas, L. D.; Teichert, F.; Perez-Trujillo, M.; Svendsen, C.; Spurgeon, D. J.; Singh, R.; Jarup, L.; Bundy, J. G.; Keun, H. C., Metabolic profiling detects early effects of environmental and lifestyle exposure to cadmium in a human population. *BMC Med* **2012,** *10*, 61.
75. Huang, S. M.; Zuo, X.; Li, J. J.; Li, S. F.; Bay, B. H.; Ong, C. N., Metabolomics studies show dose-dependent toxicity induced by SiO(2) nanoparticles in MRC-5 human fetal lung fibroblasts. *Adv Healthc Mater* **2012,** *1* (6), 779-84.
76. Du, Y.; Xu, X.; Chu, M.; Guo, Y.; Wang, J., Air particulate matter and cardiovascular disease: the epidemiological, biomedical and clinical evidence. *J Thorac Dis* **2016,** *8* (1), E8-E19.
77. Messerlian, C.; Martinez, R. M.; Hauser, R.; Baccarelli, A. A., 'Omics' and endocrine-disrupting chemicals - new paths forward. *Nat Rev Endocrinol* **2017,** *13* (12), 740-748.
78. Casati, L.; Sendra, R.; Sibilia, V.; Celotti, F., Endocrine disrupters: the new players able to affect the epigenome. *Front Cell Dev Biol* **2015,** *3*, 37.
79. Bonvallot, N.; Tremblay-Franco, M.; Chevrier, C.; Canlet, C.; Warembourg, C.; Cravedi, J. P.; Cordier, S., Metabolomics tools for describing complex pesticide exposure in pregnant women in Brittany (France). *PLoS One* **2013,** *8* (5), e64433.
80. Carrizo, D.; Chevallier, O. P.; Woodside, J. V.; Brennan, S. F.; Cantwell, M. M.; Cuskelly, G.; Elliott, C. T., Untargeted metabolomic analysis of human serum samples associated with exposure levels of Persistent organic pollutants indicate important perturbations in Sphingolipids and Glycerophospholipids levels. *Chemosphere* **2017,** *168*, 731-738.
81. Adkesson, M. J.; Levengood, J. M.; Scott, J. W.; Schaeffer, D. J.; Langan, J. N.; Cardenas-Alayza, S.; de la Puente, S.; Majluf, P.; Yi, S., Assessment of Polychlorinated Biphenyls, Organochlorine Pesticides, and Polybrominated Diphenyl Ethers in the Blood of Humboldt Penguins (Spheniscus Humboldti) from the Punta San Juan Marine Protected Area, Peru. *J Wildl Dis* **2018,** *54* (2), 304-314.
82. Holmes, E.; Li, J. V.; Marchesi, J. R.; Nicholson, J. K., Gut microbiota composition and activity in relation to host metabolic phenotype and disease risk. *Cell Metab* **2012,** *16* (5), 559-64.
83. O'Kane, A. A.; Chevallier, O. P.; Graham, S. F.; Elliott, C. T.; Mooney, M. H., Metabolomic profiling of in vivo plasma responses to dioxin-associated dietary contaminant exposure in rats: implications for identification of sources of animal and human exposure. *Environ Sci Technol* **2013,** *47* (10), 5409-18.
84. Hu, W. Y.; Shi, G. B.; Hu, D. P.; Nelles, J. L.; Prins, G. S., Actions of estrogens and endocrine disrupting chemicals on human prostate stem/progenitor cells and prostate cancer risk. *Molecular and cellular endocrinology* **2012,** *354* (1-2), 63-73.
85. Jeng, H. A., Exposure to endocrine disrupting chemicals and male reproductive health. *Frontiers in public health* **2014,** *2*, 55.
86. Nohynek, G. J.; Borgert, C. J.; Dietrich, D.; Rozman, K. K., Endocrine disruption: fact or urban legend? *Toxicology letters* **2013,** *223* (3), 295-305.
87. Prins, G. S., Endocrine disruptors and prostate cancer risk. *Endocr Relat Cancer* **2008,** *15* (3), 649-56.

88. Louis, L. M.; Lerro, C. C.; Friesen, M. C.; Andreotti, G.; Koutros, S.; Sandler, D. P.; Blair, A.; Robson, M. G.; Beane Freeman, L. E., A prospective study of cancer risk among Agricultural Health Study farm spouses associated with personal use of organochlorine insecticides. *Environ Health* **2017,** *16* (1), 95.
89. Boada, L. D.; Sangil, M.; Alvarez-Leon, E. E.; Hernandez-Rodriguez, G.; Henriquez-Hernandez, L. A.; Camacho, M.; Zumbado, M.; Serra-Majem, L.; Luzardo, O. P., Consumption of foods of animal origin as determinant of contamination by organochlorine pesticides and polychlorobiphenyls: results from a population-based study in Spain. *Chemosphere* **2014,** *114*, 121-8.
90. Bell, M. R., Endocrine-disrupting actions of PCBs on brain development and social and reproductive behaviors. *Curr Opin Pharmacol* **2014,** *19*, 134-44.
91. El Majidi, N.; Bouchard, M.; Carrier, G., Systematic analysis of the relationship between standardized biological levels of polychlorinated biphenyls and thyroid function in pregnant women and newborns. *Chemosphere* **2014,** *98*, 1-17.
92. Kalluri, R., EMT: when epithelial cells decide to become mesenchymal-like cells. *The Journal of clinical investigation* **2009,** *119* (6), 1417-9.
93. Wang, H.; Fang, R.; Wang, X. F.; Zhang, F.; Chen, D. Y.; Zhou, B.; Wang, H. S.; Cai, S. H.; Du, J., Stabilization of Snail through AKT/GSK-3beta signaling pathway is required for TNF-alpha-induced epithelial-mesenchymal transition in prostate cancer PC3 cells. *European journal of pharmacology* **2013,** *714* (1-3), 48-55.
94. Kiesslich, T.; Pichler, M.; Neureiter, D., Epigenetic control of epithelial-mesenchymal-transition in human cancer. *Molecular and clinical oncology* **2013,** *1* (1), 3-11.
95. Ha, B.; Ko, H.; Kim, B.; Sohn, E. J.; Jung, J. H.; Kim, J. S.; Yoon, J. J.; Won, G.; Kim, J. H.; Jung, D. B.; Yun, M.; Shim, B.; Kim, S. H., Regulation of crosstalk between epithelial to mesenchymal transition molecules and MMP-9 mediates the antimetastatic activity of anethole in DU145 prostate cancer cells. *Journal of natural products* **2014,** *77* (1), 63-9.
96. Lamouille, S.; Xu, J.; Derynck, R., Molecular mechanisms of epithelial-mesenchymal transition. *Nature reviews. Molecular cell biology* **2014,** *15* (3), 178-96.
97. Tsao, H.; Chin, L.; Garraway, L. A.; Fisher, D. E., Melanoma: from mutations to medicine. *Genes Dev* **2012,** *26* (11), 1131-55.
98. Noonan, F. P.; Zaidi, M. R.; Wolnicka-Glubisz, A.; Anver, M. R.; Bahn, J.; Wielgus, A.; Cadet, J.; Douki, T.; Mouret, S.; Tucker, M. A.; Popratiloff, A.; Merlino, G.; De Fabo, E. C., Melanoma induction by ultraviolet A but not ultraviolet B radiation requires melanin pigment. *Nat Commun* **2012,** *3*, 884.
99. D'Orazio, J.; Jarrett, S.; Amaro-Ortiz, A.; Scott, T., UV radiation and the skin. *Int J Mol Sci* **2013,** *14* (6), 12222-48.
100. Morison, W. L.; Pike, R. A., Spectral power distributions of radiation sources used in phototherapy and photochemotherapy. *J Am Acad Dermatol* **1984,** *10* (1), 64-8.
101. Prost-Squarcioni, C., [Current findings on skin melanocytes and melanogenesis in human beings]. *Morphologie* **2001,** *85* (270), 5-9.
102. Downing, D. T., Lipid and protein structures in the permeability barrier of mammalian epidermis. *J Lipid Res* **1992,** *33* (3), 301-13.
103. Elias, P. M.; Menon, G. K., Structural and lipid biochemical correlates of the epidermal permeability barrier. *Adv Lipid Res* **1991,** *24*, 1-26.
104. Lin, J. Y.; Fisher, D. E., Melanocyte biology and skin pigmentation. *Nature* **2007,** *445* (7130), 843-50.
105. Ortonne, J. P., Normal and abnormal skin color. *Ann Dermatol Venereol* **2012,** *139 Suppl 4*, S125-9.
106. Chang, A. E.; Karnell, L. H.; Menck, H. R., The National Cancer Data Base report on cutaneous and noncutaneous melanoma: a summary of 84,836 cases from the past decade. The American College of Surgeons Commission on Cancer and the American Cancer Society. *Cancer* **1998,** *83* (8), 1664-78.

Capítol 3.
Validació de la metodologia ROIMCR pel tractament de dades òmiques LC-MS

3.1. Introducció

L'anàlisi de les dades metabolòmiques i lipidòmiques procedents de la cromatografia líquida acoblada a l'espectrometria de masses (LC-MS) és un dels colls d'ampolla dels estudis òmics degut a la mida i complexitat de les dades. Per aquest motiu, diferents eines d'anàlisi de dades i de programari per ordinador (*software*) han estat desenvolupades per facilitar l'extracció i interpretació de la informació rellevant dels sistemes biològics estudiats.[1-3] Existeixen dos tipus d'anàlisi, com s'ha comentat en la introducció, l'anàlisi dirigida focalitzada en l'estudi de certs grups de metabòlits o lípids pre-definits abans de començar l'estudi i l'anàlisi no-dirigida on no es predeterminen els compostos a investigar. L'aproximació no dirigida implica una anàlisi multivariant de dades més elaborada, incloent la compressió i la resolució multivariant de conjunts de dades LC-MS voluminosos. Aquests conjunts de dades contenen una gran quantitat d'informació que necessita ser processada adequadament. Un bon processament permet extreure els perfils d'elució (de concentració) i els espectres de masses més rellevants en el context del problema a estudiar. Aquest tipus d'anàlisi de dades es realitza mitjançant eines quimiomètriques multivariants.

Aquest capítol inclou la publicació:

Publicació I. *Validation of the regions of interest multivariate curve resolution (ROIMCR) procedure for untargeted LC-MS lipidomic analysis.* N. Dalmau, C. Bedia, R.Tauler. *Anal Chim Acta* **2018**,1025, 80-91

3.2. Publicació I

Validation of the regions of interest multivariate curve resolution (ROIMCR) procedure for untargeted LC-MS lipidomic analysis.

N. Dalmau, C. Bedia, R.Tauler

Anal Chim Acta **2018**,1025, 80-91

Analytica Chimica Acta 1025 (2018) 80–91

Contents lists available at ScienceDirect

Analytica Chimica Acta

journal homepage: www.elsevier.com/locate/aca

Validation of the Regions of Interest Multivariate Curve Resolution (ROIMCR) procedure for untargeted LC-MS lipidomic analysis

Núria Dalmau, Carmen Bedia, Romà Tauler*

IDEA-CSIC, Jordi Girona 18-26, 08034, Barcelona, Spain

HIGHLIGHTS

- ROIMCR procedure is a useful methodology for untargeted analysis of LC-MS data sets.
- ROI strategy reduces significantly LC-MS data size without loss of *m/z* accuracy.
- ROIMCR strategy is validated using lipid standard mixtures, also in biological samples.

GRAPHICAL ABSTRACT

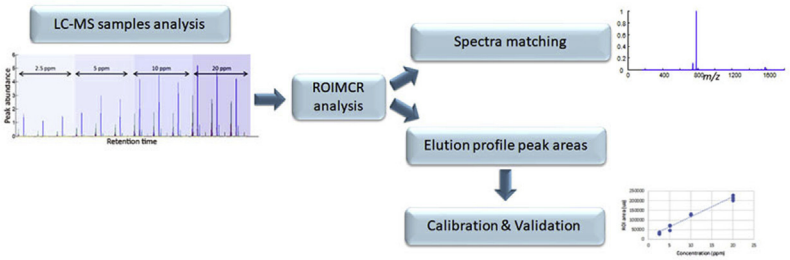

ARTICLE INFO

Article history:
Received 27 October 2017
Received in revised form
21 February 2018
Accepted 3 April 2018
Available online 17 April 2018

Keywords:
ROIMCR
Validation
Lipidomic analysis

ABSTRACT

Untargeted liquid chromatography coupled to mass spectrometry (LC-MS) analysis generates massive amounts of information-rich mass data which presents storage and processing challenges. In this work, the validation of a recently proposed procedure for LC-MS data compression and processing is presented, using as example the analysis of lipid mixtures. This method consists of a preliminary selection of the Regions of Interest of the LC-MS data (MSROI) coupled to their throughout chemometric analysis by the Multivariate Curve Resolution Alternating Least Squares method (MCR-ALS). The proposed data selection procedure is based on the search of the most significant mass traces regions with high mass densities. This allows for a drastic reduction of the MS data size and of the computer storage requirements, without any significant loss neither of spectral resolution nor of accuracy on *m/z* measures. The combination of the MSROI data compression and MCR-ALS data analysis procedures in the new ROIMCR procedure has the main advantage of not requiring neither the chromatographic peak alignment nor the chromatographic peak shape modelling used in many other procedures as a pre-treatment step of the data analysis. The proposed ROIMCR procedure is tested in the analysis of the LC-MS experimental data coming from different lipid mixtures and of a melanoma cell line culture sample with satisfactory results. The proposed strategy is shown to be a general, fast, reliable and easy to use method for general untargeted LC-MS metabolic and lipidomic data analysis type of studies.

1. Introduction

Nowadays, chromatographic techniques coupled to mass spectrometry such as LC-MS, GC-MS, CE-MS generate large volumes of data. The massive amount of information-provided by these methods presents computer storage problems and difficulties for

* Corresponding author.
E-mail address: roma.tauler@idaea.csic.es (R. Tauler).

https://doi.org/10.1016/j.aca.2018.04.003
0003-2670/

data analysis. Data pre-processing techniques are required to deal with the large data sizes generated in metabolomics studies. One very important aspect to consider is the need of preservation of the mass accuracy of the experimental measurements for optimal identification purposes. For this reason, classical data compression strategies like data binning are not the best option because the reduction of storage (bin sizes) produced using this procedure implies the consequent reduction of the instrumental accuracy of measured mass values. An alternative pre-processing approach has been proposed in the *centWave* algorithm of XCMS software [1], where the selection of the Regions of Interest in MS data (MSROI) is performed as a preliminary pre-processing step. MSROI are regions of measured data with significant mass traces and high mass densities. The MSROI selection allows for a significant reduction of the data size, without any loss of spectral accuracy on *m/z* measures. The use of this procedure allows for a faster and more accurate MS data treatment and analysis.

LC-MS analysis of complex biological samples like those needed in omics studies [2–9] require laborious data analysis tasks specially in the case of using an untargeted approach based on the analysis of the whole full scan MS detected signals. In these untargeted omic studies, the largest number of possible sample constituents (as much as possible) are simultaneously analysed, most of them strongly coeluted and in the presence of strong background and solvent contributions. To solve this type of problems, the Multivariate Curve Resolution- Alternating Least Squares method (MCR-ALS) has been proposed [10] with successful results [11–16]. One of the main advantages of using the MCR-ALS method over other proposed strategies for the analysis of full scan LC-MS data (as well as for data provided by other similar hyphenated chromatographic methods) is that the processing and resolution of a very large number (e.g. > 100) of sample constituents elution and spectra profiles do not require any preliminary step of chromatographic peak alignment nor of peak shape modelling, and that can be performed directly in a single step of the data analysis procedure.

In recent works, we have combined both strategies, the MSROI pre-processing step of mass data compression and the MCR-ALS chemometrics data analysis method in the new ROIMCR method, for the analysis of full scan LC-MS data from complex omic samples with very promising results [17–21]. A protocol of general application has been described to promote its use [13,22]. These previous studies were performed in order to estimate relative changes in concentrations of the sample constituents, but not in quantitative terms for the estimation of the real concentrations of them in analysed samples. In order to confirm the power and suitability of this new combined approach, in this work, the validation of the whole method is presented for a particular case of study. First, the two strategies are combined in the analysis of a standard lipids mixture. This allows us to check for the identification and quantitation of all the constituents, and even more important, we can check whether we missed anything that was in the sample. This study is then extended to the simultaneous analysis of multiple standard mixtures of lipids. Finally, the ROIMCR procedure is applied to the quantitative analysis of the lipids present in a biological sample. This validation examines first the recovery of the elution profiles and pure mass spectra of the lipid constituents of the standard mixture samples without any loss of spectral accuracy. Mass spectra of the resolved components are used then to identify and confirm the presence of the different lipids in the analysed mixtures. Their MCR-ALS resolved elution profiles and their corresponding peak areas/heights are further used to investigate the lipid concentration changes among the different samples simultaneously analysed, and to build calibration curves which allow for their quantitative determination. The proposed ROIMCR strategy provides a fast and efficient method for metabolomic and lipidomic studies using LC-MS analytical methods.

2. Experimental

2.1. Preparation of lipid samples

To test and validate the ROIMCR method, different lipid samples were prepared by dilution of a standard mixture of nine lipids provided by Avanti Polar Lipids. The lipid standard mixture was first prepared at 1000 ppm and it was then diluted to give four new lipid standard mixtures at 20, 10, 5 and 2.5 ppm concentrations. Furthermore, a mixture of three sphingolipid internal standards at 5 ppm was added to each sample before MS analysis. In Table 1 the list of all lipids present in the standard mixtures are given, together with their retention times and theoretical *m/z* values.

2.2. LC-MS analysis of lipids

LC-MS analysis used a Waters Acquity UHPLC system connected to a Waters LCT Premier orthogonal accelerated time of flight (ToF) mass spectrometer (Waters), operated in positive and negative electrospray ionization modes (ESI + and ESI -). Full scan spectra between 50 and 1500 Da were acquired, and individual spectra were summed to produce data points every 0.2 s. Mass accuracy and reproducibility were maintained by using an independent reference spray via the LockSpray interference. The analytical column was a 100 × 2.1 mm inner diameter, 1.7 mm C8 Acquity UPLC bridged ethylene hybrid (Waters). The two mobile phases were phase A: MeOH, 1 mM ammonium formate and phase B: H_2O, 2 mM ammonium formate, 0.2% formic acid for both solutions. The flow rate was 0.3 ml min^{-1} and the gradient of A/B solvents started at 80:20 and changed to 99:1 in 6 min until min 15; remained 99:1 until minute 18; finally returned to the initial conditions until minute 20. The column was held at 30 °C.

2.3. Lipid calibration curves

A total number of 12 different calibration samples were prepared. In each one the mixture of lipid standards at one of the lipid concentrations (at 2.5, 5, 10 and 20 ppm with three replicates) was diluted to a final volume of 170 μl. Calibration curves were built by regressing the peak areas of the elution profiles of the lipids resolved by the ROIMCR procedure (see below) in two of the three sample replicates against their known concentrations. The peak areas of the lipids resolved by ROIMCR in the third sample replicates at every concentration were then used to validate the calibration curves. Therefore these samples were used as external validation samples to test the reliability of the proposed ROIMCR method. In all cases the peak areas of the lipids were normalized by the mean value of the peak areas of the three internal standards used for each analysed sample.

To test the reliability of the calibration results, the predicted (using the calibration model) *vs* theoretical concentrations of the lipids were plotted and the linear regression parameters estimated. A good agreement between predicted vs theoretical values would give a regression line with a correlation coefficient close to 1, a slope close to one, and an offset close to zero.

2.4. Analysis of lipids in a biological sample

The human melanoma cell line A375 was purchased from ATCC and maintained in DMEM culture medium supplemented with 10% heat-inactivated fetal bovine serum, 100 U ml^{-1} streptomycin at 37 °C in a humidified atmosphere containing 5% of CO_2.

Table 1
Lipids in the mixture samples analysed by LC-MS. Different lipid families are considered: glycerols (MG, DG and TG), lyso phospholipids (LysoPE, LysoPC and LysoPG), phospholipids (PC, PE, PS) and sphingolipids (internal standards).

Lipid Standards	Abb.[a]	rt[b] (min)	*m/z*	Adduct
17:0 monoacylglycerol	MG	3.6	362.3270	M+NH4
1,3–17:0 diacylglycerol	DG	11.5	619.6037	M+NH4
1,2,3–17:0 triacylglycerol	TG	18.4	866.8177	M+NH4
17:0 Lyso phosphatidylcholine	LysoPC	3.2	510.3560	M+H
17:1 Lyso phosphatidylethanolamine	LysoPE	2.7	466.2934	M+H
17:1 Lyso phosphoglycerol	LysoPG	2.9	497.2878	M+H
16:0 D31–18:1 phosphatidylcholines	PC	9.2	791.7798	M+H
16:0 D31–18:1 phosphatidylethanolamine	PE	8.0	749.7332	M+H
16:0 D31–18:1 phosphatidylserine	PS	8.6	793.7229	M+H
C12 Ceramide	Cer	5.6	482.4573	M+H
C12 Sphingomyelin	SM	5.4	647.5128	M+H
C12 Glucosylceramide	GlcCer	5.2	644.5101	M+H

[a] Abbreviation.
[b] Retention time.

Human melanoma cell line A375 sample was used to validate the proposed ROIMCR method in the analysis of lipids in a complex biological sample. A375 cells were seeded in 6-well plates at 2×10^5 cells per well. Cells were harvested using trypsin, after medium neutralization. Cells were centrifuged at 1300 *rpm* for 3 min at 4 °C and cell pellets were washed twice with cold PBS 1X. Then, chloroform/methanol (2:1) was added to extract the lipids from the cell line samples. For this extraction, 100 μl of deionized water was added to the cell pellets and the suspension was transferred to borosilicate glass test tubes with Teflon caps. Then, 250 μl of methanol and 500 μl of chloroform were subsequently added. Samples were sonicated until they appeared dispersed, then incubated overnight at 48 °C in a heating water bath. The tubes were then cooled at 37 °C. The samples were evaporated under N_2 stream and transferred to 1.5 ml eppendorf tubes after addition of 500 μl of methanol. Samples were evaporated again and suspended in 150 μl of methanol. The tubes were centrifuged at 10000 *rpm* for 3 min and 130 μl of the supernatants was transferred to UHPLC vials for injection. Different volumes of the standard lipid mixture were added in each vial depending on the concentrations to achieve (0, 2.5, 5, 10, 15 and 20 ppm) and 5 μl of the internal standard mixture. Finally, methanol was added to all vials to achieve a final volume of 170 μl.

In this case, calibration curves followed the same procedure as the one used to build the calibration curves in the previous section with the synthetic lipids mixture samples. Predicted *vs* theoretical concentration values were also plotted in this case to further test, the reliability of the proposed ROIMCR method in the analysis of the cell culture samples.

3. Data analysis

3.1. Data acquisition and storage

One single LC-MS chromatographic run from the analysis of one sample resulted in a data file which was converted to CDF format via Databridge, MassLynx software. Data sets from the different chromatographic runs were then imported and stored in the MATLAB computational environment (release 2014b); The Mathworks Inc., Natick, MA, USA), using *mzcdfread* and *mzcdf2peaks* functions from the MATLAB Bioinformatics Toolbox™.

3.2. Selection of the regions of interest (ROI)

MS spectral data imported to the MATLAB environment were not equally sized and could not be arranged directly into a regular data table/matrix suitable for chemometric multivariate data analysis. In fact, high resolution MS instruments provide an irregular number of measured *m/z* and signal intensity pair data values at every MS scan at the considered chromatographic retention time. These paired values are not equidistant in the *m/z* direction. Measured values are only provided for those ions reaching to the mass detector. These measurements are however given with the maximum instrumental precision and resolution of the equipment, i.e. high resolution *m/z* values with up to 4 *m/z* decimal units. Building a data set with equidistant *m/z* values at this high mass resolution of the instrument would represent storing very huge sparse data matrices. For instance, in our case, for equidistant entries of the data matrix in the interval of 1000 *m/z* units with a resolution of 0.0005 *m/z* units and a number of retention times of 636 would give a total storage of 1000×20 *m/z* times 636 times $\times$ 8 bytes per value = 102 Mb. If multiple samples are examined, this value will be multiplied by the number of samples. For instance for 12 samples, this will be 1.2 Gb storage. Operating with so huge data matrices would need a considerable amount of computer storage and computation time. Current alternative approaches like data binning would reduce the storage and computation time, but with a considerable loss of mass accuracy. The method proposed in this work is based on the Regions of Interest (ROI) concept [23], and the main steps of this procedure are described below and in Fig. 1. This method takes advantage of the sparse structure of the measured MS data reducing considerably the computer storage and computation time needed without losing the instrumental mass resolution and precision of the equipment.

Regions of Interest are searched on the raw MS spectral scans looking for the spectral regions where significant intensity MS values, higher than a threshold value (estimated from the instrumental noise level), are present at high densities in specific raw data regions. Selection of the regions of interest (MSROI) for LC-MS data was proposed by Stolt et al. [23] and introduced afterwards in the *centWave* algorithm of *XCMS* software [1]. Our own MATLAB implementation of this procedure consisted on a set of MATLAB home-made functions [21,24] which require three input parameters. The first parameter is a threshold value that considers only MS signals whose intensity values are higher than this threshold value, commonly between 0.1 and 1% of the maximum measured MS peak intensity. The second parameter is the *m/z* error or admissible mass deviation of the experimental measurements, typically set to a multiple of mass accuracy of the mass spectrometer, e.g., 0.05 Da/e in our mass spectrometer MS-ToF Waters detector. The last parameter to consider is the minimum number of pair (*m/z* and MS intensity) consecutive values to be present in the same ROI. For example, in our UHPLC system, a minimum number of five values were needed in the same ROI; this corresponds to 10 s of

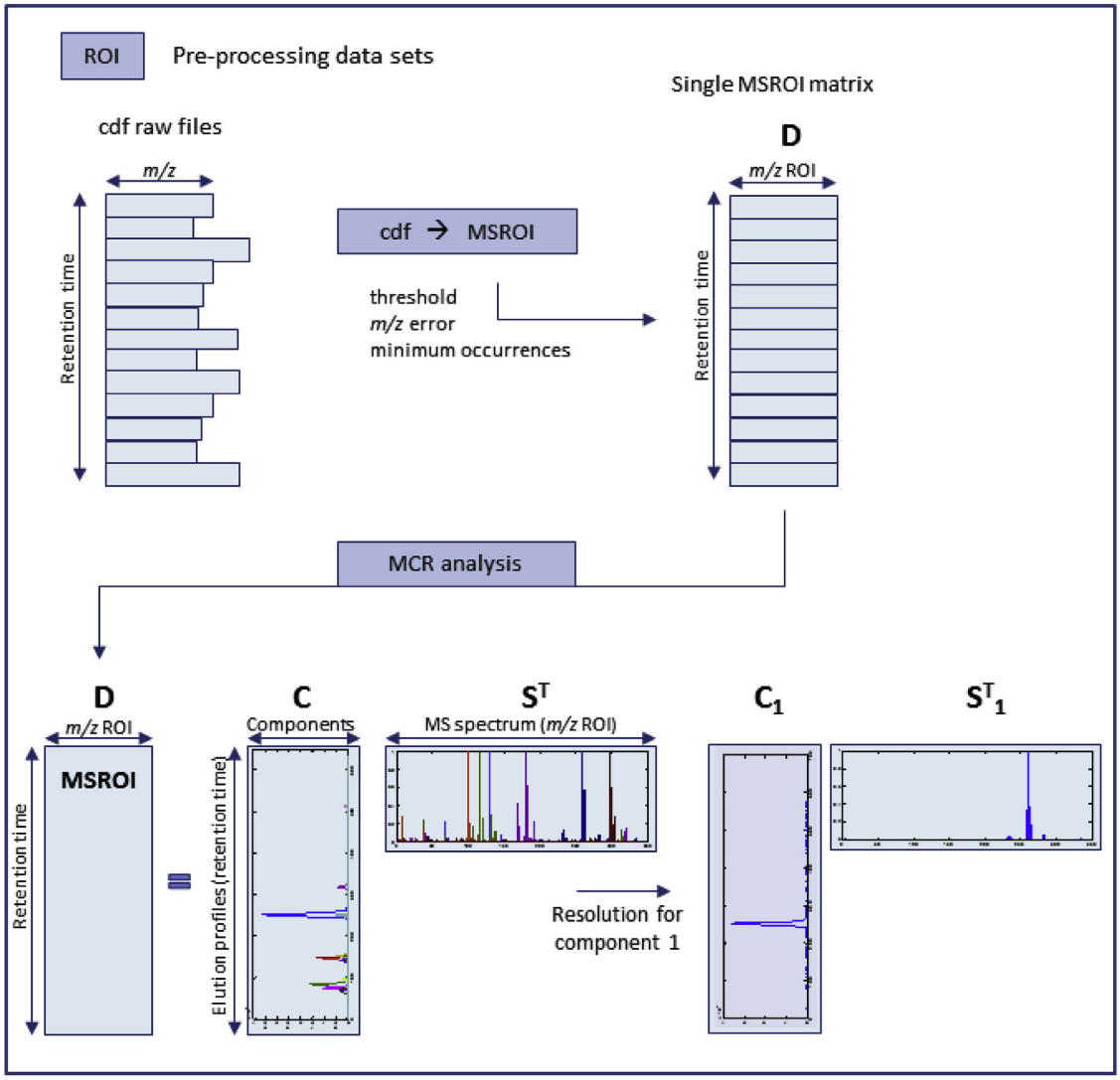

Fig. 1. Workflow of the ROIMCR data analysis method.

chromatographic peak width. More details on how this procedure is implemented and used can be found elsewhere [21,22].

The application of this MSROI procedure gives three outputs: The first one gives the finally selected *m/z* values assigned to every ROI. They are calculated as the mean of all *m/z* values belonging to the same ROI. The second output is the data matrix which contains the MSROI spectra (in the rows) at every chromatographic elution time. The final dimensions of the MSROI data matrix will be the number of spectra at every chromatographic time (in the data matrix rows) times the number of mzROI finally selected (in the data matrix columns). A considerable reduction of computer storage is achieved when only *m/z* ROI values are considered in the columns of the data matrix compared to what would be the storage needed when all equidistant *m/z* values at the instrument mass deviation would have been considered. The finally selected MSROI values can be plotted one by one for their examination and validation using the third output. The MS individual the intensities of *m/z* ROI values can be plotted *vs* the elution time, expressed in seconds. And also, the measured MSROI *m/z* mass traces corresponding to the selected MS intensities are plotted. For instance, MSROI pairs not giving a chromatographic peak shape can be detected, filtered out and not further considered for MCR analysis. In the particular case of this study, the presence of all expected lipids in the selected MSROI data matrix is checked before proceeding with the MCR-ALS data treatment analysis.

When multiple lipid mixture samples were simultaneously examined, they were grouped in a new MSROI augmented data matrix before its MCR analysis (Fig. 2). Since MSROI individual data matrices can have different ROI *m/z* values, a preliminary step of MSROI augmentation and rearrangement is performed to include all those ROI *m/z* values (common and not common) with significant traces (with MS intensity values higher than the threshold values at the considered ROI *m/z* value). This procedure has been described in more detail in Gorrochategui et al. and summarized in Fig. 1 [22].

3.3. ROIMCR analysis

MSROI individual data matrices from the lipid samples were first analysed individually by the Multivariate Curve Resolution-Alternating Least Squares (MCR-ALS) chemometric method. This method has been shown to be a powerful chemometric tool for the resolution of overlapping multivariate signals and for the bilinear decomposition of two and multi-way data arrays of different

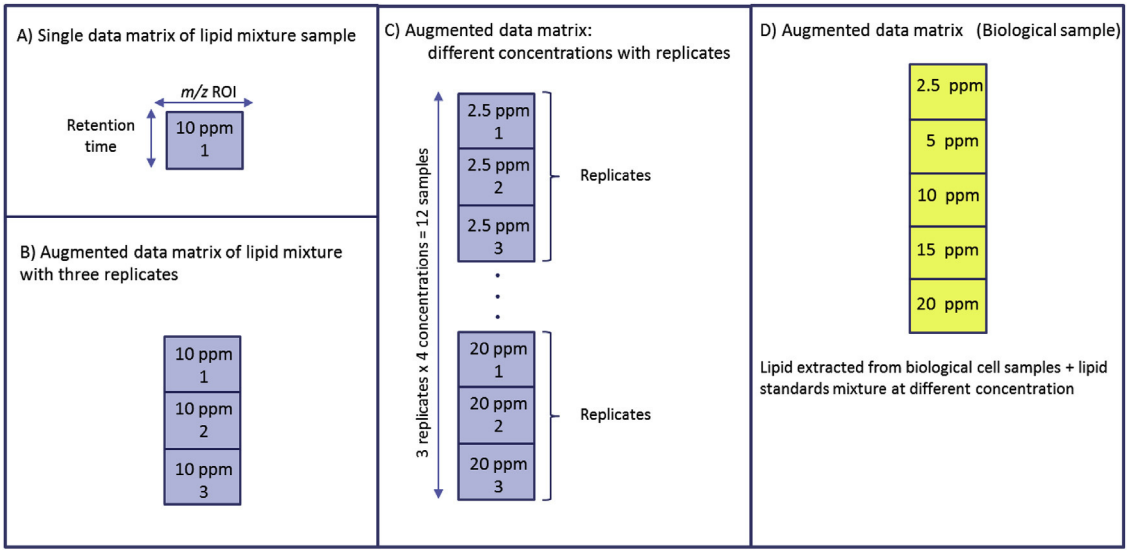

Fig. 2. Data matrices used in the analysis of the different lipid mixture samples.

complexity and structure [10,25]. MCR-ALS has been successfully applied for the resolution of LC-MS data sets with strongly coeluted and hidden peaks and it has been extended more recently to omic studies [17–19,26,27]. MCR-ALS analysis of an individual lipid mixture data matrix performs its bilinear decomposition as described by following equation:

$$D = CS^T + E \quad (1)$$

Where the matrix **D** (I × J) has the MSROI spectra at every retention time (i = 1, …I) in its rows, and the chromatograms at every *m/z* channel (j = 1, …J), in its columns. This data matrix is decomposed into the product of two factor matrices, **C** and $\mathbf{S}^T$. Column vectors in the **C** (I × N) matrix have the elution profiles of the N (n = 1, …N) resolved components (lipids). Row vectors in the $\mathbf{S}^T$ (N × J) matrix, have the MSROI spectra of the N resolved components (lipids). The part of **D** matrix not explained by the bilinear model is in the residuals data matrix, **E** (I × J). MCR-ALS solves Eq. (1). Starting with an initial guess of the number of components which explains sufficiently well the variance of the considered data matrix, for instance when it is analysed by the singular value decomposition (SVD) method [28]. This number of components should be large enough to include most of the lipids presents in the sample plus other contributions from the background, solvent and other instrument artifacts. MCR-ALS calculates iteratively the concentration (elution) profiles, in **C**, and the pure MSROI spectra, in $\mathbf{S}^T$, optimally fitting the experimental data matrix, **D**. During the ALS optimization, various constraints are applied to model appropriately the shapes of the **C** and $\mathbf{S}^T$ profiles and reduce rotation ambiguities [29]. For MSROI data, non-negativity constraints were applied to ensure that resolved concentration and spectra profiles are non-negative. Also, during ALS optimization, the MS spectra were normalized to equal maximum height. Results from ALS optimization are displayed as resolved elution profiles (in **C**) and pure mass spectra (in $\mathbf{S}^T$).

The data analysis strategy previously described can be easily extended to the simultaneous analysis of several MSROI data matrices coming from different samples, which facilitates the resolution of all the lipid compounds in the different investigated samples. The column-wise augmented MSROI data matrix, $\mathbf{D_{aug}}$, is submitted to MCR-ALS analysis using the extension of the bilinear model described by Equation (2):

$$\mathbf{D_{aug}} = \begin{bmatrix} \mathbf{D}1 \\ \mathbf{D}2 \\ \mathbf{D}3 \\ . \\ . \\ . \\ \mathbf{D}k \end{bmatrix} = \begin{bmatrix} \mathbf{C}1 \\ \mathbf{C}2 \\ \mathbf{C}3 \\ . \\ . \\ . \\ \mathbf{C}k \end{bmatrix} \mathbf{S}^T + \begin{bmatrix} \mathbf{E}1 \\ \mathbf{E}2 \\ \mathbf{E}3 \\ . \\ . \\ . \\ \mathbf{E}k \end{bmatrix} = \mathbf{C_{aug}}\,\mathbf{S}^T + \mathbf{E_{aug}} \quad (2)$$

In this case, the applied constraints were non-negativity (of elution, **C**, and spectra, $\mathbf{S}^T$, profiles), and spectra normalization (equal height) [30]. MCR bilinear model of the augmented data matrix enforces the resolved MS-ROI spectra in $\mathbf{S}^T$ to be the same for the common constituents in the different samples (data matrices). In contrast, elution profiles resolved in $\mathbf{C_{aug}}$ matrix area allowed to be different for each of the different samples (C_x (x = 1, 2, …12)) simultaneously analysed. Therefore, as shown in Equation (2), the bilinear modelling of the $\mathbf{D_{aug}}$ does not require the alignment of the chromatographic peaks, and this is an important advantage of the MCR-ALS method presented here.

In the case of the simultaneous analysis of the multiple lipid mixture samples by MCR-ALS, a data table that contains the peak areas or heights of the elution profiles (in $\mathbf{C_{aug}}$ matrix) of the different resolved components in the different samples is calculated. From these peak areas, concentrations of every one of the lipid components in every sample can be then estimated. Previous to this estimation, the lipid peak area values were normalized by the mean peak area of the three sphingolipids used as internal standards (Cer, SM and GluCer), which were present in all the samples always at the same concentration, 5 ppm.

MSROI pure spectra of the MCR-ALS resolved components (lipids) were recovered without any loss of spectral resolution, and they can be used afterwards for their proper identification in databases or by comparison with known standards. In this work, the MCR resolved lipid sample constituents could be identified by their exact mass values (*m/z*). The *m/z* error values representing the difference between experimentally obtained mass values and the exact adduct mass values found in databases were also calculated, to confirm that the considered resolved component corresponds really to one of the lipids in the mixture with a difference value lower than 10 ppm.

3.4. XCMS

MetaboNexus is available with its installation guide and tutorial at http://www.sph.nus.edu.sg/index.php/research-services/research-centres/ceohr/metabonexus, and is meant for the Windows Operating System, XP and onwards (preferably on 64-bit) [31]. The raw data in CDF format were also submitted to MetaboNexus. Settings for their minimum percentage of samples where the same detected peaks need to be present in at least one sample class were set to 50%. The UPLC/Q-ToF parameters were marked in the manual settings according to our instrument employed; which automatically activated centWave algorithm. Mass tolerance between successive measurements was selected to 10 ppm, peak width between 5 and 20 s, signal to noise threshold of 3, and the Obiwarp algorithm was selected for retention time alignment (*m/z* width 0.025 s, minimum fraction of samples of 2 for group validation).

3.5. Software

Software used in this work includes MassLynx V 4.1 (Waters) for raw UHPLC-TOF data exporting in cdf format and initial processing and analysis. The cdf data conversion into the MATLAB (The Mathworks Inc.) environment was performed using the Bioinformatics MATLAB Toolbox. Home-made MATLAB routines used for ROIMCR identification and data compression are given in Gorrochategui et al. [22,32] Microsoft Excel and MCR-ALS Toolbox (http://www.mcrals.info [24]) (under MATLAB) were used for the data analysis.

4. Results

This results section was structured in three different parts (see Fig. 2), according to the different data matrix arrangements and their corresponding analysis. Thus, individual LC-MS data matrices from lipid mixture samples at one of the concentrations were analysed by the proposed ROIMCR procedure to assure that all lipid constituents were correctly recovered and identified (Fig. 2A). In the second part, the LC-MS augmented data matrix composed of the three replicates of the same standard lipid mixture at the same concentration was analysed to check for the reproducibility of the procedure (Fig. 2B). Next, the LC-MS augmented data matrix composed of the twelve MSROI data matrices from the three replicate lipid mixture samples at four different concentration levels was analysed to check for the recovery of all the lipid constituents and of their concentrations from the appropriate calibration models (Fig. 2C). In the last part (Fig. 2D), a new augmented data matrix was built with the MSROI data matrices obtained in the LC-MS analysis of the lipid mixtures in the cell culture samples at different concentrations. In this last case, the proposed ROIMCR procedure was tested and validated in the LC-MS analysis of a much more complex biological sample.

4.1. ROIMCR analysis of the individual LC-MS lipid mixture samples

Results obtained in the LC-MS analysis of the individual lipid mixture samples at a particular concentration (e.g.10 ppm) and using three internal standards (5 ppm) are shown first, see Fig. 2A.

Selection of MSROI values is shown in two different subplots of every figure in Fig. 3. These subplots give information about how the LC-MS data was acquired by the instrument in different examples and situations. At the left side of every subplot, the MS intensities (red circles) of the selected *m/z* ROI values are plotted *vs* the elution time, expressed in seconds. For a correct MSROI, this plot should display the peak shape of a chromatographic profile, and should have multiple individual measurements along the same peak. At the right side of every subplot, the instrumentally measured MSROI *m/z* mass traces (in black circles) are plotted *vs* the elution time, expressed in seconds. These *m/z* mass traces are dispersed around an average *m/z* value (blue line) with one (green line) and two (red line) standard deviations respectively. These two subplots will be obtained for every selected MSROI pair (intensity and *m/z* values). Only those MSROI pairs with a reasonable chromatographic peak shape and having *m/z* traces covering a narrow region will be finally considered for the subsequent MCR-ALS analysis (see below). These plots are also useful to check for the optimal selection of the parameters during the MSROI selection procedure. For instance, the selection of the parameter fixing a too narrow *m/z* deviation would split the chromatographic peak in two different MSROIs. On the contrary, the selection of a parameter with a too wide *m/z* deviation would probably include more than one single chromatographic peak in the same MSROI. Moreover, *m/z* traces are expected to be randomly distributed respect the measured elution time in the plot, as it can see in the right plots of Fig. 3. The threshold parameter that defines the MSROI values and filters out the others should be also assessed by investigation of these plots; in our case a 0.5% of the maximum MS intensity was finally selected.

Using the proposed MSROI procedure, all lipids known to be present in the mixture samples were correctly selected and identified. Naturally, besides the analytes of interest, other MSROI values were obtained in this analysis, which were assigned to the reagents added, to the mobile phase, to possible chemical impurities from the analytical instrument, to signal background and noise and to other random interfering species. In fact, this preliminary MSROI analysis of the lipid mixtures featured a total number of 346 *m/z* ROI values, with obviously many of them having nothing to do with the lipid standards in the synthetic mixtures. Since most of them had a non-chromatographic peak shape, they could be easily distinguished from the good peak shapes obtained for the lipids present in their mixture samples and further discarded during the MCR analysis (see below).

After this initial estimation of the MSROI values, the corresponding individual MSROI data matrix was built up, with 638 retention times (rows) and only 346 *m/z* ROIs (columns) from the original number of 35000 *m/z* values in the raw equidistant (0.05 *m/z* error) data. This data matrix was then submitted to MCR-ALS analysis to resolve the elution profiles (in **C**) and pure MS spectra (in $\mathbf{S}^{\mathbf{T}}$) of all the lipids present in the lipids mixture sample. For this analysis, 30 MCR-ALS components were initially proposed from the approximate inspection of the sizes of the singular values of the data matrix. The constraints applied during the MCR-ALS analysis were non-negativity and spectral normalization (equal height). All lipids present in the mixture samples were correctly detected, resolved and confirmed together with their expected adducts, see Table 2.

In Table 2, the results of the identification and confirmation of all lipids in the mixture sample are given.

4.2. ROIMCR simultaneous analysis of multiple LC-MS lipid mixture samples

The procedure described above was extended to the simultaneous analysis of multiple lipid standards mixtures. As described in the method section, this procedure consisted in setting up an augmented MSROI data matrix which contained the common information of all MSROI values obtained in the analysis of all individual data matrices, each one related to one of the analysed lipid mixture samples.

In a first analysis, the column-wise augmented data matrix

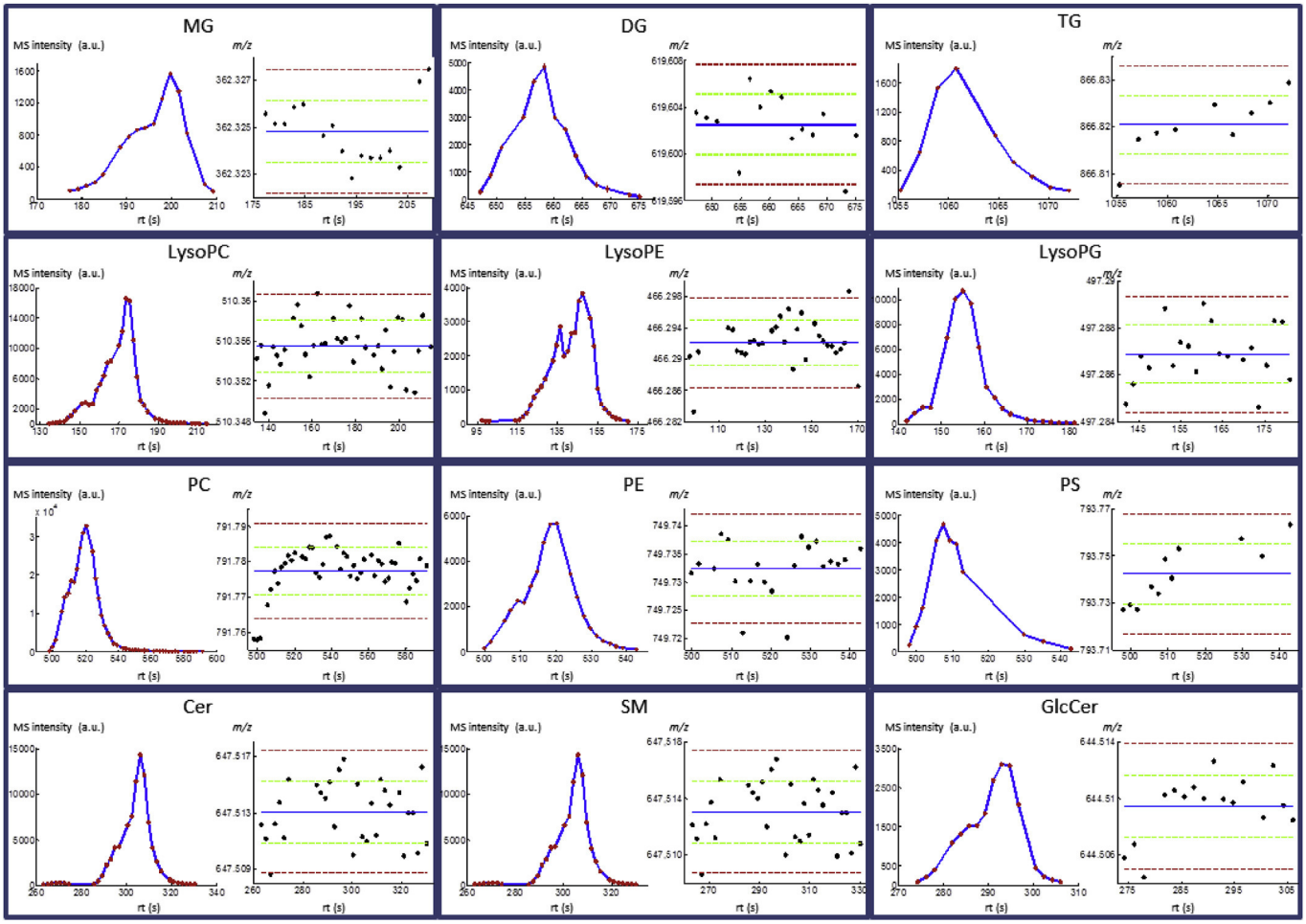

Fig. 3. Graphical representation of the MSROI obtained for the different lipids: MG, DG, TG, LysoPC, LysoPE, LysoPG, PC, PE, PS) in the analysis of the synthetic mixture samples, including the three internal standards (SM, Cer, GlcCer). In every subplot, at the left, the MS intensities (red circles) of the selected *m/z* ROI values are plotted *vs* the elution time, expressed in seconds; and at the right, the actual *m/z* ROI mass traces are plotted *vs* the elution time, expressed in seconds. (For interpretation of the references to colour in this figure legend, the reader is referred to the Web version of this article.)

Table 2
ROIMCR results of the analysis of the lipids mixture at 10 ppm concentration.

Lipid standard	Adduct	MCR component	rt (min) [a]	ROI *m/z* Value [b]	exact *m/z* [c]	*m/z* error (ppm) [d]
MG	M+NH4	16	3.33	362.3248	362.3270	6.1
DG	M+NH4	7	10.97	619.6025	619.6037	1.9
TG	M+NH4	20	17.68	866.8204	866.8177	3.1
LysoPC	M+H	2	2.89	510.3555	510.3560	1.0
LysoPE	M+H	9	2.46	466.2921	466.2934	2.7
LysoPG	M+H	4	2.58	497.2869	497.2879	2.0
PC	M+H	1	8.67	791.7774	791.7798	3.1
PE	M+H	26	8.64	749.7324	749.7332	1.1
PS	M+H	14	8.52	793.7325	793.7229	12.0
Cer	M+H	8	5.25	482.4539	482.4573	7.0
SM	M+H	3	5.10	647.513	647.5128	0.4
GlcCer	M+H	13	4.88	644.5095	644.5101	1.0

[a] Retention times at the ROI peak maximum in minutes.
[b] *m/z* values of the ROI spectra maxima in mass units.
[c] Exact *m/z* values of the considered lipids from LipidMaps database.
[d] Differences in ppm between the *m/z* values of the ROI spectra (2) and the exact *m/z* values (3).

created using the three replicates of the same lipid mixture at the same concentration was analysed (see Fig. 2B) by the ROIMCR procedure. Again, all lipids included in the mixture samples were correctly detected and resolved. The peak areas of the elution profiles of the nine lipids resolved (in $\mathbf{C_{aug}}$) by MCR-ALS were then used to validate the method reproducibility in the replicate mixture samples. These results are given in Table 3, where the coefficients of variation of all mean peak areas were rather low. This confirms that

in general, for most of the lipids, the reproducibility of the results achieved after the MSROI analysis was good.

The next step was the ROIMCR analysis of the augmented data matrix which contains lipid mixtures at different concentrations (2.5, 5, 10, 20 ppm) and their corresponding replicates, including a total number of 12 data matrices (Fig. 2C). This MSROI augmented data matrix was $12 \times 638 = 7656$ rows by 512 *m/z* ROI values. A total number of 30 components was initially proposed and the constraints applied during the MCR-ALS analysis were non-negativity and spectral normalization (equal height). Fig. 4A shows the elution profile of all the resolved lipid constituents in the 12 chromatographic runs (in $\mathbf{C_{aug}}$ matrix). Changes of the peak areas and of the heights of the elution profiles of the lipids at the four different concentration levels (2.5, 5, 10, 20 ppm) are distinguished clearly. Fig. 4B displays the corresponding pure mass spectra of the lipid constituents resolved by the MCR-ALS (in $\mathbf{S^T}$) procedure. Fig. 4C shows the resolution of the elution profile of phosphatidylcholine (PC) in the different multiple analysed samples and Fig. 4D the resolved mass spectrum of this compound given.

The peak areas of the elution profiles of the lipids resolved by MCR-ALS were used to build calibration curves by their regression against their known concentrations in the standards. These calibration curves were built using two of these replicates of every lipid mixture. Once these calibration curves were built, the concentration of the lipids in the third replicate mixture was estimated from their peak areas, and compared with their actual known concentration values. These predicted concentrations were then plotted against the known lipid concentrations in the third replicates and the regression parameters calculated. In the results shown in Table 4A, all lipid constituents were detected and quantified correctly. Good linearity (r^2) and predictions (slope and offset) were obtained for all lipids, with values close to one for the correlation coefficient and slope, and zero for the offset. Only the PE lipid did not show good linear properties, probably because this lipid is better analysed using the negative ionization mode (ESI-). RMSEP (Root Mean Square Error in Prediction) and relative prediction errors (RE% < 20%) were rather good, which confirms that the ROIMCR proposed was also appropriate for the quantification of the lipids present in the analysed mixture samples.

4.3. ROIMCR simultaneous analysis of multiple LC-MS cell culture samples

The proposed ROIMCR procedure was also applied to the analysis of the lipids in the cell culture samples, see Fig. 2D. The augmented data matrix used for this analysis was built using five samples from the same cell culture sample, each one with different concentrations of the lipids mixture (2.5, 5, 10, 15 and 20 ppm). After the MSROI preliminary compression step, a total number of 629 *m/z* ROI values were selected. This high number of ROIs needed is due to the presence of a large number of unknown lipidic compounds in the cell culture samples, which give relatively high intensity MS signals. This MSROI augmented data matrix had 3185 (5×637) rows and 629 (*m/z* ROI) columns. A total number of 130 components were used for the MCR-ALS analysis of this augmented data matrix. All nine lipids, as well as the three internal standards, were correctly resolved and identified, despite the much more complex matrix of the cell culture samples. In this case, the threshold intensity level used for MSROI selection was changed to 0.25% of maximum MS signal intensity, to recover appropriately the MS signals of all the lipids known to be present in the cell culture biological samples.

The peak areas of the elution profiles resolved by MCR-ALS for all lipids in the different cell culture samples were used to build a calibration curve. The same calibration procedure was used as for the analysis of lipid mixture samples. A good linear relationship between the concentrations of the lipids predicted from their peak areas and their known concentrations in the cell culture samples was obtained, allowing the prediction of their concentrations with low prediction errors. The results of this analysis are shown in Table 4B. Comparison between predicted and reference concentration values gave good linear correlation values, as well as regression lines with slope close to one and offsets close to zero, which indicates a good recovery of the concentrations of lipids in the tested cell culture samples. Relative errors (RE) and RMSEC (Root Mean Square Error in Calculated) values are given in Table 4B, which were also acceptable. These results confirm again that the proposed ROIMCR procedure gives reliable quantitative results and that this method can be used for the analysis of biological samples in metabolomics and lipidomics studies.

Table 3
ROIMCR results of the quantification of the lipids mixtures in the three replicates samples at 10 ppm concentration (see Fig. 2B).

Lipid standard	Adduct	MCR component	rt (min) [a]	*m/z* ROI value [b]	exact *m/z* [c]	*m/z* error (ppm) [d]	Area 1[e]	Area 2[e]	Area 3[e]	Mean [f]	standard deviation[g]	CV (%) [h]
MG	M+NH4	17	3.3	362.3243	362.327	7.45	15656	16018	14442	15372	826	5
DG	M+NH4	8	10.9	619.6029	619.6037	1.29	25063	28099	22842	25335	2639	10
TG	M+NH4	20	17.6	866.8206	866.8177	3.34	6358	7033	5293	7228	877	14
LysoPC	M+H	2	2.9	510.3549	510.356	2.24	127911	130723	126399	128344	2194	2
LysoPE	M+H	10	2.5	466.2915	466.2934	4	35005	34353	34351	34570	377	1
LysoPG	M+H	4	2.6	497.287	497.2879	1.79	55111	54964	50293	53456	2740	5
PC	M+H	1	8.6	791.7788	791.7798	1.31	53252	53638	41680	49523	6795	14
PE	M+H	31	8.6	749.733	749.7332	0.27	5235	6085	6801	6040	784	13
PS	M+H	6	8.5	793.7279	793.7229	6.3	8429	8512	8652	8531	113	1
Cer	M+H	7	5.3	482.4542	482.4573	6.41	32709	34506	33292	33503	917	3
SM	M+H	3	5.1	6,47.5127	647.5128	0.13	84688	85231	82512	84144	1439	2
GlcCer	M+H	13	4.9	644.5104	644.5101	0.52	19192	19833	18567	19197	633	3

[a] Retention times at the ROI peak maximum in minutes.
[b] *m/z* values of the ROI spectra maximum in mass units.
[c] Exact *m/z* values of the considered lipids from LipidMaps database.
[d] Differences in ppm between the *m/z* values of the ROI spectra (2) and the exact *m/z* values (3).
[e] Peak areas of the elution profiles of the corresponding MSROI in arbitrary units.
[f] Mean of the three replicate peak areas.
[g] Standard deviation of the three replicate peak areas.
[h] Coefficient of variation of the three replicate peak areas.

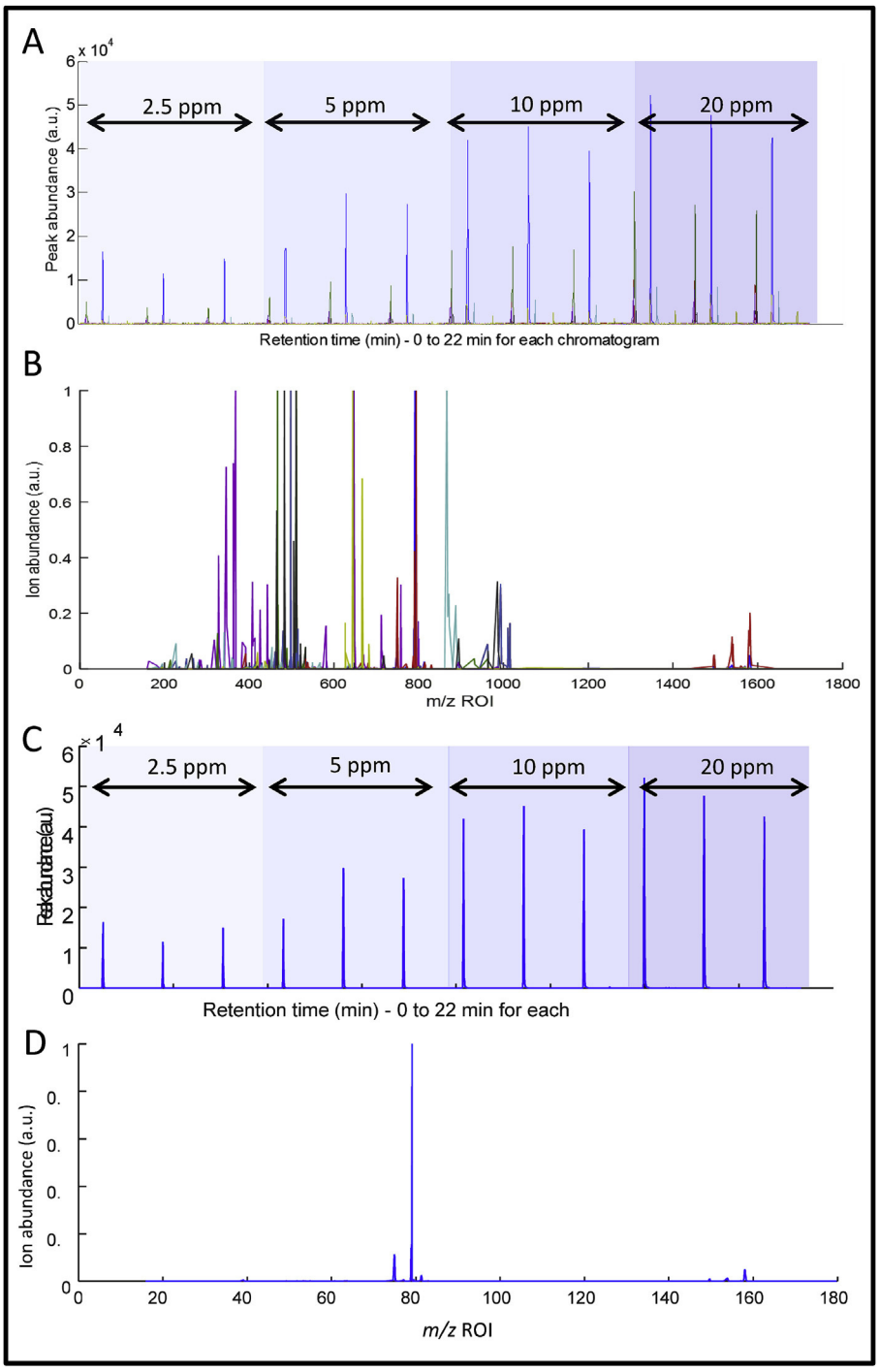

Fig. 4. A) Elution profiles and B) mass spectra of the ROIMCR resolved components. Only the selected components corresponding to the investigated lipids are shown, different colours correspond to each component. C) Elution profiles and D) pure mass spectra of the ROIMCR resolved component corresponding to PC standard (791.7788 *m*/*z*), blue. (For interpretation of the references to colour in this figure legend, the reader is referred to the Web version of this article.)

It is also important to point out, that all the estimations were performed without the need of any preliminary step of chromatographic peak alignment nor of peak shape modelling, and that they can be performed directly in a single step of the data analysis procedure when calibration and unknown samples are simultaneously processed using the MCR-ALS analysis of the augmented data matrices containing the LC-MSROI information of these samples.

4.4. Comparison study between ROIMCR and XCMS strategies

In the last years, XCMS has become a favorite method in the metabolomic community as a powerful tool for mass spectrometry feature detection, resolution and identification, and it has been used for a broad range of applications. In brief, XCMS is a tool dedicated to chromatographic feature detection which includes automatic processing of huge size full-scan LC-MS data and

Table 4
Comparison of ROIMCR and XCMS quantitative results. ROIMCR predicted *vs* actual concentrations of the different lipids analysed: A) in the mixture samples and B) in the cell culture samples. C) XCMS predicted vs actual concentrations of the different lipids analysed in the cell culture samples.

Lipid	Mixture samples[a]					Cell culture samples[b] ROIMCR					Cell culture samples[c] XCMS				
	r[b c]	Slope[d]	Offset[e]	RMSEP[f]	%RE[g]	r[b c]	Slope[d]	Offset[e]	RMSEP[f]	%RE[g]	r[b c]	Slope[d]	Offset[e]	RMSEP[f]	%RE[g]
MG	0.9997	0.9763	−0.2599	0.5448	5	0.9869	1.0128	−0.2781	1.0448	8	0.983	1.147	−2.211	1.530	12
DG	0.9975	0.9284	0.2105	1.1623	6	0.9914	0.9828	0.18	0.846	7	0.984	1.027	−0.527	1.171	9
TG	0.9975	0.8794	1.16031	1.1623	10	0.9604	0.9881	−0.1052	1.8001	14	0.981	1.097	−1.539	1.433	12
LysoPC	0.9999	0.9442	−0.0456	0.7302	6	0.9976	1.0055	−0.099	0.4427	4	0.951	0.781	2.773	2.687	21
LysoPE	0.9962	1.0004	−0.5903	0.825	7	0.9962	1.0104	−0.1862	0.5673	5	0.928	0.881	1.181	2.515	20
LysoPG	0.9996	0.8865	1.5116	1.0139	9	0.999	0.9978	0.0215	0.2873	2	0.973	0.961	0.336	1.501	12
PC	0.9908	1.0702	−2.2785	1.8188	15	0.9955	0.9911	0.0936	0.607	5	0.978	1.370	−5.474	2.449	20
PE	0.9991	1.4275	−5.6216	2.319	20	0.9723	0.9212	0.9114	1.5905	13	0.969	1.165	−2.663	1.978	16
PS	0.9932	0.7985	0.7338	2.3499	17	0.9978	0.9955	0.0471	0.4279	4	0.895	0.731	3.083	3.563	28

[a] Simultaneous analysis of 12 lipid mixture samples (see Fig. 2C).
[b] Simultaneous analysis of 5 lipid cell culture samples (see Fig. 2D).
[c] Correlation coefficient of the regression line of the ROIMCR predicted vs actual concentration values.
[d] Slope of the regression line of the regression line of the ROIMCR predicted vs actual concentration values.
[e] Offset of the regression line of the ROIMCR predicted vs actual concentration values.
[f] Root mean square error prediction of the concentrations of the lipids.
[g] Relative errors in the prediction of the ROIMCR predicted vs actual concentration values.

estimates candidate metabolites by using peak detection, retention time correction and peak shape modelling algorithms and methods.

In this work, XCMS was applied to the entire full-scan chromatograms, and the output was a table containing 329 features. Not all of these detected features could be considered to be an independent lipid compound since some of them could be adducts or isotopic masses coming from the same lipid, and others could be assigned to electric signals or other noise contributions. This together with the fact that XCMS requires peak retention time shift correction and peak shape modelling among different chromatograms makes the XCMS procedure more dependent on the selected parameters. Chromatographic information provided by XCMS and ROIMCR strategies was rather similar. As mentioned before, XCMS algorithm detects features that at a particular *m/z* value the signal is higher than a given threshold. Some of these features can be assigned to instrumental noise, background or others artifacts. Furthermore, one lipid specie could have more than one feature due to the detection of isotopic peaks or adducts. In contrast, MCR-ALS resolves components according to their elution profiles and their corresponding mass spectra. Every MCR-ALS resolved component will be associated with an elution profile and a mass spectrum which, however, may include various features at different *m/z* values. In this case these features can be easily assigned to an isotopic peak of the nominal *m/z* values or to different adducts of the same lipid. Therefore, a single MCR-ALS resolved component provides information on several features related to the same metabolite grouped together. A more difficult situation can occur when two species or more have a very strongly overlapped elution profile with practically the same mass spectrum within the mass accuracy of the mass spectrometer. Fig. 5 shows an example where three coeluted constituents were resolved without ambiguities by the MCR-ALS method.

Chemometric evaluation of the peak areas for each lipid obtained by XCMS and ROIMCR approaches allowed the statistical comparison of ROIMCR vs XCMS concentrations of the different lipids analysed in the cell culture samples, see Table 4C. The results displayed the similarity between both approaches. ROIMCR concentration values were slightly better because their relative error values were better than XCMS values.

Finally, when the use of the two approaches is compared, it may be argued that the XCMS workflow, as implemented in MetaboNexus [31], can be considered to be more straightforward for non-experienced users, but this is not always the case because of possible difficulties associated to its use as a web page platform. In contrast again, ROIMCR can perform all estimations without the need of any preliminary step of chromatographic peak alignment nor of peak shape modelling, and it can be used directly in a single step of the data analysis procedure when calibration and unknown samples are simultaneously processed using the MCR-ALS analysis of the augmented data matrices containing all the LC-MSROI information from these samples.

4.5. Comparison of targeted and non-targeted peak areas

Finally, the peak areas of the elution profiles of the lipids in the mixture samples resolved by the ROIMCR untargeted procedure were compared with the peak areas of the elution profiles of the lipids recovered by the commercial MassLynx software (Waters) using a targeted approach. In Table 5, the comparisons between the results obtained by both approaches are given.

In general, good correlations were obtained between the peak areas of all the lipids using both methods. However in targeted analysis performed using MassLynx software, background noise do interfere more than in the untargeted MSROI procedure (noise is suppressed when the threshold level is applied during ROI selection). As mentioned above (apart 4.2), PE again gave worse values because of positive ionization was not adequate for this lipid. The MG lipid resulted to be the most difficult lipid to quantify due to its low MS intensity.

In the previous comparison, the quantitation method used by the commercial Waters software should be considered a targeted approach, whereas the ROIMCR method should be classified as a non-target approach, since all the possible resolved relevant species are investigated, known or unknown, in the resolved components. Therefore, the advantage of the ROIMCR procedure compared to commercial software approaches is that the former performs directly the resolution and identification of all unknowns simultaneously present in all analysed samples in a non-targeted way, without the need of searching and matching for every component with previously known standards, one by one individually. Moreover, the complete spectral features of all resolved compounds (including unknowns) in the mixture samples can be recovered directly, with all their MS signal ions, which can facilitate their ulterior identification and differentiation. Therefore the ROIMCR approach opens and facilitates the implementation of discovery approaches, searching for unknown biomarkers in all type of omics studies and biomedical applications using

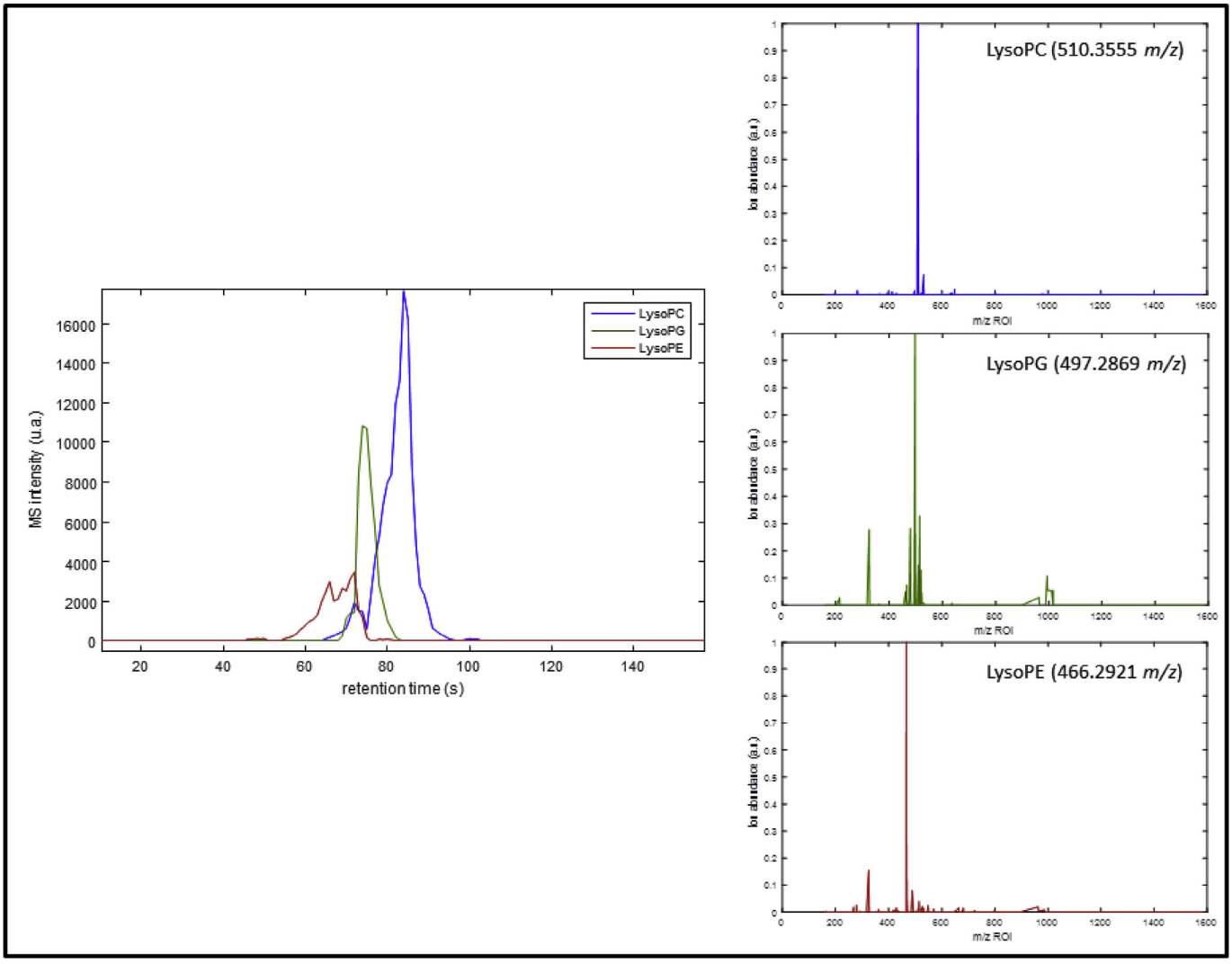

Fig. 5. Graphical description of overlapped peaks and their corresponding pure mass spectra. Each mass spectrum corresponds to one lipid: 17:0 Lyso phosphatidylcholine (LysoPC) blue, 17:1 Lyso phosphoglycerol (LysoPG) green and 17:1 Lyso phosphatidylethanolamine (LysoPE) red. (For interpretation of the references to colour in this figure legend, the reader is referred to the Web version of this article.)

Table 5
ROIMCR quantitative results of the comparison of peak areas obtained by the ROIMCR untargeted procedure *vs* the peak areas obtained by MassLynx targeted procedure in the analysis of the lipids of the mixture samples at different concentrations.

Lipid standards	slope	offset	r^2
MG	0.7801	−0.005	0.9945
DG	1.0004	−0.0183	0.9982
TG	0.9005	0.0105	0.9952
LysoPC	1.0162	−0.0298	0.9997
LysoPE	1.0568	0.0079	0.9997
LysoPG	1.9916	0.1944	0.9665
PC	1.0503	−0.1274	0.9992
PE	3.4361	−0.2417	0.9663
PS	1.9633	0.0742	0.9780

hyphenated MS chromatographic methods.

5. Conclusions

The ROIMCR method presented in this work enables a significant reduction of storage and analysis times of untargeted full scan LC-MS data sets, without any loss of instrumental mass resolution accuracy. The proposed MSROI compression method combined with the MCR-ALS strategy (ROIMCR) is confirmed for the direct analysis of LC-MS complex raw data sets, in particular for lipidomic and metabolomic studies.

In addition to the correct recovery of the elution profiles and of the MS spectra profiles of the different sample constituents with their full mass accuracy, the ROIMCR procedure presented in this work also allowed building good calibration models to perform quantitative estimations of the concentrations of the mixture constituents.

An outstanding aspect of the proposed method is that it does not require any preliminary step of chromatographic peak alignment nor of peak shape modelling, and that can be performed directly in a single step of the data analysis procedure.

Acknowledgments

This work was supported by the European Research Council under the European Union's Seventh Framework Programme (FP/2007–2013)/ERC Grant Agreement 35 no. 320737. RT also

acknowledges the Ministerio de Economía y Competividad, Spain (Grant CTQ2015-66254-C2-1-P).

Appendix A. Supplementary data

Supplementary data related to this article can be found at https://doi.org/10.1016/j.aca.2018.04.003.

References

[1] C.A. Smith, et al., XCMS: processing mass spectrometry data for metabolite profiling using nonlinear peak alignment, matching, and identification, Anal. Chem. 78 (3) (2006) 779–787.
[2] M. Navarro-Reig, et al., Evaluation of changes induced in rice metabolome by Cd and Cu exposure using LC-MS with XCMS and MCR-ALS data analysis strategies, Anal. Bioanal. Chem. 407 (29) (2015) 8835–8847.
[3] M. Farres, B. Pina, R. Tauler, Chemometric evaluation of metabolic profiles using LC-MS, Metabolomics 11 (2015) 210–224.
[4] C. Gomez-Canela, et al., Targeted metabolomics of Gammarus pulex following controlled exposures to selected pharmaceuticals in water, Sci. Total Environ. 562 (2016) 777–788.
[5] C. Bedia, et al., Phenotypic malignant changes and untargeted lipidomic analysis of long-term exposed prostate cancer cells to endocrine disruptors, Environ. Res. 140 (2015) 18–31.
[6] D. Barh, V. Zambare, V. Azevedo, OMICS: Applications in Biomedical, Agricultural and Environmental Sciences, first ed., CRC Press, 2013.
[7] T. Romero-Gutierrez, et al., A deeper examination of thorellius atrox scorpion venom components with omic techonologies, Toxins 9 (12) (2017).
[8] S.E. Dautel, et al., Lipidomics reveals dramatic lipid compositional changes in the maturing postnatal lung, Sci. Rep. 7 (2017) 40555.
[9] D.B. Foster, et al., Integrated omic analysis of a Guinea pig model of heart failure and sudden cardiac death, J. Proteome Res. 15 (9) (2016) 3009–3028.
[10] R. Tauler, Multivariate curve resolution applied to second order data, Chemometr. Intell. Lab. Syst. 30 (1) (1995) 133–146.
[11] M. Abou Fadel, et al., Extraction of pure spectral signatures and corresponding chemical maps from EPR imaging data sets: identifying defects on a CaF2 surface due to a laser beam exposure, Anal. Chem. 87 (7) (2015) 3929–3935.
[12] M. Alier, et al., Variation patterns of nitric oxide in Catalonia during the period from 2001 to 2006 using multivariate data analysis methods, Anal. Chim. Acta 642 (1–2) (2009) 77–88.
[13] M. Farres, B. Pina, R. Tauler, LC-MS based metabolomics and chemometrics study of the toxic effects of copper on Saccharomyces cerevisiae, Metall 8 (8) (2016) 790–798.
[14] S. Mas, et al., Determination of phenolic acids in strawberry samples by means of fast liquid chromatography and multivariate curve resolution methods, Talanta 71 (4) (2007) 1455–1463.
[15] G.G. Siano, et al., Multivariate curve resolution modeling of liquid chromatography-mass spectrometry data in a comparative study of the different endogenous metabolites behavior in two tomato cultivars treated with carbofuran pesticide, Talanta 85 (1) (2011) 264–275.
[16] I. Sanchez Perez, et al., Detection of unintended stress effects based on a metabonomic study in tomato fruits after treatment with carbofuran pesticide. Capabilities of MCR-ALS applied to LC-MS three-way data arrays, Anal. Chem. 81 (20) (2009) 8335–8346.
[17] C. Gomez-Canela, et al., Assessment of chlorpyrifos toxic effects in zebrafish (Danio rerio) metabolism, Environ. Pollut. 220 (Pt B) (2017) 1231–1243.
[18] M. Navarro-Reig, et al., Untargeted comprehensive two-dimensional liquid chromatography coupled with high-resolution mass spectrometry analysis of rice metabolome using multivariate curve resolution, Anal. Chem. 89 (4) (2017) 7675–7683.
[19] A.S. Marques, et al., Assessment of the effects of As(III) treatment on cyanobacteria lipidomic profiles by LC-MS and MCR-ALS, Anal. Bioanal. Chem. 408 (21) (2016) 5829–5841.
[20] E. Ortiz-Villanueva, et al., Metabolic disruption of zebrafish (Danio rerio) embryos by bisphenol A. An integrated metabolomic and transcriptomic approach, Environ. Pollut. 231 (Pt 1) (2017) 22–36.
[21] E. Gorrochategui, et al., Data analysis strategies for targeted and untargeted LC-MS metabolomic studies: overview and workflow, Trac. Trends Anal. Chem. 82 (2016) 425–442.
[22] E. Gorrochategui, J. Jaumot, R. Tauler, A Protocol for Lc-Ms Metabolomic Data Processing Using Chemometric Tools, 2015. https://doi.org/10.1038/protex.2015.102.
[23] R. Stolt, et al., Second-order peak detection for multicomponent high-resolution LC/MS data, Anal. Chem. 78 (4) (2006) 975–983.
[24] J. Jaumot, et al., A graphical user-friendly interface for MCR-ALS: a new tool for multivariate curve resolution in MATLAB, Chemometr. Intell. Lab. Syst. 76 (1) (2005) 101–110.
[25] E. Pere-Trepat, S. Lacorte, R. Tauler, Solving liquid chromatography mass spectrometry coelution problems in the analysis of environmental samples by multivariate curve resolution, J. Chromatogr. A 1096 (1–2) (2005) 111–122.
[26] N. Dalmau, et al., Epithelial-to-mesenchymal transition involves triacylglycerol accumulation in DU145 prostate cancer cells, Mol. Biosyst. 11 (12) (2015) 3397–3406.
[27] E. Ortiz-Villanueva, et al., Knowledge integration strategies for untargeted metabolomics based on MCR-ALS analysis of CE-MS and LC-MS data, Anal. Chim. Acta 978 (2017) 10–23.
[28] G.H. Golub, C. Reinsch, Singular value decomposition and least squares solutions, Numer. Math. 14 (5) (1970) 403–420.
[29] R. Tauler, Calculation of maximum and minimum band boundaries of feasible solutions for species profiles obtained by multivariate curve resolution, J. Chemometr. 15 (8) (2001) 627–646.
[30] R.M. Tauler, A. M de Juan, Multiset Data Analysis: Extended Multivaried Curve Resolution, Elsevier, 2010, pp. 473–505.
[31] S.-M. Huang, et al., MetaboNexus: an Interactive Platform for Integrated Metabolomics Analysis, 10, 2014.
[32] http://cidtransfer.cid.csic.es/descarga.php?enlace1=3adcd456c13cef5c017b66269651912c.

Informació Suplementària a la Publicació I

Validation of the regions of interest multivariate curve resolution (ROIMCR) procedure for untargeted LC-MS lipidomic analysis.

N. Dalmau, C. Bedia, R.Tauler

Anal Chim Acta **2018**, 14(3), 170-180

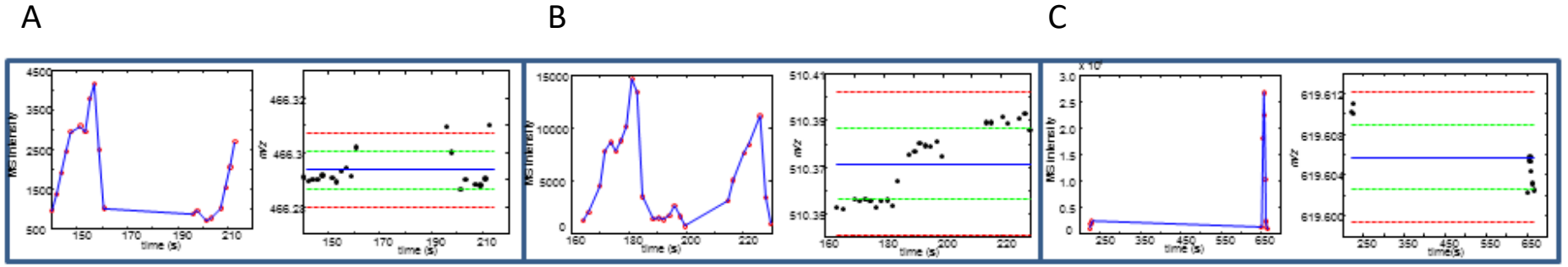

Figure S1. Graphical representation of the MSROI obtained for the different *m/z* in the analysis of cell culture samples, when are not displayed the optimal parameters, *m/z* error = 0.05; instead of 0.025 *m/z* error. In every subplot, at the left side, the MS intensities (red circles) of the selected *m/z* ROI values are plotted *vs* the elution time, expressed in seconds; and at the right, the actual *m/z* ROI mass traces are plotted vs the elution time, expressed in seconds. A) Two different regions were displayed in the same ROI. B) Two peaks are captured for the same ROI. C) Two clearly distinguished regions in this ROI. One is a defined peak and another is in the baseline.

3.3. Discussió dels resultats

Un dels objectius dins d'aquesta Tesi ha estat la realització d'una validació quantitativa de la nova metodologia quimiomètrica ROIMCR, desenvolupada dins el nostre grup de recerca pel tractament de dades òmiques.[4] Aquesta metodologia està basada en la selecció de les "Regions d'Interès (ROI)" i en el mètode de resolució multivariant de corbes per mínims quadrats alternats (Multivariate Curve resolution Alternating least Squares, MCR-ALS). Per una banda, el pre-tractament ROI es centra en la recerca i selecció de les regions de masses amb intensitats més significatives i d'elevades densitats. D'aquesta manera, a partir d'aquesta selecció selectiva de les regions s'aconsegueix una important reducció de la mida del conjunt de dades organitzat en forma de matriu de dades, sense que es produeixi pèrdua de resolució espectral ni d'exactitud en la mesura de masses. D'altra banda, en una segona fase, l'anàlisi mitjançant MCR-ALS d'aquest nou conjunt de dades ROI seleccionades, proporciona la seva resolució en els perfils d'elució cromatogràfica i espectres de masses dels components de les mostres analitzades per LC-MS.

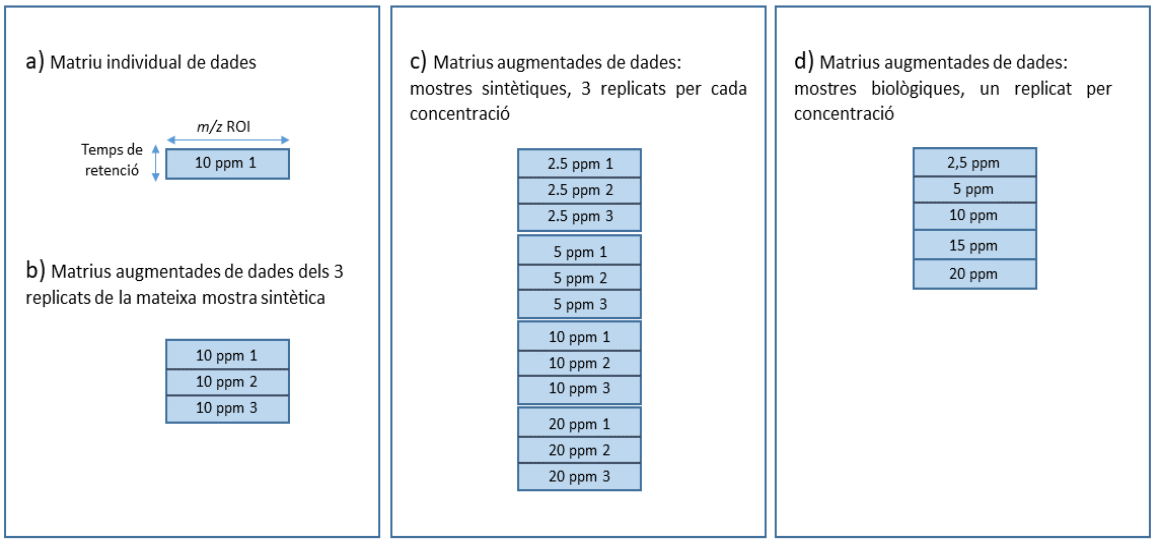

Figura 22. Matrius de dades emprades en la validació de la metodologia ROIMCR.

Seguint aquest propòsit es van analitzar diferents grups de mostres de complexitat diversa per UHPLC-ToF-MS. Les dades generades es van distribuir en quatre grups i totes elles varen ser processades seguint la metodologia ROIMCR descrita anteriorment, veure Figura 22:

a) Matrius individuals de dades obtingudes en l'anàlisi LC-MS de les diferents mostres que contenen la mescla sintètica de 13 lípids a diferents concentracions.
b) Matrius augmentades de dades obtingudes en l'anàlisi LC-MS de les tres repliques de cada mostra sintètica que contenen la mescla de 13 lípids a la mateixa concentració.
c) Matrius augmentades de dades obtingudes en l'anàlisi LC-MS de les mostres sintètiques que contenen les tres rèpliques de la mescla dels 13 lípids a quatre concentracions diferents (3 x 4 = 12 matrius de dades individuals).
d) Matrius augmentades de dades obtingudes en l'anàlisi LC-MS de diferents mostres biològiques (cultius cel·lulars) que contenen les cinc matrius de dades individuals de les mescles dels 13 lípids a concentracions diferents (cinc matrius de dades individuals). Matrius augmentades originades en l'anàlisi LC-MS de mostres biològiques enriquides amb els patrons lipídics de l'estudi a diferents concentracions.

3.3.1. Demostració qualitativa

Primerament, es va posar a prova el mètode ROIMCR de forma **qualitativa** amb el processat d'una única matriu de dades sintètica composta per la mescla dels 13 lípids. El tractament de les dades va ser qualitatiu ja que només es varen estudiar la recuperació i identificació de tots els lípids. Aquesta primera anàlisi va servir per observar com adquireix les dades l'equip UHPLC-ToF-MS emprat en aquesta Tesi i seleccionar els ROIs adequats, és a dir, aquells que donin pics amb forma gaussiana i un nombre i concentració de traces de masses suficient en una regió estreta. Per tal de realitzar una selecció correcta dels MSROI finals, es van ajustar els paràmetres a la vegada que s'observava el tipus d'adquisició que feia l'equip. Per exemple, es va assegurar no tenir una distribució aleatòria de les masses, dos pics en un mateix ROI, o pel contrari, un mateix pic dividit en dos ROIs. Finalment, es va inspeccionar que s'haguessin seleccionat les masses correctes i es van identificar els lípids de la mescla, separats de la resta de senyals provinents de la fase mòbil, impureses químiques de l'equip, senyal de fons o soroll restant, entre d'altres.

3.3.2. Demostració quantitativa

La capacitat **quantitativa** de la metodologia ROIMCR proposada va ser comprovada a partir de l'anàlisi de la matriu augmentada formada per tres rèpliques de cada mostra sintètica dels 13 lípids (Figura 1 b). Es va comprovar que tots els lípids van ser detectats pels seus ROIs i resolts adequadament amb el mètode MCR-ALS. Les àrees obtingudes de l'anàlisi ROIMCR serveixen per demostrar la reproductibilitat del mètode, obtenint uns coeficients de variació <14% per tots els lípids de la mescla.

La següent prova va ser l'anàlisi d'una matriu augmentada composta per 12 matrius individuals, incloent quatre concentracions diferents i tres replicats per a cada concentració (Figura 1c). Com a resultat es va obtenir una matriu augmentada composta per 12 x 638 = 7656 files amb un total de 512 valors de ROI. El resultat final d'aquesta anàlisi va ser primerament, l'obtenció dels valors de les àrees dels diferents lípids analitzats en funció de les diferents concentracions de les mescles i dels seus replicats corresponents. Aquestes àrees dels pics, van ser emprades en les corbes de calibratge respecte a les seves concentracions teòriques, utilitzant dos dels tres replicats que disposàvem. El tercer replicat va ser emprat per validar l'anàlisi quantitativa predictiva de les concentracions a partir de les àrees obtingudes dels lípids en les mostres no incloses en la corba de calibratge. Aquesta validació es va realitzar a partir de l'arrel quadrada de l'error quadràtic mitjà en les mostres de predicció (RMSEP) i dels errors relatius en les mostres de predicció. Aquests últims sempre van ser inferiors al 20%, la qual cosa es va considerar acceptable per a la quantificació dels lípids de les mostres analitzades a partir de la metodologia ROIMCR proposada. Prèviament, es va comprovar que la recta de calibratge acomplia els paràmetres de qualitat estadística de forma satisfactòria, possibilitant la posterior anàlisi predictiva de les concentracions dels diferents lípids.

Finalment, dins l'anàlisi ROIMCR quantitatiu, es va voler demostrar la seva resolució en matrius complexes com és la matriu composta per l'extracció de lípids de cèl·lules humanes enriquides amb la mescla sintètica de 13 lípids a diferents concentracions (Figura 1d). En aquest cas també es van resoldre i identificar tots els lípids de la mescla. Posteriorment amb les àrees ROIMCR resoltes es van realitzar les corbes de calibratge i

es va calcular l'arrel quadrada l'error quadràtic mitjà en les mostres de calibratge (RMSEC) i els errors relatius en les mostres de calibratge, obtenint sempre valors inferiors al 14% en l'anàlisi d' aquest grup de mostres.

3.3.3. Comparativa entre l'estratègia ROIMCR i el software XCMS

En aquest mateix estudi es va investigar el potencial de la metodologia ROIMCR en el tractament de dades òmiques, enfront d'altres softwares desenvolupats recentment en aquest camp. En particular l'estudi s'ha centrat en l'eina XCMS, que s'ha convertit en una de les més emprades actualment pel processat (detecció, resolució i identificació) de dades d'espectrometria de masses dins l'oferta de les plataformes online pel tractament de dades òmiques.[5-7] El mètode XCMS ha estat especialment dissenyat per a la detecció de senyals cromatogràfiques mitjançant un processat automatitzat de dades LC-MS en mode "full-scan" que permet estimar la presència dels metabòlits i/o lípids rellevants presents en la mostra.

Aquestes plataformes online realitzen l'anàlisi de dades LC-MS òmiques de forma bastant automatitzada, tot i que també necessiten l'optimització d'alguns paràmetres relacionats amb el tipus d'equip LC-MS emprat per l'anàlisi. En el cas del programa XCMS, s'ha desenvolupat una eina d'optimització automàtica dels paràmetres de selecció de pic, anomenada IPO (Isotopologue Parameter Optimization).[8] Aquesta eina permet optimitzar els paràmetres de correcció dels temps de retenció i d'agrupació. La correcció dels temps de retenció s'aconsegueix minimitzant les diferències dels temps de retenció relatiu entre els diferents grups de pics. A més, l'agrupació de paràmetres s'optimitza pel màxim nombre de combinacions de pics (grups de pics) de les diferents mostres que presentin masses i temps de retenció similars. Tots aquests pre-processats automàtics permeten el processat de les dades òmiques, però ho fan de forma desconeguda per part de l'usuari (tipus caixa negra) i no es coneixen exactament quins han estat els diferents pre-tractaments aplicats. Tot això contrasta amb l'aplicació de l'estratègia ROIMCR proposada en aquesta Tesi, on es mostren i s'aprecien clarament tots els passos i tractaments realitzats que permeten visualitzar

amb exactitud la forma i qualitat com s'adquireixen les dades dels equips LC-MS emprats.

Els resultats obtinguts en aquest estudi varen demostrar les similituds i diferències entre aquests dos procediments. Per tant, es pot concloure que la utilització del procediment XCMS, (implementat dins del programari MetaboNexus)[9], és més directe per a usuaris poc experimentats en el tractament de dades, encara que precisa d'eines d'alineament i modelat de pics no necessaris en el procediment ROIMCR. A més, quan s'aplica l'estratègia ROIMCR, les mostres són processades simultàniament i analitzades pel mètode MCR-ALS directament a partir d'una matriu augmentada que conté les dades LC-MS de totes les mostres, la qual cosa permet fer directament la comparativa quantitativa dels lípids resolts entre les diferents mostres analitzades. La realització d'aquesta comparativa entre l'estratègia ROIMCR i el software XCMS és important donat el gran nombre d'estudis amb aquesta plataforma de software online.

3.3.4. Comparativa entre l'anàlisi no dirigida i la dirigida

Per últim, es va realitzar la comparació dels resultats obtinguts emprant la metodologia ROIMCR amb els resultats extrets a partir d'una anàlisi dirigida**;** és a dir, integrant manualment aquells valors de *m/z* que sabíem que corresponien als compostos descrits prèviament (els 13 lípids de la mescla sintètica). Aquesta comparació es va realitzar amb el mateix conjunt de mostres biològiques enriquides amb la mescla de 13 lípids coneguts (cinc mostres individuals amb diferents concentracions de la mescla de lípids cadascuna), per tal de comprovar si existien diferències entre les dues aproximacions en el cas de mostres biològiques complexes. Com es pot apreciar en els resultats del treball d'aquest capítol, es va obtenir una bona correlació entre les àrees extretes seguint les dues estratègies, dirigida (integració manual) i no dirigida (processat ROIMCR). En el cas de l'anàlisi dirigida, la interferència del soroll era més gran degut a que no es va aplicar ni filtrar el senyal com si que s'aplica en el procediment ROIMCR a partir d'un valor llindar (*threshold*). Cal remarcar que encara que ambdós mètodes són igualment vàlids i proporcionen resultats similars, l'anàlisi no-dirigida permet descobrir nous compostos rellevants desconeguts i

les seves concentracions relatives en les diferents mostres. En molts casos també es detecten els adductes corresponents als nous compostos aïllats, fet que facilita la seva posterior identificació. En aquest estudi, es van comparar les àrees dels lípids detectats en les mostres biològiques mitjançant l'aproximació ROIMCR i les àrees obtingudes pels mateixos lípids mitjançant la seva integració manual. A partir dels resultats obtinguts es pot concloure que l'estratègia ROIMCR amb l'aproximació no-dirigida obté resultats similars als obtinguts amb l'aproximació dirigida. L'estratègia no-dirigida amb l'aproximació ROIMCR facilita a més, la recerca de nous biomarcadors a partir de LC-MS obtingudes. Aquests resultats poden ser de gran rellevància per a estudis futurs, obrint noves possibilitats en els estudis d'òmica mitjançant tècniques de cromatografia i d'espectrometria de masses.

3.3.5. Observacions finals

La metodologia ROIMCR presentada en aquest treball ha estat validada des d'un punt de vista qualitatiu i quantitatiu. Permet fer l'anàlisi no-dirigida de dades LC-MS, disminuint considerablement la seva complexitat i els temps d'anàlisi, sense perdre resolució ni informació espectral. L'anàlisi ROIMCR permet la resolució dels perfils d'elució i dels espectres de masses d'un gran nombre dels lípids presents en les mostres biològiques investigades, i realitzar la seva quantificació relativa en les diferents mostres analitzades.

La metodologia ROIMCR permet l'anàlisi de dades òmiques amb resultats qualitatius i quantitatius fiables. Cal destacar els següents aspectes d'aquesta metodologia:

- Extracció i identificació correcta dels lípids analitzats.
- Reproductibilitat del mètode, tant qualitativa com quantitativament.
- Calibratge de les concentracions dels lípids amb un bon coeficient de regressió, mostrant la quantificació dels lípids a les diferents concentracions proposades.
- Predicció de les concentracions dels lípids a partir dels valors de les seves àrees extretes.

- Verificació del bon funcionament del procediment ROIMCR en l'anàlisi de mostres biològiques complexes, tant a baixes com a altes concentracions de lípids.
- Resultats similars en l'anàlisi de dades òmiques amb la plataforma *open acces* (XCMS) i l'aproximació ROIMCR.
- Confirmació dels resultats de l'aproximació no-dirigida respecte a l'aproximació dirigida. Es troben els lípids que s'estudien en un anàlisi dirigit, a més d'un nombre considerable de nous lípids desconeguts abans de realitzar les anàlisis de les dades obtingudes amb el procediment ROIMCR.

En resum, es pot concloure que l'aplicació del mètode ROIMCR és una eina quimiomètrica potent i adequada per a l'anàlisi no-dirigida de dades provinents de LC-MS de manera qualitativa i quantitativa relativa de metabòlits i/o lípids en mostres sintètiques i biològiques.

3.4. Referències

1. Rohart, F.; Gautier, B.; Singh, A.; Le Cao, K. A., mixOmics: An R package for 'omics feature selection and multiple data integration. *PLoS Comput Biol* **2017,** *13* (11), e1005752.
2. Gant, T. W.; Sauer, U. G.; Zhang, S. D.; Chorley, B. N.; Hackermuller, J.; Perdichizzi, S.; Tollefsen, K. E.; van Ravenzwaay, B.; Yauk, C.; Tong, W.; Poole, A., A generic Transcriptomics Reporting Framework (TRF) for 'omics data processing and analysis. *Regul Toxicol Pharmacol* **2017,** *91 Suppl 1*, S36-S45.
3. Forsberg, E. M.; Huan, T.; Rinehart, D.; Benton, H. P.; Warth, B.; Hilmers, B.; Siuzdak, G., Data processing, multi-omic pathway mapping, and metabolite activity analysis using XCMS Online. *Nat Protoc* **2018,** *13* (4), 633-651.
4. Gorrochategui, E.; Jaumot, J.; Tauler, R., ROIMCR: a powerful analysis strategy for LC-MS metabolomic datasets. *BMC Bioinformatics* **2019,** *20* (1), 256.
5. Le Pogam, P.; Doue, M.; Le Page, Y.; Habauzit, D.; Zhadobov, M.; Sauleau, R.; Le Drean, Y.; Rondeau, D., Untargeted Metabolomics Reveal Lipid Alterations upon 2-Deoxyglucose Treatment in Human HaCaT Keratinocytes. *J Proteome Res* **2018,** *17* (3), 1146-1157.
6. Kozlowska, L.; Janasik, B.; Nowicka, K.; Wasowicz, W., A urinary metabolomics study of a Polish subpopulation environmentally exposed to arsenic. *J Trace Elem Med Biol* **2019,** *54*, 44-54.
7. Sivaram, A. K.; Subashchandrabose, S. R.; Logeshwaran, P.; Lockington, R.; Naidu, R.; Megharaj, M., Metabolomics reveals defensive mechanisms adapted by maize on exposure to high molecular weight polycyclic aromatic hydrocarbons. *Chemosphere* **2019,** *214*, 771-780.
8. Libiseller, G.; Dvorzak, M.; Kleb, U.; Gander, E.; Eisenberg, T.; Madeo, F.; Neumann, S.; Trausinger, G.; Sinner, F.; Pieber, T.; Magnes, C., IPO: a tool for automated optimization of XCMS parameters. *BMC Bioinformatics* **2015,** *16*, 118.
9. Huang, S.-M.; Toh, W.; Benke, P.; Tan, C.; Ong, C., MetaboNexus: an interactive platform for integrated metabolomics analysis. *Metabolomics $V 10* **2014,** (6), 1084-1093.

Capítol 4.
Estudi dels efectes dels disruptors endocrins i els mecanismes lipídics de la EMT en cèl·lules de càncer de pròstata DU145

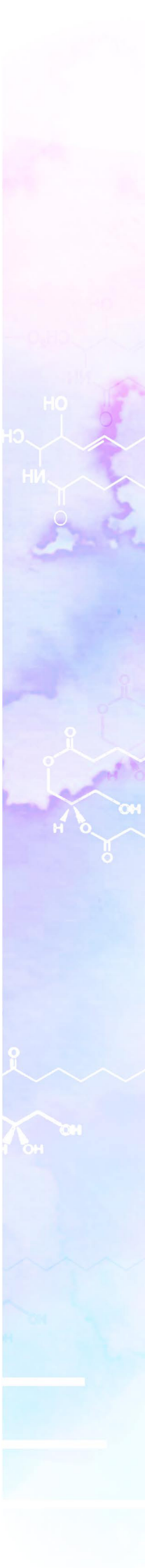

4.1. Introducció

Dins d'aquest capítol s'inclouen dos treballs centrats en l'estudi sobre l'efecte de diferents estímuls externs en el fenotip i el lipidoma de les cèl·lules de càncer de pròstata DU145. En el primer treball es van caracteritzar els efectes de l'exposició crònica a tres disruptors endocrins (Aldrin, Aroclor 1254 i Clorpirifòs) en el fenotip i lipidoma d'aquestes cèl·lules. En el segon treball es va aprofundir en l'estudi lipidòmic de les cèl·lules durant la transició epitelial mesenquimal (EMT) induïda per la citoquina inflamatòria TNFα.

Els disruptors endocrins (DEs) es consideren contaminants tòxics ambientals que interfereixen en el metabolisme normal hormonal de l'organisme. Els DEs estan presents en pesticides, la indústria dels plàstics, productes de neteja i en molts subproductes de l'industria. El major mecanisme d'exposició als DEs és a través de l'alimentació, ja que molts d'ells són bioacumulables i segueixen presents dins la cadena tròfica. Nombrosos estudis han relacionat les exposicions a DEs com a causa d'iniciació o desenvolupament de càncer, inclòs el càncer de pròstata.[1-2] En aquest treball s'han seleccionat tres DEs per realitzar l'estudi crònic de 50 dies: l'Aldrin, l'Aroclor 1254 (Aroclor) i el Clorpirifòs (CPF), explicats extensament en la Introducció. En el moment de la realització del treball no existien estudis realitzats sobre els efectes de disruptors endocrins en cèl·lules de càncer de pròstata, a nivell de fenotip i composició lipídica. En aquest estudi es va fer servir l'exposició crònica de les cèl·lules per poder fer una simulació d'un contacte amb els DEs seleccionats de manera perllongada en el temps i així poder establir una relació entre l'exposició i l'aparició d'un fenotip potencialment maligne en les cèl·lules de càncer de pròstata.

L'aparició de la transició epitelial mesenquimal (EMT) com a resultat de l'exposició a l'Aldrin, i els resultats satisfactoris obtinguts després de l'estudi lipidòmic no dirigit dut a terme en aquest primer treball, van donar peu a la segona part d'aquest capítol, és a dir, a l'estudi en més profunditat dels canvis lipidòmics que esdevenen durant la EMT. Aquest fenomen, essencial en múltiples funcions biològiques com el desenvolupament embrionari, la remodelació de teixits o la cicatrització de ferides, mai abans havia estat estudiat des del punt de vista dels lípids. L'anàlisi no dirigit va permetre conèixer els

canvis més importants que es produeixen en aquesta transició, el que suposa una contribució en l'estudi de la progressió del càncer.

Aquest capítol inclou les publicacions:

Publicació II. *Phenotypic malignant changes and untargeted lipidomic analysis of long-term exposed prostate cancer cells to endocrine disruptors.* C. Bedia, N. Dalmau, J. Jaumot, R.Tauler. *Envriron Res* **2015**, 140, 18-31

Publicació III. *Epithelial-to-mesenchymal transition involves triacylglycerol accumulation in DU145 prostate cancer cells.* N. Dalmau, J. Jaumot, C. Bedia, R.Tauler. *Mol Biosyst* **2015**, 11(12), 3397-3406

4.2. Publicació II

Phenotypic malignant changes and untargeted lipidomic analysis of long-term exposed prostate cancer cells to endocrine disruptors.

C. Bedia, N. Dalmau, J. Jaumot, R.Tauler.

Envriron Res **2015**, 140, 18-31

Environmental Research 140 (2015) 18–31

Contents lists available at ScienceDirect

Environmental Research

journal homepage: www.elsevier.com/locate/envres

Phenotypic malignant changes and untargeted lipidomic analysis of long-term exposed prostate cancer cells to endocrine disruptors

Carmen Bedia*, Núria Dalmau, Joaquim Jaumot, Romà Tauler

Department of Environmental Chemistry, Institute of Environmental Assessment and Water Research (IDAEA-CSIC), c/ Jordi Girona 18-24, 08034 Barcelona, Spain

ARTICLE INFO

Article history:
Received 4 February 2015
Received in revised form
5 March 2015
Accepted 16 March 2015
Available online 29 March 2015

Keywords:
Endocrine disruptors
Chronic exposure
Untargeted lipidomics
Prostate cancer
Chemometrics

ABSTRACT

Endocrine disruptors (EDs) are a class of environmental toxic molecules able to interfere with the normal hormone metabolism. Numerous studies involve EDs exposure to initiation and development of cancers, including prostate cancer. In this work, three different EDs (aldrin, aroclor 1254 and chlorpyrifos (CPF)) were investigated as potential inducers of a malignant phenotype in DU145 prostate cancer cells after a chronic exposure. Epithelial to mesenchymal transition (EMT) induction, proliferation, migration, colony formation and release of metalloproteinase 2 (MMP-2) were analyzed in 50-day exposed cells to the selected EDs. As a result, aldrin and CPF exposure led to an EMT induction (loss of 16% and 14% of E-cadherin levels, respectively, compared to the unexposed cells). Aroclor and CPF presented an increased migration (134% and 126%, respectively), colony formation (204% and 144%, respectively) and MMP-2 release (137% in both cases) compared to the unexposed cells. An untargeted lipidomic analysis was performed to decipher the lipids involved in the observed transformations. As general results, aldrin exposure showed a global decrease in phospholipids and sphingolipids, and aroclor and CPF showed an increase of certain phospholipids, glycosphingolipids as well as a remarkable increase of some cardiolipin species. Furthermore, the three exposures resulted in an increase of some triglyceride species. In conclusion, some significant changes in lipids were identified and thus we postulate that some lipid compounds and lipid metabolic pathways could be involved in the acquisition of the malignant phenotype in exposed prostate cancer cells to the selected EDs.

1. Introduction

Prostate cancer is the most commonly diagnosed visceral neoplasm and the second leading cause of cancer deaths in American men Jemal et al., (2008). Also, benign prostatic hyperplasia is a common benign neoplasm occurring in approximately 50% of men around 60 years. The initiation and progression of prostate cancer are still not well understood, but inappropriate levels of steroid hormones have been proposed to induce prostate carcinogenesis (Yeh et al., 2014; Prins et al., 2007).

In the context of a potential role of the environment in cancer development and progression, endocrine disruptors (EDs) have been an important subject of study. EDs are a class of environmental toxicants that interfere with the synthesis, secretion, transport, action or elimination of natural hormones. EDs are present in various commodities such as pesticide mixtures, plastic industry, cleaning and personal care products, industry sub products, and drugs. The major mechanism of exposure to EDs is food, as most of them bioaccumulate and are still present in the food chain. Many studies have evidenced that exposure to these chemicals in utero and during early life could result in birth defects, behavioral disorders, and cancer (Knower et al., 2014; Jeng, 2014; Kajta and Wojtowicz, 2013). In the case of prostate cancer, some epidemiological and animal-based studies suggest a direct association between EDs exposure and prostate cancer risk (Prins, 2008). Among all the EDs, three molecules have been chosen to carry out this work: aldrin, Aroclor 1254 and chlorpyrifos (CPF).

Aldrin is a chlorinated hydrocarbon molecule used as an insecticide on crops until 1970 and later used for killing termites until 1987 in the U.S. Other countries banned its use years later.

Abbreviations: BPA, bisphenol A; CE, cholesteryl esters; CL, cardiolipin; CPF, chlorpyrifos; DAG, diacylglycerol; EDs, Endocrine Disruptors; EMT, Endothelial-Mesenchymal Transition; GSLs, glycosphingolipids; MCC, Matthews Correlation Coefficient; MCR, Multivariate Curve Resolution; MMP-2, metalloproteinase-2; PE, phosphatidylethanolamine; PC, phosphatidylcholine; PCBs, polychlorinated biphenyls; PLS-DA, Partial Least Squares Discriminant Analysis; SLs, sphingolipids; TAG, triacylglycerols; TIC, Total Ion Current Chromatogram; TNFα, Tumor Necrosis Factor Alpha; VIP, Variable Importance in Projection

* Corresponding author.
E-mail addresses: carmen.bedia@idaea.csic.es (C. Bedia), nuria.dalmau@idaea.csic.es (N. Dalmau), joaquim.jaumot@idaea.csic.es (J. Jaumot), roma.tauler@idaea.csic.es (R. Tauler).

http://dx.doi.org/10.1016/j.envres.2015.03.014
0013-9351/

In any case, aldrin is still present in the environment from these past uses. A recent epidemiological study has suggested that aldrin exposure is associated with increased risk of aggressive prostate cancer, (Koutros et al., 2013) although some other studies reported no causal relationship between aldrin exposure and human cancer risk (Hooker et al., 2014).

Polychlorinated biphenyls (PCBs) are stable, lipophilic compounds that accumulate in the environment and the food chain. Numerous studies have demonstrated a relationship between PCBs exposure and a variety of toxic effects, such as carcinogenicity, teratogenicity or reproductive toxicology in animals (Bell, 2014; El Majidi et al., 2014; Zani et al., 2013). Also, correlation between environmental and occupational exposures to PCBs and human prostate cancer has been reported (Kling et al., 1978; Hessel et al., 2004). Aroclor 1254, hereafter aroclor, is a mixture of 60 compounds representative of PCB environmental pollution. Several publications have demonstrated its ability to decrease sperm motility and count and to alter ventral prostate antioxidant system (Selvakumar et al., 2011; Murugesan et al., 2005). Also, a recent work reported a possible association between exposure to aroclor and the induction of a cell transformation process in rat prostate (Cillo et al., 2007).

Chlorpyrifos (CPF) is an organophosphate insecticide that acts on the nervous system of insects as an acetylcholinesterase inhibitor. Although it has been described as moderately toxic to humans, it remains one of the most widely used organophosphate insecticides. Exposure to CPF has been linked to neurobehavioral and neurodevelopmental effects (Saunders et al., 2012; Grandjean and Landrigan, 2014). Concerning prostate cancer, a very large prospective cohort study reported a correlation between chlorpyrifos exposure and prostate cancer risk in farmers (Alavanja et al., 2003).

DU145 is an androgen-independent prostate cancer cell line model, known to express estrogen receptor beta (ERβ) and lacking both estrogen receptor alpha (ERα) and androgen receptor (AR) (Linja et al., 2003; Guerini et al., 2005). Nevertheless, aldrin, aroclor and CPF have shown to interact with ERβ among other intracellular targets (Luft et al., 2009). This receptor has been implicated in mediating effects of EDs; (Kuiper et al., 1998) in the case of PCBs, for example, they induce a significant reduction of ERβ in anteroventral periventricular nucleus of brain rats (Salama et al., 2003).

Lipids are molecules that modulate cellular processes such as cellular differentiation, proliferation, apoptosis and senescence, and thereby contribute to the homeostatic control of tissue growth and vascularization. These functions have shown to be altered in tumor cells, to allow them to grow locally and to metastasize to distant sites (Schulze and Harris, 2012; Hanahan and Weinberg, 2000). Therefore, a malignant phenotype or transformation towards a metastatic profile should be reflected in a characteristic lipidic signature.

Although the ED contaminants above mentioned have been the subject of epidemiological, animal and cell studies that involve them in cancer risk and progression, the phenotypic changes of a long-term exposed prostate cancer cells to EDs and the potential roles of lipids in the development of these changes has been never reported. We hypothesized that these contaminants would induce malignant alterations in DU145 prostate cancer cells when used at non-toxic concentrations and long exposure times (50 days), and that these changes would be accompanied by alterations in lipid levels and composition. The aim of this research was to investigate the potential malignant changes in cell phenotype after the ED exposure and to characterize the lipid profile of cells that accompany these changes. The novelty of this work not only resides in the exploration of the malignant effects induced by the EDs from the lipid point of view, but also in the lipidomic analysis approach used to characterize these changes. In this study, an untargeted lipidomic analysis has been performed using chemometric analysis tools which enabled the exploration of LC-MS data without any previous pre-conceived idea about the lipid candidates. In contrast to the targeted lipidomic studies, in which only a limited number of predefined lipid-specific signals are investigated, the untargeted approach used in this work had the advantage that potentially offered the discovery of novel interesting lipid molecules and metabolic pathways involved in the phenotypic changes observed.

2. Materials and methods

2.1. Reagents

Aldrin, Aroclor 1254, CPF, bisphenol A (BPA), tumor necrosis factor alpha (TNFα), tetrazolium bromide salt (MTT), cell culture media and reagents were obtained from Sigma. Analytical grade methanol and chloroform were purchased from Merck and Carlo Erba, respectively. HPLC Gradient Grade acetonitrile was from Fischer Chemicals. Lipid standards were obtained from Avanti Polar Lipids.

2.2. Cell line and culture

DU145 prostate cancer cells were obtained from the American Type Culture Collection. This cell line was cultured in RPMI 1640 medium supplemented with 10% heat inactivated fetal bovine serum (FBS), 100 U/ml penicillin and 100 μg/ml streptomycin, at 37 °C in a humidified atmosphere containing 5% of CO2.

2.3. Treatment of cells

The solutions of all the contaminants were prepared at 10 mM in DMSO. The concentration used for the chronic exposure (1 μM) was chosen on the basis of the non-toxicity at 72 h, observed in an MTT cytotoxicity assay (data not shown). From the 10 mM solutions, intermediate solutions of 100 μM were prepared diluting the concentrated solutions with non-supplemented RPMI. The vehicle solutions were also prepared with the same amounts of DMSO. DU145 cells were seeded in a 6-well plate at density of 2×10^5 per well, and 20 μl of each solution was added in the corresponding well to a final volume of 2 ml of supplemented RPMI (final concentration of DMSO 0.01%). Cells were cultured in standard conditions and diluted every 3 days. Cultures were treated after every passage to complete the 50-day treatment.

2.4. MTT proliferation assay

Cell viability was determined by using the 3–(4,5-dimethylthiazol-2-yl)–2,5–diphenyltetrazolium bromide assay on 96-well plates, according to the manufacturer's instructions.

2.5. Wound healing assay

Cells originated from the 50-day treatment were seeded in 24-well plates at a density of 1×10^5 cells per well and left grown to be confluent. The cell monolayers were scraped with a sterile 100 μl tip to create a denuded area perpendicular to the red line previously drawn in the external face of the well bottom. Cells were washed twice with PBS and non-supplemented RPMI was added (500 μl/well). Pictures of line intersections were taken from each well using a lens magnifier (1 ×, Nikon SMZ1500) fitted with a digital camera (Nikon DS-Ri1), and then plates were placed again in the incubator for 16 h. After incubation, pictures of the same

wound areas were taken. Values of wound areas were calculated with ImageJ software, and the area differences between 0 and 16 h were used for comparison and interpretation of results.

2.6. Flow cytometry

This EMT analysis was performed following the recommendations previously reported by Strauss et al., (2013). Briefly, chronic treated cells were plated at a density of 5×10^4 cells per well in 12-well plates and left grown to confluence. Cells were harvested using PBS/EDTA for 5 min to preserve the E-cadherin in the cell membrane. Cells were washed twice, and cell pellets were stained with 20 µl/sample of anti CD324/E-cadherin conjugated to FITC (Life Technologies), according to the manufacturer's instructions. Samples were incubated on ice for 1 h, and then washed with 200 µl of PBS. Green fluorescence emission of 5000 cells were measured for each sample with a Guava flow cytometer (Millipore), using Incyte software (Millipore). Calculated values of mean green fluorescence of histograms were used to compare exposed and unexposed cells.

2.7. Colony formation in agarose

Each well of a 12-well plate was first coated with 1.5 ml of low gelling temperature agarose (Sigma) mixture (0.8% agarose diluted in supplemented RPMI). After the bottom layer was solidified, 1 ml of top agarose mixture (0.4% agarose in RPMI) containing 3000 cells, coming from exposed and unexposed cultures, was added, and plates were incubated for 3 weeks. At the end of incubation, plates were stained with a crystal violet solution (0.04% in 2% EtOH/PBS) and pictures were taken using a lens magnifier (1X, Nikon SMZ1500) fitted with a digital camera (Nikon DS-Ri1). Colonies were counted using ImageJ software.

2.8. Zymography

DU145 chronically exposed cells were seeded in a 96-well plate at a density of 2×10^4 cells per well. Four wells were used for each treatment: one well was used to analyze the presence of MMP-2 in the culture supernatants, the other three wells were used to carry out a MTT viability test in order to normalize zymography results to viable cells present in the culture. 24 h after seeding, culture media were aspired and changed for non-supplemented RPMI, and plates were incubated again for 24 h more. Then, culture supernatants were collected from one well and MTT test was performed on the rest 3 wells. The supernatants were centrifuged at 1300 rpm for 3 min and 10 µl of the supernatants (corresponding to approximately 10 µg of protein) were mixed with Laemmli buffer and electrophoresed on 10% SDS-polyacrylamide gel (PAGE) containing 1% of gelatin at 100 mM for 2 h. After washing with PBS, the gel was incubated with the renaturalizing solution (200 mM NaCl, 5 mM CaCl2, 5 µM ZnCl2, 0.02% NaN3, 2.5% Triton X-100 in 50 mM Tris HCl pH 7.5) for 1 h at room temperature. Then, the gel was briefly washed with water and then submerged in the reaction buffer (200 mM NaCl, 5 mM CaCl2, 5 µM ZnCl2, 0.02% NaN3 in 50 mM Tris HCl pH 7.5) for 16 h at 37 °C. The gel was then stained with a Coomassie Brilliant Blue (Sigma) solution (0.5% Coomassie, 30% MeOH and 10% acetic acid in deionized water) for 30 min, and destained with a destaining solution (30% MeOH, 10% acetic acid in deionized water). Gelatinase areas were detected as clear bands against the blue-stained gelatin background. Pictures were taken and bands were quantified using ImageJ software. MTT absorbance values were used to normalize results.

2.9. Analysis of CDH1 mRNA expression levels

Exposed and control cells were harvested at 85% confluence using a rubber scraper into 2 ml of ice-cold PBS. Cells were centrifuged at 1300 rpm for 3 min at 4 °C and cell pellets were washed twice with cold PBS. Total RNA was extracted using the NucleoSpin RNA kit (Macherey-Nagel). RNA quality was checked in an Agilent 2100 Bioanalyzer (Agilent Technologies). RNA (2 µg) were retrotranscribed to cDNA using Transcriptor First Strand Synthesis Kit (Roche) and stored at −20 °C. Quantitative PCR analysis was carried out with a LightCycler® 78 480 Real Time PCR System (Roche) using LightCycler 480 SYBR Green I Master® (Roche). The primers used in each reaction were as follows: *CDH1* forward 5′-TACACTGCCCAGGAGCCAGA-3′ and reverse 5′-TGGCACCAGTGTCCGGATTA-3′; *GAPDH* forward 5′-GCACCGTCAAGGCTGAGAAC-3′ and reverse 5′-TGGTGAAGACGCCAGTGGA-3′. The gene *GAPDH* was used as the endogenous control reference gene. The threshold cycle number (Ct value) of *CDH1* was normalized to the Ct value of *GAPDH* from the same sample, and the fold change in expression was calculated using the delta–delta Ct method (Livak and Schmittgen, 2001). Ct values were calculated by technical triplicates.

2.10. Lipid extraction and LC-MS analysis

Exposed and control cells were seeded in triplicate in 6-well plates at 2×10^5 cells per well. After 24 h, cells were harvested using a rubber scraper into 2 ml of ice-cold PBS. Cells were centrifuged at 1300 rpm for 3 min at 4 °C and cell pellets were washed twice with cold PBS. Samples were prepared twice to perform two types of lipid extraction: (1) extraction with chloroform/methanol (2:1) that contains intact lipids from the sample; and (2) extraction chloroform/methanol (1:2) with a saponification step that removes all the ester bonds of lipids, leaving the sample cleaner to detect sphingolipids (SLs). For the extraction type 1100 µl of deionized water were added to the cell pellets and the suspension was transferred to borosilicate glass test tubes with Teflon caps. Then, 250 µl of methanol and 500 µl chloroform were subsequently added. This mixture was fortified with internal standards of lipids (1,2,3–17:0 triglyceride, 1,3–17:0 D5 diacylglyceride, 17:0 cholesteryl ester, 17:1 lyso phosphatidylethanolamine, 17:1 lyso phosphoglyceride, 17:1 lyso phosphatidylserine), 200 pmol each. Samples were vortexed and sonicated until they appeared dispersed. Then, samples were evaporated under N2 stream and transferred to 1.5 ml eppendorf tubes after addition of 500 µl of methanol. Next, samples were evaporated again and resuspended in 150 µl of methanol. Finally, tubes were centrifuged at 10,000 rpm for 3 min and 130 µl of the supernatants were transferred to UPLC vials for injection. For the extraction type 2, sphingolipids were prepared as described (Merrill et al., 2005). Briefly, 100 µl of deionized water were added to the cell pellets and the suspension was transferred to borosilicate glass test tubes with Teflon caps. Then, 500 µl of methanol and 250 µl of chloroform were subsequently added. This mixture was fortified with internal standards of sphingolipids (N-dodecanoylsphingosine, N-dodecanoylglucosylsphingosine, and N-dodecanoylsphingosylphosphorylcholine), 200 pmol each. Samples were sonicated until they appeared dispersed, and then incubated overnight at 48 °C in a heating water bath. Next, tubes were cooled and 75 µl of 1 M KOH in methanol were added. After 2 h incubation at 37 °C, KOH was neutralized with 75 µl of 1 M acetic acid. Samples were then evaporated under N2 stream and transferred to 1.5 ml eppendorf tubes after addition of 500 µl of methanol. Samples were evaporated again and resuspended in 150 µl of methanol. Finally, the tubes were centrifuged at 10000 rpm for 3 min and 130 µl of the supernatants were transferred to UPLC vials for injection.

LC/MS analysis consisted of a Waters Acquity UPLC system connected to a Waters LCT Premier orthogonal accelerated time of flight mass spectrometer (Waters), operated in both positive and negative electrospray ionization mode. Full scan spectra from 50 to 1500 Da were acquired, and individual spectra were summed to produce data points each of 0.2 s. Mass accuracy and reproducibility were maintained by using an independent reference spray via the LockSpray interference. The analytical column was a 100 × 2.1 mm inner diameter, 1.7 mm C8 Acquity UPLC bridged ethylene hybrid (Waters). The two mobile phases were phase A: MeOH/H2O/HCOOH (74:25:1, v/v) and phase B: MeOH/ HCOOH (99:1, v/v); both contained 5 mM ammonium formate. The column was held at 30 °C.

2.11. Chemometric analysis of LC-MS data

Each UPLC-MS chromatographic run recorded for every sample resulted in a data file which was converted to CDF format by the Databridge program of MassLynx software. This data set was then imported to MATLAB computational environment which is a high-performance language for technical computing that has been successfully applied to chemometrics among many diverse disciplines (Cordella and Bertrand, 2014; Martinez et al., 2011; Gemperline 2006; Qiu and Plevritis, 2013). Using mzcdfread and mzcdf2peaks functions from the MATLAB Bioinformatics Toolbox, data was loaded into the MATLAB workspace and transformed to a data matrix using an in-house written routine which bins all values with an m/z resolution of 0.05. This import process generates data matrices containing mass spectra at all retention times in their rows and the chromatograms at all m/z values in their columns. Data matrices were then normalized taken into account the internal standards added and the protein content measured for each sample. This is an important step that enables a more reliable comparison between samples.

Two types of chemometric data analysis have been carried out in this work. The first type of data analysis was performed using total ion current (TIC) chromatogram data obtained in the analysis of every sample. The goal in this case was the exploratory analysis of samples to visualize their possible differences, to discern among treated and untreated samples. The second type of analysis implied the use of the full scan chromatographic data, i.e. all individual chromatograms at all measured m/z values. In this second deeper study, the goal was to characterize the investigated samples focusing in what where the lipids showing changes because of the exposure to the contaminants and to evaluate the significance of these changes. Further interpretation of lipidomic changes was then attempted from these results.

In the first case, for the initial exploratory analysis of exposed and unexposed samples, the mass values at each retention time were summed to obtain the TIC chromatogram of every sample. Next, two data matrices containing the TICs of exposed and unexposed samples were built up in both positive and negative ionization modes (24 rows corresponding to 6 samples of each of the three exposures and the control, and 662 columns corresponding to the retention times). Both TIC data matrices were baseline corrected using the asymmetric least squares algorithm (Eilers, 2003) and mean-centered. Then, matrices were analyzed using Partial Least Squares Discriminant Analysis (PLS-DA) to discriminate between exposed and unexposed samples to contaminants. PLS-DA is a supervised classification analysis tool that requires prior knowledge of class membership. This classification study was performed on matrices containing the normalized TICs of samples, in order to see if exposed and unexposed samples could be segregated by their lipidomic profiles.

In the second type of data treatment, every analyzed sample represented a full scan data matrix. Due to the huge dimensions of these data matrices (e.g. 662 retention times (rows) × 35000 m/z values (columns)), each individual sample data matrix was subdivided in twelve time windows. Windows were not equal sized; narrow divisions were made in chromatographic zones were peak signals were more abundant. Every data matrix corresponding to the same time window but to different sample was then adjoined in a single column-wise augmented data matrix (see previous works), (Farrés et al., 2014; Gorrochategui et al., 2015; Lima et al., 2014) containing the six exposed and six unexposed samples. Additionally, these twelve new augmented data matrices were scaled using an adaptation of the MinMax transformation, also known as feature scaling, in order to favor the resolution of lipid profiles present at low concentrations. MinMax procedure rescales each column of the raw data matrix by subtracting the minimum value to each element of the column and dividing the result by the range of the column. In order to avoid unwanted noise effects, only values clearly above the noise level of each data matrix were considered. Then, the twenty-four data matrices generated (twelve raw and twelve scaled) for each exposure were subjected separately to multivariate curve resolution-alternating least squares (MCR-ALS) (Jaumot et al., 2005) data analysis. MCR-ALS is a powerful chemometric tool for the resolution of overlapping multivariate signals and for the bilinear decomposition of two and multi-way data arrays of different complexity and structure (Tauler 1995; Pere-Trepat et al., 2005). This method has been successfully applied for the resolution of extensive LC-MS data sets with strongly coeluted and hidden peaks in recent -omic studies (Farrés et al., 2014; Gorrochategui et al., 2015). Application of MCR-ALS to the windowed augmented data matrices resulted in the resolution of a number of components, each one represented by a dyad of profiles that described their chromatographic time elution and their mass spectra profiles. From the relative areas of these MCR-ALS resolved elution profiles, it is possible to estimate the relative amounts of components in every analyzed sample. However, only those components with significant differences in their elution profile peak areas between exposed and unexposed samples were then finally considered for further analysis. Although their MCR-ALS resolved MS spectra profiles at 0.05 m/z resolution may already allow a preliminary identification of the involved lipid, a more exact identification is possible using original raw data of samples (Farrés et al. 2014, Gorrochategui et al., 2015). Exact mass at the mass spectrum read by the instrument at the selected times of the peak maxima of the MCR-ALS resolved elution profiles can be searched in the original instrument files using the MassLynx software. The corresponding elution peaks at these m/z values were subsequently integrated in order to obtain an accurate estimation of the amount of each lipid (identified by its m/z value) in each sample. This is extremely useful in the case of considering scaled data in which each MCR-ALS resolved component could present a relatively high number of candidate m/z values and assignation of MCR-ALS resolved area to a particular peak is not straightforward. The calculated areas were then normalized to protein content and the internal standards specifically added in each type of extraction. For the identification of compounds, both a home-made database of lipids built using the same chromatographic conditions described above, and also external databases available on-line such as LipidMaps (Sud et al., 2007) and Human Metabolome Database (Wishart et al., 2013) were used. The assigned compound corresponded to the lipid molecule with the minimum mass error value respect to the measured m/z, considering the possible adducts in the corresponding ionization modes. The lipid annotated also had to fulfill an adequate retention time regarding its polarity. Fold change was calculated from the arithmetic mean values of each group. To check whether the differences observed in lipid peak areas between exposed and unexposed samples were statistically significant, a Welch's *t*-test

was used. Additionally, a discriminant analysis with PLS-DA was applied to the data matrix containing the integrated and normalized values of the selected peak areas for each sample (X-data). PLS-DA y-vector had the class labels, unexposed (class 0) and exposed (class 1) cells to the specific EDs. This peak areas data matrix was autoscaled before PLS-DA. Results were cross-validated by the leave-one-out method. The Matthews Correlation Coefficient (MCC) (Matthews, 1975) was calculated to validate the goodness of each discrimination model. The MCC is a correlation coefficient between the observed and predicted binary classifications; the returned values are between -1 and $+1$. A coefficient of $+1$ indicates a perfect prediction, a value of 0 indicates no better classification than a random prediction and a value of -1 represents total disagreement between prediction and observation. In the PLS-DA model obtained, the Variable Importance in Projection (VIP) scores, (Wold et al., 2001) which estimate the importance of each variable in the projection used in a PLS model, were calculated to investigate which were the most influent lipids in the discrimination of samples. Only identified compounds with VIP values greater than one and statistically significant in the Welch's *t*-test ($p < 0.05$) were finally selected for further interpretation of lipidomic results.

2.12. Statistical analysis

Results are expressed as mean ± SD of three independent experiments unless otherwise specified. One-way ANOVA analysis of variance was used to assess the difference of means among groups in the biological assays. Two-way ANOVA and Tukey's multiple-comparison test have been used for the analysis of variance in the proliferation tests.

2.13. Software

Software used in this work includes MassLynx V 4.1 (Waters) for raw UPLC-TOF data analysis. For matrix data processing and statistical analyses, Bioinformatics Toolbox (The Mathworks Inc.), Statistics ToolBox (The Mathworks Inc.), PLS-Toolbox (Eigenvector Research Inc.) and MCR-ALS Toolbox (Jaumot et al., 2015) were used in MATLAB 8.3.0-R2014a (The Mathworks Inc.) environment. ImageJ (National Institutes of Health) was used for image processing and analysis.

3. Results

3.1. Malignant phenotypic changes induced by chronic exposure to endocrine disruptors

DU145 prostate cancer cells were exposed to varying concentrations (0.8–100 μM) of aldrin, aroclor and CPF to determine their cytotoxicity over 72 h (data not shown). The concentration 1 μM (as non-lethal concentration) was selected to perform the chronic exposure of cells to the EDs. DU145 cells were exposed to the indicated doses of contaminants for 50 days under standard cell culture conditions. After chronic treatment, cultured cells were subjected to several biological assays in order to assess potential changes in the DU145 cell line that suggest the acquirement of an aggressive phenotype.

3.1.1. Epithelial-mesenchymal transition

Epithelial-mesenchymal transition (EMT) is an essential process in cell biology involved in embryonic development, tissue remodeling and wound healing. During the EMT process, epithelial cells reduce their intercellular adhesion and increase their invasive and migratory properties. Recently, EMT has been shown to play a

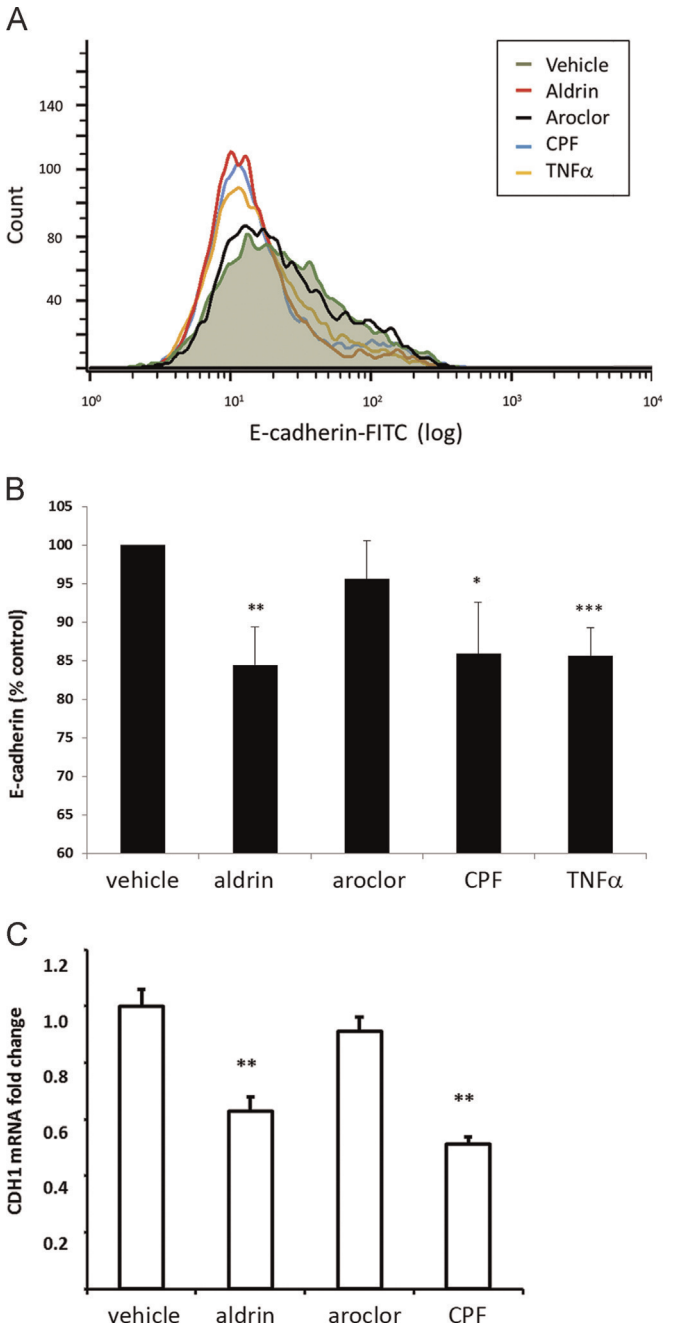

Fig. 1. Analysis of EMT by E-cadherin measurement. (A) Representative histograms of the E-cadherin flow cytometry assay. 50- day exposed and unexposed DU145 cells to aldrin, aroclor, CPF (1 μM each) and TNFα (10 ng/ml) were stained with the antibody anti-E-cadherin-FITC for 1 h. Green fluorescence emission of 5000 cells was measured for each sample. (B) Bar diagram representation of mean green fluorescence percentages respect unexposed cells (vehicle). Results are represented as the mean ± SE of four independent experiments ($n=4$) performed in duplicate. (C) Real-time quantitative PCR analysis of *CDH1* expression. Ct values were normalized to the Ct value of *GAPDH* from the same sample, and fold change expression was obtained using the delta–delta Ct method. Results are represented the mean ± SE of three independent experiments ($n=3$) performed in triplicate. * $p < 0.05$, ** $p < 0.01$, *** $p < 0.005$.

crucial role in tumor invasion and metastasis (Thiery et al., 2009). In order to assess the induction of EMT in our exposed cell cultures, a flow cytometry assay was performed to detect the presence of E-cadherin in the cell membrane, (Strauss et al., 2013) of which loss is an indicator of the process. In this assay, 50-day treated cells with TNFα (1 ng/ml), a cytokine that induces EMT, (Wang et al., 2013; Bates and Mercurio, 2003) was used as a

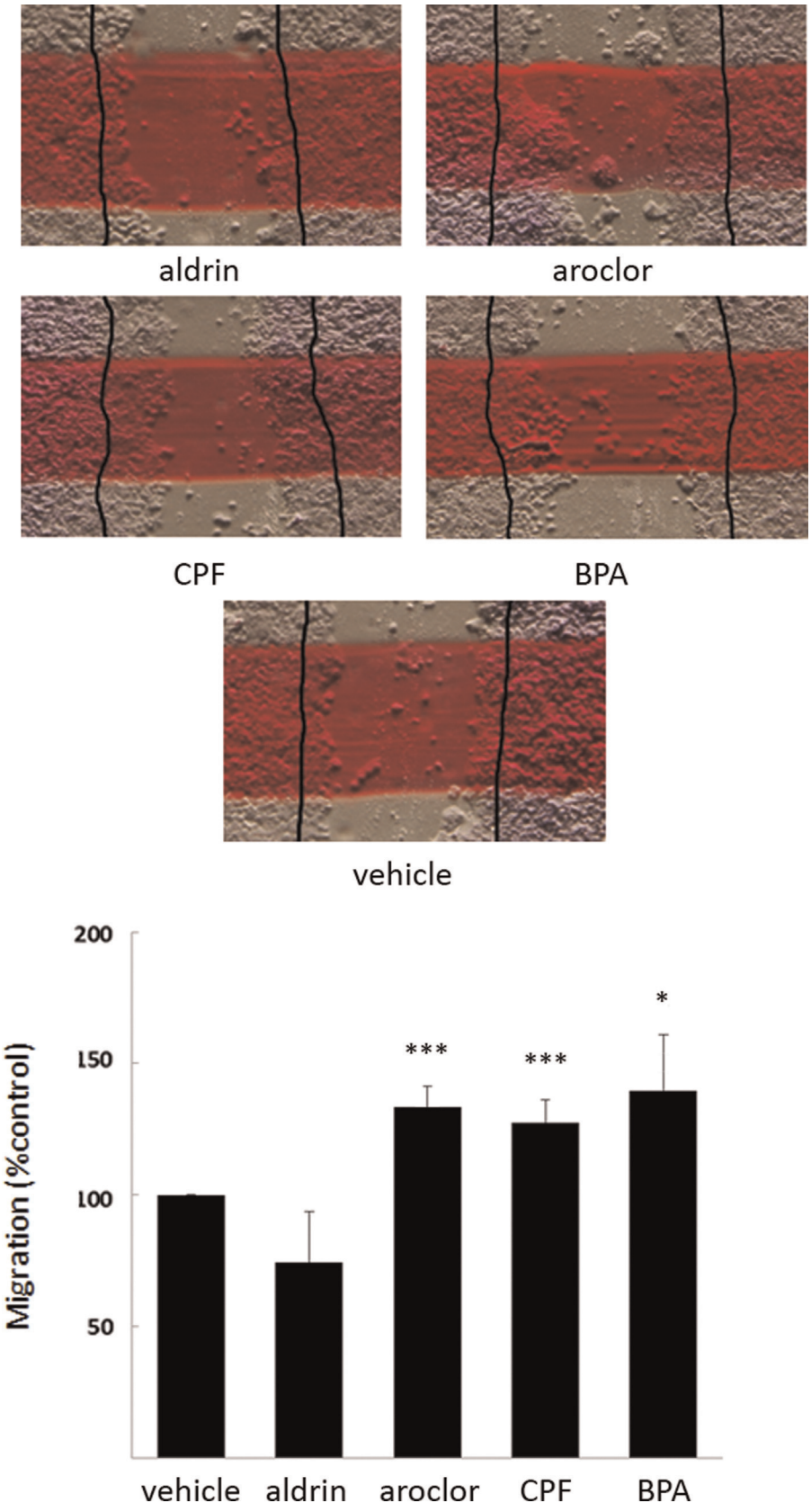

Fig. 2. Effect of chronic exposure to EDs on cell migration. Cell migration was assessed by the wound healing assay. Cell monolayers of 50-day exposed and unexposed cells (vehicle) were scratched with a pipette tip, crossing the red line drawn on the bottom of the cell plate. Cells were washed with PBS and pictures of the wounds were taken at 0 h and after 16 h of incubation under non-supplemented media. Bold lines on each picture show the original edge of the scratched area at 0 h. Bar diagram represents the percentage of cell migration respect to the control. Results are represented as mean ± SE of three independent experiments ($n=3$) performed in triplicate. *$p < 0.05$, **$p < 0.01$, ***$p < 0.005$.

positive control. As depicted in Fig. 1, our results showed that aldrin and CPF exposed cells reduced their E-cadherin levels significantly (84% and 86% of E-cadherin out of control, respectively) in a similar degree to TNFα treated cells (86%). This indicated that aldrin and CPF can induce cell changes leading to a mesenchymal-like phenotype, comparable to those induced by a chronic treatment of low TNFα doses. In contrast, aroclor exposure resulted in similar levels of E-cadherin compared to the control, indicating that aroclor was not inducing EMT under chronic exposure. These results were corroborated by a significant decrease in *CDH1* transcript in aldrin and CPF exposed cells (63% and 51% out of control, respectively) but not for aroclor treated cells.

3.1.2. Migration of cells

In order to escape the tumor, enter the circulation and establish secondary growth in distant organs, cancer cells must develop an enhanced propensity to migrate. A wound healing assay was performed to investigate the migration and motility abilities of contaminant exposed cells on confluent cultures of treated and control cells. Recently, bisphenol A (BPA), an endocrine disruptor

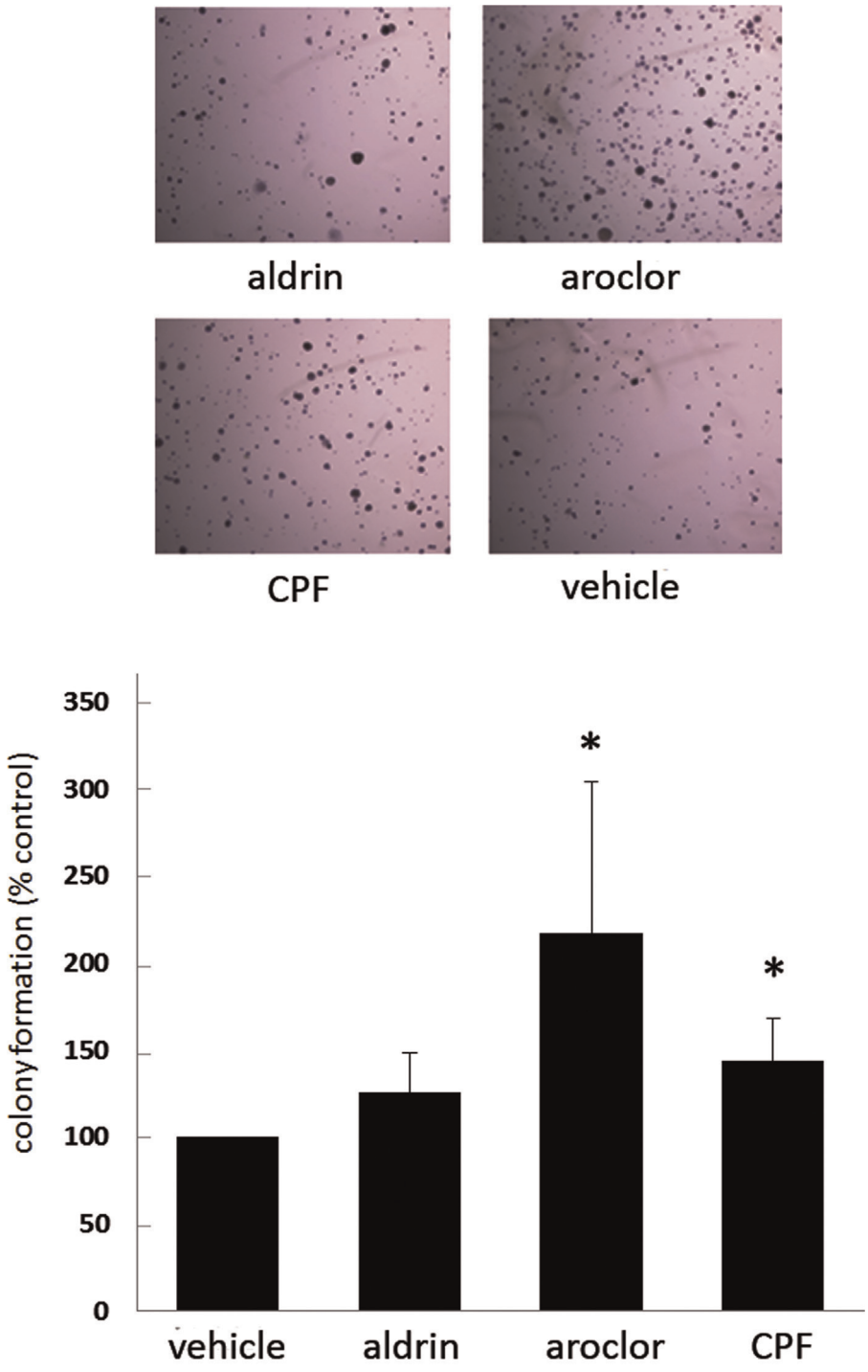

Fig. 3. Soft agar colony formation assay. Three thousand cells coming from unexposed and exposed cell cultures to the different EDs were seeded in 12-well agarose plates (0.35% agarose) and incubated for 3 weeks. Representative pictures of crystal violet stained colonies are shown, bar diagram represents the percentage of colonies formed respect to the unexposed cells (vehicle). Results are expressed as the mean of three independent experiments ($n=3$) performed in duplicate for each exposure. $^{*}p < 0.05$.

employed in the plastics industry known to be involved in prostate carcinogenesis (Prins et al., 2014; Tarapore et al., 2014), has been demonstrated to induce cell migration in prostate cancer cells (Derouiche et al., 2013). Therefore, to conduct this assay, 50-day treated cells with BPA (1 μg/ml) were used as positive control for migration. As a result, aldrin treated cells did not show migration compared to untreated cells (Fig. 2). However, aroclor and CPF treated cells showed a significant increase in the coverage of the wounds (134% and 126% out of control, respectively) compared to untreated cells and at a similar degree to BPA treated cells (140% out of control). This suggests that these exposures increase the pro-metastatic behavior of cells necessary to escape from tumor solid mass.

3.1.3. Colony formation

Anchorage-independent formation (colony formation) is also indicative of an aggressive phenotype. Cells were seeded in an agarose layer to prevent cell–cell interaction and attachment. Colony number was obtained by photographing and counting after 3-week incubation. As it is shown in Fig. 3, aldrin treatment resulted in no increase in colony number compared to control. However, a significant increase in colony number formation was observed for aroclor and CPF (204% and 144% out of control, respectively). Such observations suggest that both CPF and aroclor promoted an anchorage-independent survival of cells, which is associated with a metastatic phenotype of cells.

3.1.4. Release of metalloproteinase 2

Matrix metalloproteinases (MMPs) are a family of enzymes found in the extracellular milieu of tissues which play important roles in degrading extracellular matrix in tumor invasion and metastasis. To assess changes in the release of MMP-2 to the cell media of exposed and control cells, the activity of MMP-2 was determined by zymography. As depicted in Fig. 4, among all the treatments, only aroclor and CPF showed a significant increase of active MMP-2 released to the media (37% in both cases). This reinforces the previous results suggesting that long-term exposure to these endocrine disruptors induces a malignant phenotype in DU145 prostate cancer cells.

3.1.5. Cell proliferation

The possibility of altered proliferation of exposed cells was explored. Cells were left to grow in 96-well plates at low confluences (125 cells/well) for 3, 6 and 9 days, and MTT viability test was performed. The results showed that all the exposed cells followed the same proliferation curve pattern that unexposed cells with no significant changes in their proliferation rates.

3.2. Lipidomic study of chronic exposition of DU145 cells to aldrin, aroclor and CPF

The lipidome profile of these exposed cultures was explored in order to characterize the changes in lipid species that accompany the malignant features observed.

The lipidomic study was performed on cell cultures exposed to aldrin, aroclor, CPF, and vehicle (6 samples/each). For each sample, two types of lipid extraction were performed: extraction (1) with chloroform/methanol (2:1) to recover most of the lipids from the sample; extraction (2) with chloroform/methanol (1:2) and a saponification step, to remove all the ester lipids from the sample favoring the recovery of sphingolipids (SLs). As described in the experimental section, samples were injected in a UPLC-MS instrument system and raw data was imported to MATLAB environment. First, a preliminary study on total ion current chromatograms (TICs) was carried out by PLS-DA giving the scores plotted in Fig. 5. In general, exposed samples were well separated from unexposed samples, especially in the positive ionization mode of type 1 lipid extraction injections (intact lipids) and in the negative ionization mode of type 2 lipid extraction injections (only sphingolipids, after saponification). Although in the latter case aroclor samples showed a not so clear separation from controls, MCC of this PLS-DA model was equal to 0.81 indicating a good classification of samples. These results suggested that the exposure to the different EDs induced changes in the lipidomic profiles of DU145 prostate cancer cells. Therefore, a deeper data analysis was performed to extract more exhaustive information about changes in specific lipid compounds and their possible interpretation. To do this, only data that allowed a good separation between exposed and control samples (positive ionization data from extraction type 1 and negative ionization data from extraction type 2) were used.

Full scan LC-MS data matrices containing all intensity values measured at different mass and retention times were analyzed by MCR-ALS. Selected mass peaks with statistically significant changes between exposed and unexposed samples were subsequently integrated using raw data files and identified as described in the methodology section.

A new matrix containing the areas of the different selected compounds in every sample (X-data) was constructed and subjected to a PLS-DA in order to confirm the separation of exposed

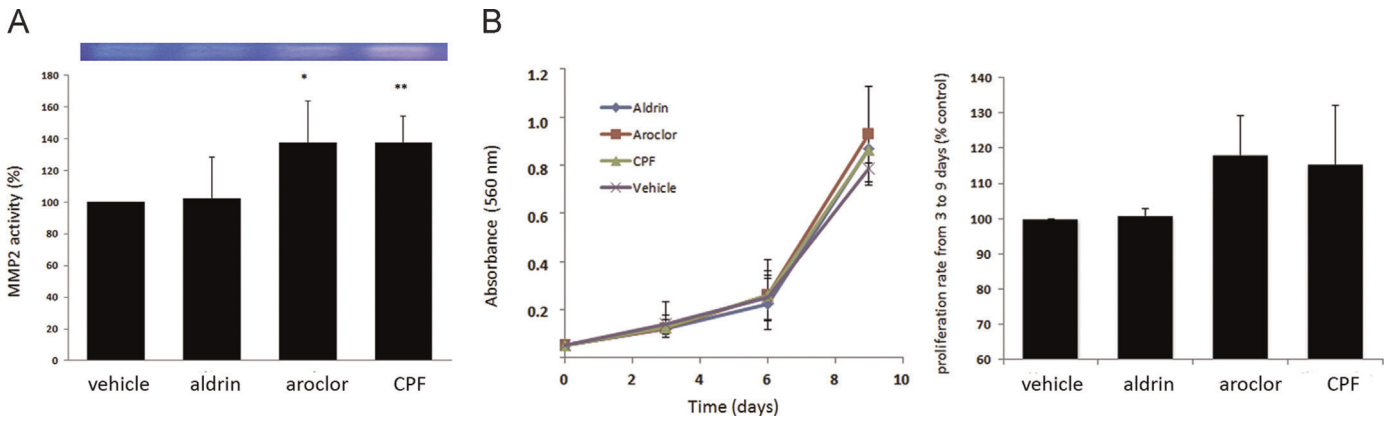

Fig. 4. MMP-2 activity and proliferation assays. (A) SDS-PAGE zymography of culture supernatants of unexposed and exposed cells to EDs. Representative picture of MMP-2 gelatin digestion of gel and bar diagram of percentages of MMP-2 activity respect to the unexposed cells (vehicle). Results are represented as mean ± SE of four independent experiments (n=4) performed in duplicate. *$p < 0.05$, **$p < 0.01$. (B) MTT proliferation assay of unexposed and exposed cell cultures to EDs. Left panel shows the proliferation curves for 9 days, right panel represents the proliferation rates from 3 to 9 days, referred to the unexposed cells rate. Results are represented as mean ± SE of three independent experiments ($n=3$) performed in quadruplicate.

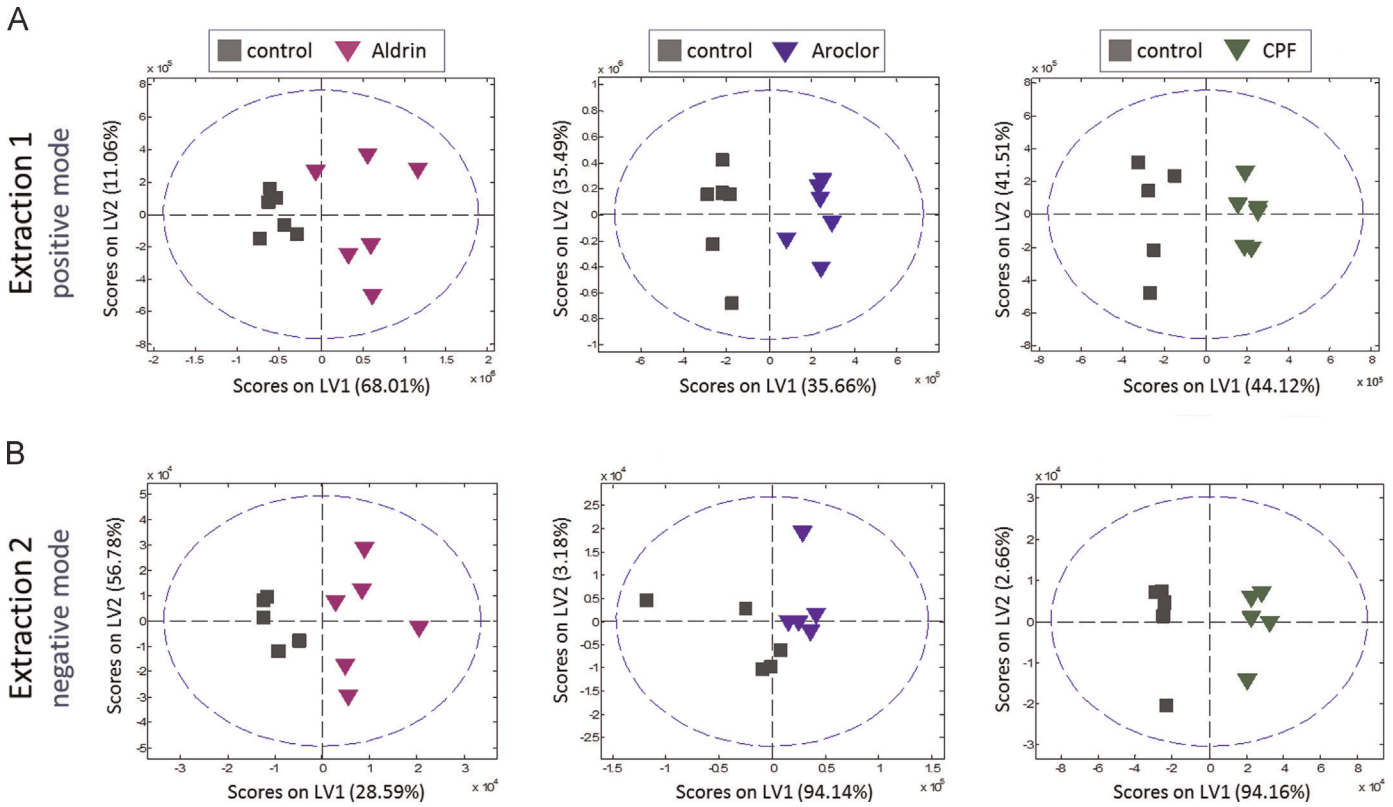

Fig. 5. PLS-DA sample scores of total ion chromatograms (TICs) obtained for EDs-exposed and unexposed cell cultures. Each exposure is compared to the unexposed cell samples. (A) PLS-DA scores plots of TICs in a positive ionization mode of samples coming from total extract of lipids (extraction 1), (B) PLS-DA scores plots of TICs in a negative ionization mode of samples coming from sphingolipid extraction (extraction 2).

and unexposed samples (Y-vector). PLS-DA scores obtained in the analysis are plotted in Fig. 6. For aldrin exposure results, one latent variable was enough to explain most of the Y-variance (90%) using 50% of X-variance (related to the peak areas changes), with an MCC equal to 1.0 (Matthews, 1975). In the case of aroclor exposure, 97% of Y-variance was explained by a 52% of X-variance using two latent variables and an MCC of 0.71. Finally, in the case of CPF exposure data, 89% of Y-variance was explained by a 70% of X-variance using two latent variables with an MCC of 0.67. These results seem to indicate that specific lipid molecules whose profiles were resolved in the MCR-ALS analysis presented significant changes in peak areas between exposed and unexposed samples to EDs, allowing their discrimination. PLS-DA VIP values greater than one indicated which X-variables and therefore, which lipid molecules, were more influent to discriminate between exposed and unexposed samples to EDs.

The complete detailed lists of the m/z values that presented a significant difference in their peak areas (p-value in the Welch's test less than 0.05) between unexposed and exposed cells to aldrin, aroclor and CPF can be consulted in Supplementary Table 1. This table includes the annotation of lipids, performed as described in the experimental section. For each m/z found, the corresponding chromatographic retention time, the name of the lipid, the calculated m/z, the mass error, the fold change, the p-value and the VIP value are detailed.

For a further analysis and biological interpretation of lipidomic results, only listed lipid molecules with a VIP score value greater than one and a mass error less than 10 ppm in lipid identification

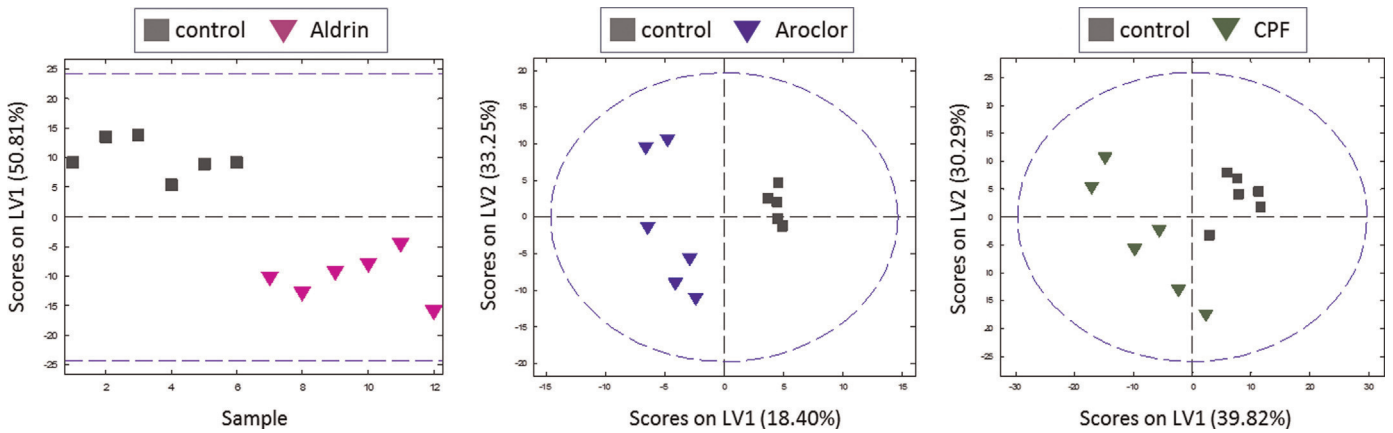

Fig. 6. PLS-DA scores plots of matrix containing MassLynx integrated peak areas of selected compounds in the different samples. Each exposure is compared to the unexposed samples data.

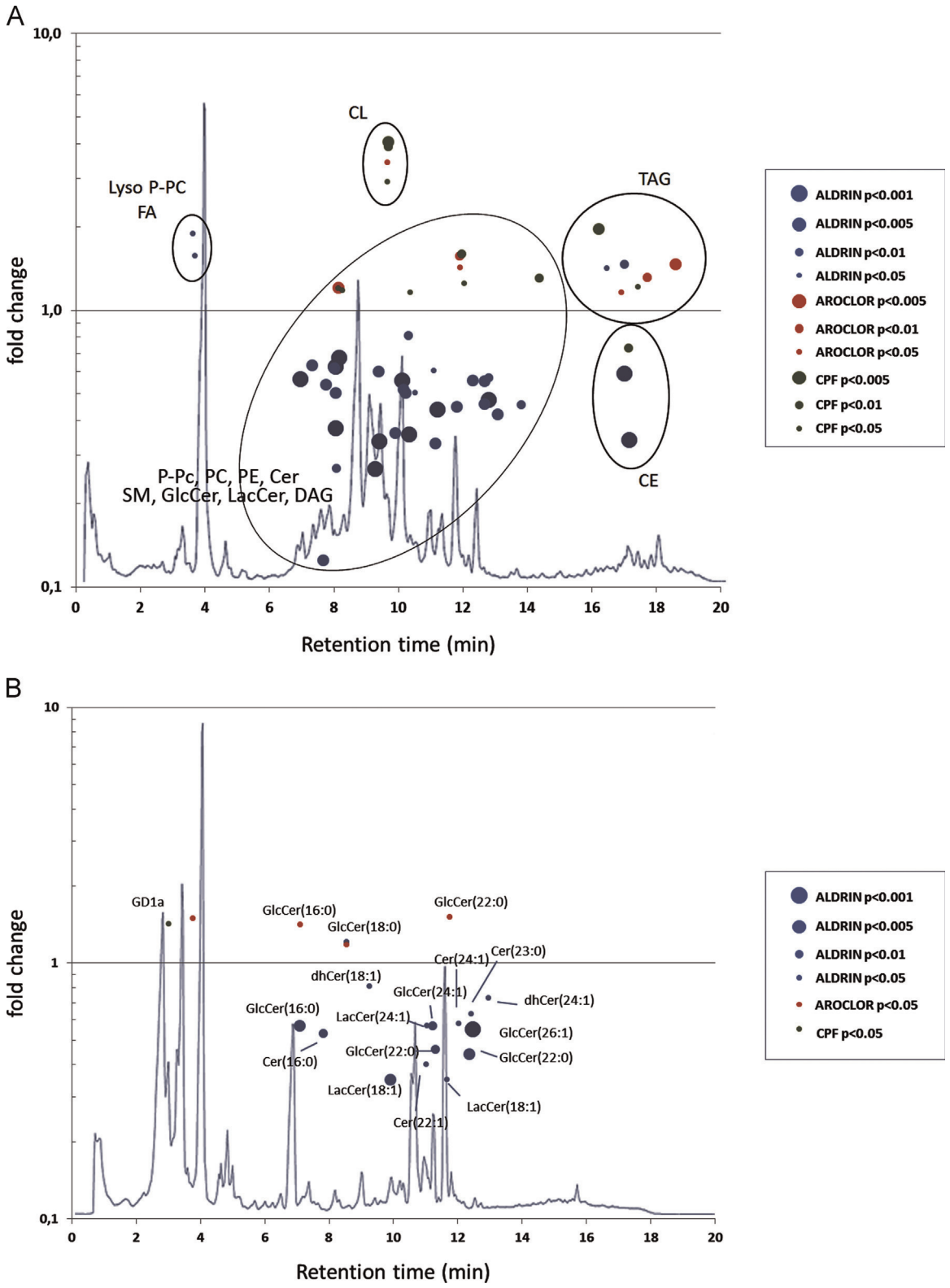

Fig. 7. Lipids species that present significant changes in the lipidomic profile of cells exposed to the different EDs, compared to unexposed cells. Graphical representation of lipids with significant changes along the chromatogram. Lipids from extraction 1 and 2 are represented in A and B pictures, respectively. *Y*-axis gives their fold change in logarithmic scale, and *x*-axis represents their chromatographic retention time. For more interpretability of results, some subclasses of lipids are enclosed in circles. The size of dots represent their *p*-value of statistical significance (bigger dot corresponds to higher significance). Only identified compounds with an m/z error < 10 ppm that meet the requirements of *p*-value < 0.05 and VIP value > 1 are represented in this figure and are used for further biological interpretation. CE: cholesteryl esters; Cer: ceramides; CL: cardiolipin; DAG: diacylglycerol; FA: fatty alcohol; GlcCer: glucosylceramides; LacCer: Lactosylceramides; P: plasmalogen; PC: phosphatidylcholines; PE:phosphatidylethanolamines; SM: sphingomyelins; TAG: triacylglycerols; THCer: trihexosylceramide.

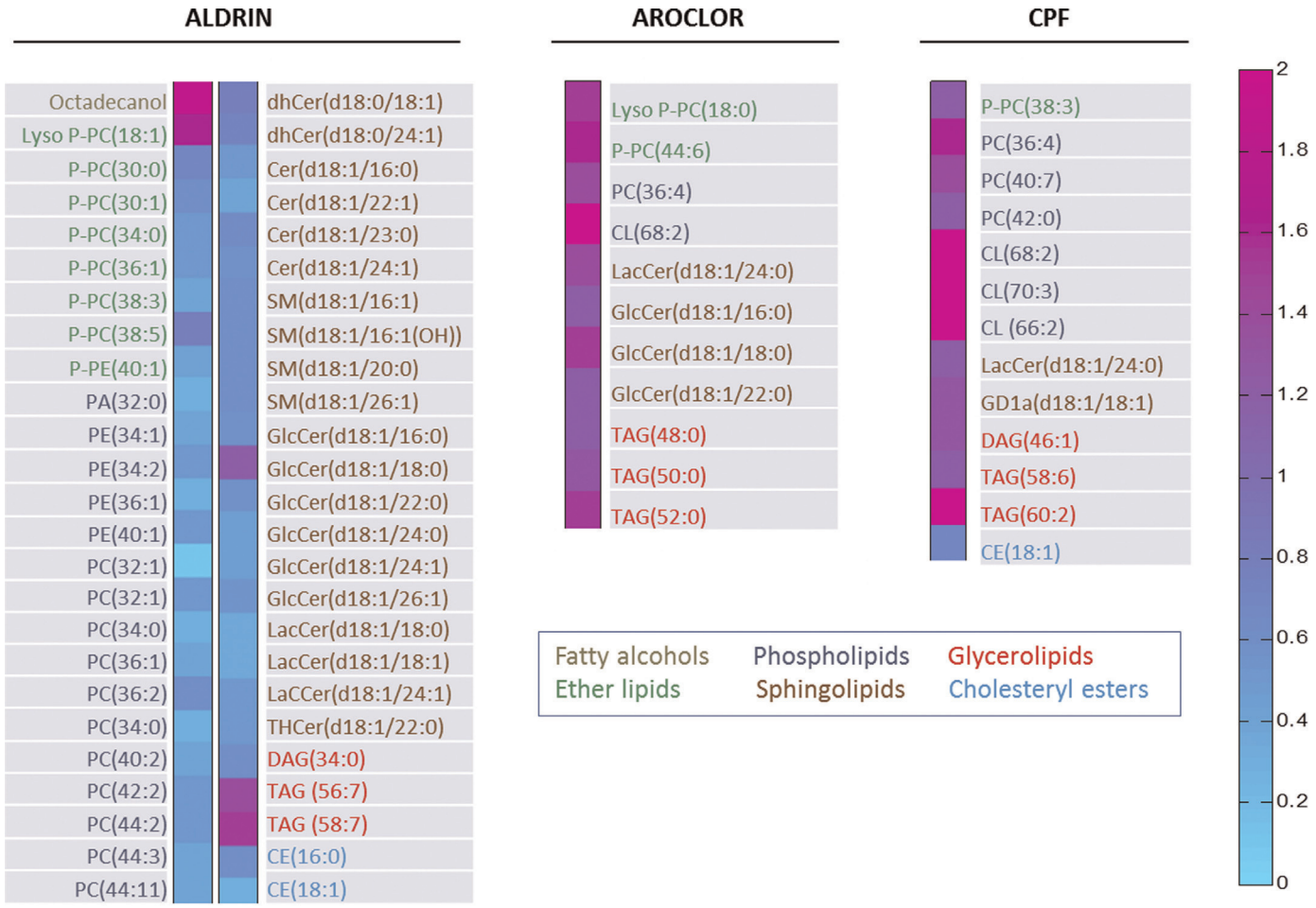

Fig. 8. Heat map of relative fold change of lipid species with significant changes in the lipidomic profile, under aldrin, aroclor and CPF exposure. Different colors in compound names correspond to the different lipid subclasses listed.

were considered. Among all the lipids listed, 50, 11 and 13 lipids fulfilled these requirements in aldrin, aroclor and CPF exposure samples, respectively. These selected lipids are represented in Fig. 7A (extraction 1) and 7B (extraction 2). In these figures, lipids from the three analyses are represented along of their corresponding chromatograms and their fold change in logarithmic scale is represented in the *Y*-axis. These plots allow a rapid overview of differences and similarities in relevant lipids (organized in lipid subclasses) between the three different exposures. For better understanding of results, Fig. 8 contains a list of the relevant lipids organized in subclasses together with a heat map representing their relative fold change under every exposure.

3.3. *Biological interpretation of lipidomic analysis*

In the case of aldrin exposure, a general decrease of phosphatidylethanolamines (PE), phosphatidylcholines (PC) and plasmalogen PC species of different length chain is observed. This could be due to the hydrolytic action of various phospholipases (A, C and D) leading to the formation of lipid second messengers. The hypothesis of an enhanced hydrolytic action is supported by the observation of increased levels of lyso plasmalogen PC (18:1) and the fatty alcohol octadecanol. Among the various phospholipases, phospholipase D has been demonstrated to have a critical role in many aspects of cell proliferation and metastasis (Foster and Xu, 2003). This enzyme catalyzes the hydrolysis of PC to choline and phosphatidic acid, a potent oncogenic signaling lipid involved in processes like growth signaling, proliferation, survival, migration, invasion and increased endothelial permeability (Bruntz et al., 2014). Also, saturated diacylglycerol (DAG (34:0)), cholesteryl esters (CE (16:0) and CE(18:1)) and SLs were reduced compared to unexposed cells. The specific extraction for SLs allowed the detection of a significant decrease in glycosphingolipids (GSLs, glucosyceramides, lactosylceramides and trihexosylceramide), sphingomyelins, dihydroceramides and ceramides of varying acyl chain length. The reduction of sphingomyelins and ceramides is in agreement with recent findings of Legembre group (Edmond et al., 2014) showing that EMT is involved in the decrease of C16 ceramide and C16 sphingomyelin production (through down-regulation of *CerS6*). Additionally, they demonstrate that increased levels of C16 ceramide prevented membrane fluidization and cell migration which are characteristic features of EMT. Besides its role in plasma membrane, ceramide is a well-known signaling lipid involved in anti-proliferative responses and programmed cell death, also known as apoptosis. According to this, the reduction of ceramide levels observed may be involved in an increase in cell survival, necessary for tumor progression. Ceramides are also the biosynthetic precursor of sphingomyelin and glucosylceramide, therefore, a loss of their natural substrate could explain the decrease in these species. In contrast, other lipids were significantly increased such as some unsaturated TAG. This increase is consistent with the recent work of Fhaner et al., (2012) which showed

a substantial increase of these species in a lipidomic study on SW620 metastatic colorectal cancer cell line, compared to SW480 cell line, its primary colorectal cancer counterpart.

Aroclor and CPF exposures to prostate cancer cells have resulted in lipidomic profiles very similar to each other. Both exposures showed an increase of certain PC and plasmalogen PC species. Also, as showed by aldrin exposure results, the levels of some TAG (saturated species for aroclor and unsaturated for CPF) were increased. Interestingly, both exposures shared a huge increase (from 3 to 4 fold) of cardiolipin species (CL (68:2) for aroclor and CL (66:2), CL (68:2) and CL (70:3) for CPF). CLs are a group of lipids found almost exclusively in the mitochondrial membranes of eukaryote cells. Recent research suggests that CLs exert control over the mitochondrial apoptotic pathway through the interaction with Bcl-2 family proteins (Zhang and Saghatelian, 2013). However, CL species and metabolites may have dual roles in apoptosis regulation as they have different affinities for the distinct Bcl-2 proteins and to other protein components of the apoptotic machinery, which could result in either promotion or inhibition of apoptosis. Regarding the SL species, both exposures presented changes in GSLs levels. Aroclor exposure led to a significant increase in three different glucosylceramide species of varying acyl chain length (16, 18 and 22 carbons). Also, both aroclor and CPF exposures had in common a significant increase of lactosylceramide (24:0). GSLs are plasma membrane components with the lipid portion embedded in the outer leaflet with the sugar chain extending to the extracellular space. GSLs are known to be implicated in many fundamental cellular processes and are also described as functionally crucial molecules in tumor cell attachment. Specifically, glucosylceramide has proliferative functions in various cells and plays an important role in the metastatic spread of tumor cells (Kartal Yandim et al., 2013). CPF also showed a significant increase of ganglioside GD1a. Gangliosides are acidic GSLs characterized by the presence of at least one sialic acid linked to their oligosaccharide chain. Cumulative evidence indicates that gangliosides have different roles in tumor progression such as angiogenesis, cell adhesion and motility and metastasis (Birkle et al., 2003). More specifically, GD1a is involved in cancer cell adhesion to endothelial cells during metastasis (Taki et al. 1997; Hatano et al., 2011).

4. Discussion

Even though the environmental and agricultural use of aldrin and PCBs is prohibited, residues are frequently found due to their persistence in the environment and bioaccumulation along the food chains. For instance, aldrin is still observed in human breast milk from developing countries (Yalcin et al., 2014) or in placenta of pregnant women from Southern Spain, (Lopez-Espinosa et al., 2007) meaning that these contaminants accumulate in body fats, which may have potential impact on human health. On the other hand, CPF is not a lipophilic compound but is a currently used pesticide in more than 80 countries, whose residues can be found in fruits and vegetables (Angioni et al., 2011). In this work, we have tested these compounds for 50 days using a dose which did not produce signs of lethality to DU145 prostate cancer cells. Some interesting changes in phenotype were observed, together with changes in lipid profiles.

DU145 exposure to aldrin caused a reduction of E-cadherin levels, characteristic of EMT phenotype, similar to that obtained under TNFα exposure, without a significant increase in colony formation, migration, proliferation or release of MMP-2. The lipidomic profile of these cells showed a global reduction of phospholipids and sphingolipids. On one hand, the decrease in phospholipid levels could have been due to an enhanced phospholipid hydrolysis by phospholipases leading to the release of the pro-oncogenic lipid PA. PA could have been in turn metabolized to other signaling lipids like lysophosphatidic acid (LPA) or diacylglycerol (DAG) both of which have second messenger functions that could have contributed to the effects observed (Mills and Moolenaar, 2003). In this context, interestingly, highly unsaturated DAG (40:9) was found elevated in the lipidomic analysis of the three studied exposures (see Supplementary Table 1), although this fact has not been mentioned in the results due to the high m/z error value found in the identification process. Due to the elevated fold changes and VIP values found in the analyses, this lipid and other highly unsaturated DAG will be further studied, focusing on its correct identification and its potential role in the acquisition of the malignant phenotype. On the other hand, the decrease in ceramide levels reduced the apoptotic signaling in cells. This reduction has been shown to be involved in the EMT process (Edmond et al., 2014). These both pathways are involved in tumor cell survival and progression any may reflect the incipient transformation of aldrin exposed cells.

Aroclor and CPF exposures resulted in similar phenotypic changes and lipid profiles. Both exposures induced cell migration, an increase in anchorage-independent survival and the release of MMP-2 to the extracellular milieu. However, only CPF was able to reduce E-cadherin levels on the cell membrane. Regarding the lipid profile of these cells, both presented an increase of certain PC and plasmalogen PC species, lactosylceramide (24:0), TAG and CLs. Interestingly, these last compounds showed the highest fold increase in the whole lipidomic study, suggesting an important role of certain CLs in the acquisition of a metastatic phenotype. CLs are considered bioactive lipids as they participate in the optimal functioning of oxidative phosphorylation enzymes such as ATP synthase and respiratory chain complexes (Dumas et al., 2013) present in the mitochondrial membrane. In addition, CL also supports conformational changes undergone by proteins of the Bcl-2 family, which has a role in the regulation of apoptotic cell death (Zhang and Saghatelian, 2013). Abnormalities in CL content have been already reported in mouse brain tumors (Kiebish et al., 2008) or breast cancer cells (Hardy et al., 2003). Moreover, a functional link between CL acyl chains composition (length and saturation) and cell proliferation has been suggested (Schild et al., 2012). Recently, strong expression of tafazzin protein, a phospholipid-lysophospholipid transacylase responsible for cardiolipin remodeling in mitochondrial membranes, has been demonstrated to be related to rectal cancer development and radiotherapy response (Pathak et al., 2014). A deeper research focused on CL species needs to be performed in different malignant phenotype scenarios to confirm these results and to explore if specific CL compounds could be considered as metastatic phenotype biomarkers. Altogether, the lipidomic analyses suggested that cell exposure to aroclor and CPF induced a malignant phenotype through signaling and metabolic pathways similar to each other, of which, on the other hand, were very different to those observed in cells exposed to aldrin.

Another interesting feature found in the lipidic profiles is the increase of TAG species, which is common in all of the three exposures studied. This is in agreement to a previous work that reported an increase of TAG associated with a malignant phenotype in colorectal cancer cells (Fhaner et al., 2012). This increase of TAG production is likely to be part of a general metabolic transformation of cancer cells. TAGs are stored in lipid droplets and can be used by cancer cells as a source of energy, membrane components and signaling molecules, which are essential to guarantee the autonomy of malignant cells in terms of enhanced growth, migration and proliferation (Zadra et al. 2013). In the context of cell exposure to contaminants, a TAG increase has been recently reported in placenta cells under acute exposure to tributyltin (TBT),

another ED (Gorrochategui et al., 2015). TBT has been shown to be an agonist of the peroxisome proliferator-activated receptor γ (PPARγ), (Grun et al., 2006) a nuclear receptor and transcription factor whose activation increases the expression of genes that promote triglyceride storage (Ferre, 2004). The activation of PPARγ and their downstream targets by aldrin, aroclor and CPF deserves to be further investigated to understand the metabolic mechanisms involved in this increase and also to consider some specific TAG species as potential biomarkers of cancer cell malignancy.

5. Conclusions

This study demonstrates that chronic exposure to aldrin, aroclor and CPF induced a pro-metastatic phenotype in the prostate cancer cell line DU145. To our knowledge, this work reported for the first time an EMT process induction under aldrin and CPF exposure. The use of chemometrics in the untargeted lipidomic study of these exposed cells allowed the identification of lipid species and lipid metabolic pathways that may have a potential role in the acquisition of the observed malignant behavior. Besides the toxicological information about the exposure to the endocrine disruptors used in this study, the lipidic signatures obtained were found relevant to better understand the lipid metabolic pathways and lipid species involved in EMT and metastasis and thereby shed a light in the discovery of new biomarkers and therapeutic targets in cancer research.

Funding sources

This work was supported by the European Research Council under the European Union's Seventh Framework Programme (FP/2007-2013)/ERC Grant Agreement 35 no. 320737. J.J acknowledges a CSIC JAE-Doc contract cofounded by FSE. Also, recognition from the Catalan government (grant 2014SGR1106) is acknowledged.

Acknowledgements

We greatly appreciate Dr. Gemma Fabriàs and Dr. Josefina Casas for their technical advice and Dr. Melissa Faria for reviewing and proof-reading this manuscript.

Appendix A. Suplementary Information

Supplementary data associated with this article can be found in the online version at http://dx.doi.org/10.1016/j.envres.2015.03.014.

References

Alavanja, M.C., Samanic, C., Dosemeci, M., Lubin, J., Tarone, R., Lynch, C.F., Knott, C., Thomas, K., Hoppin, J.A., Barker, J., Coble, J., Sandler, D.P., Blair, A., 2003. Use of agricultural pesticides and prostate cancer risk in the Agricultural Health Study cohort. Am. J. Epidemiol. 157, 800–814.

Angioni, A., Dedola, F., Garau, A., Sarais, G., Cabras, P., Caboni, P., 2011. Chlorpyrifos residues levels in fruits and vegetables after field treatment. J. Environ. Sci. Health B 46, 544–549.

Bell, M.R., 2014. Endocrine-disrupting actions of PCBs on brain development and social and reproductive behaviors. Curr. Opin. Pharmacol. 19C, 134–144.

Bates, R.C., Mercurio, A.M., 2003. Tumor necrosis factor-alpha stimulates the epithelial-to-mesenchymal transition of human colonic organoids. Mol. Biol. Cell 14, 1790–1800.

Bruntz, R.C., Lindsley, C.W., Brown, H.A., 2014. Phospholipase D signaling pathways and phosphatidic acid as therapeutic targets in cancer. Pharmacol. Rev. 66, 1033–1079.

Birkle, S., Zeng, G., Gao, L., Yu, R.K., Aubry, J., 2003. Role of tumor-associated gangliosides in cancer progression. Biochimie 85, 455–463.

Cillo, F., de Eguileor, M., Gandolfi, F., Brevini, T.A., 2007. Aroclor-1254 affects mRNA polyadenylation, translational activation, cell morphology, and DNA integrity of rat primary prostate cells. Endocr. Relat. Cancer 14, 257–266.

Cordella, C.B.Y., Bertrand, D., 2014. SAISIR: A new general chemometric toolbox. TrAC-Trends in Anal. Chem. 54, 75–82.

Derouiche, S., Warnier, M., Mariot, P., Gosset, P., Mauroy, B., Bonnal, J.L., Slomianny, C., Delcourt, P., Prevarskaya, N., Roudbaraki, M., 2013. Bisphenol A stimulates human prostate cancer cell migration remodelling of calcium signalling. Springerplus 2, 54.

Dumas, J.F., Peyta, L., Couet, C., Servais, S., 2013. Implication of liver cardiolipins in mitochondrial energy metabolism disorder in cancer cachexia. Biochimie 95, 27–32.

El Majidi, N., Bouchard, M., Carrier, G., 2014. Systematic analysis of the relationship between standardized biological levels of polychlorinated biphenyls and thyroid function in pregnant women and newborns. Chemosphere 98, 1–17.

Eilers, P.H., 2003. A perfect smoother. Anal. Chem. 75, 3631–3636.

Edmond, V., Dufour, F., Poiroux, G., Shoji, K., Malleter, M., Fouque, A., Tauzin, S., Rimokh, R., Sergent, O., Penna, A., Dupuy, A., Levade, T., Theret, N., Micheau, O., Segui, B., Legembre, P., 2014. Downregulation of ceramide synthase-6 during epithelial-to-mesenchymal transition reduces plasma membrane fluidity and cancer cell motility. Oncogene.

Farrés, M., Piña, B., Tauler, R., 2014. Chemometric evaluation of Saccharomyces cerevisiae metabolic profiles using LC–MS. Metabolomics.

Foster, D.A., Xu, L., 2003. Phospholipase D in cell proliferation and cancer. Mol. Cancer Res. 1, 789–800.

Fhaner, C.J., Liu, S., Ji, H., Simpson, R.J., Reid, G.E., 2012. Comprehensive lipidome profiling of isogenic primary and metastatic colon adenocarcinoma cell lines. Anal. Chem. 84, 8917–8926.

Ferre, P., 2004. The biology of peroxisome proliferator-activated receptors: relationship with lipid metabolism and insulin sensitivity. Diabetes 53 (Suppl 1), S43–S50.

Grandjean, P., Landrigan, P.J., 2014. Neurobehavioural effects of developmental toxicity. Lancet Neurol. 13, 330–338.

Guerini, V., Sau, D., Scaccianoce, E., Rusmini, P., Ciana, P., Maggi, A., Martini, P.G., Katzenellenbogen, B.S., Martini, L., Motta, M., Poletti, A., 2005. The androgen derivative 5alpha-androstane-3beta,17beta-diol inhibits prostate cancer cell migration through activation of the estrogen receptor beta subtype. Cancer Res. 65, 5445–5453.

Gemperline, P., 2006. Practical Guide to Chemometrics. CRC Press. Taylor & Francis Group, Boca Raton.

Gorrochategui, E., Casas, J., Porte, C., Lacorte, S., Tauler, R., 2015. Chemometric strategy for untargeted lipidomics: biomarker detection and identification in stressed human placental cells. Anal. Chim. Acta 854, 20–33.

Grun, F., Watanabe, H., Zamanian, Z., Maeda, L., Arima, K., Cubacha, R., Gardiner, D. M., Kanno, J., Iguchi, T., Blumberg, B., 2006. Endocrine-disrupting organotin compounds are potent inducers of adipogenesis in vertebrates. Mol. Endocrinol. 20, 2141–2155.

Hooker, E.P., Fulcher, K.G., Gibb, H.J., 2014. Aldrin and dieldrin: a reevaluation of the cancer and noncancer dose-response assessments. Risk Anal. 34, 865–878.

Hessel, P.A., Kalmes, R., Smith, T.J., Lau, E., Mink, P.J., Mandel, J., 2004. A nested case-control study of prostate cancer and atrazine exposure. J. Occup. Environ. Med. 46, 379–385.

Hanahan, D., Weinberg, R.A., 2000. The hallmarks of cancer. Cell 100, 57–70.

Hatano, K., Miyamoto, Y., Nonomura, N., Kaneda, Y., 2011. Expression of gangliosides, GD1a, and sialyl paragloboside is regulated by NF-kappaB-dependent transcriptional control of alpha2,3-sialyltransferase I, II, and VI in human castration-resistant prostate cancer cells. Int. J. Cancer 129, 1838–1847.

Hardy, S., El-Assaad, W., Przybytkowski, E., Joly, E., Prentki, M., Langelier, Y., 2003. Saturated fatty acid-induced apoptosis in MDA-MB-231 breast cancer cells. A role for cardiolipin. J. Biol. Chem. 278, 31861–31870.

Jemal, A., Siegel, R., Ward, E., Hao, Y., Xu, J., Murray, T., Thun, M.J., 2008. Cancer statistics, 2008. CA Cancer J. Clin. 58, 71–96.

Jeng, H.A., 2014. Exposure to endocrine disrupting chemicals and male reproductive health. Front Public Health 2, 55.

Jaumot, J., Gargallo, R., de Juan, A., Tauler, R., 2005. A graphical user-friendly interface for MCR-ALS: a new tool for multivariate curve resolution in MATLAB. Chemom. Intell. Lab. Syst. 76, 101–110.

Jaumot, J., de Juan, A., Tauler, R., 2015. MCR-ALS GUI 2.0: New features and applications. Chemom. Intell. Lab. Sys. 140, 1–12.

Knower, K.C., To, S.Q., Leung, Y.K., Ho, S.M., Clyne, C.D., 2014. Endocrine disruption of the epigenome: a breast cancer link. Endocr. Relat. Cancer 21, T33–T55.

Kajta, M., Wojtowicz, A.K., 2013. Impact of endocrine-disrupting chemicals on neural development and the onset of neurological disorders. Pharmacol. Rep. 65, 1632–1639.

Koutros, S., Beane Freeman, L.E., Lubin, J.H., Heltshe, S.L., Andreotti, G., Barry, K.H., DellaValle, C.T., Hoppin, J.A., Sandler, D.P., Lynch, C.F., Blair, A., Alavanja, M.C., 2013. Risk of total and aggressive prostate cancer and pesticide use in the Agricultural Health Study. Am. J. Epidemiol. 177, 59–74.

Kling, D., Kunkle, J., Roller, A.S., Gamble, W., 1978. Polychlorinated biphenyls: in vivo and in vitro modifications of cholesterol and fatty acid biosynthesis. J. Environ. Pathol. Toxicol. 1, 813–828.

Kuiper, G.G., Lemmen, J.G., Carlsson, B., Corton, J.C., Safe, S.H., van der Saag, P.T., van der Burg, B., Gustafsson, J.A., 1998. Interaction of estrogenic chemicals and phytoestrogens with estrogen receptor beta. Endocrinology 139, 4252–4263.

Kartal Yandim, M., Apohan, E., Baran, Y., 2013. Therapeutic potential of targeting ceramide/glucosylceramide pathway in cancer. Cancer Chemother. Pharmacol.

71, 13–20.
Kiebish, M.A., Han, X., Cheng, H., Chuang, J.H., Seyfried, T.N., 2008. Cardiolipin and electron transport chain abnormalities in mouse brain tumor mitochondria: lipidomic evidence supporting the Warburg theory of cancer. J. Lipid Res. 49, 2545–2556.
Linja, M.J., Savinainen, K.J., Tammela, T.L., Isola, J.J., Visakorpi, T., 2003. Expression of ERalpha and ERbeta in prostate cancer. Prostate 55, 180–186.
Luft, S., Milki, E.A., Glustrom, E., Ampiah-Bonney, R., O'Hara, P.B., 2009. Binding of organochloride and pyrethroid pesticides to estrogen receptors α and β: a fluorescence polarization assay. Biophysical. J. 96, 444a.
Livak, K.J., Schmittgen, T.D., 2001. Analysis of relative gene expression data using real-time quantitative PCR and the 2Delta Delta C(T)) Method. Methods 25, 402–408.
Lima, K.M.G., Bedia, C., Tauler, R., 2014. A non-target chemometric strategy applied to UPLC-MS sphingolipid analysis of a cell line exposed to chlorpyrifos pesticide: a feasibility study. Microchem. J. 117, 255–261.
Lopez-Espinosa, M.J., Granada, A., Carreno, J., Salvatierra, M., Olea-Serrano, F., Olea, N., 2007. Organochlorine pesticides in placentas from Southern Spain and some related factors. Placenta 28, 631–638.
Murugesan, P., Senthilkumar, J., Balasubramanian, K., Aruldhas, M.M., Arunakaran, J., 2005. Impact of polychlorinated biphenyl Aroclor 1254 on testicular antioxidant system in adult rats. Hum. Exp. Toxicol. 24, 61–66.
Merrill Jr., A.H., Sullards, M.C., Allegood, J.C., Kelly, S., Wang, E., 2005. Sphingolipidomics: high-throughput, structure-specific, and quantitative analysis of sphingolipids by liquid chromatography tandem mass spectrometry. Methods 36, 207–224.
Martinez, W.L., Martinez, A.R., Solka, J.L., 2011. Exploratory Data Analysis with MATLAB. CRC Press. Taylor & Francis Group, Boca Raton.
Matthews, B.W., 1975. Comparison of the predicted and observed secondary structure of T4 phage lysozyme. Biochim. Biophys. Acta 405, 442–451.
Mills, G.B., Moolenaar, W.H., 2003. The emerging role of lysophosphatidic acid in cancer. Nat. Rev. Cancer 3, 582–591.
Prins, G.S., Birch, L., Tang, W.Y., Ho, S.M., 2007. Developmental estrogen exposures predispose to prostate carcinogenesis with aging. Reprod. Toxicol. 23, 374–382.
Prins, G.S., 2008. Endocrine disruptors and prostate cancer risk. Endocr. Relat. Cancer 15, 649–656.
Pere-Trepat, E., Lacorte, S., Tauler, R., 2005. Solving liquid chromatography mass spectrometry coelution problems in the analysis of environmental samples by multivariate curve resolution. J. Chromatogr. A 1096, 111–122.
Prins, G.S., Hu, W.Y., Shi, G.B., Hu, D.P., Majumdar, S., Li, G., Huang, K., Nelles, J.L., Ho, S.M., Walker, C.L., Kajdacsy-Balla, A., van Breemen, R.B., 2014. Bisphenol A promotes human prostate stem-progenitor cell self-renewal and increases in vivo carcinogenesis in human prostate epithelium. Endocrinology 155, 805–817.
Pathak, S., Meng, W.J., Zhang, H., Gnosa, S., Nandy, S.K., Adell, G., Holmlund, B., Sun, X.F., 2014. Tafazzin protein expression is associated with tumorigenesis and radiation response in rectal cancer: a study of Swedish clinical trial on preoperative radiotherapy. PLoS One 9, e98317.
Qiu, P., Plevritis, S.K., 2013. TreeVis: a MATLAB-based tool for tree visualization. Comput. Methods Programs Biomed. 109, 74–76.
Selvakumar, K., Sheerin Banu, L., Krishnamoorthy, G., Venkataraman, P., Elumalai, P., Arunakaran, J., 2011. Differential expression of androgen and estrogen receptors in PCB (Aroclor 1254)-exposed rat ventral prostate: impact of alpha-tocopherol. Exp. Toxicol. Pathol. 63, 105–112.
Saunders, M., Magnanti, B.L., Correia Carreira, S., Yang, A., Alamo-Hernandez, U., Riojas-Rodriguez, H., Calamandrei, G., Koppe, J.G., Krayer von Krauss, M., Keune, H., Bartonova, A., 2012. Chlorpyrifos and neurodevelopmental effects: a literature review and expert elicitation on research and policy. Environ. Health 11 (Suppl 1), S5.
Salama, J., Chakraborty, T.R., Ng, L., Gore, A.C., 2003. Effects of polychlorinated biphenyls on estrogen receptor-beta expression in the anteroventral periventricular nucleus. Environ. Health Perspect. 111, 1278–1282.
Schulze, A., Harris, A.L., 2012. How cancer metabolism is tuned for proliferation and vulnerable to disruption. Nature 491, 364–373.
Strauss, R., Bartek, J., Lieber, A., 2013. Analysis of EMT by flow cytometry and immunohistochemistry. Methods Mol. Biol. 1049, 355–368.
Sud, M., Fahy, E., Cotter, D., Brown, A., Dennis, E.A., Glass, C.K., Merrill Jr., A.H., Murphy, R.C., Raetz, C.R., Russell, D.W., Subramaniam, S., 2007. LMSD: LIPID MAPS structure database. Nucleic Acids Res. 35, D527–D532.
Schild, L., Lendeckel, U., Gardemann, A., Wiswedel, I., Schmidt, C.A., Wolke, C., Walther, R., Grabarczyk, P., Busemann, C., 2012. Composition of molecular cardiolipin species correlates with proliferation of lymphocytes. Exp. Biol. Med. Maywood 237, 372–379.
Tauler, R., 1995. Multivariate curve resolution applied to second order data. Chemom. Intell. Lab. Syst. 30, 133–146.
Thiery, J.P., Acloque, H., Huang, R.Y., Nieto, M.A., 2009. Epithelial-mesenchymal transitions in development and disease. Cell 139, 871–890.
Tarapore, P., Ying, J., Ouyang, B., Burke, B., Bracken, B., Ho, S.M., 2014. Exposure to bisphenol A correlates with early-onset prostate cancer and promotes centrosome amplification and anchorage-independent growth in vitro. PLoS One 9, e90332.
Taki, T., Ishikawa, D., Ogura, M., Nakajima, M., Handa, S., 1997. Ganglioside GD1alpha functions in the adhesion of metastatic tumor cells to endothelial cells of the target tissue. Cancer Res. 57, 1882–1888.
Wishart, D.S., Jewison, T., Guo, A.C., Wilson, M., Knox, C., Liu, Y., Djoumbou, Y., Mandal, R., Aziat, F., Dong, E., Bouatra, S., Sinelnikov, I., Arndt, D., Xia, J., Liu, P., Yallou, F., Bjorndahl, T., Perez-Pineiro, R., Eisner, R., Allen, F., Neveu, V., Greiner, R., Scalbert, A., 2013. HMDB 3.0–The Human Metabolome Database in 2013. Nucleic Acids Res. 41, D801–D807.
Wold, S., Sjöström, M., Eriksson, L., 2001. PLS-regression: a basic tool of chemometrics. Chemom. Intell. Lab. Syst. 58, 109–130.
Wang, H., Fang, R., Wang, X.F., Zhang, F., Chen, D.Y., Zhou, B., Wang, H.S., Cai, S.H., Du, J., 2013. Stabilization of Snail through AKT/GSK-3beta signaling pathway is required for TNF-alpha-induced epithelial-mesenchymal transition in prostate cancer PC3 cells. Eur. J. Pharmacol. 714, 48–55.
Yeh, C.R., Da, J., Song, W., Fazili, A., Yeh, S., 2014. Estrogen receptors in prostate development and cancer. Am. J. Clin. Exp. Urol. 2, 161–168.
Yalcin, S.S., Orun, E., Yalcin, S., Aykut, O., 2014. Organochlorine pesticide residues in breast milk and maternal psychopathologies and infant growth from suburban area of Ankara, Turkey. Int. J. Environ. Health Res., 1–9.
Zani, C., Toninelli, G., Filisetti, B., Donato, F., 2013. Polychlorinated biphenyls and cancer: an epidemiological assessment. J. Environ. Sci. Health C Environ. Carcinog. Ecotoxicol. Rev. 31, 99–144.
Zhang, T., Saghatelian, A., 2013. Emerging roles of lipids in BCL-2 family-regulated apoptosis. Biochim. Biophys. Acta 1831, 1542–1554.
Zadra, G., Photopoulos, C., Loda, M., 2013. The fat side of prostate cancer. Biochim. Biophys. Acta 1831, 1518–1532.

Informació Suplementària a la Publicació II

Phenotypic malignant changes and untargeted lipidomic analysis of long-term exposed prostate cancer cells to endocrine disruptors.

C. Bedia, N. Dalmau, J. Jaumot, R.Tauler.

Envriron Res **2015**, 140, 18-31

Supplementary table 1. Table list of the m/z values with statistically significant peak areas ($p<0.05$) between exposed and unexposed samples to EDs. The identification of lipid molecules has been performed using the on-line databases HMDB and LIPIDMAPS but also by consulting a home-made database of lipid standards built in the same chromatographic conditions. The assigned compound corresponds to the lipid molecule with the minimum mass error value respect to the measured m/z, considering all the possible adducts in the corresponding ionization modes. The lipid annotated also had to fulfill an adequate retention time considering its polarity (n.i. means that any lipid molecule has been identified with the measured m/z with a delta <0.1). Fold change was calculated from the arithmetic mean values of each group. Fold change with positive values indicates a relative higher concentration in ED exposed samples. For each exposure, there are two lists corresponding to the two different extractions made: extraction 1, of total intact lipids; and extraction 2, that includes the saponification step that favors sphingolipid recovery. Yellow highlighted lines represent the selected compounds used for a biological interpretation of results (p value <0.5, VIP value >1, ppm m/z error < 10). Compounds marked with an asterisk (*) presented an m/z error higher than 10 in their identification but they have the approximate expected retention time, according to our home-made database. CE: cholesteryl ester; Cer: ceramide; CL: cardiolipin; DAG: diacylglycerol; GluCer: glucosylceramide; PA: phosphatidic acid; PC: phosphatidylcholine; PE: phosphatidylethanolamine; LacCer: lactosylceramide; MG: monoacylglycerol; PG: phosphatidylglycerol; TAG:triacylglyceride; SM: sphingomyelin.

ALDRIN EXPOSURE

Extraction 1: Intact lipids

ret. time	m/z measured	Identified Compound	adduct	m/z calculated	mass error (ppm)	fold change	p value	VIP value	Database ID
0.81	392.7938	Tetracosatetraenoyl CoA	M+3Na	392.7917	5.4	1.4	0.001021	1.5	HMDB06516
0.811	644.6798	Ganglioside GT2 (d18:1/14:0)	M+2H+Na	644.6535	40.8	1.4	0.000562	1.6	HMDB12038
0.811	382.7654	Docosa-4,7,10,13,16-pentaenoyl CoA	M+3Na	382.7760	27.7	1.4	0.004485	1.3	HMDB06513
0.811	492.6467	n.i.				1.4	0.009989	1.1	
0.842	460.7802	n.i.				1.4	0.000628	1.6	
0.842	314.7751	n.i.				1.4	0.002477	1.4	
0.842	372.736	n.i.				1.4	0.006049	1.2	
0.87	254.82	n.i.				1.4	0.005204	1.3	
0.873	514.6749	n.i.				1.8	0.004617	1.4	
0.999	522.1728	n.i.				1.5	0.003311	1.3	
1.03	527.1309	n.i.				1.6	0.046124	0.8	
1.03	439.0963	n.i.				1.7	0.002107	1.5	
1.061	483.1221	n.i.				2.2	0.004003	1.3	
1.061	478.1677	n.i.				1.7	0.005748	1.3	
1.092	557.2993	LysoPG(22:6)	M+H	557.2874	21.3	0.5	0.047318	0.9	LMGP04050016
1.092	461.1426	n.i.				1.3	0.008388	1.2	
1.184	386.2189	n.i.				1.1	0.019192	1.0	
1.276	409.089	n.i.				2.7	0.037755	0.9	
1.648	786.1962	n.i.				1.4	0.001988	1.4	
3.23	308.2927	n.i.				2.2	0.010380	1.1	

3.633	293.2818	Octadecanol	M+Na	293.2815	1.1	1.9	0.026476	1.0	HMDB02350
3.695	327.3354	Heneicosanoic acid *	M+H	327.3258	29.4	1.6	0.014243	1.0	HMDB02345
3.695	619.6129	Arachidyl alcohol *	2M+Na	619.6364	37.8	2.8	0.029964	0.9	HMDB11619
3.695	523.3916	Lyso Plasmalogen PC (18:1)	M+NH4	523.3870	8.7	1.6	0.020327	1.0	HMDB10408
4.348	379.3673	MG(20:4)*	M+H	379.2843	218.8	1.3	0.039556	0.8	HMDB11549
4.626	934.6329	n.i.				2.4	0.008084	1.3	
4.967	372.3829	MG(18:2)*	M+NH4	372.3108	193.5	1.7	0.041136	0.8	HMDB11568
4.998	357.382	MG(18:1)*	M+H	357.2999	229.6	1.7	0.036456	0.8	HMDB11566
5.217	517.347	LysoPE(20:5)*	M+NH4	517.3037	83.6	7.4	0.021820	1.1	HMDB11519
6.953	700.5684	GluCer(d18:1/16:0)	M+H	700.5722	5.4	0.6	0.000001	2.0	HMDB04971
7.326	703.5784	SM(16:1)	M+H	703.5749	5.0	0.6	0.000250	1.9	HMDB13464
7.761	732.5567	PC(32:1)	M+H	732.5538	3.9	0.5	0.000169	1.9	HMDB08097
7.884	1194.8105	Ganglioside GA2 (24:0)	M+NH4	1194.8561	38.2	1.6	0.004423	1.4	HMDB04897
8.011	717.55	SM(16:1(OH))	M+H	717.5541	5.7	0.6	0.000073	1.8	HMDB13463
8.041	690.5383	Plasmalogen PC (30:1)	M+H	690.5432	7.1	0.6	0.000016	1.9	HMDB13402
8.041	716.5211	PE(34:2)	M+H	716.5225	1.9	0.5	0.000069	2.0	HMDB09056
8.041	880.5879	PC(44:11)	M+H	880.5851	3.2	0.4	0.000000	2.1	HMDB08682
8.072	666.5013	PA(32:0)	M+NH4	666.5068	8.3	0.3	0.003469	1.6	HMDB00674
8.165	692.5558	Plasmalogen PC(30:0)	M+H	692.5589	4.4	0.7	0.000022	1.9	HMDB13341
8.63	1469.1282	Plasmalogen PE (36:3) *	2M+NH4	1469.1057	15.3	0.5	0.000080	1.8	HMDB11378
9	1520.1826	PC(34:1) *	2M+H	1520.1629	12.9	0.5	0.000261	1.9	HMDB08100
9.28	1546.1836	PC(34:0)	2M+Na	1546.1761	4.8	0.3	0.000017	2.1	HMDB08034
9.376	786.6072	PC(36:2)	M+H	786.6007	8.2	0.6	0.000434	1.8	HMDB07920
9.4	1530.1494	PC(34:0)	2M+K	1530.1602	7.0	0.3	0.000041	2.1	HMDB08060
9.653	1210.946	n.i.				4.3	0.014778	1.2	
9.468	1506.1772	Plasmalogen PC (34:2)*	2M+Na	1506.1237	35.5	0.3	0.000058	2.1	HMDB08030
9.684	695.4796	n.i.				3.1	0.001999	1.7	

9.684	680.4839	DAG (40:9)*	M+NH4	680.5248	60.1	3.4	0.004940	1.5	HMDB07771
9.715	663.4514	n.i.				3.7	0.005630	1.5	
9.903	702.5434	PE(34:1)	M+H	702.5432	0.2	0.4	0.000132	2.0	HMDB08952
9.964	800.6279	PE(40:2)	M+H	800.6164	14.3	0.6	0.000077	2.0	HMDB08981
10.118	759.6337	SMC20:0	M+H	759.6375	4.9	0.6	0.000008	2.0	HMDB12102
10.149	746.6028	Plasmalogen PC (34:0)	M+H	746.6058	4.0	0.5	0.000189	2.0	HMDB13405
10.211	772.625	Plasmalogen PC (36:1)	M+H	772.6215	4.5	0.5	0.000062	2.0	HMDB11243
10.3	1560.2361	Plasmalogen PE 40:4	2M+H	1560.1731	40.4	0.4	0.005143	1.3	HMDB09610
10.306	794.6064	Plasmalogen PC (38:5)	M+H	794.6058	0.7	0.8	0.004727	1.3	HMDB13432
10.337	1576.2384	PC(36:1)	2M+H	1576.2255	8.2	0.4	0.000038	1.9	HMDB08526
10.522	1108.7688	Trihexosylceramide (22:0)	M+H	1108.7717	2.6	0.5	0.013005	1.2	HMDB04882
10.8	972.7263	LacCer (24:1)	M+H	972.7346	8.5	0.5	0.000537	1.6	HMDB04872
10.803	679.4245	DAG(38:6)*	M+K	679.4698	66.7	9.0	0.017806	1.2	HMDB56175
11.1	555.5323	n.i.				0.5	0.000013	1.9	
11.1	810.6794	GluCer (24:1)	M+H	810.6817	2.9	0.6	0.013117	1.2	HMDB04975
11.11	754.5657	PE(38:3)*	M+H	754.5745	11.7	0.4	0.030906	0.9	HMDB11415
11.142	730.5731	PE(36:1)	M+H	730.5745	1.9	0.3	0.000148	2.0	HMDB09049
11.2	798.6331	Plasmalogen PC (38:3)	M+H	798.6371	5.0	0.4	0.000046	2.0	HMDB13439
11.2	677.6158	n.i.				1.2	0.007145	1.2	
11.268	663.6088	n.i.				1.2	0.042917	0.8	
11.8	842.6593	PC(40:2)	M+H	842.6633	4.7	0.4	0.000100	1.8	HMDB08340
11.8	624.5864	DAG(36:2)*	M+NH4	624.5561	48.4	0.5	0.006658	1.3	HMDB56024
11.98	647.4609	n.i.				8.0	0.013860	1.3	
12.3	583.5637	DAG(34:0)	M+H	583.5660	3.9	0.6	0.000205	1.8	HMDB11146
12.66	802.6331	PE(40:1)	M+H	802.6320	1.3	0.5	0.000181	1.7	HMDB09262
12.665	841.7139	SM(26:1)	M+H	841.7157	2.1	0.6	0.000070	1.8	HMDB13461
12.665	609.5714	DAG (35:1)*	M+H	609.5453	42.9	0.3	0.001398	1.7	HMDB07079

12.8	650.6417	Cer(24:1)	M+H	650.6446	4.4	0.6	0.005036	1.4	HMDB11769
12.8	870.6895	PC (42:2)	M+H	870.6946	5.9	0.5	0.000010	2.0	HMDB08348
13.069	896.7049	PC (44:3)	M+H	896.7103	6.0	0.4	0.000161	1.8	HMDB08356
13.22	874.6476	PE(46:7)*	M+H	874.6320	17.8	0.4	0.000009	1.9	HMDB09707
13.65	830.6547	PE(42:1)*	M+H	830.6633	10.3	0.3	0.005676	1.5	HMDB09270
13.658	843.7263	TAG (51:3)*	M+H	843.7436	20.5	0.6	0.000157	1.8	HMDB42521
13.812	898.7206	PC (44:2)	M+H	898.7259	5.9	0.5	0.000957	1.8	HMDB08323
15.147	902.7555	TAG (54:10)*	M+NH4	902.7232	35.7	0.6	0.007831	1.3	HMDB55447
16.48	922.7779	TAG (56:7)	M+NH4	922.7858	8.5	1.4	0.024038	1.1	HMDB45356
16.98	1272.1364	CE(16:0)*	2M+Na	1272.1583	17.2	0.3	0.002619	1.7	HMDB00885
17.011	950.8229	TAG (58:7)	M+NH4	950.8171	6.0	1.5	0.009555	1.2	HMDB50738
17.011	642.6166	CE(16:0)	M+NH4	642.6184	2.7	0.6	0.000006	2.0	HMDB00885
17.165	1319.2366	CE (18:1)	2M+NH4	1319.2342	1.8	0.3	0.000037	2.0	HMDB05189

Extraction 2: Saponification

retention time	m/z measured	Identified Compound	adduct	m/z calculated	m/z error (ppm)	fold change	p value	VIP value	Database ID
9.251	610.5387	Cer(d18:0/18:1(11Z))	M+FA-H	610.5416	4.7	0.8	0.025429	1.1	HMDB11762
12.969	762.6274	Cer(d18:0/24:1(15Z))	M+TFA-H	762.6229	5.9	0.7	0.022845	1.0	HMDB11769
7.824	650.4978	Cer (d18:1/16:0)	M+TFA-H	650.4977	0.2	0.5	0.008101	1.2	HMDB04949
11.02	732.5773	Cer(d18:1/22:1)	M+TFA-H	732.5759	1.9	0.4	0.033675	1.0	HMDB11775
12.412	748.6065	Cer(d18:1/23:0)	M+TFA-H	748.6072	0.9	0.6	0.034897	1.1	HMDB35472
12.04	760.605	Cer(d18:1/24:1(15Z))	M+TFA-H	760.6072	2.9	0.6	0.025325	1.2	HMDB04953
7.083	812.5489	GluCer (d18:1/16:0)	M+TFA-H	812.5505	1.9	0.6	0.002322	1.4	HMDB04971
8.539	840.5746	GluCer (d18:1/18:0)	M+TFA-H	840.5818	8.6	1.2	0.027850	1.0	HMDB04972
7.548	1450.172	GluCer (d18:1/18:1)	2M-H	1450.1539	12.5	0.6	0.005373	1.2	HMDB04970

11.207	896.6451	GluCer (d18:1/22:0)	M+TFA-H	896.6444	0.7	0.6	0.006007	1.2	HMDB04974
12.351	924.674	GluCer (d18:1/24:0)	M+TFA-H	924.6757	1.8	0.4	0.001596	1.5	HMDB04978
11.299	922.6602	GluCer (d18:1/24:1)	M+TFA-H	922.6601	0.2	0.5	0.009426	1.2	HMDB04975
12.473	950.6961	GluCer (d18:1/26:1)	M+TFA-H	950.6914	5.0	0.6	0.000332	1.6	HMDB04976
6.802	974.5926	LacCer (d18:1/16:0)*	M+TFA-H	974.6033	11.0	0.6	0.004424	1.3	HMDB06750
11.672	948.6661	LacCer (d18:1/18:0)	M+Hac-H	948.6629	3.3	0.4	0.013860	1.1	HMDB11591
9.904	868.6117	LacCer (d18:1/18:1)	M+TFA-H	868.6131	1.6	0.4	0.003002	1.4	HMDB11592
11.05	1084.723	LacCer (d18:1/24:1)	M+TFA-H	1084.7129	9.3	0.6	0.019323	1.0	HMDB04872
12.351	992.6741	Plasmalogen PC (44:4)*	M+TFA-H	992.6937	19.7	0.7	0.030399	0.9	HMDB13455
7.517	1518.1863	Plasmalogen PE (34:0)*	2M-H	1518.2211	22.9	0.6	0.015104	1.0	HMDB11380
12.692	786.62	Plasmalogen PE (40:0)*	M-H	786.6382	23.1	0.2	0.003174	1.3	HMDB09741
11.794	766.6086	Plasmalogen PE (40:1)*	M-H20-H	766.6115	3.7	0.4	0.038051	0.8	HMDB11421

AROCLOR 1254 EXPOSURE

Extraction 1: Intact lipids

retention time	m/z measured	Identified Compound	adduct	m/z calculated	mass error (ppm)	fold change	p value	VIP value	Database ID
2.083	269.0977	n.i.				1.3	0.0070	3.2	
2.206	514.3055	Ganglioside GD3	M+3Na	514.2744	60.5	1.2	0.0002	4.6	HMDB11859
2.206	479.2726	Ganglioside GM2	M+2H+Na	479.2931	42.7	1.2	0.0017	4.4	HMDB11900
2.206	497.2849	Leukotriene D4	M+H	497.2680	34.0	1.2	0.0056	3.4	HMDB03080
2.237	519.2684	Leukotriene D4	M+Na	519.2499	35.6	1.3	0.0350	2.4	HMDB03080
2.299	510.2773	LysoPC (18:0)*	M+H	510.3918	224.4	1.2	0.0334	2.2	HMDB11149
2.456	466.2906	n.i.				1.2	0.0172	2.9	
7.979	928.5833	PC (46:1)	M+H	928.7729	204.2	1.2	0.0438	0.0	HMDB08553
8.134	782.5728	PC (36:4)	M+H	782.5694	4.3	1.2	0.0010	4.3	HMDB08623
8.134	1194.8167	Ganglioside GA2 (d18:1/24:0)	M+NH4	1194.8561	33.0	1.6	0.0011	4.0	HMDB04897
9.6	695.4796	CL(66:3)*	M+2H	695.4934	19.8	3.1	0.0018	4.5	HMDB56701
9.653	1437.0627	CL(68:2)	M+NH4	1437.0530	7.7	3.4	0.0222	3.0	HMDB56402
9.684	1342.9247	DAG (40:9)*	2M+NH4	1343.0159	67.9	10.9	0.0245	3.0	HMDB56371
10.833	998.7313	TAG (62:11)*	M+NH4	998.8171	85.9	0.5	0.0076	3.1	HMDB49672
11.207	619.6035	DAG (36:3)*	M+H	619.5296	119.3	1.1	0.0102	2.9	HMDB56147
11.888	876.6804	Plasmalogen PC (44:6)	M+H	876.6841	4.2	1.6	0.0096	3.4	HMDB13450
11.919	974.7460	LacCer 24:0	M+H	974.7502	4.3	1.4	0.0354	2.2	HMDB11595
11.95	1000.7487	TAG (63:9)*	M+H	999.8375	910.5	1.3	0.0323	2.2	HMDB44820
11.981	857.4091	PG (40:8)	M+K	857.4729	74.5	5.4	0.0016	4.5	HMDB10659
16.918	824.7676	TAG 48:0	M+NH4	824.7702	3.2	1.2	0.0449	1.5	HMDB42065
17.726	852.8028	TAG 50:0	M+NH4	852.8015	1.5	1.3	0.0054	2.4	HMDB42154
18.592	880.8309	TAG 52:0	M+NH4	880.8327	2.1	1.5	0.0023	3.0	HMDB05358

Extraction 2: Saponification

ret. time	m/z measured	Identified Compound	adduct	m/z calculated	mass error (ppm)	fold change	p value	VIP value	Database ID
3.768	554.3860	Lyso plasmalogen PC (18:0)	M+FA-H	554.3827	5.9	1.5	0.02078	1.7	HMDB11149
7.113	744.5593	GluCer (d18:1/16:0)	M+FA-H	744.5631	5.1	1.4	0.02356	1.3	HMDB04971
8.539	840.5746	GluCer (d18:1/18:0)	M+TFA-H	840.5818	8.6	1.2	0.03427	1.1	HMDB04972
11.763	842.6715	GluCer (d18:1/22:0)	M+Hac-H	842.6727	1.4	1.5	0.02010	2.1	HMDB04974
8.073	817.5746	SM(d18:0/22:3)	M+K-2H	817.5631	14.0	1.4	0.03625	2.2	HMDB13468

CHLORPYRIFOS EXPOSURE

Extraction 1: Intact lipids

retention time	m/z measured	Identified Compound	adduct	m/z calculated	mass error (ppm)	fold change	p value	VIP value	Database ID
0.811	644.6798	Ganglioside GT2	M+2H+Na	644.6535	40.7	1.4	0.00108	2.7	HMDB12038
0.811	690.5803	n.i.				1.6	0.00610	2.1	
0.873	1142.2054	n.i.				1.9	0.01521	1.7	
0.904	1138.2325	tetracosaheptaenoyl-CoA	M+K	1138.2924	52.6	2.0	0.00055	3.2	HMDB06260
0.904	922.3887	Decanoyl-CoA	M+H	922.2583	141.3	1.5	0.01599	1.9	LMFA07050022
1.092	557.2993	Ganglioside GM1 (d18:22:0)	M+3Na	557.3091	17.6	0.4	0.00002	4.4	HMDB11882
3.014	650.4371	LysoPC (24:1)*	M+2Na-H	650,4132	36.7	0.3	0.02934	2.3	HMDB10406
5.62	884.54	PC (44:9)*	M+H	884.6164	86.3	1.5	0.00006	3.9	HMDB08648
5.62	867.5084	PG (40:6)	M+H	867.5122	4.4	1.3	0.00900	2.6	HMDB10614
7.884	586.4296	Cer (d18:1/18:1)*	M+Na	586.5170	148.9	13.6	0.01775	2.1	HMDB04948
8.134	782.5728	PC (36:4)		782.5694	4.3	1.2	0.01396	2.5	HMDB08623
8.257	832.579	PC (40:7)	M+H	832.5851	7.3	1.2	0.02873	1.8	HMDB08123
9.653	1453.0228	CL (70:8)*	M+NH4	1452.9904	22.3	6.1	0.01477	2.2	HMDB57512
9.653	1449.0388	CL (70:3)	M+NH4	1449.0530	9.8	2.9	0.01548	2.2	HMDB06260
9.684	707.4865	CL (66:2)	M+H+Na	707.4921	8.0	4.1	0.00209	3.1	HMDB56392
9.684	1437.0419	CL (68:2)	M+NH4	1437.0530	7.7	3.9	0.00819	2.6	HMDB56402
9.684	1342.9247	DAG (40:9)*	2M+NH4	1343.0159	67.8	14.0	0.03097	1.8	HMDB07771
9.7	1397.0021	CL (66:1)*	M+NH4	1397.0217	14.0	6.7	0.01091	2.4	HMDB56932
10.149	820.6332	Plasmalogen PC (40:5)*	M+H	820.6215	14.2	1.2	0.04309	1.6	HMDB11260
10.368	796.6177	Plasmalogen PC (38:3)	M+H	796.6215	4.7	1.2	0.03093	1.8	HMDB08391
11.95	857.402	PG (40:8)	M+K	857.47294	82.7	5.8	0.00326	2.9	HMDB12096
11.95	974.7473	Lactosylceramide (d18:1/24:0)	M+H	974.75022	2.9	1.6	0.00555	2.6	HMDB04947

11.981	647.4609	DAG (38:3)*	M+H	647.5609	154.4	9.1	0.00949	2.5	HMDB08648
12.043	801.6779	DAG (46:1)	M+K	801.6733	5.7	1.3	0.04457	1.4	HMDB56096
14.371	874.7191	PC (42:0)	M+H	874.7259	7.8	1.3	0.00737	2.7	HMDB56962
16.202	988.9244	TAG (60:2)	M+NH4	988.9267	2.2	2.0	0.00226	2.6	HMDB04948
17.134	1319.2384	CE (18:1)	2M+NH4	1319.2342	3.1	0.7	0.00768	2.4	HMDB05189
17.445	952.8281	TAG (58:6)	M+NH4	952.8328	4.9	1.2	0.02555	1.9	HMDB08123

Extraction 2: Saponification

retention time	m/z measured	Identified Compound	adduct	m/z calculated	mass error (ppm)	fold change	p value	VIP value	Database ID
3.024	610.3120	Ganglioside GD1a (d18:1/18:1(9Z))	M-3H		1.8	1.4	0.02352	2.0	HMDB11796

4.3. Publicació III

Epithelial-to-mesenchymal transition involves triacylglycerol accumulation in DU145 prostate cancer cells.

N. Dalmau, J. Jaumot, C. Bedia, R.Tauler.

Mol Biosyst **2015**, 11(12), 3397-3406

Molecular BioSystems

PAPER

View Article Online
View Journal | View Issue

Cite this: *Mol. BioSyst.*, 2015, 11, 3397

Epithelial-to-mesenchymal transition involves triacylglycerol accumulation in DU145 prostate cancer cells†

Núria Dalmau, Joaquim Jaumot, Romà Tauler and Carmen Bedia*

Received 19th June 2015,
Accepted 6th October 2015

DOI: 10.1039/c5mb00413f

www.rsc.org/molecularbiosystems

Epithelial to mesenchymal transition (EMT) is a biological process that plays a crucial role in cancer metastasis. Although studies regarding the EMT mechanisms are usual in terms of gene expression and protein functions, little is known about the involvement of lipids in EMT. In this work, an untargeted lipidomic analysis was performed to reveal which lipids are involved in the EMT process. DU145 prostate cancer cells were treated with TNFα, a well-known EMT inducer. After 6 hours of treatment, a decrease of cell membrane E-cadherin as well as a reduction in its gene expression were observed. Also, the mesenchymal markers Vimentin and Snail were up-regulated, suggesting that EMT started below 6 hours of treatment. Lipid extracts of untreated and TNFα-treated cells at short times were analyzed using ultra-performance liquid chromatography coupled to high-resolution mass spectrometry (UPLC-MS). Multivariate data analysis methods were applied to decipher which lipids presented significant changes after EMT induction. Among the results obtained, a significant increase of twelve unsaturated triacylglycerides (TAGs) was observed. This increase of TAGs was also observed for cells treated with TGFβ (another EMT inducer), suggesting that this feature is a common mechanism in the EMT process. In conclusion, this work reported for the first time a TAG accumulation through EMT induction. These TAG lipids could play a key role in providing cells with the energy, cell membrane components and signaling lipids necessary to guarantee the enhanced cell migration and proliferation of metastatic cells.

Introduction

Epithelial-to-mesenchymal transition (EMT) is an essential process involved in multiple biological tasks such as tissue repair, wound healing and embryonic development. During EMT, epithelial cells lose their intercellular adhesion and apical-basal polarization, leading to an increase in their migratory and invasive properties.[1,2] In cancer cells, this transition to a mesenchymal phenotype has been shown to be involved in tumour invasion and metastasis.[3,4] EMT is characterized by the loss of epithelial markers such as membrane E-cadherin and β-catenin and the up-regulation of the transcription factors Snail, Twist, Slug and ZEB1 as well as mesenchymal markers such as vimentin and fibronectin.[5]

Many cytokines and growth factors such as transforming growth factor beta (TGFβ), IL-6 and tumour necrosis factor alpha (TNFα) can induce EMT.[6] TNFα is a pro-inflammatory cytokine, involved in the regulation of multiple physiological and pathological processes including inflammation, immunity, cell proliferation and apoptosis. Increased TNFα expression levels have been associated with an increased grade malignancy and metastasis in prostate cancer.[7] This cytokine has been shown to induce EMT through the activation of nuclear factor kappa beta (NF-κB), a transcription factor involved in cancer initiation and progression.[8]

Lipids are a very diverse group of compounds with crucial roles in living organisms. Among their multiple biological functions, they contribute to cell compartmentalization, energy storage and production, cell signalling, protein trafficking, and membrane organization. Despite the importance of lipids in cell homeostasis, little is known about the lipid composition of cells during EMT. Lipidomics is a branch of metabolomics consisting in the large-scale study of cellular lipids and their interaction with other lipids, proteins and metabolites.[9] It includes the comprehensive analysis of lipid species within a biological sample and the analysis of alterations in lipid content and composition after cell perturbation or pathogenesis.[10] These studies have been proven to be useful in the study of the mechanism of many diseases, as well as in the finding of specific disease biomarkers.[11–13] Two different analytical approaches exist

Department of Environmental Chemistry, Institute of Environmental Assessment and Water Research (IDAEA-CSIC), c/Jordi Girona 18-24, 08034 Barcelona, Spain. E-mail: carmen.bedia@idaea.csic.es

† Electronic supplementary information (ESI) available. See DOI: 10.1039/c5mb00413f

in lipidomics: targeted and untargeted analyses. Whereas targeted lipidomic analyses are focused on the detection and quantitative analysis of some selected compounds, the aim of the untargeted analyses is to detect which lipid species show significant changes under specific stimuli, without any previous hypothesis of the lipids involved. The advantage of this approach is that it enables the discovery of unexpected lipid species associated with a certain biological process. This untargeted approach often involves the use of chemometric analysis methods in complex and massive amounts of data obtained in the LC/GC-MS full scan analysis of samples.

In the present study, an untargeted lipidomic approach on EMT-induced prostate cancer cells under TNFα treatment was carried out. Data obtained from LC-MS on lipid extracts were further processed using chemometric analysis methods. The aim of this lipidomic research was to explore the changes in lipid composition in EMT-induced cells and to detect which lipid species are involved in the EMT process.

Results

TNFα induces EMT in DU145 cells

First of all, EMT induction was confirmed under TNFα exposure in DU145 prostate cancer cells. EMT was assessed by flow cytometry on cells exposed to TNFα (20 ng ml^{-1}) for 24 hours, using a specific antibody against E-cadherin, a characteristic epithelial cell marker. The results showed a reduction of the fluorescence associated with membrane E-cadherin (Fig. S1, ESI†), indicating that the reported conditions induced EMT in DU145 cells.

Immunofluorescence images taken after 6 and 24 hours of TNFα treatment confirmed the loss of E-cadherin in the cell membrane (Fig. 1a). Interestingly, 6 hours were sufficient to observe a decrease of E-cadherin green fluorescence. Also, the formation of pseudopodia was found in plasma membranes after 6 hours of TNFα exposure. Pseudopodia are projections of cell membranes that involve changes in the cytoskeleton dynamics. Their formation has long been associated with tumour cell migration and invasion,[14] and recently, to the acquisition of a motile and migratory phenotype in EMT.[15] According to this, qRT-PCR analysis further corroborated the EMT induction at early exposure times. As represented in Fig. 1b, TNFα significantly induced the down-regulation of E-cadherin at 5 and 6 hours. In addition, mRNA levels of the mesenchymal markers Vimentin and Snail increased significantly at 6 hours.

These observations suggested that changes leading to EMT under TNFα treatment occurred at early incubation times. According to this, the subsequent lipidomic study was performed at different exposure times below 6 hours.

Lipidomic study of EMT

The lipidomic study was performed on cell cultures exposed to TNFα for 0, 3, 4, 5 and 6 hours (3 samples/each). Every sample was then subjected to two types of lipid extraction: (1) extraction using chloroform/methanol (2 : 1) that contained intact lipids from the sample and (2) extraction using chloroform/methanol

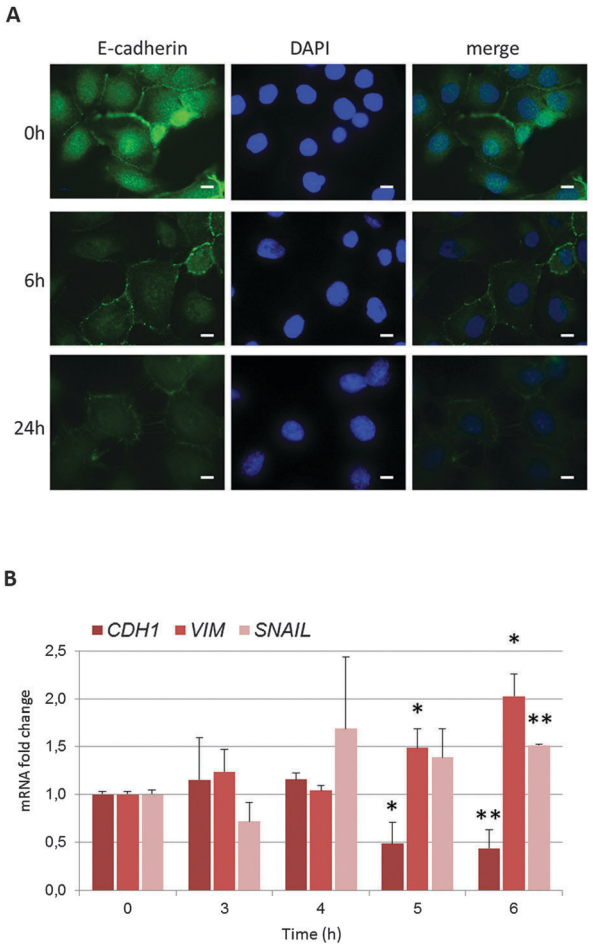

Fig. 1 EMT induction in DU145 prostate cancer cells under TNFα treatment. (A) Immunofluorescence assay on DU145 cells treated with TNFα (20 ng ml^{-1}) for 6 and 24 hours. After fixation, E-cadherin (green) was examined by green immunofluorescence staining with E-cadherin-FITC antibody. Nuclei were stained with DAPI (blue). Images are representative pictures of three independent experiments. Scale bars: 10 μm. (B) Bar diagram of real-time quantitative PCR analysis of E-cadherin (CDH1), Vimentin (VIM) and Snail expression. C_t values were normalized to the C_t value of GAPDH from the same sample, and fold change expression was obtained using the delta–delta Ct method. The results represented the mean ± SE of three independent experiments (n = 3) performed in triplicate. The indicated significant differences are considered with respect to the untreated cells. *$p < 0.05$, **$p < 0.01$.

(1 : 2) with a saponification step to remove all the ester lipids from the sample favouring the detection of sphingolipids. LC-MS profiles of lipid extractions and internal standards are available in the ESI† (Fig. S3–S6).

First, a preliminary study on total ion current (TIC) chromatograms, obtained in both positive and negative ionization modes was carried out by Partial Least Squares-Discriminant Analysis (PLS-DA). This classification study was performed on matrices containing the normalized TICs of samples, in order to evaluate if their lipidomic profiles could separate samples corresponding to different times of TNFα exposure. PLS-DA is a supervised classification analysis tool that requires prior knowledge of class membership. In this case, two classes were chosen and defined

as pre-EMT and post-EMT: samples at 0 and 3 hours were grouped into the pre-EMT class and samples at 5 and 6 hours into the post-EMT class. These classes were defined considering that at 0 and 3 hours mRNA levels of the EMT markers were similar and significantly different to the expression levels observed at 5 and 6 hours. As a result, we observed a clear separation between pre-EMT and post-EMT samples in the positive mode (see Fig. S2, ESI†) suggesting that substantial changes in the lipidomic profile occurred as a consequence of the EMT induction under TNFα treatment. In contrast, the TICs of samples acquired in the negative mode in both extractions 1 and 2 could not be separated in the PLS-DA models, thus these data were not considered for further analysis.

In order to investigate which specific lipids were altered during the EMT induction process, a deeper analysis of these data were carried out. Full scan LC-MS data matrices containing all intensity values measured at different mass and retention times in the positive ionization mode were analysed by means of Multivariate Curve Resolution – Alternating Least Squares (MCR-ALS). The mass values of the resolved peaks that presented significant changes between pre- and post-EMT samples were integrated using raw data files, and further normalized and identified as described in the Methodology section. A new matrix containing the concentrations of the selected compounds in every sample (X-data) was constructed and subjected to a PLS-DA in order to confirm the discrimination between pre- and post-EMT classes (Y-data). Fig. 2 shows PLS-DA scores obtained in the analysis. For extraction 1 (intact lipids), 85.10% of *Y*-variance was explained by cumulative *X*-variance of 74.67% of two latent variables with a Matthews Correlation Coefficient (MCC)[16] equal to 0.7. In the case of extraction 2 (sphingolipids), 89.84% of *Y*-variance was explained by cumulative *X*-variance of 82.64% of three latent variables with a MCC of 0.8.

These results indicated that specific lipid molecules whose profiles were resolved in the MCR-ALS analysis allowed the discrimination between pre-EMT and post-EMT samples. In the PLS-DA model obtained, the Variable Importance in Projection (VIP) scores[17] were calculated to investigate which were the most influent lipids in the discrimination of pre- and post-EMT samples.

The complete detailed list of *m*/*z* values corresponding to the lipids that showed changes from 0–3 h to 5–6 h under TNFα treatment within both extractions 1 and 2 can be consulted in Table 1. This table, in which compounds are sorted by their chromatographic retention time, includes the annotation of lipids, performed as described in the Experimental section. Only the listed lipids with a VIP score value greater than 1 and a mass error less than 10 ppm (rows in italics) were selected for a further interpretation of lipidomic results.

The most relevant aspect of the results obtained was the increase of twelve different unsaturated triacylglycerides (TAGs) containing from 50 to 58 carbon atoms with fold-change values ranging from 1.6 to 2.5. Also, a 1.4 fold increase was observed for phosphatidylcholine (40 : 5). Regarding sphingolipid species, an important decrease of ceramide 16 : 0 (Cer(16 : 0)) was detected (0.5 fold) with a VIP value of 2.2. Although Cer(16 : 0) is the only identified sphingolipid that presented substantial changes, its VIP value suggested that this reduction of ceramide is influencing sufficiently to allow the discrimination between pre- and post-EMT samples. This decrease is consistent with the results of Edmond *et al.*'s work,[18] in which a down-regulation of CerS6 gene, responsible for the enzyme that synthesizes Cer(16 : 0), is reported in EMT.

Confirmation of TAG enhancement in EMT induced DU145 cells

To further explore the increase of TAG observed under TNFα treatment, the behaviour of all the TAGs listed in Table 1 was investigated. A time course was performed by exposing cells to TNFα (20 ng ml^{-1}) for 0, 6, 24 and 48 hours. The time course results showed a dependence of TAG increase over time under TNFα exposure. After 6 hours of treatment, TAG levels increased in similar proportions to that observed in the previous lipidomic study, reaching maximum levels at 24 hours. At 48 hours of

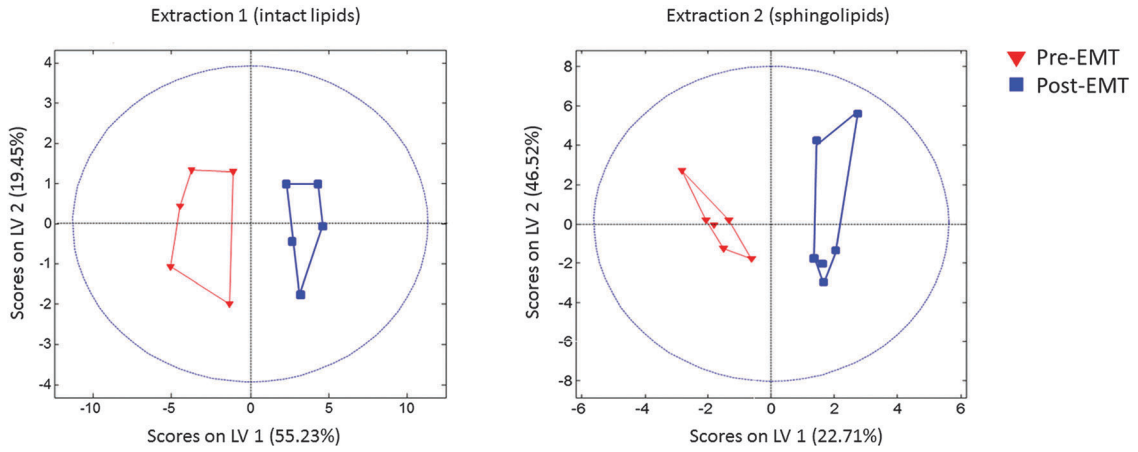

Fig. 2 PLS-DA analysis of lipidomic data. Lipid extracts of DU145 cells treated with TNFα at different times were analysed through UPLC-TOF and data were imported into the MATLAB environment. PLS-DA score plots of matrices containing the concentrations of the selected compounds obtained by MCR-ALS analysis on full scan data matrices in the positive ionization mode.

Table 1 A list of the *m/z* values that presented significant changes (p-value <0.05) in their levels between pre-EMT and post-EMT group samples in both types of lipid extraction. The absolute concentrations of lipids were calculated considering the area of the corresponding internal standards added in the extraction (Cer, TAG and PC) and the protein content in each sample as follows: (200 × mg of protein)/area of specific standard. The assigned compound corresponds to the lipid molecule with the minimum mass error value with respect to the measured *m/z*, considering all the possible adducts in the positive ionization mode. The list only contains the compounds with a Benjamini–Hochberg's corrected p-value <0.05. Rows in italics indicate the lipids considered for further interpretation of the results. Cer: ceramide; PC: phosphatidylcholine; TAG: triacylglyceride

Ret. time	*m/z* measured	Identified compound	Adduct	*m/z* calculated	Mass error (ppm)	pmol mg^{-1} protein in pre-EMT	pmol mg^{-1} protein in post-EMT	Fold change	*p* value	VIP value	Database ID
7.8	*538.5208*	*Cer(16:0)*	*M + H*	*538.5194*	*2.60*	*194 ± 100*	106 ± *18*	*0.5*	*0.0209*	*2.2*	*HMBD04949*
9.7	*836.6181*	*PC(40:5)*	*M + H*	*836.6164*	*1.94*	*425 ± 83*	581 ± *100*	*1.4*	*0.0362*	*1.0*	*HMDB08218*
16.1	*846.7559*	*TAG(50:3)*	*M + NH4*	*846.7545*	*1.64*	*326 ± 116*	737 ± *228*	*2.2*	*0.0209*	*1.3*	*HMDB47737*
16.5	*848.7717*	*TAG(50:2)*	*M + MH4*	*848.7701*	*2.16*	*419 ± 137*	866 ± *269*	*2.1*	*0.0209*	*1.2*	*HMDB44034*
16.5	*922.7806*	*TAG(56:7)*	*M + MH4*	*922.7858*	*5.22*	*305 ± 152*	753 ± *167*	*2.5*	*0.0136*	*1.5*	*HMDB45356*
16.6	*948.7969*	*TAG(58:8)*	*M + NH4*	*948.8014*	*4.70*	*233 ± 111*	582 ± *135*	*2.5*	*0.0136*	*1.6*	*HMDB51044*
16.7	*874.787*	*TAG(52:3)*	*M + NH4*	*874.7858*	*1.36*	*326 ± 104*	724 ± *235*	*2.2*	*0.0136*	*1.3*	*HMDB45489*
16.9	*950.8147*	*TAG(58:7)*	*M + NH4*	*950.8171*	*2.22*	*241 ± 112*	574 ± *123*	*2.3*	*0.0136*	*1.6*	*HMDB50738*
17.1	*850.7863*	*TAG(50:1)*	*M + NH4*	*850.7858*	*0.22*	*623 ± 114*	1025 ± *269*	*1.6*	*0.0136*	*1.1*	*HMBD45481*
17.3	*876.8036*	*TAG(52:2)*	*M + NH4*	*876.8014*	*2.89*	*958 ± 229*	1878 ± *467*	*2.0*	*0.0136*	*1.4*	*HMDB42488*
17.5	*902.8262*	*TAG(54:3)*	*M + MH4*	*902.8171*	*9.81*	*744 ± 195*	1483 ± *392*	*2.0*	*0.0136*	*1.4*	*HMBD46267*
17.9	878.8126	TAG(52:1)	M + NH4	878.8711	4.68	417 ± 90	628 ± 153	1.5	0.0362	0.9	HMDB42453
17.9	*916.8317*	*TAG(55:3)*	*M + NH4*	*916.8328*	*1.16*	*186 ± 53*	372 ± *87*	*2.0*	*0.0136*	*1.5*	*HMDB43548*
13.1	*904.8357*	*TAG(54:2)*	*M + NH4*	*904.8327*	*3.58*	*502 ± 116*	882 ± *186*	*1.8*	*0.0136*	*1.4*	*HMBD46436*
18.6	*956.8592*	*TAG(58:4)*	*M + MH4*	*956.8640*	*5.29*	*140 ± 36*	298 ± *71*	*2.1*	*0.0136*	*1.5*	*HMDB46326*

treatment, most of the TAGs still showed significantly enhanced levels (Fig. 3). This increase was also obtained by a MCR-ALS simultaneous analysis of 0 and 24 hours samples (data not shown), which confirmed the rise of TAG levels. Also, we explored if the increase of TAG was accompanied by a rise of lipid droplets, which are lipid storage organelles consisting of a phospholipid monolayer that surrounds a core of neutral lipids, mainly TAGs and cholesterol esters. As depicted in Fig. 4a and b, lipid droplets, stained using Nile Red, were significantly increased in cells at 6 hours, with sustained elevated levels at 24 and 48 hours of TNFα treatment, confirming the lipid deposition of the newly synthesized TAG in these organelles. The increased levels of TAGs suggested an activation of lipogenic mechanisms. Thus, the expression of some lipogenic enzymes such as acetyl-CoA carboxylase α (ACACA) and fatty acid synthase (FASN) was investigated after 6 hours of TNFα exposure. As a result, whereas any significant change was observed for the expression of ACACA, FASN was found overexpressed (Fig. 4c). This observation suggested that FASN, which is responsible for the synthesis of new fatty acids and has been found to be highly expressed in prostate cancer,[19] could be involved in the TAG accumulation observed.

To confirm that this rise of TAG was not a specific event of TNFα treatment, another widely known EMT inducer cytokine, transforming growth factor-beta (TGFβ),[20–22] was used. DU145 cells were treated with TGFβ (20 ng ml^{-1}) for 0, 6, 24 and 48 hours. The induction of EMT was confirmed by the reduction of E-cadherin levels on the cell membrane at 6 and 24 hours (see Fig. 5a). Concerning the TAG species listed in Table 1, for most of them, TGFβ treatment induced a time-dependent rise in the levels of TAGs with significant fold increases for some of them at 24 hours (Fig. 5b), which was consistent with the observations obtained under TNFα treatment. In addition, we observed that lipid droplets also increased, with a maximum at 24 hours

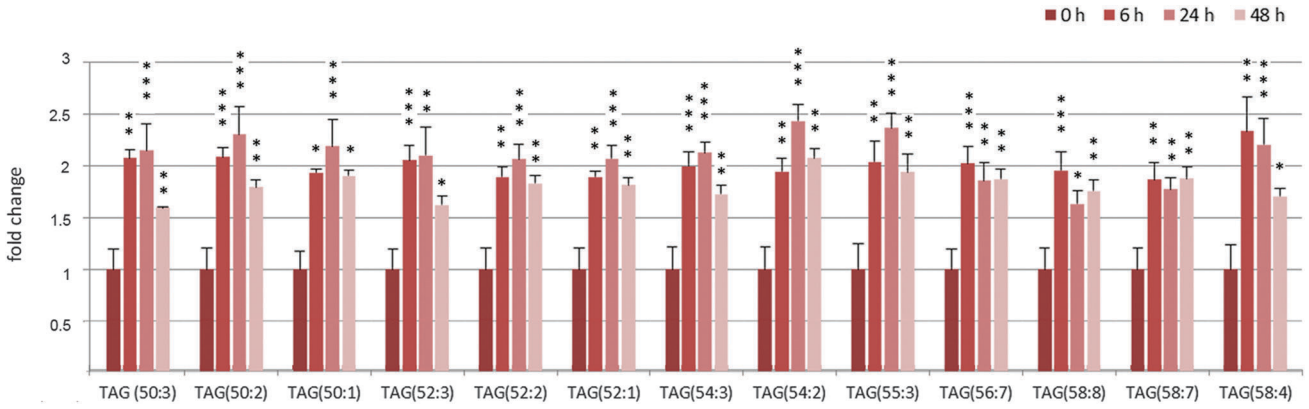

Fig. 3 Time dependence of TAGs increase under TNFα treatment. DU145 cells were exposed to TNFα (20 ng ml^{-1}) for 0, 6, 24 and 48 hours. Bar diagram of fold changes in the levels of the selected TAGs at the indicated times. The results are representative of two independent experiments performed in triplicate. The indicated significant differences are considered with respect to the untreated cells. *$p < 0.05$, **$p < 0.01$, ***$p < 0.005$.

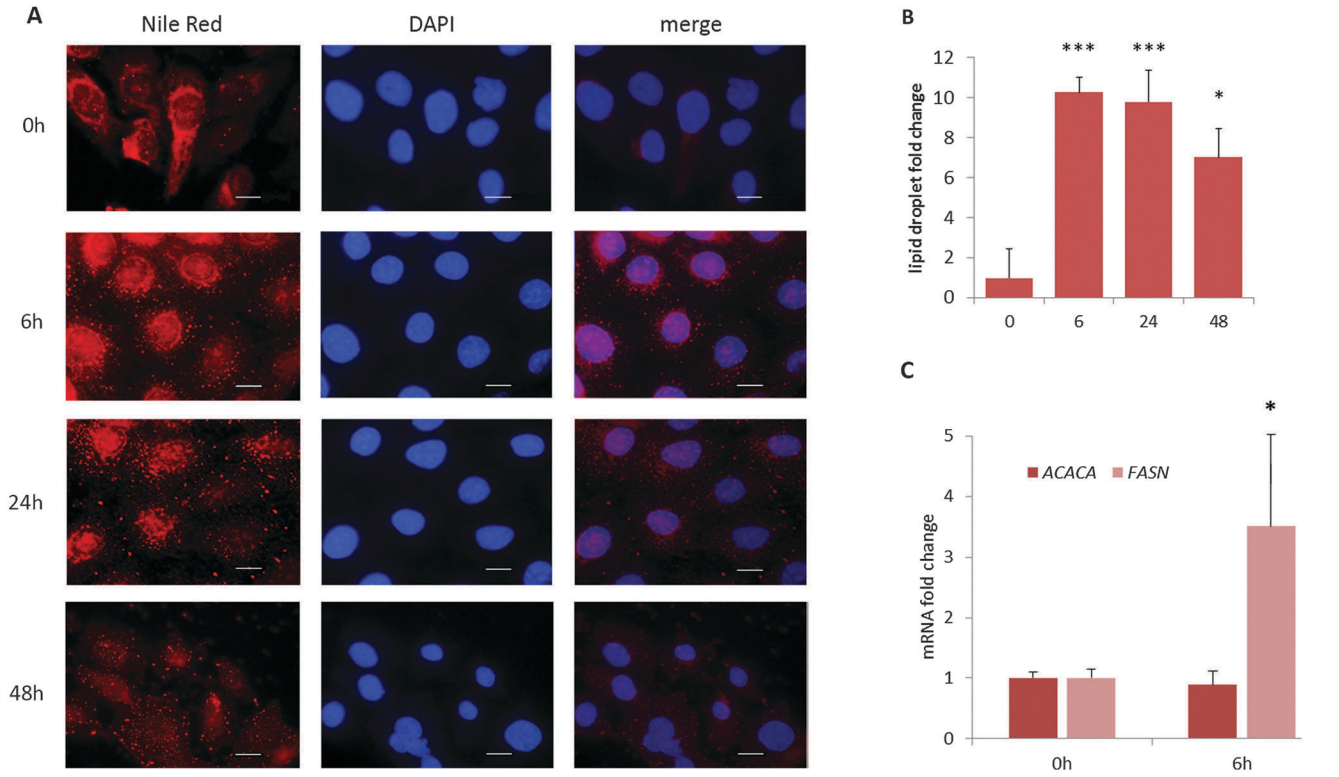

Fig. 4 Lipid droplet accumulation and mRNA expression of lipogenic enzymes in EMT induced cells. (A) Pictures of DU145 cells treated with TNFα (20 ng ml^{-1}) for 0, 6 24 and 48 hours and then stained with Nile Red for 20 minutes and DAPI. Representative fluorescence images of the stained cells using red and blue filters are shown. Scale bars: 20 μm. (B) Bar diagram of lipid droplet quantification. The results are representative of pictures of three independent experiments. (C) Bar diagram of real-time quantitative PCR of ACACA and FASN expression in samples of untreated and 6 hour treated cells with TNFα (20 ng ml^{-1}). The results represented the mean ± SE of three independent experiments (n = 3) performed in triplicate. *$p < 0.05$, **$p < 0.01$, ***$p < 0.005$.

(Fig. 5c and d). Even though these results were not identical to those of TNFα, these similar features observed under both treatments suggested that TAGs have a relevant role in EMT.

Discussion

Lipids contribute to several biological functions in cancer cells. First, they have a structural role in the production of cell membranes to support the high proliferation rate of cancer cells. Second, some of them such as diacylglycerol, sphingosine-1-phosphate or ceramide, act as second messengers in signalling transduction pathways controlling diverse cellular functions such as cell migration, proliferation or survival. Third, fatty acids (FAs) are able to induce post-translational modifications of proteins (*i.e.* palmitoylation) which control the function of various signalling processes.[23] Finally, FAs also can serve as a source of energy through β-oxidation to assure cancer cell survival.

Due to the essential functional roles of lipids in cancer cell maintenance and survival, we considered relevant the study of lipid changes involved in EMT, which constitutes a critical process involved in the transdifferentiation of epithelial cells into an invasive phenotype, a crucial mechanism that mediates cancer metastasis. In the context of EMT, few publications have reported changes in lipids during EMT. Guan *et al.* have shown that some specific glycosphingolipids (gangliotetraosylceramide and GM2) are reduced in an EMT process induced by TGFβ in mouse and human epithelial cell lines.[24,25] In another recent article, CerS6 gene, responsible for Cer (16:0) synthesis, has shown to be down-regulated in EMT induced cells.[18]

The untargeted lipidomic approach of the present work was carried out in order to detect changes in specific lipids without any pre-conceived idea about the lipid candidates, which potentially enabled the discovery of novel interesting molecules that could have never been a focus of study in EMT. The main results of this untargeted lipidomic study revealed a significant rise of twelve unsaturated TAG species during the EMT induction in DU145 cells under TNFα treatment. A similar TAG increase was observed under TGFβ exposure, another well-known EMT inducer, suggesting that this common feature could be important for the transition process in epithelial cells. Also, we observed that in EMT induced cells by TNFα and TGFβ, the newly synthesized TAGs accumulated in lipid droplets. TAGs act not only as a reservoir of energy, but also of FAs, which in turn could be used for protein modification, incorporation into other lipid species for cell membrane building and the generation of pro-tumorigenic signals. Thus, this increase of TAG levels could be interpreted as a preparation process of cells for the increasing need of energy, membrane production and signalling lipids essential to guarantee survival and proliferation of metastatic cells.

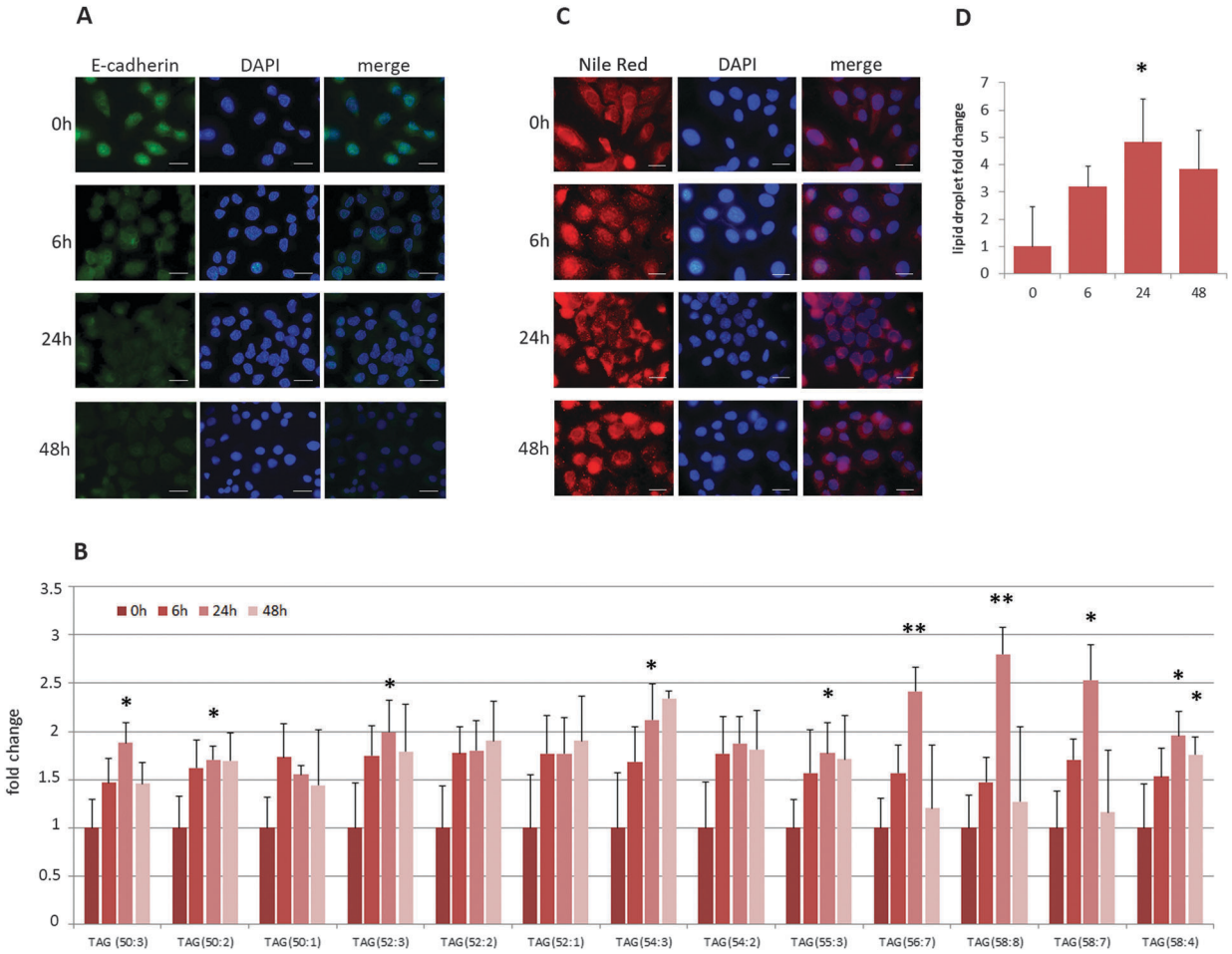

Fig. 5 EMT induction in DU145 cells using TGFβ. DU145 cells were treated with TGFβ (20 ng ml^{-1}) for 0, 6, 24 and 48 hours. (A) Immunofluorescence assay of EMT induced cells. After fixation, E-cadherin (green) was examined by green immunofluorescence staining with E-cadherin-FITC antibody. Nuclei were stained with DAPI (blue). Images are representative of several pictures taken in random fields. Scale bars: 20 μm. (B) Bar diagram of fold changes in the levels of the selected TAGs at the indicated doses. The results are representative of two independent experiments performed in triplicate. The indicated significant differences are considered with respect to the untreated cells. (C) Pictures of TGFβ treated cells (20 ng ml^{-1}) for 0, 6, 24 and 48 hours stained with Nile Red for 20 minutes and DAPI. Representative fluorescence images of the stained cells using red and blue filters are shown. Scale bars: 20 μm. (D) Bar diagram of lipid droplet quantification. The results are representative of pictures of three independent experiments. *$p < 0.05$, **$p < 0.01$.

These results are in agreement with a previous work of Goto *et al.* on fibrosarcoma cells, in which hypoxia has been shown to upregulate TAG synthesis and to promote the formation of lipid droplets.[26] In addition, pharmacological inhibition of this TAG synthesis has been shown to cancel proliferation and motility of hypoxic cancer cells, indicating that newly synthesized TAGs played an important role in tumour growth and metastasis under hypoxic conditions. Several publications have linked hypoxia and EMT induction.[27,28] Since in solid tumours most cells exist in chronic hypoxia, TAG synthesis could be an interesting subject of study in cancer progression research.

An aberrant increase in *de novo* lipogenesis has been observed in many cancers,[29] including prostate cancer, in which it is significantly associated with tumour progression and worse prognosis.[30] Fatty acid synthase (FASN), which produces palmitate (16 : 0), has been found to be overexpressed in prostate cancer and to be associated with progression and metastasis.[29] In addition, FASN has been reported to mediate EMT in breast and ovarian cancer cells.[31,32] In the present study, we have also found a significant increase of FASN under TNFα exposure. This FASN overexpression could be related to the increased TAGs levels, since the newly synthesized FAs are rapidly incorporated into neutral- and phospholipid stores. In contrast to normal cells, these FAs have been reported to account for more than 93% of triacylglycerol FAs in tumour cells.[29] Although our results suggest that FASN overexpression could be responsible for the rise of TAG under our conditions, the direct involvement of FASN in the TAG synthesis under EMT induction needs to be further investigated.

The generation and accumulation of TAG in metastatic cells has sense if these malignant cells have a complementary lipolytic mechanism able to liberate stored fatty acids for metabolic and signalling needs. This TAG lipolysis is performed through the action of a series of lipases such as hormone-sensitive lipase,

adipose triglyceride lipase and monoacylglycerol lipase (MAGL). In this context, the lipolytic enzyme MAGL has been found to be highly elevated in aggressive cells from multiple tissues of origin.[33] This enzyme has demonstrated to generate a wide array of second messenger signals that support migration, survival, and *in vivo* tumour growth.

Besides the increase of TAGs, our untargeted lipidomic analysis also detected a reduction of Cer (16 : 0) levels, which is in agreement with the findings of Edmond *et al.*[18] These authors reported a down-regulation of CerS6 in EMT, the enzyme responsible for its synthesis. They demonstrated that lowered levels of Cer (16 : 0) enhance membrane fluidity and stimulate cell motility in epithelial tumour cells. In addition to its role in the plasma membrane, ceramide is a well-known signalling lipid involved in anti-proliferative responses and apoptosis. According to this, the reduction of ceramide levels observed could be traduced in a decrease of pro-apoptotic signals leading to an enhanced cell survival, necessary for tumour progression.

Conclusions

The untargeted lipidomic analysis performed in this work revealed a significant increase of twelve unsaturated TAG species in EMT-induced prostate cancer cells. To our knowledge, this feature has never been reported before under EMT induction. This rise of TAGs is concomitant with lipid droplet formation and FASN overexpression, suggesting an activation of the *de novo* lipogenesis in EMT induced cells. This TAG storage could be explained by an increasing cell need for energy, membrane components and signalling lipids for the enhanced cell migration, proliferation and aggressiveness characteristic of metastatic cells. Since TAGs seem to be the fuel of cancer cells necessary to acquire a malignant phenotype, further research should be addressed to find new therapeutic targets throughout the lipogenic and lipolytic enzymatic pathways that control TAG accumulation.

Experimental

Chemicals and reagents

TNFα, TGFβ, cell culture media and reagents were obtained from Sigma. Analytical grade methanol and chloroform were purchased from Merck and Carlo Erba, respectively. HPLC Gradient Grade acetonitrile was purchased from Fischer Chemicals. Lipid standards were obtained from Avanti Polar Lipids.

Cell culture

The human prostate cancer cell line DU145 was purchased from the American Type Culture Collection and maintained in RPMI1640 culture medium supplemented with 10% heat-inactivated foetal bovine serum, 100 U ml^{-1} penicillin and 100 μg ml^{-1} streptomycin at 37 °C in a humidified atmosphere containing 5% of CO_2.

Immunofluorescence

DU145 cells were seeded in 12-well plates containing glass coverslips at a density of 1.5×10^5 cells per well and left in culture until next day. Cells were treated with TNFα (20 ng ml^{-1}) or TGFβ for 0, 6, 24 and 48 hours. Media was aspirated and cells washed with PBS. Cells were fixed with cold methanol for 20 minutes and washed three times with PBS. Next, 20 μl of anti-CD324/E-cadherin-FITC was added to each sample. Samples were incubated on ice for one hour, and then washed three times with PBS. Cells were mounted onto glass slides using ProLong® Diamond Antifade Mountant with DAPI (Life Technologies) and left in the dark for 30 minutes, according to the manufacturer's instructions. Samples were examined under a fluorescence microscope (40×, Nikon SMZ 1500, using DAPI and FTIC filters) fitted with a digital camera (Nikon DS-Ri1).

Quantitative real-time PCR

Total mRNA of DU145 cells was extracted after treatment with TNFα for the indicated times (0, 3, 4, 5, 6 hours). Cells were harvested using a rubber scraper into 2 ml of ice-cold PBS. Cells were centrifuged at 1300 rpm for 3 minutes at 4 °C and cell pellets were washed twice with cold PBS. Total RNA was extracted using the NucleoSpin RNA kit (Macherey-Nagel). RNA quality was checked using an Agilent 2100 Bioanalyzer (Agilent Technologies). RNA (2 μg) were retro-transcribed to cDNA using a Transcriptor First Strand Synthesis Kit (Roche) and stored at −20 °C. Quantitative PCR analysis was carried out using a LightCycler® 480 Real Time PCR System (Roche) using LightCycler SYBR Green I Master® (Roche). The primers used in each reaction are as follows: CDH1 forward 5′-TACACTGCCC AGGAGCCAGA-3′ and reverse 5′-TGGCACCAGTGTCCGGATTA-3′; SNAIL forward 5′-GACCACTATGCCGCGCTCTT-3′ and reverse 5′-GTGGGATGGCTGCCAGC-3′; VIM forward 5′-TGAGTACCGGA GACAGGTGCAG and reverse 5′- TAGCAGCTTCAACGGCAAAGTT C-3′; ACACA forward 5′-CAGAGACTACGTCCTCAAGCAAATC-3′ and reverse 5′-CGTAT-GACTTCTGCTCGCTGAGT-3′; FASN forward 5′-GCACCTCTCAGGCATCGA-3′ and reverse 5′-CTGTGGTC CCACTTGATGAG-3′. The gene GAPDH was used as the endogenous control reference gene. The threshold cycle number (C_t value) of different genes was normalized to the C_t value of GAPDH from the same sample, and the fold change in expression was calculated using the ΔΔCt method.[34] C_t values were calculated by technical triplicates.

Visualization of neutral lipids using Nile Red staining

DU145 cells were seeded at 5×10^4 cells per well density in 12-well plates containing glass coverslips. Next day, cells were treated with TNFα (20 ng ml^{-1}) or TGFβ (20 ng ml^{-1}) for 0, 6, 24 and 48 hours. Next, media was aspirated and cells were fixed for 20 min using cold methanol. Cells were stained for 1 hour by adding 1 ml of a 0.5 mg L^{-1} Nile Red (Sigma) solution in acetone. Then, cells were washed with PBS and left in PBS until further use. Finally, coverslips were mounted onto glass slides using ProLong® Diamond Antifade Mountant with DAPI (Life Technologies) and left in the dark for 30 minutes, according to the manufacturer's instructions. Samples were examined under a fluorescence microscope (60×, Nikon SMZ 1500, using DAPI and Red filters) fitted with a digital camera (Nikon DS-Ri1).

Quantification of lipid droplets was carried out using ImageJ software on three independent measurements.

Lipid extraction and LC-MS analysis

DU145 cells were seeded in triplicate in 6-well plates at 2×10^5 cells per well. After 24 hours, cells were treated with TNFα (20 ng ml^{-1}) for 0, 3, 4, 5 and 6 hours. Cells were harvested using a rubber scraper into 2 ml of ice-cold PBS. Cells were centrifuged at 1300 rpm for 3 minutes at 4 °C and pellets were washed twice with cold PBS. Samples were prepared twice to perform two types of lipid extraction: (1) extraction with chloroform/methanol (2 : 1) that contained intact lipids from the sample and (2) extraction with chloroform/methanol (1 : 2) with a saponification step that enabled the recovery of sphingolipids. For extraction 1, 100 μl of deionized water were added to the cell pellets and the suspension was transferred to borosilicate glass test tubes with Teflon caps. Then, 250 μl of methanol and 500 μl of chloroform were subsequently added. This mixture was fortified with internal standards of lipids (1, 2, 3–17 : 0 triglyceride, 1, 3–17 : 0 D5 diacylgliceride, 17 : 0 cholesteryl ester, 17 : 1 lyso phosphatidylethanolamine, 17 : 1 lyso phosphoglyceride, and 17 : 1 lyso phosphatidylcholine), 200 pmol each (10 μL of 20 μM stock solutions in absolute ethanol). Samples were vortexed and sonicated until they appeared dispersed. Next, the samples were evaporated under a N_2 stream and transferred to 1.5 ml eppendorf tubes after addition of 500 μl of methanol. Samples were evaporated again and resuspended in 150 μl of methanol. The tubes were centrifuged at 10 000 rpm for 3 minutes and 130 μl of the supernatants were transferred to UPLC vials for injection. For extraction 2, sphingolipids were prepared as described.[35] Briefly, 100 μl of deionized water were added to the cell pellets and the suspension was transferred to borosilicate glass test tubes with Teflon caps. Afterwards, 500 μl of methanol and 250 μl of chloroform were subsequently added. This mixture was fortified with internal standards of sphingolipids (*N*-dodecanoyl-sphingosine, *N*-dodecanoylglucosyl-sphingosine and *N*-dodecanoyl-sphingosylphosphorylcholine), 200 pmol each (10 μL of 20 μM stock solutions in absolute ethanol). Samples were sonicated until they appeared dispersed, and incubated overnight at 48 °C in a heating water bath. The tubes were cooled and 75 μl of 1 M KOH in methanol were added. After 2 h incubation at 37 °C, KOH was neutralized with 75 μl of 1 M acetic acid. The samples were then evaporated under a N_2 stream and transferred to 1.5 ml eppendorf tubes after the addition of 500 μl of methanol. Samples were evaporated again and resuspended in 150 μl of methanol. Finally, the tubes were centrifuged at 10 000 rpm for 3 minutes and 130 μl of the supernatants were transferred to UPLC vials for injection.

The LC/MS analysis consisted of a Waters Acquity UPLC system connected to a Waters LCT Premier orthogonal accelerated time of flight mass spectrometer (Waters), operated in both positive and negative electrospray ionization modes. Full scan spectra from 50 to 1500 Da were acquired, and individual spectra were summed to produce data points each of 0.2 s. Mass accuracy and reproducibility were maintained by using an independent reference spray *via* the LockSpray interference. The analytical column was a 100 × 2.1 mm inner diameter, 1.7 mm C8 Acquity UPLC bridged ethylene hybrid (Waters). The two mobile phases were phase A: MeOH 1 mM ammonium formate and phase B: H_2O 2 mM ammonium formate. The flow rate was 0.3 ml min^{-1} and the gradient of A/B solvents started at 80 : 20 and changed to 90 : 2 in 3 min; from 3 to 6 min remained at 90 : 10; changed to 99 : 1 in 6 minutes until min 15; remained 99 : 1 until minute 18; finally returned to the initial conditions until minute 20. The column was held at 30 °C.

Kinetic study of TAG increase

DU145 cells were seeded in triplicate in 6-well plates at 2×10^5 cells per well. After 24 hours, cells were treated with TNFα (20 ng ml^{-1}) for 0, 6, 24 and 48 hours. Cells were harvested using a rubber scraper into 2 ml of ice-cold PBS. Then, cells were centrifuged at 1300 rpm for 3 minutes at 4 °C and pellets were washed twice with cold PBS. Lipids were extracted using lipid extraction 1 and analysed using the same system mentioned above. Specific TAG species were integrated using the Masslynx software on the original raw data of samples and areas were further normalized by the protein content and the area of the internal TAG standard.

Chemometric analysis of LC-MS data

Each UPLC-MS chromatographic run recorded for every sample resulted in a data file which was converted to a CDF format by the Databridge program of the MassLynx software. Data were imported into MATLAB environment using mzcdfread and mzcdf2peaks functions from the MATLAB Bioinformatics Toolbox. Working data matrices were built up using in-house functions which bin all values with an m/z resolution of 0.05. This import process generated data matrices containing mass spectra at all retention times in their rows and the chromatograms at all m/z values in their columns. Next, data matrices were normalized taking into account the areas of the internal standards added and the protein content measured for each sample. This normalization was done by multiplying each matrix by a factor obtained as follows: (200 × mg protein)/mean area of standards; where 200 refers to the pmol of standards added in the lipid extraction.

These data were analysed in two different steps. First, an exploratory analysis of TIC chromatograms of treated and untreated samples was done by PLS-DA. This step gave us an initial idea about the differences and classification of samples, between pre- and post-EMT (see Fig. S2, ESI†). Second, a full scan LC-MS data analysis was performed by using MCR-ALS to detect the specific lipids that presented changes under EMT induction and to evaluate the significance of these changes.

In the second data treatment, the detection of specific lipid changes was done using full scan data matrices of every sample only in the positive ionization mode (negative mode samples were not considered as the samples could not be separated in the exploratory PLS-DA models). Due to huge dimensions of these data matrices (*e.g.* 612 retention times (rows) × 29 000 m/z values (columns)), each individual data matrix was subdivided into 11 time windows. These windows were not equal sized and

narrower divisions were made in chromatographic zones where peak signals were more abundant. Every data matrix corresponding to the same time window but to different samples (pre-EMT and post-EMT samples) was then adjoined to a single column-wise augmented data matrix.[36–38] Thus, 11 augmented data matrices were obtained for each type of extraction (a total of 22 matrices). Each augmented matrix was baseline corrected and subsequently scaled using an adaptation of the MinMax algorithm, also known as feature scaling, in order to favour the resolution of lipid profiles present low concentrations. MinMax algorithm rescales each column of the raw data matrix by subtracting the minimum value to each element of the column and dividing the result by the range of the column. A total of 44 matrices (22 raw and 22 scaled) were subjected separately to MCR-ALS data analysis. This chemometric tool allows the improved mathematical resolution of overlapping multivariate signals of different structure and complexity.[39–41] The successful application of MCR on LC-MS data in – omic studies for the resolution of coeluted and embedded peaks has been recently reported.[36–38,42] Application of MCR-ALS to the windowed augmented data matrices resulted in the resolution of a number of components, each one represented by a dyad of profiles that described their chromatographic elution and their mass spectra profiles. From the relative areas of these MCR-ALS resolved elution profiles, it is possible to estimate the relative amounts of components in every analysed sample. However, only those components with a significant difference in their elution profile peak areas between pre- and post-EMT samples were finally considered for further analysis. Although their MCR-ALS resolved MS spectra profiles at 0.05 *m*/*z* resolution may already allow a preliminary identification of the lipid species, a more exact identification is possible using original raw high-resolution data.[36,37,42] The corresponding elution peaks at these *m*/*z* values were subsequently integrated using the MassLynx software in order to obtain an accurate estimation of the amount of each lipid (identified by its *m*/*z* value) in each sample. This is extremely useful in the case of considering normalized data in which each MCR-ALS resolved component could present a relatively high number of candidate *m*/*z* values and assignation of MCR-ALS resolved area to a particular peak is not straightforward. The calculated areas were then normalized to the concentration of lipids (pmol mg^{-1} protein) as follows: (200 × mg of protein)/mean area of standards.

For these normalized concentrations of lipids, fold changes were calculated from the arithmetic mean values of each group. To check whether the difference observed in lipid peak areas between pre- and post-EMT samples were statistically significant, a Mann–Whitney *U* test was applied considering as a factor the different treatment times. Additionally, a discriminant analysis with PLS-DA was applied to the data matrix containing the concentrations of the selected lipids for each sample (X-data). PLS-DA y-vector had the class labels, pre-EMT (class 0) and post-EMT (class 1) samples for each extraction. These lipid concentration matrices were autoscaled before PLS-DA. The results were cross-validated by the leave-one-out method. Two out of the twenty-four samples analysed were removed appearing as outliers in the *Q* residuals *vs.* T^2 plots. The MCC[16] was calculated to validate the goodness of each discrimination model. The MCC is a correlation coefficient between the observed and predicted binary classifications; the returned values are between −1 and +1. A coefficient of +1 indicates a perfect prediction, a value of 0 indicates no better classification than a random prediction and a value of −1 represents total disagreement between prediction and observation. In the PLS-DA model obtained, the VIP scores,[17] which estimate the importance of each variable in the projection used in a PLS-DA model, were calculated.

The identification of compounds was only performed for *m*/*z* values with statistically significant differences in their areas (*p*-value of Mann–Whitney *U* test <0.05). LipidMaps[43] and Human Metabolome Database (HMDB)[44] were used for the identification of lipid species. The assigned compound corresponded to the lipid molecule with the minimum mass error value with respect to the measured *m*/*z*, considering all the possible adducts in the positive ionization mode. The annotated lipid also had to fulfil an adequate retention time regarding its polarity.

Finally, only identified compounds with a VIP score value greater than 1 and a mass error less than 10 ppm in the lipid identification were selected for further interpretation of lipidomic results.

Statistical analysis

The results are expressed as mean ± SD of three independent experiments unless otherwise specified. To check whether the differences observed in qRT-PCR and kinetic experiments were statistically significant, a Welch's *t*-test was used. The Mann–Whitney *U* test was used to assess the difference of means between the areas of the identified compounds in the different treatment times. The Benjamini–Hochberg procedure has been used to control the false discovery rate.

Software

The software used in this work includes MassLynx V 4.1 (Waters) for raw UPLC-TOF data analysis. For matrix data processing and statistical analyses, the Bioinformatics Toolbox (The Mathworks Inc.), PLS-Toolbox (Eigenvector Research Inc.) and MCR-ALS Toolbox[45] were used in the MATLAB 8.3.0 – R2013a (The Mathworks Inc.) environment. ImageJ (National Institutes of Health) was used for image processing and analysis.

Acknowledgements

This work was supported by the European Research Council under the European Union's Seventh Framework Programme (FP/2007-2013)/ERC Grant Agreement 320737. J.J. acknowledges a CSIC JAE-Doc contract cofounded by FSE.

References

1 K. Polyak and R. A. Weinberg, *Nat. Rev. Cancer*, 2009, **9**, 265–273.
2 J. P. Thiery and J. P. Sleeman, *Nat. Rev. Mol. Cell Biol.*, 2006, **7**, 131–142.

3 J. P. Thiery, H. Acloque, R. Y. Huang and M. A. Nieto, *Cell*, 2009, **139**, 871–890.
4 H. E. Zhau, V. Odero-Marah, H. W. Lue, T. Nomura, R. Wang, G. Chu, Z. R. Liu, B. P. Zhou, W. C. Huang and L. W. Chung, *Clin. Exp. Metastasis*, 2008, **25**, 601–610.
5 H. Peinado, D. Olmeda and A. Cano, *Nat. Rev. Cancer*, 2007, **7**, 415–428.
6 Y. Wu and B. P. Zhou, *Cell Cycle*, 2009, **8**, 3267–3273.
7 V. Michalaki, K. Syrigos, P. Charles and J. Waxman, *Br. J. Cancer*, 2004, **90**, 2312–2316.
8 M. Kumar, D. F. Allison, N. N. Baranova, J. J. Wamsley, A. J. Katz, S. Bekiranov, D. R. Jones and M. W. Mayo, *PLoS One*, 2013, **8**, e68597.
9 G. van Meer, *EMBO J.*, 2005, **24**, 3159–3165.
10 K. Sandra and P. Sandra, *Curr. Opin. Chem. Biol.*, 2013, **17**, 847–853.
11 D. Touboul and M. Gaudin, *Bioanalysis*, 2014, **6**, 541–561.
12 P. L. Wood, *Neuropsychopharmacology*, 2014, **39**, 24–33.
13 M. Oresic, V. A. Hanninen and A. Vidal-Puig, *Trends Biotechnol.*, 2008, **26**, 647–652.
14 R. Guirguis, I. Margulies, G. Taraboletti, E. Schiffmann and L. Liotta, *Nature*, 1987, **329**, 261–263.
15 J. Shankar, A. Messenberg, J. Chan, T. M. Underhill, L. J. Foster and I. R. Nabi, *Cancer Res.*, 2010, **70**, 3780–3790.
16 B. W. Matthews, *Biochim. Biophys. Acta*, 1975, **405**, 442–451.
17 S. Wold, M. Sjöström and L. Eriksson, *Chemom. Intell. Lab. Syst.*, 2001, **58**, 109–130.
18 V. Edmond, F. Dufour, G. Poiroux, K. Shoji, M. Malleter, A. Fouque, S. Tauzin, R. Rimokh, O. Sergent, A. Penna, A. Dupuy, T. Levade, N. Theret, O. Micheau, B. Segui and P. Legembre, *Oncogene*, 2015, **34**, 996–1005.
19 X. Wu, G. Daniels, P. Lee and M. E. Monaco, *Am. J. Clin. Exp. Urol.*, 2014, **2**, 111–120.
20 J. Fuxe and M. C. Karlsson, *Semin. Cancer Biol.*, 2012, **22**, 455–461.
21 C. H. Heldin, M. Vanlandewijck and A. Moustakas, *FEBS Lett.*, 2012, **586**, 1959–1970.
22 J. Xu, S. Lamouille and R. Derynck, *Cell Res.*, 2009, **19**, 156–172.
23 M. E. Linder and R. J. Deschenes, *Nat. Rev. Mol. Cell Biol.*, 2007, **8**, 74–84.
24 F. Guan, K. Handa and S. I. Hakomori, *Proc. Natl. Acad. Sci. U. S. A.*, 2009, **106**, 7461–7466.
25 F. Guan, L. Schaffer, K. Handa and S. I. Hakomori, *FASEB J.*, 2010, **24**, 4889–4903.
26 K. Goto, T. Asai, S. Hara, I. Namatame, H. Tomoda, M. Ikemoto and N. Oku, *Cancer Lett.*, 2005, **219**, 215–222.
27 J. Guo, B. Wang, Z. Fu, J. Wei and W. Lu, *Technol. Cancer Res. Treat.*, 2015, DOI: 10.1177/1533034614566413.
28 J. V. Joseph, S. Conroy, K. Pavlov, P. Sontakke, T. Tomar, E. Eggens-Meijer, V. Balasubramaniyan, M. Wagemakers, W. F. den Dunnen and F. A. Kruyt, *Cancer Lett.*, 2015, **359**, 107–116.
29 J. A. Menendez and R. Lupu, *Nat. Rev. Cancer*, 2007, **7**, 763–777.
30 G. Zadra, C. Photopoulos and M. Loda, *Biochim. Biophys. Acta*, 2013, **1831**, 1518–1532.
31 J. Li, L. Dong, D. Wei, X. Wang, S. Zhang and H. Li, *Int. J. Biol. Sci.*, 2014, **10**, 171–180.
32 L. Jiang, H. Wang, J. Li, X. Fang, H. Pan, X. Yuan and P. Zhang, *Int. J. Mol. Sci.*, 2014, **15**, 11539–11554.
33 D. K. Nomura, J. Z. Long, S. Niessen, H. S. Hoover, S. W. Ng and B. F. Cravatt, *Cell*, 2010, **140**, 49–61.
34 K. J. Livak and T. D. Schmittgen, *Methods*, 2001, **25**, 402–408.
35 A. H. Merrill, Jr., M. C. Sullards, J. C. Allegood, S. Kelly and E. Wang, *Methods*, 2005, **36**, 207–224.
36 M. Farrés, B. Piña and R. Tauler, *Metabolomics*, 2014, **11**, 210–224.
37 E. Gorrochategui, J. Casas, C. Porte, S. Lacorte and R. Tauler, *Anal. Chim. Acta*, 2015, **854**, 20–33.
38 K. M. G. Lima, C. Bedia and R. Tauler, *Microchem. J.*, 2014, **117**, 255–261.
39 J. Jaumot, R. Gargallo, A. de Juan and R. Tauler, *Chemom. Intell. Lab. Syst.*, 2005, **76**, 101–110.
40 E. Pere-Trepat, S. Lacorte and R. Tauler, *J. Chromatogr. A*, 2005, **1096**, 111–122.
41 R. Tauler, *Chemom. Intell. Lab. Syst.*, 1995, **30**, 133–146.
42 C. Bedia, N. Dalmau, J. Jaumot and R. Tauler, *Environ. Res.*, 2015, **140**, 18–31.
43 M. Sud, E. Fahy, D. Cotter, A. Brown, E. A. Dennis, C. K. Glass, A. H. Merrill, Jr., R. C. Murphy, C. R. Raetz, D. W. Russell and S. Subramaniam, *Nucleic Acids Res.*, 2007, **35**, D527–D532.
44 D. S. Wishart, T. Jewison, A. C. Guo, M. Wilson, C. Knox, Y. Liu, Y. Djoumbou, R. Mandal, F. Aziat, E. Dong, S. Bouatra, I. Sinelnikov, D. Arndt, J. Xia, P. Liu, F. Yallou, T. Bjorndahl, R. Perez-Pineiro, R. Eisner, F. Allen, V. Neveu, R. Greiner and A. Scalbert, *Nucleic Acids Res.*, 2013, **41**, D801–D807.
45 J. Jaumot, A. de Juan and R. Tauler, *Chemom. Intell. Lab. Syst.*, 2015, **140**, 1–12.

Informació Suplementària a la Publicació III

Epithelial-to-mesenchymal transition involves triacylglycerol accumulation in DU145 prostate cancer cells.

N. Dalmau, J. Jaumot, C. Bedia, R.Tauler.

Mol Biosyst **2015**, 11(12), 3397-3406

Epithelial-to-mesenchymal transition involves triacylglycerol accumulation in DU145 prostate cancer cells

Núria Dalmau, Joaquim Jaumot, Romà Tauler and Carmen Bedia

Supplementary material

EMT assessment by flow cytometry

EMT induction was confirmed under TNFα exposure in DU145 prostate cancer cells. EMT was assessed by flow cytometry on cells exposed to TNFα (20 ng/ml) for 24 hours, using a specific antibody against E-cadherin, a characteristic epithelial cell marker. The results showed a reduction of the fluorescence associated to membrane E-cadherin (Fig. S1), indicating that the reported conditions induced EMT in DU145 cells.

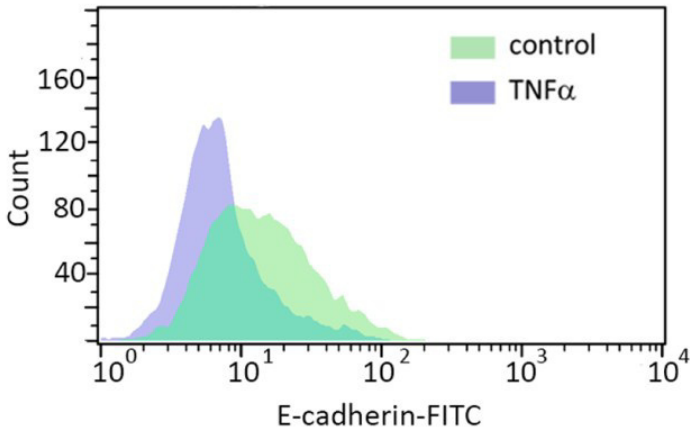

Fig S1. EMT induction in DU145 prostate cancer cells under TNFα treatment. Histogram of E-cadherin fluorescence intensity (FITC). DU145 prostate cancer cells were treated for 24 h with TNFα (20ng/ml) and stained with the anti E-cadherin-FITC antibody for 1 hour. The image illustrates a representative histogram of three independent measurements.

Exploratory analysis of TICs

A preliminary study on total ion current (TIC) chromatograms, obtained in both positive and negative ionization modes was carried out by Partial Least Squares-Discriminant Analysis (PLS-DA). This classification study was performed on matrices containing the normalized TICs of samples, in

order to see if their lipidomic profiles could separate samples corresponding to different times of TNFα exposure. PLS-DA is a supervised classification analysis tool that requires prior knowledge of class membership. In this case, two classes were chosen and defined as pre-EMT and post-EMT: samples at 0 and 3 hours were grouped into the pre-EMT class and samples at 5 and 6 hours into the post-EMT class. These classes were defined considering that at 0 and 3 hours mRNA levels of the EMT markers were similar and significantly different to the expression levels observed at 5 and 6 hours. As shown in the scores plot of the PLS-DA model (Fig. S2), the use of this class assignment resulted in a good discrimination between pre-EMT and post-EMT classes for both extraction 1 and 2 samples in the positive ionization mode. Samples at 4 hour-treatment were left out of the calculations as its inclusion in either pre or post-EMT classes impeded the correct separation of samples, probably due to an intermediate lipidic profile between pre and post-EMT samples. In contrast, the TICs of samples acquired in the negative mode in both extraction 1 and 2 could not be separated in the PLS-DA models, thus these data was not considered for further analysis. The clear separation between classes considering the TIC chromatograms in the positive mode suggested that substantial changes in the lipidomic profile occurred as a consequence of the EMT induction under TNFα treatment.

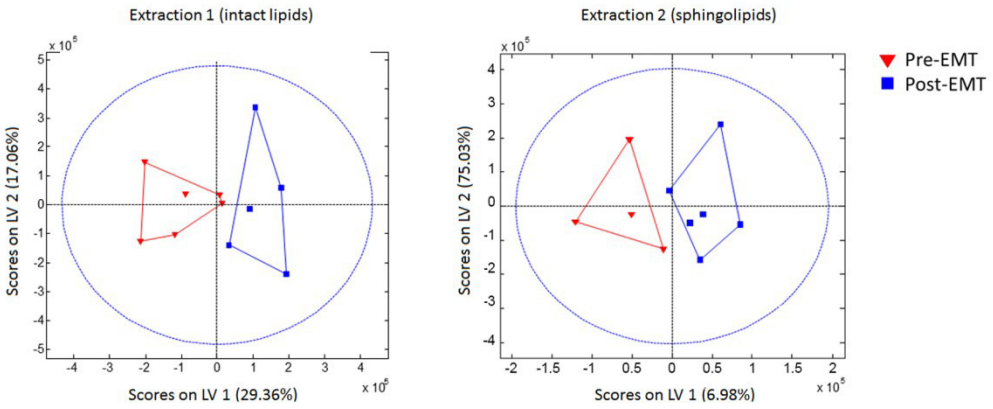

Figure S2. PLS-DA analysis of lipidomic data. Lipid extracts of DU145 cells treated with TNFα at different times were analysed through UPLC-TOF and data was imported into MATLAB environment. PLS-DA scores plots of matrices containing TICs data in the positive ionization mode of both types of extractions. Two classes were defined: pre-EMT, containing samples of 0 and 3h treatment and post-EMT, with the samples of 5 and 6h.

LC-MS profiles of samples and internal standards

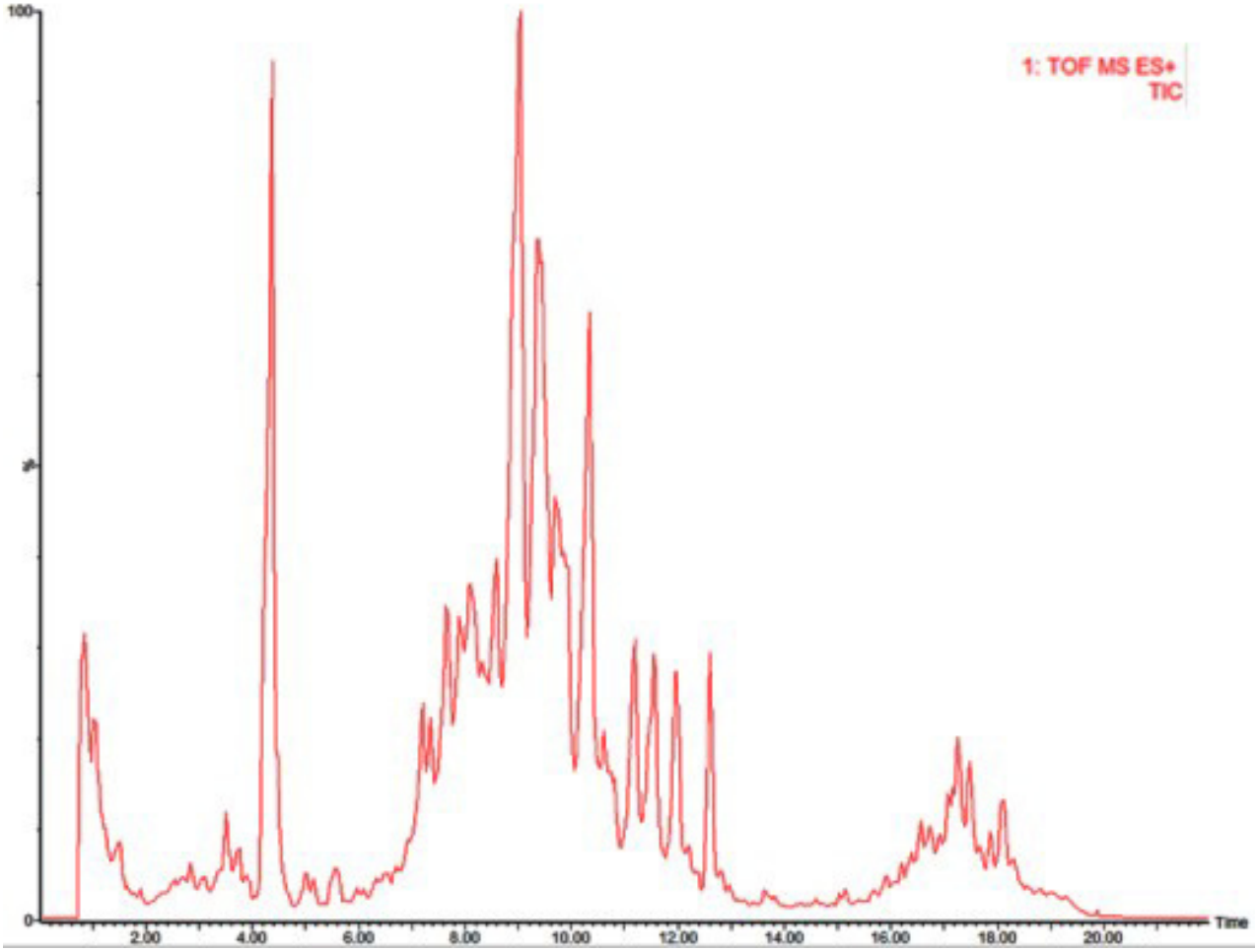

Figure S3. Representative LC-MS profile of extraction 1 samples

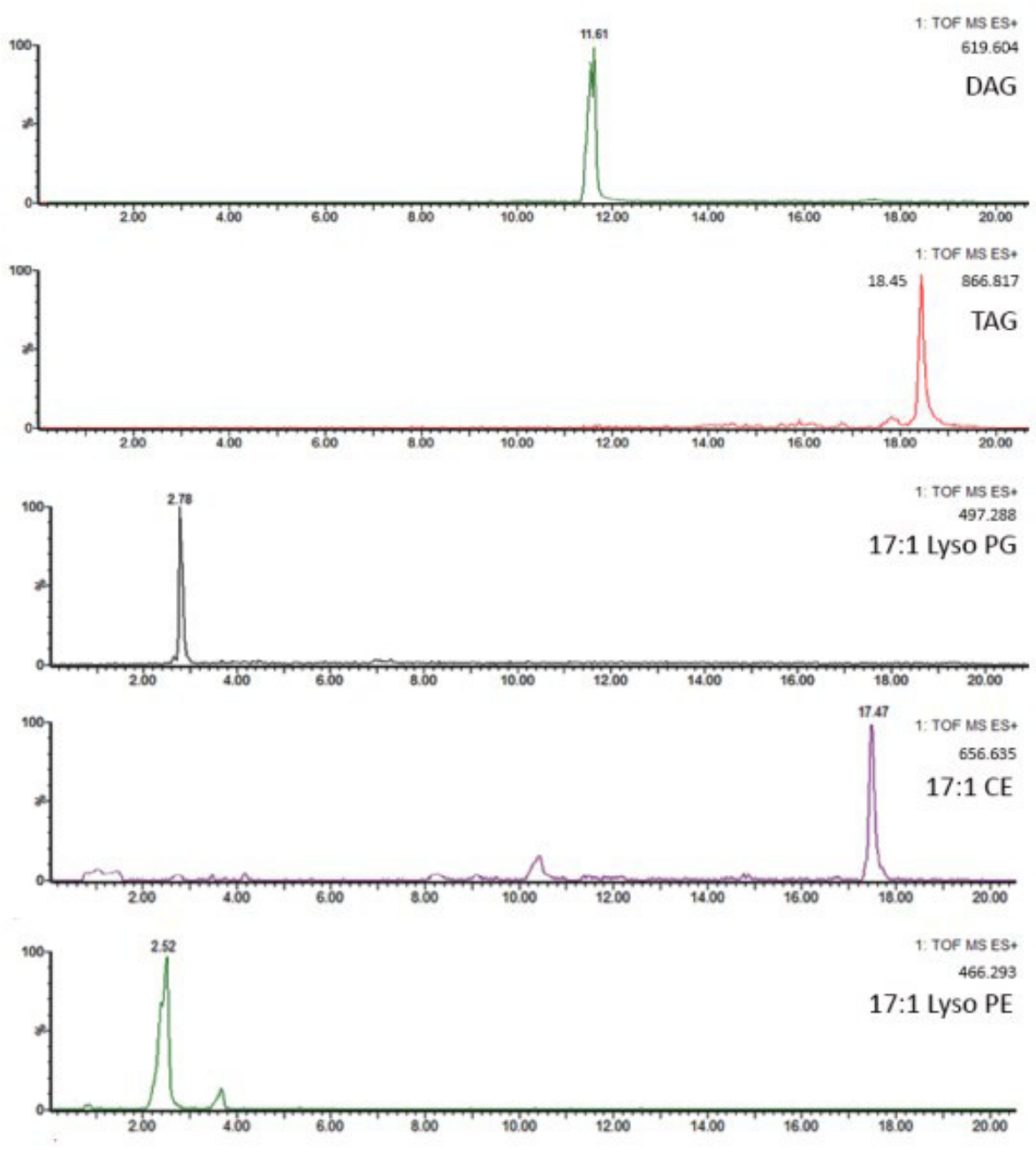

Figure S4. LC-MS profiles of internal standards added in extraction 1. DAG: 1,3-17:0 D5 diacylgliceride; TAG: 1,2,3-17:0 triacylglyceride; 17:1 Lyso PG: 17:1 lyso phosphoglyceride; 17:0 CE: 17:0 cholesteryl ester; 17:1 lysoPE: 17:1 lyso phosphatidylethanolamine.

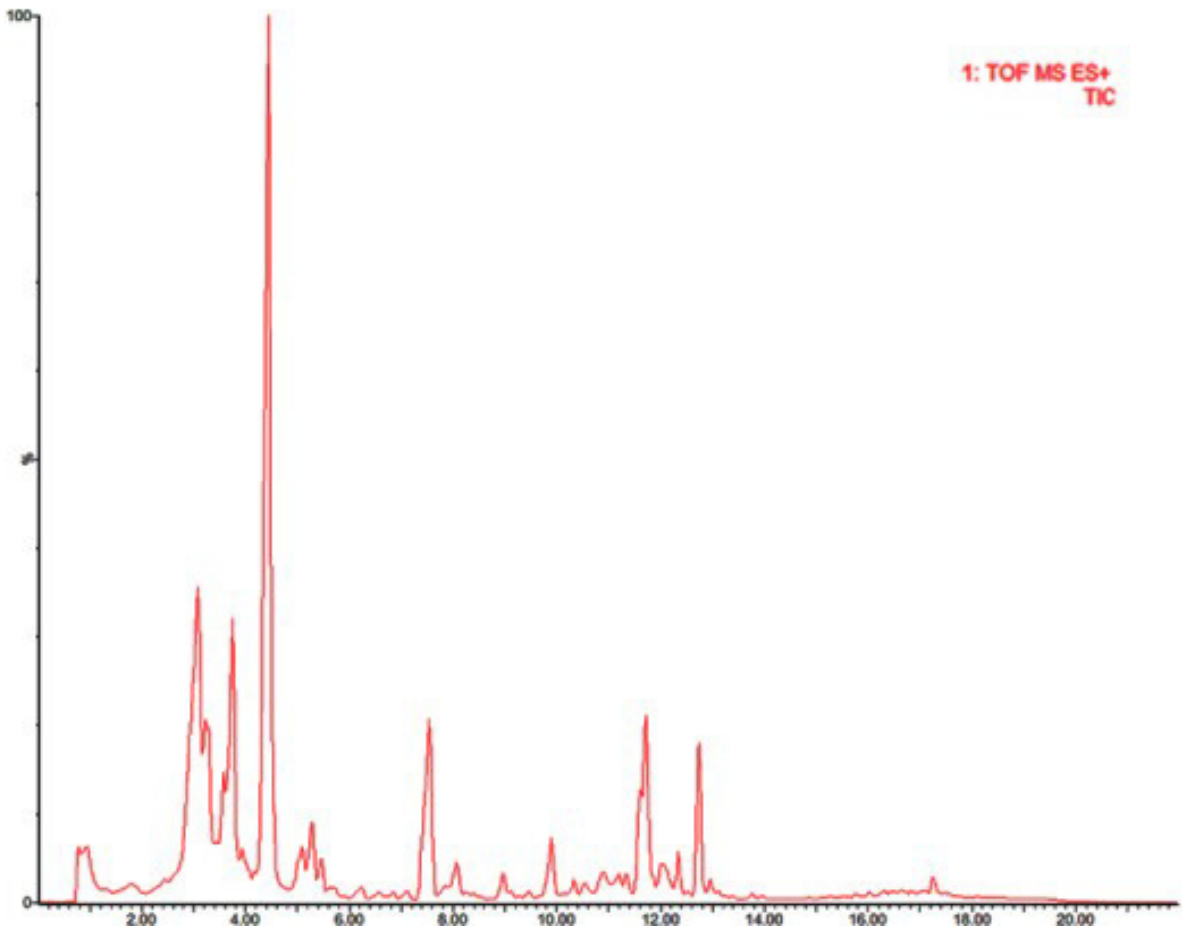

Figure S5. Representative LC-MS profile of extraction 2 samples

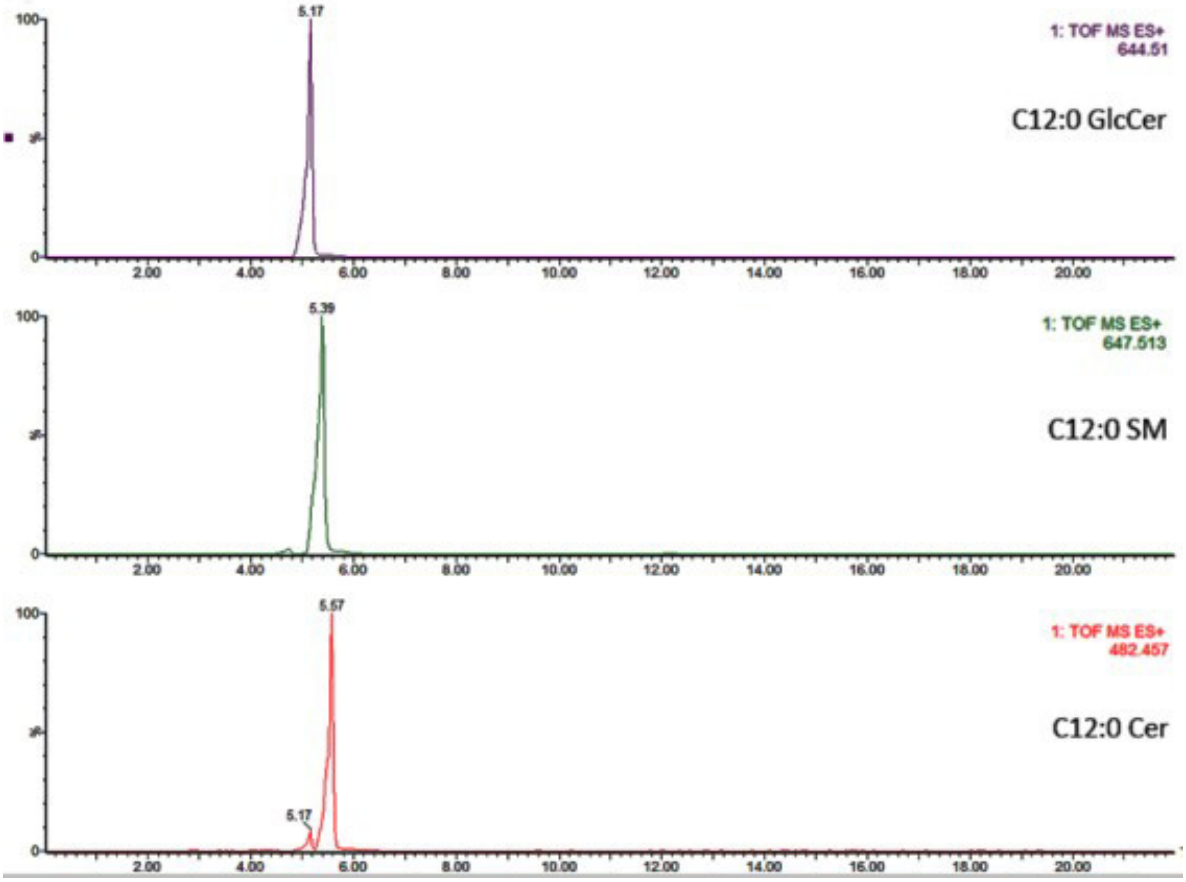

Figure S6. LC-MS profiles of internal standards added in extraction 2. C12:0 GlcCer: C12 glucosylceramide or N-dodecanoylglucosyl-sphingosine; C12:0 SM: C12 sphingomyelin or N-dodecanoylsphingosylphosphorylcholine; C12:0 Cer: C12 ceramide or N-dodecanoylsphingosine.

Experimental

Flow Cytometry Analysis

The EMT assessment by flow cytometry was performed following the recommendations previously reported by Strauss et al.[1] Briefly, cells were plated at a density of 2x105 cells per well in 12-well plates and left in culture until next day. Cells were treated with 20 ng/ml TNFα for 24 hours. Cells were harvested using PBS/EDTA for 5 minutes to preserve the E-cadherin in the cell membrane. Cells were washed twice, and cell pellets were stained with 20 µl/sample of anti CD324/E-cadherin conjugated to FITC (Life Technologies), according to the manufacturer's instructions. Samples were incubated on ice for one hour, and then washed with 200 µl of PBS. Green fluorescence emission of 5000 cells was measured for each sample with a Guava flow cytometer (Millipore), using Incyte software (Millipore). Calculated values of mean green fluorescence of histograms were used to compare TNF treated and untreated cells.

Exploratory analysis

For the preliminary analysis on TICS, mass values at each retention time were summed to obtain the TIC of each sample. Then, two matrices containing the TICs of treated samples at different times were constructed in both positive and negative ionization modes. Matrices were baseline corrected using the asymmetric least squares algorithm 2 and mean-centered. Then, the matrices were analysed by PLS-DA using the PLS Toolbox software for MATLAB. Data was cross-validated by applying the leave-one-out method, which was adequate for the small number of samples in this study. Three out of the twenty-four samples analysed were removed from the study as they appeared as outliers in the Q residuals *vs* T^2 plots. Taking into account the correct separation between classes and the results of qRT-PCR, pre-EMT class was defined by 0 and 3h samples and post-EMT class by 5 and 6h samples.

References

1. R. Strauss, J. Bartek and A. Lieber, *Methods in molecular biology*, 2013, **1049**, 355-368.
2. P. H. Eilers, *Analytical chemistry*, 2003, **75**, 3631-3636.

4.4. Discussió dels resultats

En aquest capítol es discuteixen els resultats obtinguts en els treballs de recerca portats a terme sobre els efectes de l'exposició crònica a diferents disruptors endocrins sobre el fenotip i la composició lipídica de les cèl·lules de càncer de pròstata DU145 i, l'assaig i caracterització de la EMT induïda per TNFα, en el mateix model cel·lular.

4.4.1. Efectes de l'exposició a disruptors endocrins sobre cèl·lules DU145 de càncer de pròstata

L'exposició crònica de les cèl·lules DU145 de càncer de pròstata als diferents disruptors endocrins ha permès detectar diversos canvis cel·lulars que denoten una fenotip més agressiu a causa de l'exposició.

Per tal de poder estudiar les alteracions causades per l'exposició crònica a diferents disruptors endocrins (DE), es van sembrar les cèl·lules de càncer de pròstata DU145 en 4 plaques de 6 pous. Es van disposar de manera que es tinguessin dos replicats independents per cada tractament. Les cèl·lules van ser tractades de forma crònica durant 50 dies, aplicant el tractament al finalitzar cada dilució cel·lular. La concentració utilitzada pel tractament crònic (1 μM) es va basar en un estudi previ de toxicitat per determinar que les concentracions no fossin tòxiques per cap dels DEs. El TNFα es va fer servir com a control positiu d'augment de mobilitat i agressivitat.

Per tal de detectar la transició cap a fenotips cel·lulars més agressius i/o malignes en les cèl·lules a causa de l'exposició crònica als diferents DEs, es van realitzar varies proves de biologia cel·lular. En la Taula 4.1 es mostren totes les proves que es van realitzar en els diferents tractaments per tal de determinar si s'apreciaven canvis en les cèl·lules respecte les control.

Taula 4.1. Resultats fenotípics de l'exposició als diferents DEs (Aldrin, Aroclor i CPF) respecte els controls.

Assaig	Aldrin	Aroclor	CPF
Inducció EMT (% reducció E-caderina respecte el control)	↓ 16%	No varia	↓ 14%
Migració cel·lular	No varia	↑ 134 %	↑ 126 %
Formació colònies	No varia	↑ 204 %	↑ 144 %
MMP-2 (invasivitat i metàstasi)	No varia	↑ 37 %	↑ 37 %
Proliferació cel·lular	No varia	No varia	No varia

Primer es va voler estudiar si s'havia induït la EMT en el nostre model de cèl·lules exposades durant 50 dies a Aldrin, Aroclor i CPF. Per fer-ho es va avaluar la presència de la E-caderina en els cultius cel·lulars. La E-caderina és una proteïna d'adhesió intercel·lular que ajuda en el manteniment de la integritat dels teixits. La progressiva desaparició de la E-caderina està relacionada amb la progressió de la EMT i l'adquisició de mobilitat cel·lular. Com a resultats, l'Aroclor no va mostrar cap variació respecte les cèl·lules no tractades, en canvi, l'Adrin i el CPF van mostrar una disminució significativa de la E-caderina, tant en els resultats de la citometria de flux com en la qPCR-RT, comparable a la induïda al control positiu (emprant TNFα). El següent assaig realitzat per avaluar un potencial increment de la invasivitat de les cèl·lules va ser el de la curació de ferida o *wound healing assay*, en el que es va mesurar la capacitat de les cèl·lules d'envair un espai creat en una placa de cultiu de cèl·lules confluent. Només l'Aroclor i el CPF van mostrar un augment significatiu respecte els controls en els nivells de migració. Posteriorment, es va portar a terme l'estudi de formació de colònies en cultius d'agar per determinar l'agressivitat de les cèl·lules tractades i la seva capacitat de colonitzar en medis adversos. En aquest assaig, només les cèl·lules DU145 tractades amb Aroclor i CPF van mostrar un increment en el nombre de colònies respecte el control, denotant així un increment considerable en les propietats migratòries i invasives de les cèl·lules. En el cas de l' Aldrin, no es va percebre cap increment significatiu en la formació de colònies. Un altre assaig que es va portar a terme va ser l'estudi de l'activitat de l'enzim metal·loproteïnasa 2 (MMP-2) mitjançant la tècnica de la zimografia. En aquest assaig només l'Aroclor i el CPF van mostrar un augment en l'enzim MMP-2, fet que indicava una capacitat augmentada de degradació

de la matriu extracel·lular, el que està relacionat amb una major habilitat invasiva i metastàsica de les cèl·lules. Per últim, també es va voler analitzar la proliferació cel·lular dels diferents tractaments (Aldrin, Aroclor i CPF), però cap d'ells va presentar canvis significatius. Tots aquests resultats demostren que es van produir diferents canvis fenotípics en les cèl·lules degut a les diferents exposicions cròniques a DEs. Cal destacar que les cèl·lules exposades a l'Aroclor i el CPF presenten canvis fenotípics similars, diferenciats dels observats sota l'exposició amb Aldrin.

4.4.2. Estudi lipidòmic sobre l'exposició a disruptors endocrins sobre cèl·lules DU145 de càncer de pròstata

L'estudi lipidòmic es va realitzar a partir de dues extraccions lipídiques, una general per tots els lípids i una d'altra més específica pels esfingolípids (SLs). Ambdues extraccions es van injectar en positiu i negatiu (ESI+ i ESI-) en el UHPLC-MS. L'exploració preliminar de les dades obtingudes amb un anàlisi de components principals (PCA) va evidenciar que l'exposició crònica als diferents DEs havia produït canvis en la composició lipídica de les cèl·lules. Un cop constatada aquesta observació es van processar les dades mitjançant la metodologia MCR-ALS, prèvia divisió per finestres del cromatograma. La Figura 8 de la publicació II mostra totes les especies lipídiques que presentaven canvis significatius (p-valor < 0.05) i VIPs >1) en les diverses extraccions de lípids i segons el contaminant. Es van trobar un total de 53 lípids diferentment presents en les cèl·lules exposades a l'Aldrin, 11 en el cas d'Aroclor i 12 pel que fa al CPF.

En el cas de l'**Aldrin**, es va detectar una reducció general de fosfolípids (PE i PC) de diferents llargades de cadena i d'alguns plasmalògens (P-PC i P-PE). Aquesta disminució pot ser deguda a l'acció hidrolítica de diverses fosfolipases (A, C i D) que condueix a la formació de missatgers secundaris lipídics. D'altra banda, es va detectar una disminució general dels esfingolípids: dhCer, Cer, SM, GlcCer i LacCer. Tant la reducció de SMs com de Cer estan en concordança amb un estudi previ de Edmond *et al.,* el qual relaciona una reducció dels nivells de Cer i SM amb una disminució de l'expressió de la CerS6 en el procés de la EMT.[3] La reducció dels nivells de ceramides està relacionada amb la disminució de la senyal apoptòtica en les cèl·lules. Això està

directament relacionat amb la supervivència cel·lular i la progressió tumoral, el que podria explicar la incipient transformació de les cèl·lules DU145 exposades a l'Aldrin.

En el cas de l'exposició crònica a l'**Aroclor** i el **CPF**, es van observar uns canvis significatius molt similars en ambdós tractaments. En les dues exposicions es va apreciar un increment de certes espècies PC i P-PC, LacCer(24:0), triacilglicèrids (TAGs) i de les cardiolipines. Les cardiolipines (CLs) identificades presentaven un gran increment respecte les mostres control. Aquest augment tant significatiu de les CLs pot suggerir un important rol en l'adquisició d'un fenotip metastàtic a causa de l'exposició crònica a l'Aroclor i el CPF. Les cardiolipines són considerades lípids bioactius que participen en el funcionament òptim de la fosforilació oxidativa d'enzims com l'ATP sintasa i en les cadenes respiratòries complexes[4] presents en la membrana mitocondrial. A més, les CLs suporten canvis conformacionals experimentats per les proteïnes de la família Bcl-2, que tenen un rol en la regulació de la mort cel·lular apoptòtica.[5] També s'ha suggerit una relació funcional entre la composició de les cadenes acil de les CLs (llargades i insaturacions) i la proliferació cel·lular.[6] Una recerca més extensa s'hauria de realitzar per tal de determinar el rol del les CLs en diferents escenaris d'adquisició de fenotips malignes. En quant als SLs, ambdues exposicions presenten canvis en els nivells de glicoesfingolípids (GSLs). L'exposició crònica a l'Aroclor presenta un increment significatiu de tres GluCer de llargades de cadena diferent (16, 18 i 22 carbonis). En comú per l'Aroclor i el CPF s'observa l'increment de la LacCer (24:0). Els GSLs són coneguts per la seva implicació en nombrosos processos cel·lulars fonamentals i són descrits com molècules crucials en l'adherència de cèl·lules tumorals. En l'exposició crònica al CPF, també destaca l'increment significatiu del gangliòsid GD1a. Els gangliòsids són GSLs caracteritzats per la presència de com a mínim un àcid siàlic lligat a la seva cadena d'oligosacàrids. Diverses evidències senyalen que els gangliòsids tenen diferents rols en la progressió tumoral com la angiogènesi, l'adhesió cel·lular i la metàstasi.[7] Especialment, el GD1a es troba involucrat en l'adhesió de les cèl·lules cancerígenes a les cèl·lules endotelials durant el procés de la metàstasi.[8-9]

En conjunt, les anàlisis realitzades suggereixen que l'exposició cel·lular a l'Aroclor i el CPF indueixen un fenotip maligne mitjançant mecanismes similars en ambdós exposicions, però ben diferents als resultats observats de l'exposició crònica a l'Aldrin.

4.4.3. Inducció de la EMT sobre cèl·lules DU145 de càncer de pròstata

Paral·lelament, el mateix model cel·lular va ser exposat al TNFα per tal d'induir la EMT i poder-ne estudiar l'evolució de la inducció EMT i poder-ne estudiar el seu patró en un procés tan essencial en les cèl·lules.

L'aparició de la EMT en cèl·lules exposades a l'Aldrin i la manca d'estudis sobre els lípids que participen en la seva inducció van propiciar un estudi separat sobre aquest tema. Es va emprar l'anàlisi lipidòmic no dirigit per tal d'explorar les dades de UHPLC-MS i descobrir quins canvis de lípids estan estretament relacionats amb la EMT. La inducció de EMT es va estimular amb la citoquina TNFα (20 ng/ml) i el seu seguiment es va fer mitjançant la citometria de flux i imatges d' immunofluorescència utilitzant anticossos anti E-caderina. En aquests assaigs s'aprecia com 6 hores de tractament són suficients per a la inducció de la EMT en el nostre model cel·lular. A part, en les imatges de les cèl·lules a les 6 hores s'observava la formació de pseudòpodes a la membrana plasmàtica de les cèl·lules. Els pseudòpodes són projeccions de la membrana cel·lular estretament relacionats amb la migració i invasió de cèl·lules tumorals. Per concretar més sobre el temps d'inducció de EMT, es va estudiar l'expressió dels gens relacionats en temps inferiors a 6 hores. Com a resultat es va observar que *CDH1* (E-caderina) disminuïa significativament a les 5 hores, i que els gens *VIM* (vimentin) i *SNAIL* (marcadors de EMT) presentaven un increment a partir de les 5 i 6 hores, respectivament. Totes aquestes observacions posen de manifest la inducció de la EMT en les cèl·lules DU145 a les 6 hores de ser tractades amb TNFα. Seguint els resultats presentats, es va procedir a un estudi lipidòmic no-dirigit que es va fer sobre mostres d'extraccions de lípids i esfingolípids de les cèl·lules a diferents temps d'exposició al TNFα (0, 3, 4, 5 i 6 hores). Segons els resultats dels temps d'inducció de EMT, es van agrupar les mostres en pre- EMT (0 i 3 hores de tractament) i post-EMT (5 i 6 hores de tractament). Les dades van ser processades mitjançant el

mètode MCR-ALS, prèvia divisió per finestres dels cromatogrames, degut al gran volum de dades. Els resultats obtinguts es mostren en la Taula 4.2. Clarament, s'aprecia que els majors canvis significatius s'han localitzat en els triacilglicèrids (TAGs) insaturats de diferents llargades, des de 50 fins a 58 carbonis, i amb uns increments (*fold change*) entre 1.6 i 2.5 vegades els valors del controls.

Taula 4.2. Llistat dels valors m/z que presenten canvis significatius (p-value>0.05) en els seus nivells entre els grups de mostres pre-EMT i post-EMT.

Temps retenció (min)	*m/z mesurat*	*Compost identificat*	*m/z calculat*	*Error masses (ppm)*	*Fold change*	*p-value*	*Valor VIP*	*ID base de dades*
7.8	538.5208	Cer(16:0)	538.5194	3	0.5	0.0209	2.2	HMDB04949
9.7	836.6181	PC(40:5)	836.6164	2	1.4	0.0362	10	HMDB08218
16.1	846.7559	TAG(50:3)	846.7545	2	2.2	0.0209	1.3	HMDB47737
16.5	848.7717	TAG(50:2)	848.7701	2	2.1	0.0209	1.2	HMDB44034
16.5	922.7806	TAG(56:7)	922.7858	5	2.5	0.0136	1.5	HMDB45356
16.6	948.7969	TAG(58:8)	948.8014	5	2.5	0.0136	1.6	HMDB51044
16.7	874.7870	TAG(52:3)	874.7858	1	2.2	0.0136	1.3	HMDB45489
16.9	950.8147	TAG(58:7)	950.8171	2	2.3	0.0136	1.6	HMDB50738
17.1	850.7863	TAG(50:1)	850.7858	0	1.6	0.0136	1.1	HMDB45481
17.3	876.8036	TAG(52:2)	876.8014	3	2.0	0.0136	1.4	HMDB42488
17.5	902.8262	TAG(54:3)	902.8171	10	2.0	0.0136	1.4	HMDB46267
17.9	878.8126	TAG(52:1)	878.8711	5	1.5	0.0362	0.9	HMDB42453
17.9	916.8317	TAG(55:3)	916.8328	1	2.0	0.0136	1.5	HMDB43548
13.1	904.8357	TAG(54:2)	904.8327	4	1.8	0.0136	1.4	HMDB46436
18.6	956.8592	TAG(58:4)	956.8640	5	2.1	0.0136	1.5	HMDB46326

Per corroborar l'increment de TAGs, es va realitzar un anàlisi lipidòmic dirigit dels TAGs identificats a més llarga exposició: 0, 6, 24 i 24 hores. Es van confirmar els resultats i es va detectar que l'increment màxim era a les 24 hores de tractament. A les 48 hores, moltes de les espècies de TAGs mantenien els nivells. A part, amb el mateix cultiu cel·lular tractat, es van analitzar els *lipid droplets,* que són orgànuls d'emmagatzematge de lípids consistents en una monocapa de fosfolípids que envolta un nucli de lípids neutres, TAGs o èsters de colesterol. Les imatges de fluorescència de cèl·lules incubades amb *Nile Red* van mostrar un increment significatiu de *lipid droplets* a les 6 hores, el que es mantenia fins a 24 i 48 hores després del tractament amb TNFα.

Un augment similar de TAGs va ser observat mitjançant la inducció de la EMT a les cèl·lules DU145 amb el factor de creixement transformant beta (TGFβ), un altre ben

conegut inductor de la EMT[10], suggerint que aquest augment de TAGs és un fenomen comú i important en el procés de la transició de les cèl·lules epitelials cap a un fenotip més agressiu. També, s'ha observat que els TAGs generats pel tractament amb TNFα i TGFβ són emmagatzemats en *lipid droplets* en ambdós casos. Els TAGs a més a més d'actuar com a reserves d'energia, poden actuar com a modificadors de proteïnes, incorporar-se a d'altres espècies de lípids per formar part de les membranes cel·lulars o com a generadors de senyals pro-oncogèniques. Per tot això, aquest increment significatiu de TAGs pot ser interpretat com un procés de preparació de les cèl·lules per una necessitat creixent d'energia, producció de membranes o de senyalització per tal de garantir la supervivència i proliferació de cèl·lules metastàtiques.

En el moment en que es va realitzar l'estudi, les publicacions referents als TAG en la progressió del càncer eren escasses. Un estudi previ de Goto *et al.* feia referència a com la hipòxia regula l'augment de la síntesi de TAGs i promociona la formació de lípid droplets.[11] A més, s'ha demostrat que inhibicions farmacològiques de la síntesis de TAGs poden cancel·lar la proliferació i motilitat de les cèl·lules cancerígenes en condicions d'hipòxia, indicant així que els nous TAGs sintetitzats juguen un rol clau en el creixement tumoral i de la metàstasis sota aquestes condicions. Diverses publicacions han relacionat la inducció de la EMT amb la hipòxia.[12-13] Actualment hi ha algun treball amb resultats molt similars al nostre estudi, com per exemple l'estudi de Giudetti *et al*., el qual mostra com les cèl·lules que han adquirit un perfil mesenquimal han reduït la lipogènesis, incrementen els nivells d'àcids grassos poliinsaturats i incrementen l'expressió de gens involucrats en la síntesis de TAGs i la formació de *lípid droplets*.[14]

En el nostre estudi també vam estudiar l'afectació en alguns mecanismes lipogènics mitjançant l'estudi de l'expressió de diferents enzims lipogènics com l'acetil-CoA carboxilasa a (ACACA) i l'àcid gras sintasa (FASN). L'expressió d'ambdós enzims va ser analitzada després de tractar les cèl·lules durant 6 hores amb TNFα. Com a resultat, no vam detectar cap canvi significatiu en l'expressió de l'ACACA, en canvi, el FASN, responsable de la producció de palmitat, va presentar una sobrexpressió. En nombrosos estudis s'ha reportat la mediació del FASN en la EMT en càncer d'ovari i de mama.[15] A més a més, en l'estudi de Giudetti *et al.* mostra la directa correlació del

increment de TAGs amb la diacilgliceroltransferasa (DGAT-1), un altre enzim important en la síntesis de TAGs en el càncer de mama.[14]

A més de l'increment significatiu dels TAGs, també es va detectar l'increment de la fosfatidilcolina (PC(40:5)) i de la disminució significativa de la ceramida (Cer(16:0). La disminució d'aquesta ceramida es mostra també en l'estudi de Edmond *et al.*[3] Els autors del treball reporten una disminució de la CerS6 en la EMT, l'enzim responsable de la síntesis de la Cer (16:0). Mostren com nivells baixos de Cer(16:0) incrementa la fluïdesa de la membrana i estimula la motilitat en cèl·lules epitelials tumorals. Les ceramides són característiques pel seu paper com senyalitzadors lipídics en respostes anti-proliferatives i en apoptosis. D'acord amb tot això, la reducció dels nivells de la ceramida (16:0) podria ser traduït en una disminució de les senyals pro-apoptòtiques, millorant la supervivència cel·lular, necessària per la progressió tumoral.

Per últim, cal mencionar que l'increment de TAGs s'ha observat en la inducció de la EMT com a canvi principal, però també en l'exposició crònica als diferents DEs: Aldrin, Aroclor i CPF. Tot fa indicar, com ja s'ha mencionat anteriorment, que l'augment de TAGs podria estar relacionat en una etapa de preparació de les cèl·lules com a font de reserves energètiques, components estructurals de la membrana o com a senyalitzadors moleculars. Un estudi previ de Fahner *et al.,* associava l'increment de TAGs amb el fenotip maligne en cèl·lules de càncer de colon.[16] L'increment de producció de TAGs es considera una part general de la transformació metabòlica de les cèl·lules cancerígenes.

4.4.4. Observacions finals

L'exposició crònica de les cèl·lules a DEs a dosis baixes no tòxiques té en les nostres condicions efectes sobre el fenotip i composició lipídica. Tot i que el model utilitzat són cèl·lules en cultiu i pot ser allunyat de la realitat, aquest estudi evidencia que una exposició prolongada en el temps a DEs a concentracions subtòxiques pot tenir conseqüències que no es poden arribar a predir quan només es té en compte la toxicitat aguda. Aquests resultats s'han de tenir en compte alhora de caracteritzar el risc d'exposició a aquests productes.

Pel que fa la EMT, s'ha realitzat una anàlisi lipidòmica no dirigida per caracteritzar el procés EMT des del punt de vista dels lípids, cosa que mai no havia estat explorada fins el moment. Entre altres resultats, les dades obtingudes evidencien un rol important dels triacilglicèrids en aquest procés, el que concorda amb resultats del primer treball d'exposició crònica a diferents DEs. Aquests resultats suposen una contribució al coneixement de la biologia cel·lular del càncer i poden ser útils en la recerca bàsica sobre la progressió tumoral.

4.5. Referències

1. Prins, G. S., Endocrine disruptors and prostate cancer risk. *Endocr Relat Cancer* **2008,** *15* (3), 649-56.
2. Sanchez de Badajoz, E.; Lage-Sanchez, J. M.; Sanchez-Gallegos, P., Endocrine disruptors and prostate cancer. *Arch Esp Urol* **2017,** *70* (3), 331-335.
3. Edmond, V.; Dufour, F.; Poiroux, G.; Shoji, K.; Malleter, M.; Fouque, A.; Tauzin, S.; Rimokh, R.; Sergent, O.; Penna, A.; Dupuy, A.; Levade, T.; Theret, N.; Micheau, O.; Segui, B.; Legembre, P., Downregulation of ceramide synthase-6 during epithelial-to-mesenchymal transition reduces plasma membrane fluidity and cancer cell motility. *Oncogene* **2015,** *34* (8), 996-1005.
4. Dumas, J. F.; Peyta, L.; Couet, C.; Servais, S., Implication of liver cardiolipins in mitochondrial energy metabolism disorder in cancer cachexia. *Biochimie* **2013,** *95* (1), 27-32.
5. Zhang, T.; Saghatelian, A., Emerging roles of lipids in BCL-2 family-regulated apoptosis. *Biochim Biophys Acta* **2013,** *1831* (10), 1542-54.
6. Schild, L.; Lendeckel, U.; Gardemann, A.; Wiswedel, I.; Schmidt, C. A.; Wolke, C.; Walther, R.; Grabarczyk, P.; Busemann, C., Composition of molecular cardiolipin species correlates with proliferation of lymphocytes. *Exp Biol Med (Maywood)* **2012,** *237* (4), 372-9.
7. Birkle, S.; Zeng, G.; Gao, L.; Yu, R. K.; Aubry, J., Role of tumor-associated gangliosides in cancer progression. *Biochimie* **2003,** *85* (3-4), 455-63.
8. Taki, T.; Ishikawa, D.; Ogura, M.; Nakajima, M.; Handa, S., Ganglioside GD1alpha functions in the adhesion of metastatic tumor cells to endothelial cells of the target tissue. *Cancer Res* **1997,** *57* (10), 1882-8.
9. Hatano, K.; Miyamoto, Y.; Nonomura, N.; Kaneda, Y., Expression of gangliosides, GD1a, and sialyl paragloboside is regulated by NF-kappaB-dependent transcriptional control of alpha2,3-sialyltransferase I, II, and VI in human castration-resistant prostate cancer cells. *Int J Cancer* **2011,** *129* (8), 1838-47.
10. Steller, E. J.; Raats, D. A.; Koster, J.; Rutten, B.; Govaert, K. M.; Emmink, B. L.; Snoeren, N.; van Hooff, S. R.; Holstege, F. C.; Maas, C.; Borel Rinkes, I. H.; Kranenburg, O., PDGFRB promotes liver metastasis formation of mesenchymal-like colorectal tumor cells. *Neoplasia* **2013,** *15* (2), 204-17.
11. Goto, K.; Asai, T.; Hara, S.; Namatame, I.; Tomoda, H.; Ikemoto, M.; Oku, N., Enhanced antitumor activity of xanthohumol, a diacylglycerol acyltransferase inhibitor, under hypoxia. *Cancer Lett* **2005,** *219* (2), 215-22.
12. Guo, Q.; Qin, W., DKK3 blocked translocation of beta-catenin/EMT induced by hypoxia and improved gemcitabine therapeutic effect in pancreatic cancer Bxpc-3 cell. *J Cell Mol Med* **2015,** *19* (12), 2832-41.

13. Joseph, J. V.; Conroy, S.; Pavlov, K.; Sontakke, P.; Tomar, T.; Eggens-Meijer, E.; Balasubramaniyan, V.; Wagemakers, M.; den Dunnen, W. F.; Kruyt, F. A., Hypoxia enhances migration and invasion in glioblastoma by promoting a mesenchymal shift mediated by the HIF1alpha-ZEB1 axis. *Cancer Lett* **2015,** *359* (1), 107-16.
14. Giudetti, A. M.; De Domenico, S.; Ragusa, A.; Lunetti, P.; Gaballo, A.; Franck, J.; Simeone, P.; Nicolardi, G.; De Nuccio, F.; Santino, A.; Capobianco, L.; Lanuti, P.; Fournier, I.; Salzet, M.; Maffia, M.; Vergara, D., A specific lipid metabolic profile is associated with the epithelial mesenchymal transition program. *Biochim Biophys Acta Mol Cell Biol Lipids* **2019,** *1864* (3), 344-357.
15. Jiang, L.; Wang, H.; Li, J.; Fang, X.; Pan, H.; Yuan, X.; Zhang, P., Up-regulated FASN expression promotes transcoelomic metastasis of ovarian cancer cell through epithelial-mesenchymal transition. *Int J Mol Sci* **2014,** *15* (7), 11539-54.
16. Fhaner, C. J.; Liu, S.; Ji, H.; Simpson, R. J.; Reid, G. E., Comprehensive lipidome profiling of isogenic primary and metastatic colon adenocarcinoma cell lines. *Anal Chem* **2012,** *84* (21), 8917-26.

Capítol 5.
Estudis fenotípics i lipidòmics sobre els efectes de la radiació UV en melanòcits i queratinòcits primaris

5.1. Introducció

La pell té funció de barrera ja que és la part més exposada del cos humà a agressions ambientals, entre les quals es troba la radiació solar. La llum ultraviolada (UV) està formada per la radiació UVA, de 315 a 400 nm, i la radiació UVB, de 285 a 315 nm. La radiació UVA penetra més profundament en l'epidermis cap a la dermis i pot promoure la generació d'espècies reactives d'oxigen (ROS) i induir la carcinogènesi de la pell *in vivo*.[1-2] Per altra banda, la radiació UVB afecta més a la capa basal de l'epidermis i és responsable directe dels danys en l'DNA i dels canvis més visibles com les cremades, el fotoenvelliment, la pèrdua d'elasticitat i to de la pell, la sequedat, la pigmentació irregular i la formació d'arrugues profundes.[3]

Els estudis sobre la radiació UV i els efectes que originen tan a curt com a llarg termini són importants ja que tota la població hi està exposada. En els darrers anys s'ha detectat que la radiació solar pot esdevenir més intensa degut a la disminució del gruix en la capa d'ozó i els forats que han sorgit en algunes zones, com els pols o algunes regions d'Australia.[4-5] Per tot això, resulta de gran interès estudiar els efectes de la radiació UV sobre la nostra pell i poder així entendre millor les seves conseqüències.

En aquesta secció es discuteixen els resultats obtinguts en els treballs de recerca portats a terme sobre els efectes de la radiació UV sobre el fenotip i la composició lipídica de les cèl·lules més importants de la pell (queratinòcits i melanòcits). En la realització d'aquests treballs es van fer servir cultius primaris de melanòcits i queratinòcits, que són models de cèl·lules més semblants a les condicions que poden produir-se *in vivo*. Les cèl·lules es van exposar de forma aguda i crònica una radiació UV a una proporció UVA/UVB similar a la de la llum solar en l'hora de la màxima exposició en la nostre regió (728 mJ cm^{-2} UVA i 25 mJ cm^{-2} UVB). A continuació, es discutiran els canvis fenotípics i del cicle cel·lular observats, i per altra banda, la petjada lipídica associada a l'exposició aguda i crònica de queratinòcits i melanòcits a la radiació UV.

Aquest capítol inclou les publicacions:

Publicació IV. *Untargeted lipidomic analysis of primary human epidermal melanocytes acutely and chronically exposed to UV radiation.* N. Dalmau, N. Andrieu-Abadie, R.Tauler, C. Bedia. *Mol Omics* **2018**, 14(3), 170-180

Publicació V. *Phenotypic and lipidomic characterization of primary human epidermal keratinocytes exposed to simulated solar UV radiation. .* N. Dalmau, N. Andrieu-Abadie, R.Tauler, C. Bedia. *J Dermatol Sci* **2018**, 92(1), 97-105

5.2. Publicació IV

Untargeted lipidomic analysis of primary human epidermal melanocytes acutely and chronically exposed to UV radiation.

N. Dalmau, N. Andrieu-Abadie, R.Tauler, C. Bedia.

Mol Omics **2018**, 14(3), 170-180

Molecular Omics

RESEARCH ARTICLE

View Article Online
View Journal | View Issue

Cite this: *Mol. Omics*, 2018, **14**, 170

Untargeted lipidomic analysis of primary human epidermal melanocytes acutely and chronically exposed to UV radiation†

Núria Dalmau,[a] Nathalie Andrieu-Abadie,[b] Romà Tauler [a] and Carmen Bedia *[a]

Received 7th March 2018,
Accepted 23rd April 2018

DOI: 10.1039/c8mo00060c

rsc.li/molomics

Ultraviolet (UV) radiation present in sunlight has been related to harmful effects on skin such as premature aging and skin cancer. In order to study the effects of UV radiation on skin, many investigations have been carried out at transcriptomic and proteomic levels. However, studies on the effects of UV radiation on lipid composition are scarce. In this work, primary cultures of melanocytes were exposed to UV radiation in a similar UVA/UVB ratio to that found in solar light. The UV exposure was carried out twice a week and different endpoints were investigated at 0.5 (acute exposure), 1.5 and 3 weeks. As a result, dendrite formation and a progressive reduction in cell viability were observed. Also, cell cycle arrest and a reduced E-cadherin content were detected at 0.5 and 1.5 weeks. In the second stage of the study, lipid extracts of melanocytes were analysed by liquid chromatography coupled to mass spectrometry (LC-MS) and subjected to an untargeted lipidomic approach using the ROIMCR chemometric method. Among the most important changes observed under UV irradiation, lipid raft components such as sphingomyelins and GM3 gangliosides as well as other signalling molecules such as phosphatidylinositols decreased progressively with time. These modifications indicated strong effects on important functions such as cell signalling and recognition. In contrast, triacylglycerol species, associated with energy storage, increased progressively, which could be interpreted as a survival mechanism under adverse conditions. Further studies are needed to better understand the functional implications of the changes observed.

1. Introduction

Ultraviolet (UV) light is known to produce a variety of biological effects on skin cells. While acute exposure to UV has been associated with erythema and pigment darkening, chronic exposure has been related to skin cancer, skin aging, and local and systemic immunosuppression.[1] UV radiation is composed of UVA (315–400 nm) and UVB (285–315 nm). UVA penetrates deeply through the epidermis into the dermis and is able to promote the production of reactive oxygen species (ROS) and to induce skin carcinogenesis *in vivo*.[2,3] UVB radiation mostly affects the epidermal basal cell layer of the skin.[4] It is responsible for direct DNA damage in epidermal and dermal cells and results in a variety of harmful effects on human skin, including sunburn, photoaging, and increased susceptibility to skin cancers such as melanoma.[5]

Lipids play a key role in living organisms. Among their multiple biological functions, they contribute to cell compartmentalization, energy production and storage, cell signalling, protein trafficking, and membrane organization. Lipidomics is a relatively new field that quantitatively evaluates a range of lipid species at once, and can be used to generate a lipid profile for most pathophysiological states. Lipidomics has been recently applied as a useful tool in the study of lipid-mediated mechanisms in many diseases such as diabetes,[6] obesity,[7] some types of human cancer[8,9] and also biological processes such as epithelial to mesenchymal transition.[10]

In recent years, the development of high-throughput analytical approaches has enabled the identification of UV-responsive changes at different molecular levels, such as in gene expression,[11–13] proteins[14,15] or metabolites.[16–18] Despite the importance of lipids in cell membrane structure and signalling functions, few studies are dedicated to the study of cell lipids under UV radiation. Some investigations have focused on the changes in ceramide levels in the mitochondria of HeLa cells,[19] the activation of sphingomyelinases in keratinocytes[20] or the time-dependent effect on the levels of phospholipids in skin fibroblasts upon different types of UV irradiation.[21] Also, Reich *et al.* published a more complete

[a] *Department of Environmental Chemistry, Institute of Environmental Assessment and Water Research (IDAEA-CSIC), c/Jordi Girona 18-24, 08034 Barcelona, Spain. E-mail: carmen.bedia@idaea.csic.es; Tel: +34-934006140-1410*

[b] *INSERM UMR 1037, Centre de Recherches en Cancérologie de Toulouse (CRCT), 31037, Toulouse, France*

† Electronic supplementary information (ESI) available. See DOI: 10.1039/c8mo00060c

lipidomic analysis of UVB narrow band-irradiated HaCaT keratinocytes.[22] In spite of these studies, the untargeted analysis of lipids from skin cells, and pigmented cells in particular, exposed to simulated solar UV radiation has not yet been explored.

The present study aimed to elucidate the changes in the lipid profile of melanocytes induced under UV irradiation. Melanocytes are located in the epidermis where they play a photoprotective role through the production of melanin, which, afterwards, is transferred to the surrounding keratinocytes. In this work, primary human epidermal melanocytes were exposed to simulated solar UV radiation at different endpoints and the accompanying changes in the morphology, cell cycle and cell proliferation upon UV irradiation were studied. Melanocyte lipid extracts were analysed together with non-exposed melanocytes by liquid chromatography–mass spectrometry (LC-MS). Then, an untargeted analysis of LC-MS data was performed using a chemometric approach, ROIMCR. The lipid profiles of UV irradiated melanocytes sufficiently differed from those of controls to enable a clear discrimination between groups. The most relevant lipid changes in melanocytes under UV are presented and discussed.

2. Materials and methods

2.1. Cell culture

Primary human epidermal melanocytes were a gift from Dr Corine Bertolotto (C3M, Nice, France). Melanocytes were cultured in Medium 254 (Gibco) supplemented with Human Melanocyte Growth Supplement (HMGS, Gibco) and 100 U per ml penicillin and 100 μg per ml streptomycin (Thermo Fisher Scientific), at 37 °C in a humidified atmosphere containing 5% of CO_2.

2.2. UV irradiation

Cultured melanocytes were irradiated in a Suntest CPS (Atlas, USA) solar simulation unit. This simulator is equipped with a xenon arc lamp that provides irradiance that simulates sunlight. The UVA/UVB radiation intensity was controlled using a VLX-3W radiometer (Vilber Lourmat). The simulated UV daylight applied in this work presented a UVA/UVB irradiance ratio of 29 (it has been estimated that a UVA/UVB ratio between 23 and 32 is representative of the UV daylight spectrum).[23] This irradiation was selected taking into account the UVB irradiation intensities used in the literature for studies related to sunlight exposure[20,24–26] and the results of a previous melanocyte viability test carried out after UV exposure at different irradiation intensities. The chosen UV dose (728 mJ cm^{-2} UVA and 25 mJ cm^{-2} UVB) was the highest dose that did not produce any change in cell viability 72 h post-irradiation (data not shown).

Melanocytes were seeded into 6-well plates (Nunclon surface, Thermo Scientific) and kept in culture under standard conditions. Just before irradiation, an acetate plastic sheet was placed above the plate to adapt the UVA/UVB ratio to 29 : 1. Cells were placed inside the Suntest chamber and were irradiated for five min, which represented the final UV radiation dose of 728 mJ cm^{-2} UVA and 25 mJ cm^{-2} UVB. After irradiation, cells were rinsed with PBS 1×, fresh medium was added to the cells, and plates were incubated again under standard conditions. Following this procedure, irradiations were applied twice a week to the melanocyte cultures. In this work, three different exposure endpoints were tested: 0.5 week (0.5W) which is equivalent to one irradiation (acute irradiation), and 1.5 weeks (1.5W) and 3 weeks (3W) that are equivalent to 3 and 6 exposures to UV irradiation, respectively. At each time, cells exposed to sham light were used as a control reference and were subjected to identical culture conditions to those used for UV-irradiated cells. In the second phase of the work, longer exposures to UV were performed at five weeks (5W) and twelve weeks (12W), representing 10 and 24 exposures to UV radiation, respectively.

2.3. Cell viability

Cell viability was determined using the 3-(4,5-dimethylthiazol-2-yl)-2,5-diphenyltetrazolium bromide (MTT, Sigma) assay on 96-well plates, according to the manufacturer's instructions.

2.4. Western blot

Cells were harvested by trypsinization, centrifuged and washed twice with PBS 1×. Then, cells were lysed using mammalian lysis buffer 1× (ab179835, Abcam) and cocktail protein inhibitor 1× (Thermo Scientific). Proteins in cell lysates were quantified using the BCA assay (Thermo Scientific) and 90 μg of proteins per sample was resolved by 10% SDS-PAGE. Proteins were transferred to PVDF membranes (Roche). Membranes were blocked with TBS 1× containing 0.1% Tween 20 and probed with the cell cycle antibody cocktail (ab136810, Abcam). The membranes were developed using the chemiluminescent signal detection kit ECL™ Prime Western Blotting detection reagent (GE Healthcare) and visualized using a LICOR C-DiGit blot scanner. Relative quantification of western blot band intensity was performed using Image Studio Lite ver. 5.0 software; values were normalized to those of β-actin, and differences between irradiated and control samples were calculated.

2.5. Quantitative real-time PCR

At each endpoint (0.5W, 1.5W and 3W), cells were harvested by trypsinization, centrifuged and washed twice with PBS 1×. Total RNA was extracted using the NucleoSpin RNA kit (Macherey-Nagel). RNA (1.5 μg) was retro-transcribed to cDNA using a Transcriptor First Strand Synthesis Kit (Roche) and stored at −20 °C. Quantitative PCR was carried out using a LightCycler® 480 Real Time PCR system (Roche). The primers used in each reaction were as follows: *CDH1* forward 5′-TACACTGCCCAGGAGCCAGA-3′ and reverse 5′-TGGCACCAGTGTCCGGATTA-3′; *SNAI1* forward 5′-GACCACTATGCCGCGCTCTT-3′ and reverse 5′-GTGGGATGGCTGCCAGC-3′; *VIM* forward 5′-TGAGTACCGGAGACAGGTGCAG-3′ and reverse 5′-TAGCAGCTTCAACGGCAAAGTTC-3′.

The GAPDH and ACTB genes were used as endogenous control reference genes. The threshold cycle numbers (C_t values) of different genes were normalized to the C_t value of mean control genes from the same sample, and the fold change in expression was calculated using the $\Delta\Delta C_t$ method.[27] C_t values were calculated from technical triplicates.

2.6. Reactive oxygen species (ROS) assay

To evaluate the formation of ROS after UV acute irradiation, melanocytes were seeded into 96-well plates at 10^5 cells per ml and incubated for 24 hours. Immediately prior to use, a fresh stock solution of carboxy-H_2DCFDA (Sigma) was prepared in dimethyl sulfoxide (DMSO). Melanocytes were washed twice with PBS 1×, and the dye (carboxy-H_2DCFDA) was added at a final concentration of 32 μM to cell wells. After 30 min under regular incubation conditions, the dye solution was removed, cells were washed twice with PBS 1× and incubated with fresh medium. Then, cells were irradiated in the Suntest CPS, and immediately after that, fluorescence was measured using a plate reader (485/535 nm exc./em.).

2.7. Lipid extraction and LC-MS analysis

Cells were harvested using trypsin and centrifuged at 1300 rpm for 3 min at 4 °C and cell pellets corresponding to 10^6 cells per sample were washed twice with cold PBS 1×. Two types of extraction were used in this work, one to extract all lipids and the other to specifically extract sphingolipids, as previously described.[10] LC-MS analysis used a Waters Acquity UHPLC system connected to a Waters LCT Premier orthogonal acceleration time of flight (ToF) mass spectrometer (Waters), operated in positive and negative electrospray ionization modes (ESI + and ESI −). Full scan spectra between 50 and 1500 Da were acquired, and individual spectra were summed to produce data points every 0.2 second. Mass accuracy and reproducibility were maintained using an independent reference spray *via* the LockSpray interference. The analytical column was a 100 × 2.1 mm inner diameter, 1.7 mm C8 Acquity UPLC ethylene bridged hybrid (Waters). The two mobile phases were phase A (MeOH, 1 mM ammonium formate) and phase B (H_2O, 2 mM ammonium formate, 0.2% formic acid for both solutions). The flow rate was 0.3 ml min^{-1} and the gradient of A/B solvents started at 80 : 20 and changed to 99 : 1 in 6 min until min 15; remained at 99 : 1 until minute 18; and finally returned to the initial conditions until minute 20. The column was held at 30 °C.

2.8. Chemometric analysis of LC-MS data

One single LC-MS chromatographic run from the analysis of one sample resulted in a data file which was converted to the CDF format *via* DataBridge (MassLynx software, Waters). Data sets from the different chromatographic runs were then imported and stored in the MATLAB computational environment (release R2016b; The MathWorks Inc.), using *mzcdfread* and *mzcdf2peaks* functions from the MATLAB Bioinformatics Toolbox™.

The method used here to analyse the LC-MS data comprises two steps: first, a data compression step based on the Region of Interest (ROI) concept,[28] and second, the analysis of the compressed data using the Multivariate Curve Resolution-Alternating Least Squares (MCR-ALS)[29] methodology. This combined approach (ROIMCR) has been successfully used in different untargeted metabolomics investigations using LC-MS.[30–33]

In the first compression step, significant intensity MS values, higher than a threshold value (estimated from the instrumental noise level), were searched on the raw MS spectral scans. These ROI values also have to be represented by a minimum of consecutive data points in the chromatogram, as well as to have a particular m/z deviation error.[30–33] The ROI compression step takes advantage of the sparse structure of the measured MS data reducing considerably the computer storage and computation time needed without losing the instrumental mass resolution. This procedure has been described in more detail by Gorrochategui *et al.*[34] In our study, control and UV-exposed samples at each UV exposure endpoint were analysed together, either using positive and negative ionization data. This procedure was repeated for each of the endpoints studied. As a result of the ROI compression step, a matrix containing all the ROI m/z values for the different samples (common and not common) with significant traces was built (D_{aug}).

Then, the compressed matrices were analysed using MCR-ALS. This method has been shown to be a powerful chemometric tool for the resolution of overlapping multivariate signals and for the bilinear decomposition of two and multi-way data arrays of different complexity and structure.[35,36] MCR-ALS has been successfully applied for the resolution of LC-MS data sets with strongly coeluted and hidden peaks, and it has been extended more recently to omic studies.[10,37–43]

Initialization of the MCR-ALS procedure when applied to augmented data matrices (D_{aug}) was performed using estimates of spectral profiles found at the purest elution times. The applied constraints were the non-negativity of elution and spectral profiles, and spectral normalization (equal height).[44] Results of MCR-ALS generated a data table that contains the peak areas of the elution profiles of the different resolved components in the different samples. The pure spectra of the MCR-ALS resolved components (lipids) were recovered without any loss of spectral resolution, and identified using the Human Metabolome database (HMDB).[45]

To investigate if lipidomic profiles were different enough to discriminate between irradiated and non-irradiated samples, Partial Least Squares Discriminant Analysis (PLS-DA) was performed. The data matrix of areas obtained from the MCR-ALS resolved components was used for PLS-DA analysis, previously refined with the variables (lipids) identified. The classes considered were control (class 0) and UV irradiated (class 1) for each endpoint. These lipid area matrices were autoscaled before PLS-DA and the results were cross-validated by the leave-one-out method. The Matthews Correlation Coefficient (MCC)[46] was calculated to validate the goodness of each discrimination model. The MCC is a correlation coefficient between the observed and predicted binary classifications; the values move between +1 and −1. A coefficient of +1 indicates a perfect prediction, a value of 0 indicates no better classification than random prediction and a value of −1 represents a total disagreement between prediction and observation. In the PLS-DA model obtained, the VIP scores,[47] which estimate the importance of each variable (lipids) in the projection used in the PLS-DA model, were calculated.

2.9. Statistical analysis

The results are expressed as means ± SD of three independent experiments unless otherwise indicated. To check whether the

differences observed in qRT-PCR and kinetic experiments were statistically significant, Welch's *t*-test was used.

2.10. Software

Software used in this work includes MassLynx V 4.1 (Waters) for raw UPLC-TOF data analysis and data conversion to the *cdf* format. For matrix data processing and statistical analyses, the Bioinformatics Toolbox (The MathWorks Inc.), Statistics Toolbox (The MathWorks Inc.), PLS-Toolbox (Eigenvector Research Inc.) and MCR-ALS Toolbox[48] were used in a MATLAB 8.3.0-R2016a (The MathWorks Inc.) environment.

3. Results

3.1. Effects of UV exposure on cell viability, the cell cycle and cell proliferation

Cells were irradiated (728 mJ cm^{-2} UVA and 25 mJ cm^{-2} UVB) twice a week for different periods: 0.5 week, 1.5 weeks and 3 weeks (designated as 0.5W, 1.5W and 3W). In the first approach, cell viability, the cell cycle and the potential acquirement of a malignant phenotype under UV exposure were explored. With increasing exposure times, a progressive decrease of cell viability was observed, as shown by the reduction of protein amounts in the irradiated melanocyte cultures (Fig. 1A). UV exposure also affected the morphology of melanocytes. As shown in Fig. 1B, a remarkable increase in the number and length of dendrites in 3W irradiated melanocytes was observed.

One of the best known consequences of UV-radiation is the production of reactive oxygen species (ROS) that, in turn, are able to elicit DNA damage. Previous studies on cell cultures have also reported changes in the cell cycle as a response to DNA damage induced by UV radiation.[20,49,50] DNA damage can trigger the activation of DNA checkpoints that trigger cycle arrest at various points of the cell cycle.[51] In our primary cell cultures of melanocytes, ROS were generated after UV exposure, just after irradiation (Fig. 1C). When the effects on the cell cycle were explored, increased levels of Cdk2 pTyr15, a marker of G1/S phase arrest, and histone 3, a marker of M phase arrest, were observed at 0.5W and 1.5W (Fig. 2A), suggesting that DNA checkpoints are activated in order to pause the replication of a damaged genome and to buy time for the activation of DNA repair systems. However, 3W irradiated cells returned to normal levels as they did not present any significant difference in cell cycle markers compared to control melanocytes.

To determine the ability of cells to proliferate after the different UV irradiation periods, irradiated and control cells were seeded into 96-well plates and left to grow for 72 h under the standard incubation conditions used in this study. An MTT viability test was performed every day. No statistically significant differences were observed in proliferation rates between control and irradiated melanocytes in any of the UV irradiation endpoints (Fig. 2B). The possibility that UV radiation induces epithelial-to-mesenchymal transition (EMT) was also explored in 0.5W, 1.5W and 3W melanocytes. Expression levels of E-cadherin (*CDH1*), Vimentin (*VIM*) and Snail (*SNAI1*), three of the most important EMT markers, were analysed by qRT-PCR. As illustrated in Fig. 2C, 0.5W and 1.5W irradiated cells presented a significant decrease of *CDH1*, whereas no changes were observed for *VIM* or *SNAI1*. However, in 3W samples, *CDH1* levels were equal to those of non-irradiated cells, as well as those of *SNAI1* and *VIM* (Fig. 2C). After three-week incubation, melanocytes were maintained in culture for four weeks and further analysis of EMT markers was repeated, but no changes in these markers were observed (see Fig. S1, ESI†).

The migration ability of irradiated cells was also investigated at the different UV irradiation endpoints by the means of the wound healing assay, but no differences were noted between irradiated and non-irradiated melanocytes (data not shown).

3.2. Lipidomic study of UV exposed melanocytes

In order to explore the changes in lipids that may occur upon UV radiation at the different endpoints, an untargeted lipidomic study was carried out. Two types of lipid extraction were performed: one to measure intact lipids of the samples, and the other to specifically detect sphingolipids. Full scan LC-MS data matrices containing all intensity values measured at different mass and retention times in the positive and negative ionization modes were analysed through the ROIMCR procedure. Data corresponding to the UV exposed cells and controls at each specific UV endpoint were analysed together. The results obtained from ROIMCR analysis were subjected to a PLS-DA in order to investigate if the lipidomic profiles of control and

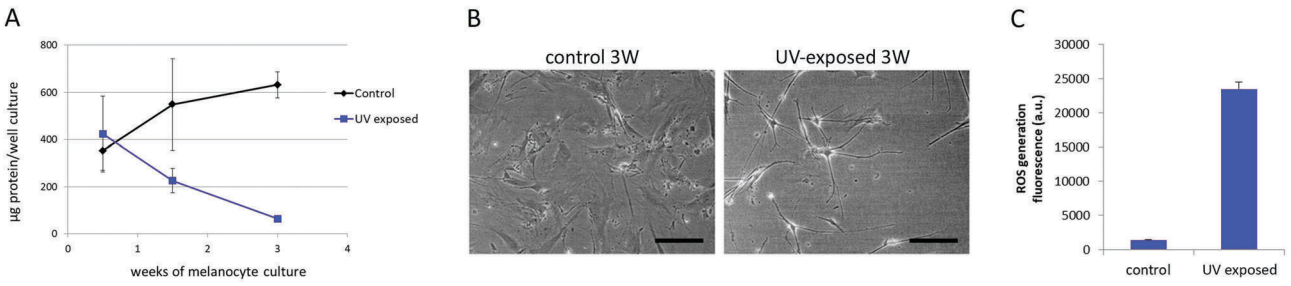

Fig. 1 Melanocyte viability, morphology and intracellular ROS generation upon UV irradiation. (A) Time course of protein content in the plate wells of UV exposed and non-exposed melanocyte cultures. Results are represented as means ± SE of three independent experiments (n = 3) performed in triplicate. (B) Representative microscopy images of control and exposed cells at 3W. Scale bar = 100 μm. (C) Intracellular generation of ROS in melanocyte cultures just after UV irradiation. Results are represented as means ± SD of three independent experiments (n = 3) performed with more than 5 replicates.

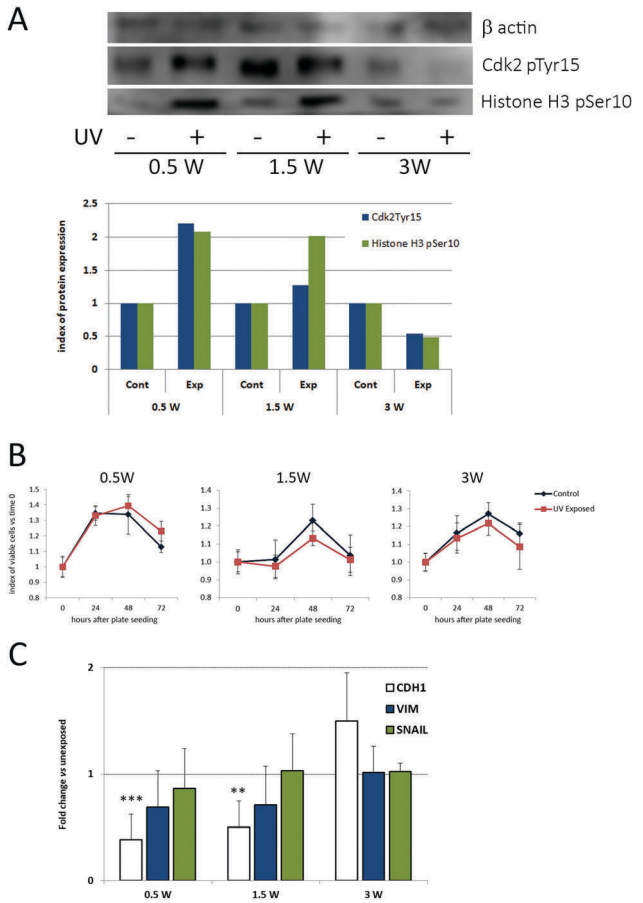

Fig. 2 Assessment of changes in the cell cycle, proliferation and EMT biomarkers in irradiated melanocytes at 0.5W, 1.5W and 3W irradiation endpoints. (A) Western blot bands and relative quantification corresponding to Cdk2 pTyr15 (marker of G1/S arrest) and histone H3 pSer10 (marker of GM2/M arrest). (B) Cell proliferation test. UV and non-exposed cells at 0.5W, 1.5W and 3W were seeded into a 96-well plate and left to grow for 72 h. Cell viability was assessed using the MTT test every 24 h. (C) Bar diagram of the real-time quantitative PCR analysis of E-cadherin (CDH1), Vimentin (VIM) and Snail expression. Results are represented as means ± SE of three independent experiments (n = 3) performed in triplicate. The indicated significant differences are considered with respect to the untreated cells. $^{**}p < 0.01$, $^{***}p < 0.005$.

irradiated melanocytes were different enough to discriminate between the two groups of samples. The PLS-DA plots of 0.5W, 1.5W and 3W are depicted in Fig. 3. For 0.5W samples, 82.7% of the *Y*-variance was explained by the cumulative *X*-variance of two latent variables (43.7%). For samples corresponding to the 1.5W endpoint, 68.8% of the *Y*-variance was explained by an *X*-variance of 36.2% of one latent variable. In the last case, 3W, 94.6% of the *Y*-variance was explained by the *X*-variance of two latent variables (72.9%). The Matthews Correlation Coefficients (MCCs) of the cross-validated models were 0.7, 0.7 and 0.8 for the 0.5W, 1.5W and 3W groups of samples, respectively, indicating that the lipidomic profiles of the samples enabled a good discrimination between UV-irradiated and non-irradiated melanocytes.

Using the PLS-DA models obtained, the Variable Importance in Projection (VIP) scores[47] were calculated. The values of these VIP scores indicate which were the most influent lipids that enabled the observed discrimination. Only the lipids with VIP scores higher than 1 were considered for further analysis and discussion. In order to facilitate the visualization of the lipidomic results and the importance of lipid species in the irradiated and non-irradiated samples, plots representing the fold changes of these lipids, grouped in subfamilies, are presented in Fig. 4, together with the information on the VIP score values. The detailed information about the individual lipid species, *m*/*z* values, retention times, fold changes and VIP score values is available in the Table S1 (ESI†).

Concerning sphingolipids (SLs), a common feature found in the three irradiation endpoints was the decrease of sphingomyelins (SMs) and GM3 ganglioside species, about 0.5 and 0.8 fold with respect to the non-irradiated melanocytes. In both cases, SMs and GM3 were represented by numerous lipid species with a broad range of acyl chain lengths (from 14 : 0 to 24 : 1). Glucosylceramide (GlcCer) species also appeared to be altered in irradiated cells at 0.5W and 1.5W. In most cases, GlcCer appeared decreased compared to controls (16 : 0, 22 : 0, 24 : 0 and 24 : 1 species at 0.5W, and 24 : 0 at 1.5W), but some other species showed an increase (14 : 0 and 24 : 0 at 0.5W and 1.5W, respectively). A modest decrease of 16 : 0 ceramide (Cer) at 0.5W and a 1.9-fold increase of 24 : 0 Cer at 3W accompanied the variations in SLs observed in melanocytes under UV irradiation.

Among the glycerophospholipid (PL) changes under UV radiation, decreased levels of phosphatidylglycerol (PG) and phosphatidylinositol (PI) species were observed in the three irradiation endpoints studied (decreases ranging from 0.7 fold in 0.5W to 0.2–0.6 in 1.5W and 3W). Two of the PI species (38 : 3 and 38 : 4) found decreased in all the endpoints are among the most abundant PI in cells,[52] and these species were found as important lipids to differentiate irradiated cells from controls in all the endpoints studied, with elevated VIP score values. In general, phosphatidylcholines (PCs) and phosphatidylethanolamines (PEs) tended to decrease in irradiated cells at all times of exposure in the range of 0.3 to 0.7 fold. However, at 0.5W, some PC species (28 : 0, 34 : 2, 36 : 1, 36 : 2 and 40 : 7) exhibited a significant increase (1.2 to 1.7 fold), and at 3W, the saturated PC (32 : 0) was also increased (2.6 fold). At 0.5W and 1.5W, an important decrease of lysoPC species was also observed. Regarding plasmalogen species of PC (PC-P) and PE (PE-P), some PC-P compounds were augmented at 0.5W and 1.5W (1.2 to 2.1 fold increase), whereas in the case of PE-P increasing and decreasing species were observed, in the three exposure times studied.

Regarding glycerolipids (GLs), the most remarkable features were an increase of saturated monoacylglycerides (16 : 0 and 18 : 0) detected at 3W (16 and 5 fold, respectively), together with a 10-fold increase of palmitic acid (C16:0). This could be indicative of an increased hydrolysis of more complex GLs and PLs. Triacylglyceride (TAG) levels increased in cells irradiated at 0.5W (1.3 fold) and 3W (3.5 fold) but some species were decreased at 1.5W and 3W (0.6 fold in both cases).

Given the fact that important lipid changes occurred upon UV radiation, the effects of irradiation were investigated beyond three weeks. UV exposure to melanocytes was carried out twice a week for a total exposure time of twelve weeks. During this

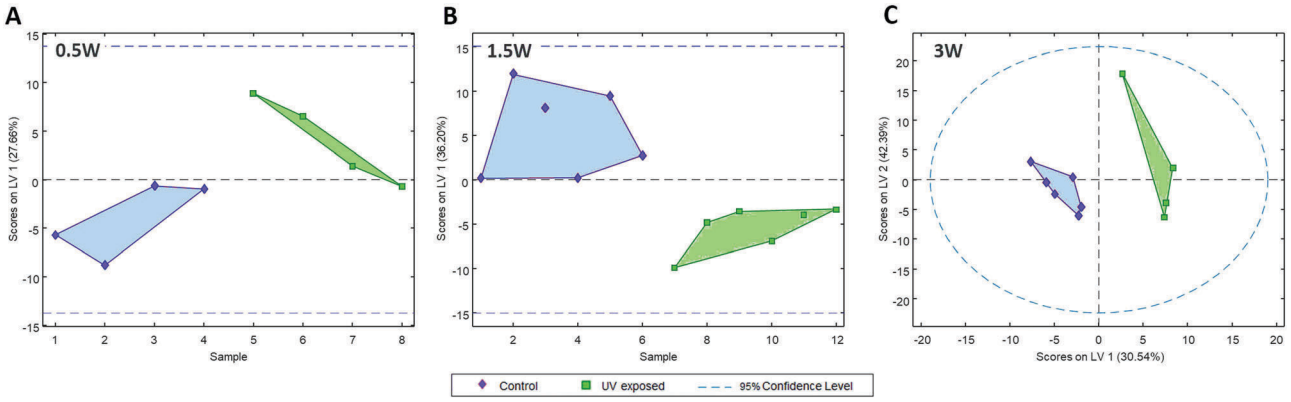

Fig. 3 PLS-DA analysis of the lipidomic data. UPLC-TOF positive and negative ionization data of melanocyte lipid extracts were processed using the ROIMCR strategy. At each endpoint studied (0.5W (A), 1.5W (B) and 3W (C)), a matrix containing the areas for each MCR component in the irradiated and non-irradiated samples was used to build the two-class PLS-DA models.

period, irradiated melanocytes grew very slowly and had a morphology similar to that observed at 3W (data not shown). Cell samples for lipidomic analysis were taken at five weeks (5W) and twelve weeks (12W). The analysis was carried out following the same untargeted strategy and PLS-DA models were elaborated (Fig. S2, ESI†). Irradiated and non-irradiated cells could be separated and the most influent lipids for the separation were identified. A detailed list of the results is available in Table S2 (ESI†). The most remarkable results consisted of a decrease of SM, GM3, PC, PE, PG and PI species in irradiated cells, as was observed at 0.5W, 1.5W and 3W. In contrast, 5W and 12W samples presented a clear increase of several TAG species that ranged from 2 to 10-fold in UV-irradiated cells. The time course progression of the fold changes was represented using the fold changes found for each individual relevant lipid species (VIP score $>$ 1) at their corresponding UV-radiation endpoint in order to visualize the decreasing and increasing tendencies in lipid changes. As shown in Fig. 5, in general terms, the fold changes found in 5W and 12W for SM, GM3, PC, PE, PG and PI were more pronounced than those found in previous endpoints. For instance, SMs were the lipids with more representative compounds that enabled the discrimination between irradiated and non-irradiated cells. In this case, seven SM species (ranging from 14 to 24 : 1 acyl chain length) presented fold changes from 0.6 to 0.1 at 5W and 12W, respectively, which represent higher decreases compared to those found for SM species until 3W, which ranged from 0.5 to 0.8. In addition, the loss of SM was accompanied by an increase of long-chain Cer species (24 : 0 and 24 : 1) at 12W (8 and 2 fold, respectively). These observations suggest that longer repeated UV exposures aggravated the already exceptional lipid composition detected at 0.5W, 1.5W and 3W. In contrast to the general reduction of SL and PL levels in UV irradiated cells, TAG levels showed a huge increment upon longer UV irradiation exposures.

4. Discussion

The primary function of melanocytes is the production of the melanin pigment that protects against UV radiation from sunlight. However, melanocytes are also the origin of melanoma, one of the most aggressive and deadly forms of skin cancer. Evidence of the involvement of UV radiation in the development of melanoma is abundant and epidemiologic studies have shown that sporadic UV exposure is a significant risk factor for melanoma. In particular, intense, intermittent exposure and sunburns early in childhood and adolescence are associated with an increased risk.[53,54] Due to the omnipresence of UV radiation and its ability to interact with melanocytes, the identification of the molecular changes involved in the cellular response to UV radiation is of paramount importance in order to evaluate the risk of potential malignant changes and to elaborate strategies of photoprotection.

The first part of the present study was dedicated to the evaluation of the UV irradiation effects on the melanocytes' viability and its possible influence on the acquisition of malignant properties such as an increase of cell proliferation, cell migration or EMT induction. We observed that the number of cells was progressively reduced as long as melanocytes were subjected to cumulative UV irradiations. The reduced viability of cells has been previously reported under acute irradiation[55] or under repeated UV exposures.[56] A morphological characteristic of melanocytes is their ability to form dendrites, which are specialized cell structures that transport melanosomes to their tips for transfer to the surrounding keratinocytes in response to growth factors and UV irradiation.[57] In the present work, dendritic prolongations conferring a neuron-like appearance to UV-irradiated melanocytes were observed. This UV-induced dendricity is triggered by hormone stimulation by keratinocytes, but it can also occur as a direct effect of UV in the absence of keratinocytes,[58] as demonstrated by Friedmann *et al.* on cultured melanocytes after seven consecutive solar irradiation simulations.[56] Interestingly, a different behaviour was observed in melanocytes subjected to acute UV irradiation (0.5W, single irradiation) compared to longer exposures. The cell viability at 0.5W was not affected and decreased E-cadherin levels and cell cycle arrest in G1/S and M phases were observed after acute irradiation. This is in agreement with previous investigations reporting that UV can induce E-cadherin reduction in melanocytes and melanoma cells.[59] In melanocytes, E-cadherin is responsible for the adhesion of

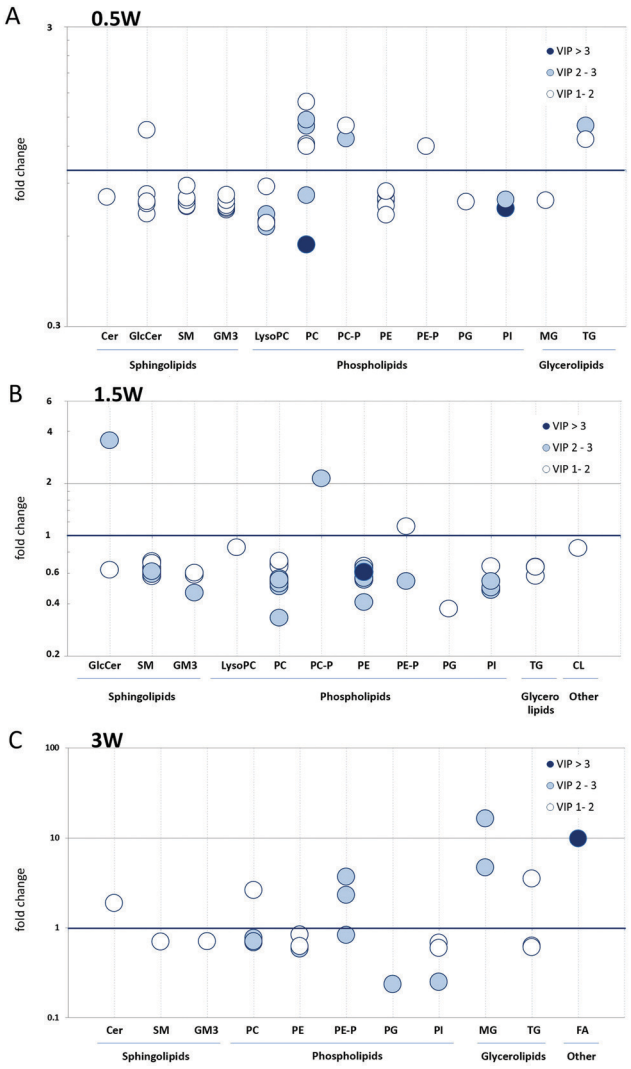

Fig. 4 Representative lipid changes at each of the UV irradiation endpoints studied. Only lipids with VIP scores >1 in the PLS-DA models were used to elaborate these plots. Fold changes of UV exposed melanocytes for 0.5W (A), 1.5W (B) and 3W (C) compared to the non-exposed are depicted for each lipid. Darker circles represent higher VIP score values in the PLS-DA models built.

human melanocytes to keratinocytes, and is a recognized tumour invasion suppressor which is downregulated in most melanoma cells.[60] Both the reduced EMT levels and the cell cycle arrest were also observed at 1.5 W, but with less intensity, and at 3 W no significant change in EMT or cell cycle markers was detected in irradiated melanocytes when compared to controls. These results suggest that surviving cells, after some time in culture and being exposed to UV, are able to adapt to the adverse environment and return to the original cell cycle rates and EMT levels. Despite the fact that UV-exposed melanocytes did not present any changes in the proliferation and migration tests performed at the different endpoints, the behaviour of acutely and chronically exposed melanocytes deserves further attention at transcriptomic and protein levels to investigate potentially acquired malignant properties.

The present lipidomic study disclosed different lipid profiles at all the UV endpoints studied. The results obtained at very long exposure times (5W and 12W) helped in visualizing the general trends of the main lipid groups under chronic exposure to UV.

Regarding sphingolipids, a subfamily of lipids that play a crucial role in cell signalling, inflammatory responses, and cell survival and differentiation,[61] the major changes detected in the study concerned SMs and the GM3 gangliosides. Previous studies have reported a SM hydrolysis when HeLa cells were subjected to an oxidative stress, such as UV radiation.[19] This stress could induce apoptosis and alteration in cell proliferation rates due to the accumulation of Cer.[50] In the present work, the most common SM species (from 14:0 to 26:0 chain lengths) showed a progressive reduction of their levels in melanocytes, along with longer UV exposure times. Together with this loss of SMs, increases of 24:0 and 24:1 Cer species were observed for long exposure times (3W and 12W), which suggest that ceramide-induced apoptosis could be related to the reduced cell viability observed upon chronic UV radiation. Besides, gangliosides are complex sphingolipids that contain one or more sialic acids in their structure. They are enriched in the plasma membrane and play important roles in cell adhesion, proliferation and recognition processes. In melanocytes, the predominant type of ganglioside is GM3 (90%), and the corresponding disialo derivative GD3 represents a minor component (2–6%). However, in melanoma cells, GD3 is the most abundant ganglioside.[62] In a previous study, the ratio of the GM3/GD3 gangliosides has been proposed as an index for the classification of melanoma patients, based on biopsy specimens from 42 melanoma patients. The progressive reduction of the GM3/GD3 ratio correlated with a worse overall survival of patients.[63] Furthermore, high levels of GM3 are able to inhibit cell growth and differentiation, acting as an antitumor agent against human brain tumors[64] and bladder cancer.[65] In our lipidomics results, the progressive decrease of GM3 species of varied length chains (from 14:0 to 24:0) may have potential implications in the aggressive behaviour of melanocytes, including their proliferation and recognition functions.

Both SMs and GM3 are important constituents of lipid rafts, which are lipid microenvironments on the cell surface that participate in signal transduction processes. Lipid rafts are present in the outer leaflet of the plasma membrane and they are able to change their composition in response to intra- or extracellular stimuli, such as UV irradiation, favouring specific protein–protein interactions and subsequent activation of signalling cascades.[66] In a study on the effects of UV radiation on lipid raft composition, Grether-Beck and co-workers demonstrated that only specific ratios of lipids present in rafts are able to initiate UV-induced signaling cascades.[67] In the present study, a continued reduction of the important constituents of lipid rafts, which are SMs and GM3, may lead to serious alterations in signal transduction processes.

PCs and PEs are the first and second most abundant phospholipids in human cell membranes, respectively. Although both are key components of membrane bilayers, they participate in

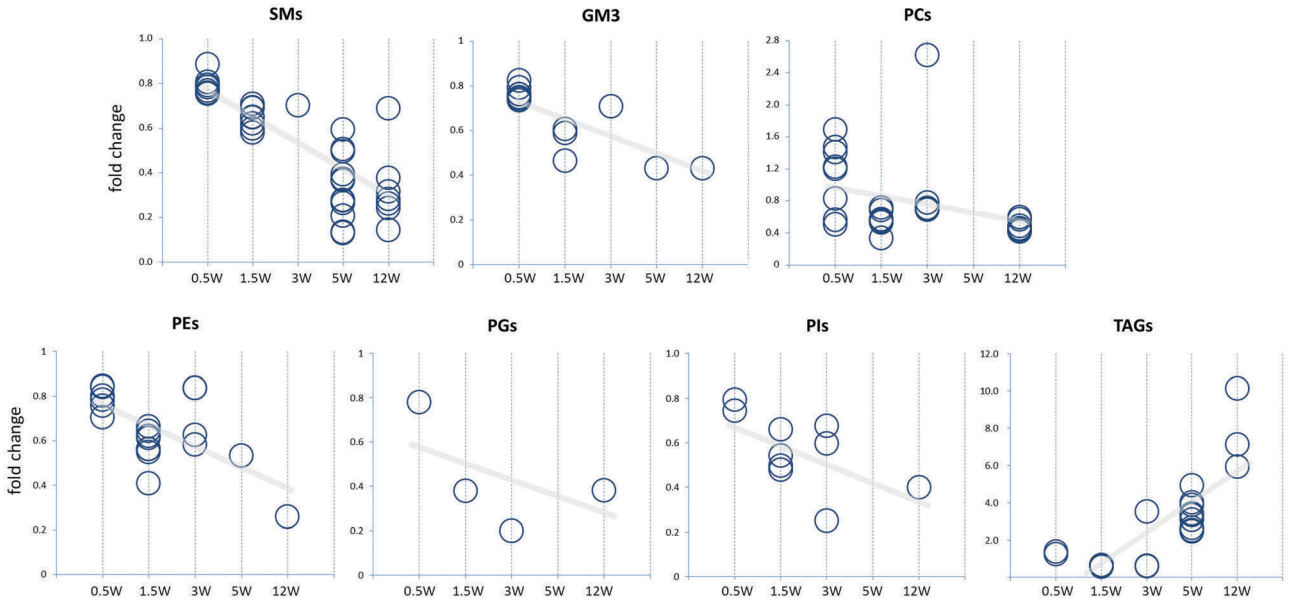

Fig. 5 Time-course representation of the most representative lipid changes in melanocytes under UV exposure. Each circle represents a lipid compound of the respective lipid type (SM, GM3, PC, PE, PG and TAG) that resulted relevant for the discrimination between UV exposed and non-exposed melanocytes (VIP score >1), at each of the five UV irradiation endpoints (0.5W, 1.5W, 3W, 5W and 12W). The grey lines represent the increasing or decreasing tendencies for each lipid group.

different biological functions. The general effect of UV radiation on the levels of PC and PE was a progressive decrease, with the exception of 0.5W, where significant increments and reductions of PC molecules were found. Indeed, similar to what occurred for the cell cycle and E-cadherin expression, the acute exposure to UV resulted in a different lipid profile compared to the rest of the endpoints, especially for PC, PC-P and lysoPC. At 0.5W, some species of PC-P appeared to have increased and, in contrast, four lysoPC species were decreased. This observation was also present at 1.5W, although with a lower number of representative species, indicating an intermediate situation between acute and chronic UV exposure.

The progressive loss of PCs and PEs may reflect huge structural changes of the lipid balance in melanocyte membranes that may translate into crucial changes in membrane fluidity and morphology, possibly related to the formation of melanocyte dendrites. In addition to an essential role in membrane structure, PC and PE participate in cell signal transduction. For instance, PC is a reservoir for second messengers such as fatty acids, DAG, lysoPC and phosphatidic acid (PA). Previous studies have demonstrated that lysoPC is able to stimulate melanocyte dendricity,[68] and that this effect is mediated by its metabolite lysophosphatidic acid (lysoPA), which is produced from lysoPC by the action of lysophospholipase D (lysoPLD).[69] In this context, an explanation for the reduced levels of the different lysoPC species observed in UV irradiated cells at 0.5 and 1.5W could be an increased transformation of lysoPC to lysoPA, in order to modulate cell shape and induce dendrite formation. In addition, changes in the lysoPC species imply alterations in the normal turnover of the sn-2 acyl moiety of phospholipids which is accomplished through the so-called Lands cycle.[70] This metabolic cycle involves the deacylation of PC through the activity of phospholipase A2 (PLA_2), followed by reacylation of the resulting lysoPC species to regenerate PC. In the context of this work, the low levels of several lysoPC species (as a consequence of either enhanced lysoPLD or reduced PLA_2 activities) would explain the increased and decreased changes in different PC species at 0.5W.

Other phospholipids that presented important reduction rates are PIs and PGs. PG family members have a crucial role in cell physiology, mainly involving the stress response. PG is a membrane constituent and acts as a key intermediate in the biosynthesis of a number of lipids, especially cardiolipins (also found decreased in 1.5W), which are located in the inner mitochondrial membrane and are required for proper functioning of the enzymes involved in oxidative phosphorylation.[71] PIs are precursors of PI phosphates (or phosphoinositides), which have specific roles in cell signalling cascades and intracellular membrane trafficking. In this study, the reduced levels of two of the most abundant PIs (38 : 3 and 38 : 4) under UV irradiation could reflect an increased turnover of phosphoinositides, which suggests that some of the functions regulated by the different phosphoinositides, such as membrane trafficking, protein recruitment, cell survival, proliferation or cytoskeletal rearrangement,[72,73] could be altered to some extent. Bellono *et al.*[74] demonstrated that the UV-induced increase of melanin is produced through the activation of the $G\alpha_{q/11}$ signalling cascade in human melanocytes that hydrolyzes PI4,5-biphosphate (PIP2) to release DAG and inositol triphosphate. This activation has been reported to result in a rapid increase of intracellular Ca^{2+} and increased melanin content.[75] Also, in the same sense, the activation of the PI3 kinase–Akt pathway

has been reported to be critical for the survival response of melanocytes to UV.[76]

Finally, an increase of numerous triacylglycerides (TAGs), with acyl chains from 46 to 56 carbons, was observed under UV exposure. This increase was not very clear in the samples up to 3W, but was dramatic for longer incubation times. This TAG accumulation could be interpreted as a cell survival mechanism, a lipid storage that serves as a source of energy, membrane components and signalling molecules essential to provide autonomy to cells in adverse environments. A TAG increase has been recently reported in placental cells under acute exposure to tributyltin (TBT)[77] and in chronic exposure of prostate cancer cells to endocrine disruptors.[39]

Overall, this study reveals that the acute exposure to low doses of UV can cause changes in the cell cycle and E-cadherin expression, as well as important changes in the lipid composition of cells. After several consecutive UV irradiations, the cell cycle and E-cadherin levels returned to normal levels and a progressive transformation in the lipid profile of melanocytes was observed. The lipid changes observed involving SMs, GM3, PCs, PEs, PGs, PIs and TAGs under chronic exposure may underlie not only deep changes in membranes' structure but also in cell signalling, trafficking and transport functions.

5. Conclusion

To our knowledge, this is the first comprehensive lipidomic study performed in primary cultured melanocytes exposed and non-exposed to UV radiation under acute and chronic conditions. On the one hand, our observations revealed that UV exposure produced changes in the E-cadherin expression cell cycle and cell morphology. On the other hand, the untargeted lipidomic analysis revealed many changes in the lipid profiles of melanocytes in each of the UV-exposure endpoints tested. Among the important changes observed under repeated UV exposures, some of them deserve to be highlighted: (1) numerous SM and GM3 ganglioside species, constituents of membrane lipid rafts with important signalling and recognition functions, showed a progressive decrease; (2) two of the most abundant PIs in cells, crucial for their role in cell signalling and trafficking, presented lower levels under UV exposure; (3) many PC and PE species also presented a decreasing tendency which may be related to the morphological changes observed in UV-exposed cells; and (4) several TAG species increased for long exposure times, which could be interpreted as a survival mechanism in a hostile environment. The phenotype of these UV-irradiated melanocytes should be taken into consideration in near future research in order to assign a functional role to our findings and to investigate potential signs of malignant behaviour.

Conflicts of interest

The authors report no conflicts of interest. The authors alone are responsible for the content and writing of the paper.

Acknowledgements

The research leading to these results received funding from the European Research Council under the European Union's Seventh Framework Programme (FP/2007-2013)/ERC Grant Agreement No. 320737. We thank Dr Thierry Levade (Toulouse, France) for critical reading and discussion.

References

1 L. R. Sklar, F. Almutawa, H. W. Lim and I. Hamzavi, Effects of ultraviolet radiation, visible light, and infrared radiation on erythema and pigmentation: a review, *Photochem. Photobiol. Sci.*, 2013, **12**, 54–64.
2 A. de Laat, J. C. van der Leun and F. R. de Gruijl, Carcinogenesis induced by UVA (365 nm) radiation: the dose-time dependence of tumor formation in hairless mice, *Carcinogenesis*, 1997, **18**, 1013–1020.
3 G. Kelfkens, F. R. de Gruijl and J. C. van der Leun, Tumorigenesis by short-wave ultraviolet A: papillomas *versus* squamous cell carcinomas, *Carcinogenesis*, 1991, **12**, 1377–1382.
4 M. Meinhardt, R. Krebs, A. Anders, U. Heinrich and H. Tronnier, Wavelength-dependent penetration depths of ultraviolet radiation in human skin, *J. Biomed. Opt.*, 2008, **13**, 044030.
5 F. Afaq, V. M. Adhami and H. Mukhtar, Photochemoprevention of ultraviolet B signaling and photocarcinogenesis, *Mutat. Res.*, 2005, **571**, 153–173.
6 S. A. Murfitt, *et al.*, A metabolomics and lipidomics study of mouse models of type 1 diabetes highlights divergent metabolism in purine and tryptophan metabolism prior to disease on-set, *J. Proteome Res.*, 2017, **17**, 946–960.
7 M. Nam, *et al.*, Lipidomic Profiling of Liver Tissue from Obesity-Prone and Obesity-Resistant Mice Fed a High Fat Diet, *Sci. Rep.*, 2015, **5**, 16984.
8 E. I. Braicu, *et al.*, High-grade ovarian serous carcinoma patients exhibit profound alterations in lipid metabolism, *Oncotarget*, 2017, **8**, 102912.
9 M. Ros-Mazurczyk, *et al.*, Serum lipid profile discriminates patients with early lung cancer from healthy controls, *Lung Cancer*, 2017, **112**, 69–74.
10 N. Dalmau, J. Jaumot, R. Tauler and C. Bedia, Epithelial-to-mesenchymal transition involves triacylglycerol accumulation in DU145 prostate cancer cells, *Mol. BioSyst.*, 2015, **11**, 3397–3406.
11 Y. Zheng, *et al.*, Transcriptome analysis of ultraviolet A-induced photoaging cells with deep sequencing, *J. Dermatol.*, 2017, **45**, 175–181.
12 O. Bruning, *et al.*, A range finding protocol to support design for transcriptomics experimentation: examples of *in vitro* and *in vivo* murine UV exposure, *PLoS One*, 2014, **9**, e97089.
13 A. Sample, B. Zhao, L. Qiang and Y. Y. He, Adaptor protein p62 promotes skin tumor growth and metastasis and is induced by UVA radiation, *J. Biol. Chem.*, 2017, **292**, 14786–14795.
14 J. Song, *et al.*, The Role of FABP5 in Radiation-Induced Human Skin Fibrosis, *Radiat. Res.*, 2017, **189**, 177–186.

15 J. Y. Fang, *et al.*, Skin aging caused by intrinsic or extrinsic processes characterized with functional proteomics, *Proteomics*, 2016, **16**, 2718–2731.

16 H. M. Park, *et al.*, Mass spectrometry-based metabolite profiling in the mouse liver following exposure to ultraviolet B radiation, *PLoS One*, 2014, **9**, e109479.

17 H. M. Park, *et al.*, MS-based metabolite profiling reveals time-dependent skin biomarkers in UVB-irradiated mice, *Metabolomics*, 2014, **10**, 663–676.

18 A. R. Svobodova, *et al.*, Acute exposure to solar simulated ultraviolet radiation affects oxidative stress-related biomarkers in skin, liver and blood of hairless mice, *Biol. Pharm. Bull.*, 2011, **34**, 471–479.

19 Q. Dai, *et al.*, Mitochondrial ceramide increases in UV-irradiated HeLa cells and is mainly derived from hydrolysis of sphingomyelin, *Oncogene*, 2004, **23**, 3650–3658.

20 C. Magnoni, *et al.*, Ultraviolet B radiation induces activation of neutral and acidic sphingomyelinases and ceramide generation in cultured normal human keratinocytes, *Toxicol. In Vitro*, 2002, **16**, 349–355.

21 A. Gegotek, K. Bielawska, M. Biernacki, I. Dobrzynska and E. Skrzydlewska, Time-dependent effect of rutin on skin fibroblasts membrane disruption following UV radiation, *Redox Biol.*, 2017, **12**, 733–744.

22 A. Reich, D. Schwudke, M. Meurer, B. Lehmann and A. Shevchenko, Lipidome of narrow-band ultraviolet B irradiated keratinocytes shows apoptotic hallmarks, *Exp. Dermatol.*, 2010, **19**, e103–e110.

23 F. J. Christiaens, A. Chardon, A. Fourtanier and J. E. Frederick, Standard Ultraviolet Daylight for Nonextreme Exposure Conditions, *Photochem. Photobiol.*, 2005, **81**, 874–878.

24 C. S. Wu, C. L. Yu, C. S. Wu, C. C. Lan and H. S. Yu, Narrow-band ultraviolet-B stimulates proliferation and migration of cultured melanocytes, *Exp. Dermatol.*, 2004, **13**, 755–763.

25 Y. Takagi, H. Nakagawa, T. Yaginuma, Y. Takema and G. Imokawa, An accumulation of glucosylceramide in the stratum corneum due to attenuated activity of beta-glucocerebrosidase is associated with the early phase of UVB-induced alteration in cutaneous barrier function, *Arch. Dermatol. Res.*, 2005, **297**, 18–25.

26 P. Waster, I. Rosdahl, B. F. Gilmore and O. Seifert, Ultraviolet exposure of melanoma cells induces fibroblast activation protein-alpha in fibroblasts: implications for melanoma invasion, *Int. J. Oncol.*, 2011, **39**, 193–202.

27 K. J. Livak and T. D. Schmittgen, Analysis of relative gene expression data using real-time quantitative PCR and the 2(-Delta Delta C(T)) Method, *Methods*, 2001, **25**, 402–408.

28 R. Stolt, *et al.*, Second-order peak detection for multicomponent high-resolution LC/MS data, *Anal. Chem.*, 2006, **78**, 975–983.

29 R. Tauler, Multivariate curve resolution applied to second order data, *Chemom. Intell. Lab. Syst.*, 1995, **30**, 133–146.

30 M. Navarro-Reig, *et al.*, Untargeted Comprehensive Two-Dimensional Liquid Chromatography Coupled with High-Resolution Mass Spectrometry Analysis of Rice Metabolome Using Multivariate Curve Resolution, *Anal. Chem.*, 2017, **89**, 7675–7683.

31 E. Ortiz-Villanueva, *et al.*, Knowledge integration strategies for untargeted metabolomics based on MCR-ALS analysis of CE-MS and LC-MS data, *Anal. Chim. Acta*, 2017, **978**, 10–23.

32 C. Gómez-Canela, E. Prats, B. Piña and R. Tauler, Assessment of chlorpyrifos toxic effects in zebrafish (Danio rerio) metabolism, *Environ. Pollut.*, 2017, **220**, 1231–1243.

33 A. S. Marques, C. Bedia, K. M. G. Lima and R. Tauler, Assessment of the effects of As(III) treatment on cyanobacteria lipidomic profiles by LC-MS and MCR-ALS, *Anal. Bioanal. Chem.*, 2016, **408**, 5829–5841.

34 E. Gorrochategui, J. Jaumot, S. Lacorte and R. Tauler, Data analysis strategies for targeted and untargeted LC-MS metabolomic studies: overview and workflow, *TrAC, Trends Anal. Chem.*, 2016, **82**, 425–442.

35 R. Tauler, A. K. Smilde and B. R. Kowalski, Multivariate curve resolution applied to second order data, *Chemom. Intell. Lab. Syst.*, 1995, **30**, 133–146.

36 E. Pere-Trepat, S. Lacorte and R. Tauler, Solving liquid chromatography mass spectrometry coelution problems in the analysis of environmental samples by multivariate curve resolution, *J. Chromatogr. A*, 2005, **1096**, 111–122.

37 M. Navarro-Reig, J. Jaumot, A. Garcia-Reiriz and R. Tauler, Evaluation of changes induced in rice metabolome by Cd and Cu exposure using LC-MS with XCMS and MCR-ALS data analysis strategies, *Anal. Bioanal. Chem.*, 2015, **407**, 8835–8847.

38 M. Farres, B. Pina and R. Tauler, Chemometric evaluation of Saccharomyces cerevisiae metabolic profiles using LC-MS, *Metabolomics*, 2015, **11**, 210–224.

39 C. Bedia, N. Dalmau, J. Jaumot and R. Tauler, Phenotypic malignant changes and untargeted lipidomic analysis of long-term exposed prostate cancer cells to endocrine disruptors, *Environ. Res.*, 2015, **140**, 18–31.

40 C. Gomez-Canela, E. Prats, B. Pina and R. Tauler, Assessment of chlorpyrifos toxic effects in zebrafish (Danio rerio) metabolism, *Environ. Pollut.*, 2017, **220**, 1231–1243.

41 M. Navarro-Reig, *et al.*, Untargeted Comprehensive Two-Dimensional Liquid Chromatography Coupled with High-Resolution Mass Spectrometry Analysis of Rice Metabolome Using Multivariate Curve Resolution, *Anal. Chem.*, 2017, **89**, 7675–7683.

42 E. Ortiz-Villanueva, *et al.*, Knowledge integration strategies for untargeted metabolomics based on MCR-ALS analysis of CE-MS and LC-MS data, *Anal. Chim. Acta*, 2017, **978**, 10–23.

43 A. S. Marques, C. Bedia, K. M. Lima and R. Tauler, Assessment of the effects of As(III) treatment on cyanobacteria lipidomic profiles by LC-MS and MCR-ALS, *Anal. Bioanal. Chem.*, 2016, **408**, 5829–5841.

44 R. Tauler, M. Maefer and A. de Juan, *Multiset Data Analysis: Extended Multivaried Curve Resolution*, Elsevier, 2010, vol. 2, pp. 473–505.

45 D. S. Wishart, *et al.*, HMDB 3.0—The Human Metabolome Database in 2013, *Nucleic Acids Res.*, 2013, **41**, D801–D807.

46 B. W. Matthews, Comparison of the predicted and observed secondary structure of T4 phage lysozyme, *Biochim. Biophys. Acta*, 1975, **405**, 442–451.

47 S. Wold, M. Sjöström and L. Eriksson, PLS-regression: a basic tool of chemometrics, *Chemom. Intell. Lab. Syst.*, 2001, **58**, 109–130.
48 J. Jaumot and R. Tauler, Potential use of multivariate curve resolution for the analysis of mass spectrometry images, *Analyst*, 2015, **140**, 837–846.
49 J. U. Bertrand, *et al.*, UVB represses melanocyte cell migration and acts through beta-catenin, *Exp. Dermatol.*, 2017, **26**, 875–882.
50 A. Reich and K. Medrek, Effects of narrow band UVB (311 nm) irradiation on epidermal cells, *Int. J. Mol. Sci.*, 2013, **14**, 8456–8466.
51 A. G. Paulovich, D. P. Toczyski and L. H. Hartwell, When checkpoints fail, *Cell*, 1997, **88**, 315–321.
52 Y. V. Shulga, *et al.*, Molecular Species of Phosphatidylinositol-Cycle Intermediates in the Endoplasmic Reticulum and Plasma, *Membr. Biochem.*, 2010, **49**, 312–317.
53 B. K. Armstrong and A. Kricker, The epidemiology of UV induced skin cancer, *J. Photochem. Photobiol., B*, 2001, **63**, 8–18.
54 S. D. Walter, W. D. King and L. D. Marrett, Association of cutaneous malignant melanoma with intermittent exposure to ultraviolet radiation: results of a case-control study in Ontario, Canada, *Int. J. Epidemiol.*, 1999, **28**, 418–427.
55 D. Barker, *et al.*, Comparison of the responses of human melanocytes with different melanin contents to ultraviolet B irradiation, *Cancer Res.*, 1995, **55**, 4041–4046.
56 P. S. Friedmann and B. A. Gilchrest, Ultraviolet radiation directly induces pigment production by cultured human melanocytes, *J. Cell. Physiol.*, 1987, **133**, 88–94.
57 S. S. Sulaimon and B. E. Kitchell, The biology of melanocytes, *Vet. Dermatol.*, 2003, **14**, 57–65.
58 G. Scott, Rac and Rho: The Story Behind Melanocyte Dendrite Formation, *Pigm. Cell Res.*, 2002, **15**, 322–330.
59 S. Jamal and R. J. Schneider, UV-induction of keratinocyte endothelin-1 downregulates E-cadherin in melanocytes and melanoma cells, *J. Clin. Invest.*, 2002, **110**, 443–452.
60 M.-Y. Hsu, *et al.*, E-Cadherin Expression in Melanoma Cells Restores Keratinocyte-Mediated Growth Control and Down-Regulates Expression of Invasion-Related Adhesion Receptors, *Am. J. Pathol.*, 2000, **156**, 1515–1525.
61 Y. A. Hannun and L. M. Obeid, Sphingolipids and their metabolism in physiology and disease, *Nat. Rev. Mol. Cell Biol.*, 2018, **19**, 175–191.
62 J. M. Carubia, R. K. Yu, L. J. Macala, J. M. Kirkwood and J. M. Varga, Gangliosides of normal and neoplastic human melanocytes, *Biochem. Biophys. Res. Commun.*, 1984, **120**, 500–504.
63 M. H. Ravindranath, T. Tsuchida, D. L. Morton and R. F. Irie, Ganglioside GM3:GD3 ratio as an index for the management of melanoma, *Cancer*, 1991, **67**, 3029–3035.
64 Y. Nakatsuji and R. H. Miller, Selective cell-cycle arrest and induction of apoptosis in proliferating neural cells by ganglioside GM3, *Exp. Neurol.*, 2001, **168**, 290–299.
65 R. Watanabe, *et al.*, Ganglioside GM3 Overexpression Induces Apoptosis and Reduces Malignant Potential in Murine Bladder Cancer, *Cancer Res.*, 2002, **62**, 3850–3854.
66 K. Simons and D. Toomre, Lipid rafts and signal transduction, *Nat. Rev. Mol. Cell Biol.*, 2000, **1**, 31–39.
67 S. Grether-Beck, *et al.*, Ceramide and raft signaling are linked with each other in UVA radiation-induced gene expression, *Oncogene*, 2008, **27**, 4768–4778.
68 G. A. Scott, S. E. Jacobs and A. P. Pentland, sPLA2-X stimulates cutaneous melanocyte dendricity and pigmentation through a lysophosphatidylcholine-dependent mechanism, *J. Invest. Dermatol.*, 2006, **126**, 855–861.
69 J. Aoki, *et al.*, Serum Lysophosphatidic Acid Is Produced through Diverse Phospholipase Pathways, *J. Biol. Chem.*, 2002, **277**, 48737–48744.
70 W. E. Lands, Metabolism of glycerolipids. 2. The enzymatic acylation of lysolecithin, *J. Biol. Chem.*, 1960, **235**, 2233–2237.
71 H. Matsuo, *et al.*, Role of LBPA and Alix in multivesicular liposome formation and endosome organization, *Science*, 2004, **303**, 531–534.
72 G. v. Meer and H. Sprong, Membrane lipids and vesicular traffic, *Curr. Opin. Cell Biol.*, 2004, **16**, 373–378.
73 M. R. Wenk, *et al.*, Phosphoinositide profiling in complex lipid mixtures using electrospray ionization mass spectrometry, *Nat. Biotechnol.*, 2003, **21**, 813.
74 N. W. Bellono, J. A. Najera and E. Oancea, UV light activates a Gα(q/11)-coupled phototransduction pathway in human melanocytes, *J. Gen. Physiol.*, 2014, **143**, 203–214.
75 N. L. Wicks, J. W. Chan, J. A. Najera, J. M. Ciriello and E. Oancea, UVA phototransduction drives early melanin synthesis in human melanocytes, *Curr. Biol.*, 2011, **21**, 1906–1911.
76 A. L. Kadekaro, *et al.*, α-Melanocortin and Endothelin-1 Activate Antiapoptotic Pathways and Reduce DNA Damage in Human Melanocytes, *Cancer Res.*, 2005, **65**, 4292–4299.
77 E. Gorrochategui, J. Casas, C. Porte, S. Lacorte and R. Tauler, Chemometric strategy for untargeted lipidomics: biomarker detection and identification in stressed human placental cells, *Anal. Chim. Acta*, 2015, **854**, 20–33.

Informació Suplementària a la Publicació IV

Untargeted lipidomic analysis of primary human epidermal melanocytes acutely and chronically exposed to UV radiation.

N. Dalmau, N. Andrieu-Abadie, R.Tauler, C. Bedia.

Mol Omics **2018**, 14(3), 170-180

Figure S1

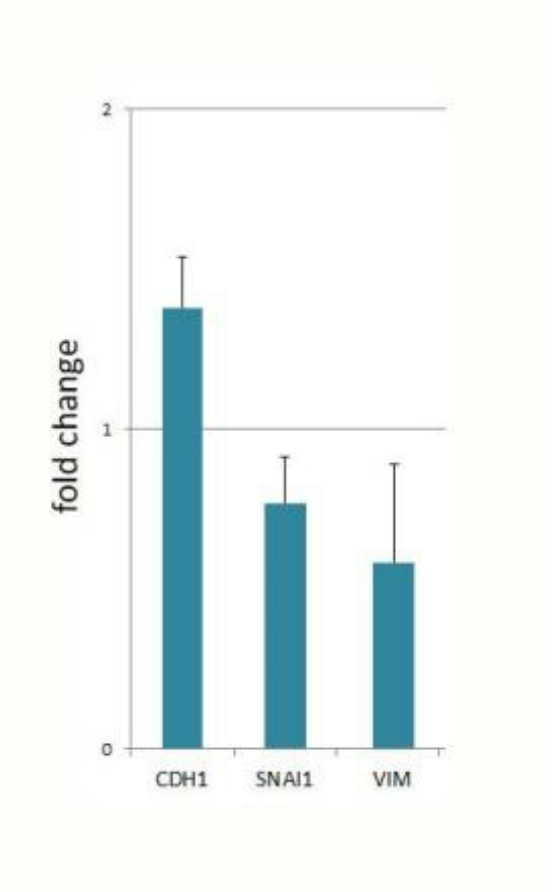

Figure S1. qRT-PCR of EMT related genes on cultured 3-week exposed cells vs non exposed. No particular EMT induction profile was detected. Results represented the mean ± SE of three independent experiments (n=3) performed in duplicate.

Figure S2

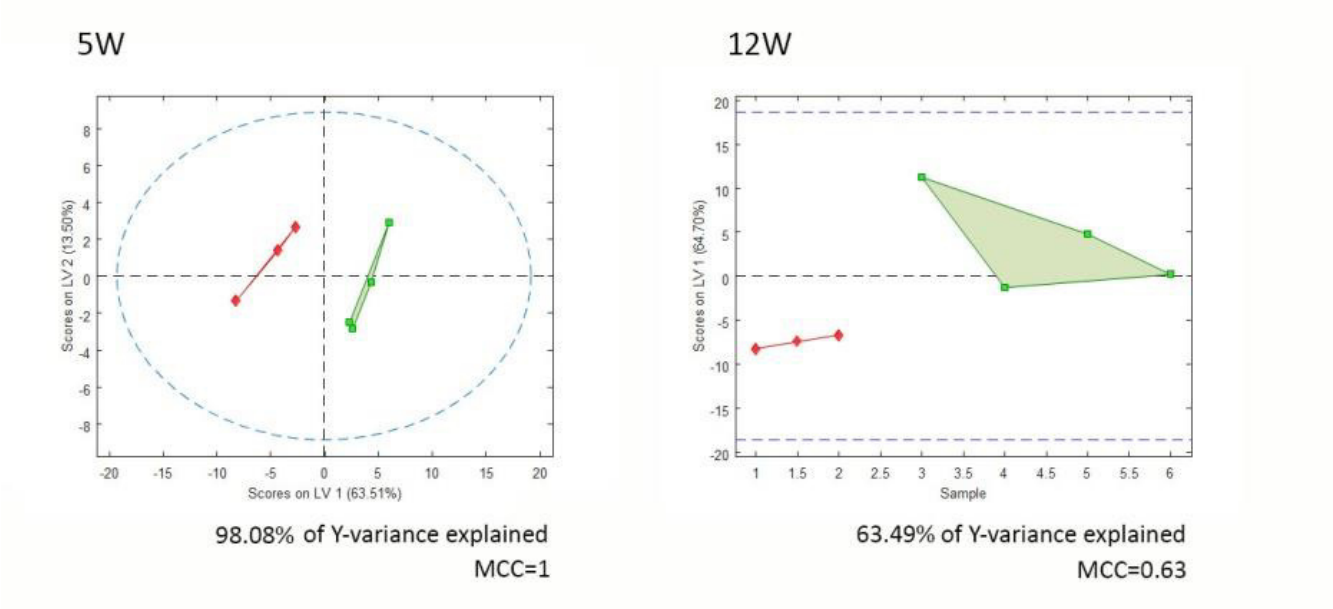

Figure S2. PLS-DA analysis of the lipidomic data at 5W and 12W. UPLC-TOF positive and negative ionization data of melanocyte lipid extracts was processed using the ROIMCR strategy. At each endpoint studied a matrix containing the areas for each MCR component in the irradiated and non-irradiated samples was used to build the two-class PLS-DA models.

Supplementary Table 1. Detailed information about the individual lipid species, retention times, *m/z* values, mass error, fold changes and VIP values of the resolved lipids used for the lipidomics results representation of Figure 4.

0.5W

Identified compound	Rt (min)	m/z measured	Adduct	m/z calculated	Mass error (ppm)	Fold change	VIP value	Database ID
Ceramide (d18:1/16:0)	7,1	582,5069	M+FA-H	582,5103	6	0,81	1,42	HMDB0004949
Glucosylceramide (d18:1/14:0)	5,3	716,5311	M+FA-H	716,5318	1	1,36	1,90	HMDB0012321
Glucosylceramide (d18:1/16:0)	6,3	744,5600	M+FA-H	744,5631	4	0,77	1,42	HMDB0004971
Glucosylceramide (d18:1/22:0)	10,4	828,6709	M+FA-H	828,657	17	0,71	1,48	HMDB0004974
Glucosylceramide (d18:1/24:0)	11,7	856,6810	M+FA-H	856,6883	9	0,83	1,48	HMDB0004978
Glucosylceramide (d18:1/24:1)	10,7	854,6709	M+FA-H	854,6727	2	0,78	1,08	HMDB0004975
SM(d18:1/14:0)	5,5	719,5317	M+FA-H	719,5345	4	0,76	1,36	HMDB0012097
SM(d18:0/16:1)	6,6	747,5623	M+FA-H	747,5658	5	0,77	1,65	HMDB0013464
SM(d18:0/18:1)	8,1	775,5951	M+FA-H	775,5971	2	0,81	1,10	HMDB0012088
SM(d18:1/22:0)	10,8	831,6578	M+FA-H	831,6597	2	0,79	1,29	HMDB0012103
SM(d18:1/24:0)	12,0	859,6853	M+FA-H	859,691	7	0,78	1,41	HMDB0012095
SM(d18:1/24:1)	11,0	857,6753	M+FA-H	857,6753	0	0,75	1,42	HMDB0012107
Ganglioside GM3 (d18:1/14:0)	4,4	1123,6803	M-H	1123,6746	5	0,82	1,01	HMDB0011928
Ganglioside GM3 (d18:1/16:0)	5,1	1151,7127	M-H	1151,7059	6	0,76	1,39	HMDB0004844
Ganglioside GM3 (d18:1/18:0)	6,1	1179,7428	M-H	1179,7372	5	0,74	1,81	HMDB0004845
Ganglioside GM3 (d18:1/22:0)	8,7	1235,8090	M-H	1235,7998	7	0,75	1,55	HMDB0004847
Ganglioside GM3 (d18:1/22:1)	7,6	1233,7946	M-H	1233,7841	8	0,76	1,43	HMDB0011930
Ganglioside GM3 (d18:1/24:0)	10,0	1263,8383	M-H	1263,8311	6	0,79	1,39	HMDB0004851
Ganglioside GM3 (d18:1/24:1)	8,9	1261,8269	M-H	1261,8154	9	0,74	1,67	HMDB0004848
LysoPC(14:1)	2,4	464,2779	M-H	464,2783	1	0,88	0,99	HMDB0010380
LysoPC(16:0)	2,5	540,3270	M+FA-H	540,3307	7	0,64	2,29	HMDB0010382
LysoPC(16:1)	2,1	494,3176	M+H	494,3241	13	0,68	2,40	HMDB0010383
LysoPC(18:1)	2,7	522,3517	M+H	522,3554	7	0,71	2,10	HMDB0002815
PC(28:0)	5,6	678,5183	M+H	678,5068	17	1,20	1,00	HMDB0007866
PC(32:0)	8,1	778,5604	M+FA-H	778,5604	0	0,82	2,42	HMDB0000564
PC(34:0)	9,4	762,5961	M+H	762,6007	6	0,56	4,50	HMDB0007878
PC(34:2)	7,5	1516,1298	2M+H	1516,1316	1	1,22	1,47	HMDB0007880
PC(36:1)	9,8	832,6071	M+FA-H	832,6073	0	1,47	2,15	HMDB0008526
PC(36:2)	8,9	1572,1980	2M+H	1572,1942	2	1,40	2,30	HMDB0000593
PC-P(30:1)	7,3	705,5821	M+NH4	705,5541	40	1,27	2,52	HMDB0011204
PC-P(38:1)	10,7	844,6599	M+FA-H	844,6437	19	1,41	1,12	HMDB0008325
PE(34:0)	9,4	700,5273	M-H20-H	700,5281	1	0,84	1,60	HMDB0008925
PE(36:1)	6,5	744,5549	M-H	744,5549	0	0,80	1,93	HMDB0009482
PE(36:2)	9,7	788,5404	M+FA-H	788,5447	6	0,79	2,70	HMDB0009547
PE(38:4)	9,0	766,5372	M-H	766,5392	3	0,85	1,27	HMDB0009420
PE(42:2)	9,4	826,6380	M-H	826,6331	6	0,76	1,55	HMDB0009559
PE-P(34:0)	6,9	704,5536	M+H	704,5589	7	1,20	1,62	HMDB0011371
PG(34:0)	7,2	749,5740	M-H	749,5338	54	0,78	1,51	HMDB0010572
PI(38:3)	10,0	887,5658	M-H	887,5655	0	0,74	3,98	HMDB0009907
PI(38:4)	9,2	885,5515	M-H	885,5499	2	0,79	2,64	HMDB0009914
MG(20:4)	3,0	423,2491	M+FA-H	423,2752	62	0,79	1,67	HMDB0011578
TG(52:4)	15,9	872,7758	M+NH4	872,7702	6	1,40	2,23	HMDB0044529
TG(50:1)	16,5	850,7868	M+NH4	850,7858	1	1,26	0,99	HMDB0043279

1.5W

Identified compound	Rt (min)	m/z measured	Adduct	m/z calculated	Mass error (ppm)	Fold change	VIP value	Database ID
Glucosylceramide (d18:1/24:0)	11,1	856,6691	M+FA-H	856,6883	22	3,55	2,95	HMDB0004978
Glucosylceramide (d18:1/24:1)	10,1	854,6569	M+FA-H	854,6727	19	0,63	1,28	HMDB0004975
SM(d18:1/14:0)	5,1	675,5437	M+H	675,5436	0	0,58	1,63	HMDB0012097
SM(d18:1/16:0)	6,2	703,5760	M+H	703,5749	2	0,65	1,56	HMDB0013464
SM(d18:1/22:0)	10,4	831,6502	M+FA-H	831,6597	11	0,62	2,17	HMDB0012092
SM(d18:1/24:0)	11,6	815,7102	M+H	815,7001	12	0,65	1,93	HMDB0012095
SM(d18:1/24:1)	10,6	857,6693	M+FA-H	857,6753	7	0,60	2,41	HMDB0012107
Ganglioside GM3 (d18:1/16:0)	4,6	1151,7060	M-H	1151,7059	0	0,59	1,34	HMDB0004844
Ganglioside GM3 (d18:1/18:0)	5,6	1179,7380	M-H	1179,7372	1	0,61	1,16	HMDB0004845
Ganglioside GM3 (d18:1/20:0)	6,6	1207,7690	M-H	1207,7685	0	0,46	2,07	HMDB0004846
LysoPC(14:1)	1,9	466,2914	M+H	466,2928	3	0,85	1,12	HMDB0010380
PC(32:0)	7,5	734,5711	M+H	734,5694	2	0,55	2,06	HMDB0008031
PC(32:1)	6,6	732,5641	M+H	732,5538	14	0,54	2,37	HMDB0008032
PC(32:3)	6,2	728,5343	M+H	728,5225	16	0,33	2,55	HMDB0008131
PC(34:1)	8,0	760,5910	M+H	760,5851	8	0,57	2,26	HMDB0007971
PC(34:3)	6,4	800,5380	M+FA-H	800,5447	8	0,51	2,63	HMDB0007882
PC(36:0)	8,9	812,6078	M+Na	812,614	8	0,53	2,17	HMDB0008525
PC(36:1)	9,4	788,6270	M+H	788,6164	13	0,68	1,81	HMDB0008558
PC(36:3)	7,4	784,5841	M+H	784,5851	1	0,54	2,63	HMDB0008591
PC(38:5)	7,2	808,5844	M+H	808,5851	1	0,71	1,15	HMDB0008692
PC-P(36:4)	7,0	783,5898	M+NH4	783,6011	14	2,14	2,06	HMDB0011279
PE(34:1)	7,9	716,5168	M-H	716,5236	9	0,41	2,97	HMDB0009055
PE(36:1)	9,2	744,5475	M-H	744,5549	10	0,62	1,43	HMDB0009253
PE(36:2)	8,3	744,5693	M+H	744,5538	21	0,56	2,20	HMDB0009059
PE(36:3)	7,1	759,5767	M+NH4	759,5647	16	0,55	2,66	HMDB0009060
PE(38:4)	8,4	766,5269	M-H	766,5392	16	0,61	3,14	HMDB0009355
PE(40:5)	8,4	811,6086	M+NH4	811,596	16	0,64	2,11	HMDB0009298
PE-P(30:0)	4,5	648,5260	M+H	648,4963	46	1,13	1,04	HMDB0008850
PE-P(34:1)	8,7	700,5295	M-H	700,5287	1	0,54	2,25	HMDB0009048
PE-P(38:5)	6,3	748,5299	M-H	748,5287	2	0,60	1,41	HMDB0009447
PG(34:0)	6,7	749,5418	M-H	749,5338	11	0,38	1,19	HMDB0010600
PI(34:1)	5,8	835,5253	M-H	835,5342	11	0,50	2,50	HMDB0009799
PI(38:3)	6,9	887,5537	M-H	887,5655	13	0,48	2,59	HMDB0009792
PI(38:4)	6,2	885,5382	M-H	885,5499	13	0,66	1,89	HMDB0009842
PI(38:5)	5,5	883,5247	M-H	883,5342	11	0,54	2,32	HMDB0009902
TG(50:1)	17,1	850,7869	M+NH4	850,7858	1	0,65	1,34	HMDB0043279
TG(50:2)	16,6	848,7742	M+NH4	848,7702	5	0,66	1,24	HMDB0048479
TG(52:2)	17,4	876,8038	M+NH4	876,8015	3	0,66	1,08	HMDB0049741
CL(78:12)	10,7	763,5280	M+2H	763,5090	25	0,85	1,65	HMDB0010305

3W

Identified compound	Rt (min)	m/z measured	Adduct	m/z calculated	Mass error (ppm)	Fold change	VIP value	Database ID
Ceramide (d18:1/24:0)	12,17	694,6252358	M+FA-H	694,6355	15	1,88	1,08	HMDB0004956
SM(d18:1/16:0)	6,26	703,5719727	M+H	703,5749	4	0,70	1,33	HMDB0013464
Ganglioside GM3 (d18:1/16:0)	4,77	1151,688159	M-H	1151,7059	15	0,71	1,11	HMDB0004844
PC(32:0)	7,44	778,5594467	M+FA-H	778,5604	1	2,62	1,16	HMDB0000564

PC(32:1)	6,57	732,5657081	M+H	732,5538	16	0,71	2,45 HMDB0008001
PC(34:1)	7,92	760,5937431	M+H	760,5851	11	0,71	3,48 HMDB0008295
PC(34:2)	7,00	758,5778247	M+H	758,5694	11	0,69	2,27 HMDB0008296
PC(38:5)	7,39	808,5839699	M+H	808,5851	1	0,69	3,86 HMDB0008692
PC-P(30:0)	6,13	707,5592127	M+NH4	707,5698	15	0,77	2,07 HMDB0007895
PE(36:2)	8,25	742,530555	M-H	742,5392	12	0,84	1,04 HMDB0009286
PE(40:6)	7,24	809,589936	M+NH4	809,5803	12	0,58	2,81 HMDB0009301
PE(44:5)	8,31	830,6063824	M-H20-H	830,6064	0	0,84	2,75 HMDB0009505
PE(44:9)	6,01	886,5408741	M+FA-H	886,5604	22	0,63	1,53 HMDB0009603
PE-P(36:1)	9,20	752,5543432	M+Na	752,5565	3	3,69	2,54 HMDB0009017
PE-P(38:5)	6,21	748,5338283	M-H	748,5287	7	0,83	2,24 HMDB0011360
PE-P(42:1)	8,64	836,6432617	M+Na	836,6504	8	2,31	2,29 HMDB0011428
PG(36:3)	8,36	790,5527213	M+NH4	790,5593	8	0,24	2,34 HMDB0010677
PI(34:1)	5,79	835,5239824	M-H	835,5342	12	0,68	1,09 HMDB0009783
PI(38:3)	6,90	906,6074595	M+NH4	906,6066	1	0,60	1,29 HMDB0009880
PI(38:4)	6,15	904,5977567	M+NH4	904,591	8	0,25	2,55 HMDB0009853
MG(18:0)	3,14	359,3254355	M+H	359,3156	27	4,70	2,22 HMDB0011535
MG(16:0)	2,52	331,3015804	M+H	331,2843	12	16,46	2,55 HMDB0011533
TG(50:2)	16,60	848,7756698	M+NH4	848,7702	6	3,53	1,77 HMDB0048479
TG(52:2)	17,37	881,7491839	M+Na	881,7569	9	0,61	1,63 HMDB0043540
TG(56:6)	17,59	907,7771165	M+H	907,7749	2	0,63	1,06 HMDB0049597
Palmitic acid	0,97	274,2719975	M+NH4	274,2741	7	9,89	3,57 HMDB0000220

Supplementary Table 2. Detailed information about the individual lipid species, retention times, *m/z* values, mass error, fold changes and VIP values of the resolved lipids used at 5W (5weeks) and 12W (12 weeks) endpoints.

5W

Identified compound	Rt (min)	m/z measured	Adduct	m/z calculated	Mass error (ppm)	Fold change	VIP value	Database ID
Glucosylceramide (d18:1/26:0)	12,0	884,7144	M+FA-H	884,7196	6	0,46	2,79	HMDB0004977
SM(d18:1/14:0)	5,1	719,5338	M+FA-H	719,5345	1	0,50	2,72	HMDB0012097
SM(d18:1/16:0)	6,1	748,5775	M+FA-H	748,5736	5	0,37	2,06	HMDB0010168
SM(d18:1/22:0)	10,2	787,6697	M+H	787,6688	1	0,27	3,32	HMDB0012103
SM(d18:1/22:1)	9,3	785,6557	M+H	785,6531	3	0,26	2,74	HMDB0012103
SM(d18:1/24:1)	10,4	813,6903	M+H	813,6844	7	0,21	3,47	HMDB0012107
SM(d18:1/26:0)	11,6	841,7215	M+H	841,7157	7	0,13	2,76	HMDB0013461
Ganglioside GM3 (d18:1/24:0)	9,1	1263,8398	M-H	1263,8311	7	0,43	2,68	HMDB0004851
LysoPC-P(18:0)	2,6	508,3762	M+H	508,3762	0	0,28	3,38	HMDB0013122
LysoPE(18:0)	2,5	462,2993	M-H20-H	462,2984	2	0,33	1,32	HMDB0011130
PC-P(36:1)	9,1	789,6348	M+NH4	789,6480	17	5,84	1,42	HMDB0011242
PE(44:0)	10,3	858,6883	M-H	858,6957	9	0,54	1,86	HMDB0009244
PE-P(16:0)	2,4	436,2822	M-H	436,2833	3	0,29	2,90	HMDB0011152
CE(22:5)	12,5	699,5971	M+H	699,6075	15	0,49	1,60	HMDB0010375
DG(38:4)	4,3	689,5468	M+FA-H	689,5362	15	7,51	1,24	HMDB0007478
DG(40:5)	11,4	671,5655	M+H	671,5609	7	4,34	1,23	HMDB0007738
DG(42:5)	12,5	699,5983	M+H	699,5922	9	10,66	1,50	HMDB0007831
TG(50:1)	16,9	850,7669	M+NH4	850,7858	22	3,90	1,60	HMDB0044081
TG(50:2)	16,4	848,7699	M+NH4	848,7702	0	2,67	1,31	HMDB0048479
TG(52:2)	17,1	876,8004	M+NH4	876,8015	1	3,41	1,41	HMDB0049741
TG(52:3)	16,6	874,7875	M+NH4	874,7858	2	2,53	1,40	HMDB0044165
TG(54:2)	17,9	904,8193	M+NH4	904,8328	15	3,10	1,27	HMDB0044389
TG(54:3)	17,3	902,8145	M+NH4	902,8171	3	4,02	1,66	HMDB0045100
TG(56:6)	16,7	924,7965	M+NH4	924,8015	5	4,95	1,59	HMDB0049597

12W

Identified compound	Rt (min)	m/z measured	Adduct	m/z calculated	Mass error (ppm)	Fold change	VIP value	Database ID
Ceramide (d18:1/24:0)	12,6	694,6527	M+FA-H	694,6355	25	8,05	1,15	HMDB0004956
Ceramide (d18:1/24:1)	11,6	692,6145	M+FA-H	692,6198	8	1,92	1,04	HMDB0004953
Glucosylceramide (d18:1/16:0)	7,9	717,5900	M+NH4	717,5987	12	4,36	1,26	HMDB0004971
Glucosylceramide (d18:1/24:1)	10,9	810,6731	M+H	810,6817	11	0,31	1,76	HMDB0004975
SM(d18:1/14:0)	6,0	719,5347	M+FA-H	719,5345	0	0,25	2,26	HMDB0012097
SM(d18:1/16:0)	7,1	747,5650	M+FA-H	747,5658	1	0,38	2,15	HMDB0013464
SM(d18:1/18:0)	8,6	731,6062	M+H	731,6062	0	0,69	1,48	HMDB0012089
SM(d18:1/22:0)	11,2	831,6610	M+FA-H	831,6597	2	0,14	1,26	HMDB0012103
SM(d18:1/22:1)	10,2	785,6618	M+H	785,6531	11	0,31	2,48	HMDB0012104
SM(d18:1/24:0)	12,4	859,6903	M+FA-H	859,691	1	0,24	1,45	HMDB0012095
SM(d18:1/24:1)	11,4	857,6802	M+FA-H	857,6753	6	0,26	1,62	HMDB0012107
Ganglioside GM3 (d18:1/16:0)	6,6	1151,7115	M-H	1151,7059	5	0,43	1,18	HMDB0004844
LysoPC(14:1)	2,5	464,2775	M-H	464,2783	2	0,82	1,07	HMDB0010380

LysoPE(18:0)	3,2	462,2970	M-H20-H	462,2984	3	0,26	2,03	HMDB0011130
PC(32:0)	8,3	778,5570	M+FA-H	778,5604	4	0,57	1,38	HMDB0000564
PC(34:0)	9,7	806,5870	M+FA-H	806,5917	6	0,44	1,17	HMDB0007878
PC(34:1)	8,8	804,5742	M+FA-H	804,576	2	0,42	1,89	HMDB0008263
PC(34:2)	7,9	802,5584	M+FA-H	802,5604	2	0,48	1,46	HMDB0008296
PC(36:2)	9,2	830,5879	M+FA-H	830,5917	5	0,59	1,49	HMDB0008559
PC(36:4)	7,9	826,5612	M+FA-H	826,5604	1	0,44	1,71	HMDB0008623
PC(38:5)	8,3	852,5813	M+FA-H	852,576	6	0,45	1,78	HMDB0008692
PE(36:2)	9,9	788,5420	M+FA-H	788,5447	3	0,26	1,16	HMDB0009286
PE-P(16:0)	3,0	438,2959	M+H	438,2979	5	0,29	2,00	HMDB0011152
PG(36:0)	7,5	777,5516	M-H	777,5651	17	0,38	1,85	HMDB0010602
PI(38:4)	9,3	885,5503	M-H	885,5499	1	0,41	1,73	HMDB0009914
MG(18:3)	3,6	351,2491	M-H	351,2541	14	0,05	1,96	HMDB0011569
TG(46:0)	8,9	796,7493	M+NH4	796,7389	13	5,93	1,10	HMDB0010411

5.3. Publicació V

Phenotypic and lipidomic characterization of primary human epidermal keratinocytes exposed to simulated solar UV radiation

N. Dalmau, N. Andrieu-Abadie, R.Tauler, C. Bedia

J Dermatol Sci **2018**, 92(1), 97-105

Journal of Dermatological Science 92 (2018) 97–105

Contents lists available at ScienceDirect

Journal of Dermatological Science

journal homepage: www.jdsjournal.com

Original Article

Phenotypic and lipidomic characterization of primary human epidermal keratinocytes exposed to simulated solar UV radiation

Núria Dalmau[a], Nathalie Andrieu-Abadie[b], Romà Tauler[a], Carmen Bedia[a,*]

[a] Department of Environmental Chemistry, Institute of Environmental Assessment and Water Research (IDAEA-CSIC), c/ Jordi Girona 18-24, 08034 Barcelona, Spain
[b] INSERM UMR 1037, Centre de Recherches en Cancérologie de Toulouse (CRCT), 31037, Toulouse, France

ARTICLE INFO

Article history:
Received 12 April 2018
Received in revised form 4 July 2018
Accepted 5 July 2018

Keywords:
Keratinocyte
UV irradiation
Untargeted lipidomics
Keratinocyte differentiation

ABSTRACT

Background: Ultraviolet (UV) radiation is known to be one of the most important environmental hazards acting on the skin. The most part of UV radiation is absorbed in the epidermis, where keratinocytes are the most abundant and exposed cell type. Lipids have an important role in skin biology, not only for their important contribution to the maintenance of the permeability barrier but also for the production and storage of energy, membrane organization and cell signalling functions. However, the effects on the lipid composition of keratinocytes under UV radiation are little explored.
Objective: The present work aims to explore the effects on the phenotype and lipid content of primary human keratinocytes exposed to simulated solar UV radiation.
Methods: Keratinocytes were exposed to a single (acute exposure) and repeated simulated solar UV irradiations for 4 weeks (chronic exposure). Cell viability and morphology were explored, as well as the production of reactive oxygen species. Then, lipid extracts were analysed through liquid chromatography coupled to mass spectrometry (LC–MS) and the data generated was processed using the ROIMCR chemometric methodology together with partial least squares discriminant analysis (PLS-DA), to finally reveal the most relevant lipid changes that occurred in keratinocytes upon UV irradiation. Also, the potential induction of keratinocyte differentiation was explored by measuring the increase of involucrin.
Results: Under acute irradiation, cell viability and morphology were not altered. However, a general increase of phosphatidylcholines (PC) phosphatidylethanolamines (PE) and phosphatidylglycerol (PG) together with a slight sphingomyelin (SM) decrease were found in UV irradiated cells, among other changes. In addition, keratinocyte cultures did not present any differentiation hallmark. Contrary to acute-irradiated cells, in chronic exposures, cell viability was reduced and keratinocytes presented an altered morphology. Also, hallmarks of differentiation, such as the increase of involucrin protein and the autophagy induction were detected. Among the main lipid changes that accompanied this phenotype, the increase of long-chain ceramides, lysoPC and glycerolipid species were found.
Conclusion: Important lipid changes were detected under acute and chronic UV irradiation. The lipid profile under chronic exposure may represent a lipid fingerprint of the keratinocyte differentiation phenotype.

1. Introduction

Sunlight is composed of a continuous spectrum of electromagnetic radiation which has three main wavelength regions: ultraviolet (UV), visible and infrared. UV radiation comprises UVA (320–400 nm), UVB (280–320 nm) and UVC (200–280 nm). Whereas UVA radiation represents 95% of the total solar UV that reaches the earth, UVC and most of the UVB radiation are absorbed by the stratospheric ozone layer [1,2]. Skin, the outermost tissue of the body, is exposed to various environmental aggressions, among which solar ultraviolet (UV) radiation is the most significant. UVA is responsible for indirect cell damage through the generation of reactive oxygen species (ROS), whereas UVB causes direct DNA damage and results in a variety of harmful effects on human skin, including epidermal thickening, collagen damage, skin wrinkling, and the development of skin tumors [3,4].

Most of the UV radiation is absorbed in the epidermis, the outermost layer of the skin, where keratinocytes are the most abundant and exposed cell type. The epidermis is continuously being regenerated through a process called differentiation, in

* Corresponding author.
E-mail address: carmen.bedia@idaea.csic.es (C. Bedia).

https://doi.org/10.1016/j.jdermsci.2018.07.002
0923-1811/

which keratinocytes are gradually modified to become flat cells named corneocytes and migrate into the upper layer of the epidermis, where they are ultimately released from the epithelial surface [5]. During this process, keratinocytes lose progressively their nucleus and cytoplasmic organelles and provide a protective barrier to retain body fluids and to prevent environmental insults. Disruption of epidermal barrier formation and abnormal keratinocyte differentiation are involved in the pathophysiology of several skin diseases, such as psoriasis, atopic dermatitis and basal and squamous skin cancer [6]. Concerning UV radiation, a recent study has demonstrated that UVB-irradiated keratinocytes present altered differentiation and impaired barrier function leading to increased permeability [7].

Lipids have an important role in skin biology. During epidermal differentiation, lipids are synthesized in the keratinocytes and extruded into the extracellular domains, where they form extracellular lipid-enriched layers. These lipids, after enzymatic processing, are incorporated in lipid lamellar membranes, which together with the keratin-filled corneocyte envelope, form the permeability barrier [8]. The impairment of sphingomyelinase activity has been shown to be involved in the aberrant differentiation of keratinocytes in atopic dermatitis, correlating with reduced ceramide content in the stratum corneum. Also, recent studies pointed out increased ceramide levels upon UV radiation [9–11]. Besides the structural role in the permeability barrier, lipids also have other important functions in cells, such as energy production and storage, cell signalling, protein trafficking and membrane organization. However, few works are dedicated to the investigation of UV effects on skin cells lipid composition.

In the recent years, the development of high-throughput analytical platforms and data analysis tools has allowed the emergence of lipidomics studies, in which the exploration of the lipid composition in a variety of biological matrices and conditions has enabled a better understanding about the lipid roles in the biological systems. The huge amounts of data obtained from these developing technologies have favoured the popularity of untargeted omic approaches, in which all data are simultaneously analysed by chemometric data analysis methodologies to extract information about the relevant molecules in the process studied.

In this work, a solar simulation unit has been used to expose primary cultures of keratinocytes to a single dose (acute exposure) and repeated doses (chronic exposure) of UV radiation. First, cell viability and morphology changes were examined and reported. Second, an untargeted LC–MS lipidomic study was performed and the obtained data were analysed by the ROIMCR (Regions of Interest Multivariate Curve Resolution) procedure. The main lipid changes that occur under acute and chronic exposures were investigated. Since differentiation is an important process in keratinocytes, its possible induction was also investigated under UV radiation. Finally, phenotype changes observed in these keratinocytes are discussed together with the observed lipid changes to hypothesize the functional role of lipids in keratinocyte differentiation.

2. Materials and methods

2.1. Cell culture

Primary cultures of human epidermal keratinocytes were obtained from Dr. P. Descargues (Genoskin, Toulouse). These cells were maintained in DermaLife K Complete Medium (CellSystems Biotechnologie) protected from sunlight and supplemented with 100 U/ml penicillin and 100 μg/ml streptomycin, at 37 °C in a humidified atmosphere containing 5% of CO_2.

2.2. UV irradiation

Cultured keratinocytes were irradiated in a Suntest CPS (Atlas, USA), solar simulation unit. This simulator is equipped with a xenon arc lamp that provides irradiance that simulates sunlight. The UVA/UVB radiation was controlled by a radiometer VLX-3 W (Vilber Lourmat). The simulated UV daylight applied in this work presented a UVA/UVB irradiance ratio of 29 (it has been estimated that a UVA/UVB ratio comprised between 23 and 32 is representative of UV daylight spectrum) [12]. The irradiation was selected taking into account the UVB irradiation intensities used in literature for studies in skin cells related to sunlight exposure [10,13–15] and the results of a previous keratinocyte viability test carried out after UV exposure at different irradiation intensities. The chosen UV dose (728 mJ/cm^2 UVA and 25 mJ/cm^2 UVB) was the highest dose that did not produce any change in cell viability after 72 h post-irradiation (data not shown).

Keratinocytes were seeded in 6-well plates (Nunclon surface, Thermo Scientific) and cultured under standard conditions. Some of the wells contained glass coverslips to perform the immunofluorescence detection of involucrin. Just before irradiation, an acetate plastic sheet was placed above the plate to adapt the UVA/UVB ratio to 29:1. Cells were placed inside the Suntest CPS and were irradiated for five min, which represented the final UV radiation dose of 728 mJ/cm^2 UVA and 25 mJ/cm^2 UVB. After light irradiation, cells were rinsed with PBS 1X and incubated again under standard conditions. Following this procedure, irradiations were applied twice a week to the keratinocyte cultures. In this work, effects of acute and chronic irradiations were investigated: 0.5 week, which is equivalent to one irradiation (acute irradiation), and 4 weeks, which represents a total of 8 exposures to UV radiation (chronic irradiation). For the evaluation of sphingomyelinase activity, involucrin increase and autophagy activation progress over time, an additional intermediate irradiation was performed for 1.5 weeks (1.5 W), equivalent to 3 UV irradiations. At each endpoint, cells exposed to sham light (regular laboratory light) were used as control references.

2.3. Cell viability

Cell viability was estimated by using the 3-(4, 5-dimethylthiazol-2-yl)-2,5-diphenyltetrazolium bromide (MTT, Sigma) assay on 96-well plates, according to the manufacturer instructions.

2.4. Autophagy assessment by western blot

Cells were harvested by trypsinization, centrifuged and washed twice with PBS 1 ×. Then, cells were lysed using mammalian lysis buffer 1X (ab179835, Abcam) and cocktail protein inhibitor 1X (Thermo Scientific). Protein in cell lysates was quantified using the BCA assay (Thermo Scientific) and 90 μg of protein per sample were resolved by 10% SDS-PAGE. Proteins were transferred to PVDF membranes (Roche). Membranes were blocked with TBS 1X containing 0.1% Tween 20 and probed with the LC3 polyclonal antibody (ab150917, Abcam). Membranes were developed using the chemiluminescent signal detection kit ECL™ Prime Western Blotting detection reagent (GE Healthcare) and visualized using LICOR C-DiGit blot scanner. Relative quantification of Western Blot band intensities was carried out using Image Studio Lite version. 5.0 software; values were normalized to those of β-actin, and the differences between UV-irradiated and control samples were calculated.

2.5. Reactive oxygen species (ROS) assay

To evaluate the formation of ROS after UV acute irradiation, keratinocytes were seeded in 96-well plates at 10^5 cells/ml and

incubated for 24 h. Immediately prior to use, a fresh stock solution of carboxy-H_2DCFDA (Sigma) was prepared in dimethyl sulfoxide (DMSO). Keratinocytes were washed twice with PBS 1X to remove traces of the original medium and a 32 μM solution of the dye (carboxy-H_2DCFDA) in culture medium was added to the cell wells. After 30 min under regular conditions, the dye solution was removed, and cells were washed twice with PBS 1X and replaced with fresh medium in the dark. Then, cells were irradiated in the Suntest CPS, and immediately after, fluorescence was measured using a plate reader (485/535 nm excitation and emission).

2.6. Protein content quantification

The protein content was quantified for each cell sample pellet using a Pierce™ BCA Protein assay kit (ThermoFisher). The protocol applied was performed following the manufacturer instructions.

2.7. Acid sphingomyelinase activity assay

Acid sphingomyelinase activity was determined using a fluorometric assay kit from Abcam (ab190554) in a 96-well plate format, following the manufacturer's instructions. The assay was performed using equal amounts of protein for each sample, previously quantified employing the BCA protein assay kit.

2.8. Involucrin immunofluorescence assay

In order to visualize involucrin, 24 h after each irradiation endpoint, media was aspirated from the culture plate wells that contained the glass coverslips specifically prepared for this purpose. Cells were fixed in cold methanol and washed with PBS 1 ×. Cells were permeabilized with Triton X-100 (0.2%) for 5 min, washed again with PBS 1X and incubated with anti-involucrin rabbit polyclonal primary antibody (Invitrogen) diluted at 1:200 in PBS-BSA 1% for 45 min at room temperature. After three washes in PBS 1X, keratinocytes were incubated 45 min at room temperature with goat Anti-Rabbit IgG (FITC) secondary antibody (ab6717) diluted at 1:500 in PBS-BSA 1%. Cells were rinsed with PBS and were mounted onto glass slides using Prolong Diamond Antifade Mountant with DAPI (Life Technologies) and left in the dark for 10 min. Samples were examined under a fluorescence microscope (Nikon SMZ 1500, using DAPI and FITC filters) fitted with a digital camera (Nikon DS-Ri1).

2.9. ***Lipid extraction and*** *LC–MS* ***analysis***

After 24 h of each irradiation endpoint, cells were harvested using trypsin, centrifuged at 1300 *rpm* for 3 min at 4 °C and cell pellets were washed twice with cold PBS 1 ×. Two types of extraction were used in this work, one to extract all lipids and another to specifically extract sphingolipids, as previously described [16].

LC–MS analysis used a Waters Acquity UHPLC system connected to a Waters LCT Premier orthogonal accelerated time of flight (ToF) mass spectrometer (Waters), operated in positive and negative electrospray ionization modes (ESI + and ESI -). Full scan spectra between 50 and 1500 Da were acquired, and individual spectra were summed to produce data points every 0.2 s. Mass accuracy and reproducibility were maintained by using an independent reference spray *via* the LockSpray interference. The analytical column was a 100 x 2.1 mm inner diameter, 1.7 μm C8 Acquity UPLC bridged ethylene hybrid (Waters). The two mobile phases were phase A: MeOH, 1 mM ammonium formate, and phase B: H_2O, 2 mM ammonium formate, 0.2% formic acid for both solutions. The flow rate was 0.3 ml min^{-1} and the gradient of A/B solvents started at 80:20 and changed to 99:1 in 6 min until min 15; remained 99:1 until minute 18; finally returned to the initial conditions until minute 20. The column was held at 30 °C.

2.10. ***Chemometric analysis of*** *LC–MS* ***data***

Every LC–MS chromatographic run from the analysis of one single sample resulted in a data file which was converted to *cdf* format *via* Databridge (MassLynx software, Waters). Data sets from the different chromatographic runs were then imported and stored in the MATLAB computational environment (release R2016b, The Mathworks Inc.), using *mzcdfread* and *mzcdf2peaks* functions from the MATLAB Bioinformatics Toolbox™.

The method used in this work to analyse the LC–MS data is called ROIMCR and comprises two steps. First, a data compression step based on the Regions of Interest (ROI) concept [17], and second, the analysis of the compressed data using Multivariate Curve Resolution- Alternating Least Squares (MCR-ALS) [18] methodology. This combined approach (ROIMCR) has been successfully used in different untargeted metabolomics investigations on LC–MS data [19–22].

In the first compression step, the ROI procedure searches for signals at *m/z* values with significant intensity MS values, higher than a threshold value (estimated from the instrumental noise level). Apart from having higher values than the threshold value, ROI values have also to be represented by a minimum of consecutive data points in the chromatogram, within a predefined *m/z* deviation error (related to the MS instrument mass accuracy) [19–22]. ROI compression step takes advantage of the sparse structure of the measured MS data reducing considerably the computer storage and computation time needed without losing the instrumental mass accuracy and resolution. This procedure has been described in more detail in Gorrochategui et al. [23] In our study, control and UV-exposed samples at each UV exposure endpoint were analysed together, both using positive and negative ionization data. This procedure was performed at acute and chronic exposures. As a result of ROI compression step, an augmented data matrix containing all significant traces at the ROI *m/z* values for the different samples (common and not common) was built.

Then, these ROI compressed augmented data matrices were analysed using MCR-ALS. This method allowed the simultaneous resolution of all the elution and MS spectral profiles of the different sample lipid constituents [24,25]. MCR-ALS has been previously applied for the resolution of the elution and spectral profiles of the constituents of complex sample mixtures analysed by LC–MS and it has been extended more recently to omic studies [16,26–32].

Initialization of the MCR-ALS procedure, when applied to augmented data matrices, was performed using estimates of spectra profiles found at the purest elution times [33]. The applied constraints were non-negativity of elution and spectra profiles, and spectra normalization (equal height) [34]. Results of MCR-ALS generated a data table containing the peak areas of the elution profiles of the different resolved components in the different samples. The calculated areas were then normalized using the areas of the internal standards used in the extraction and the protein content of each sample as follows: (calculated area/mg of protein)/mean area of internal standards. The pure spectra of the MCR-ALS resolved components (lipids) were recovered without any loss of spectral resolution and identified using the Human Metabolome Database (HMDB) [35].

To investigate if lipidomic profiles were different enough to discriminate between irradiated and non-irradiated samples, Partial Least Square Discriminant Analysis (PLS-DA) was performed. The classes considered were control (class 0) and UV irradiated (class 1) for each acute and chronic exposures. The lipid

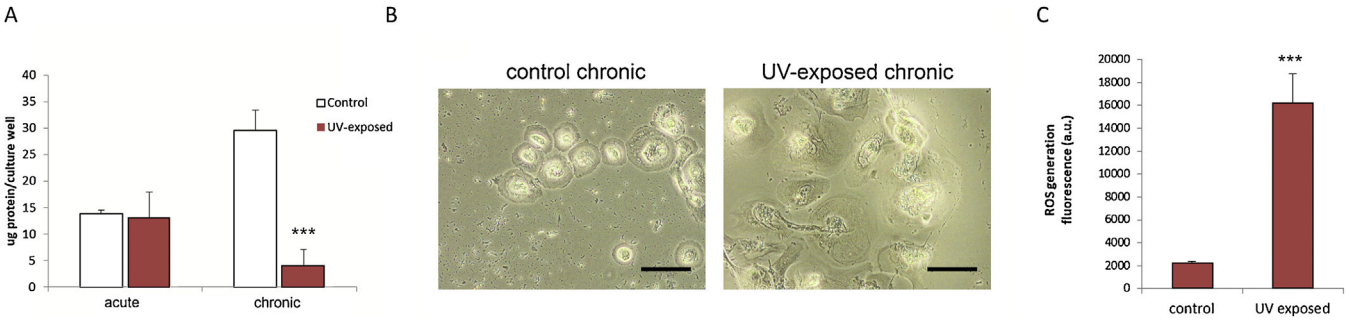

Fig. 1. Keratinocyte viability, morphology and intracellular ROS generation under UV irradiation. A) Acute and chronic protein content in the plate wells of UV exposed and non-exposed keratinocytes cultures. Results represented the mean ± SE of three independent experiments (n = 3) performed in triplicate. *** $p < 0.005$. B) Representative microscope pictures of control and UV-exposed cells at chronic exposure. Scale bar = 100 μm. C) Intracellular generation of ROS in keratinocyte cultures just after UV irradiation. Results represented the mean ± SE of three independent experiments (n = 3) performed with more than 5 replicates. *** $p < 0.005$.

peak normalized areas data matrix was autoscaled before PLS-DA and the results were cross-validated by the leave-one-out method. The Mathew's Correlation Coefficient (MCC) [36] was calculated to validate the goodness of each discrimination model. The MCC is a correlation coefficient between the observed and predicted binary classifications; the values move between +1 (perfect prediction) and -1 (total disagreement between prediction and observation). A value of 0 indicates no better classification than random prediction. The VIP scores [37] obtained in the PLS-DA model were used to estimate the importance of the different lipids in the differentiation between irradiated and non-irradiated samples.

2.11. Software

Software used in this work includes MassLynx V 4.1 (Waters) for raw UPLC-TOF data analysis and data conversion to *cdf* format. For matrix data processing and statistical analyses, Bioinformatics Toolbox (The Mathworks Inc.), Statistics Toolbox (The Mathworks Inc.), PLS-Toolbox (Eigenvector Research Inc.) and MCR-ALS Toolbox [38] were used in MATLAB 8.3.0-R2016a (The Mathworks Inc.) environment.

3. Results

3.1. Effects of UV exposure on cell viability, morphology and ROS production

First, the effects of acute and chronic exposure to UV radiation were explored in terms of cell viability, morphology and ROS production. Regarding cell viability, it was not affected after acute exposure; but at chronic irradiation, the protein amounts measured in the cell culture wells indicated that control keratinocytes proliferated during these 4 weeks, whereas irradiated cells reduced dramatically their number (Fig. 1A). UV radiation also affected the morphology of keratinocytes. As shown in Fig. 1B, keratinocytes at chronic exposure presented deformations in the cell membrane and these were much more intense in UV irradiated cells than in controls. One of the most important cell responses to UV radiation is the formation of reactive oxygen species (ROS) which are able to induce cellular oxidative stress and DNA damage. In the present study, the formation of ROS was confirmed after UV irradiation, as shown in Fig. 1C.

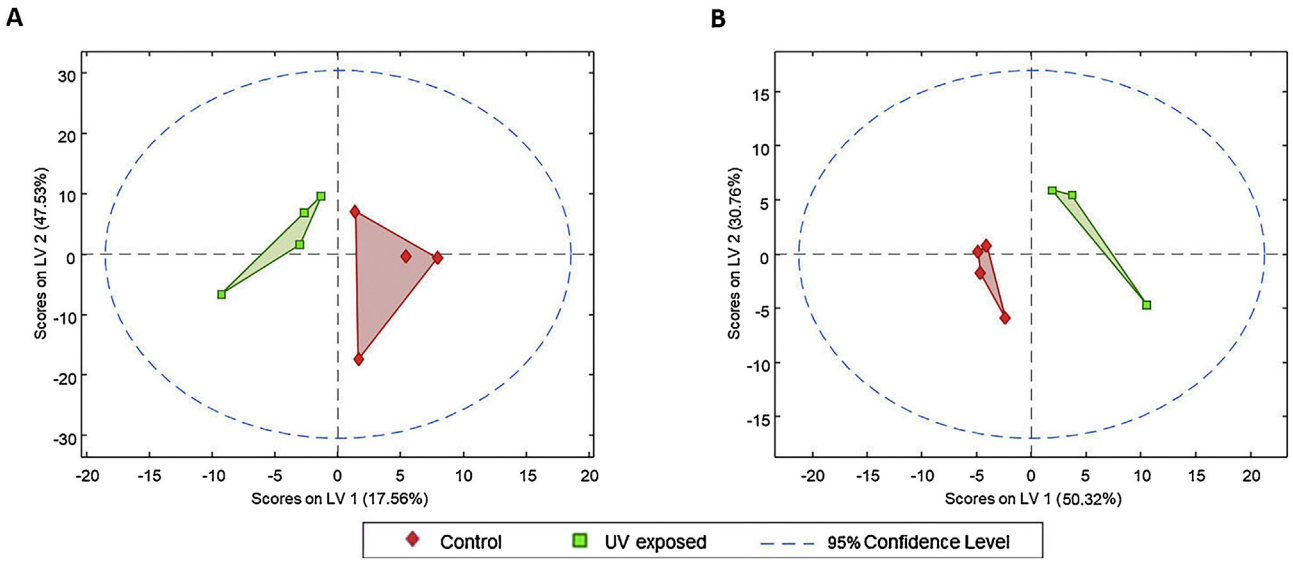

Fig. 2. Partial Least Squares – Discriminant Analysis (PLS-DA) of the lipidomic data. UPLC-ToF positive and negative ionization data of keratinocyte lipid extracts were processed using the ROIMCR strategy. At the endpoints studied: acute (A) and chronic exposures (B), a matrix containing the areas for each MCR component in the irradiated and non-irradiated samples was used to build the two-class PLS-DA models.

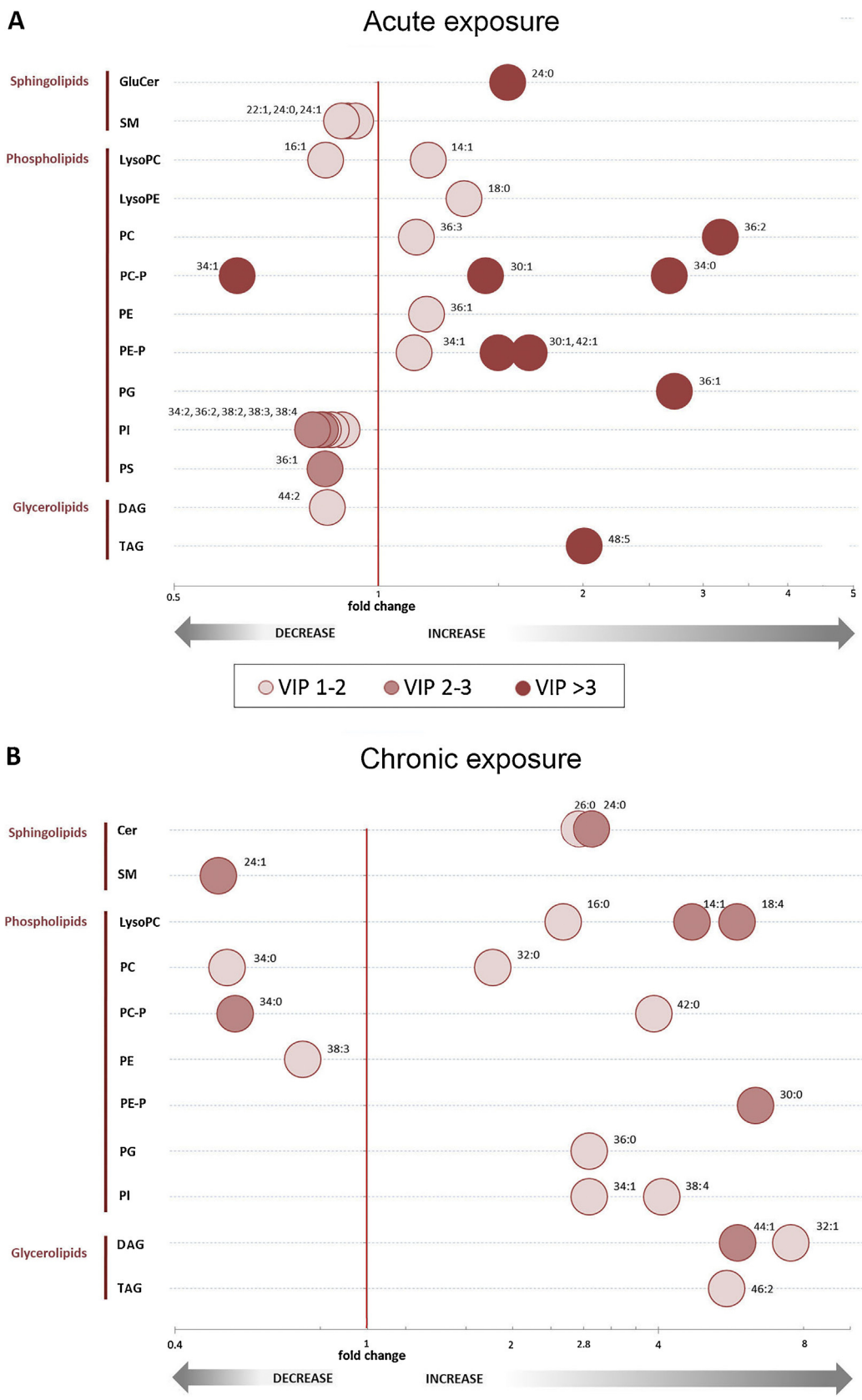

Fig. 3. Representative lipid changes in keratinocytes at acute and chronic irradiation. Fold changes of UV exposed keratinocytes for acute (A) and chronic exposures (B) compared to the non-exposed cells are depicted for each lipid. Only lipids with VIP scores >1 in the PLS-DA models were used to elaborate these plots. Darker circles represent higher VIP score values in the PLS-DA models built.

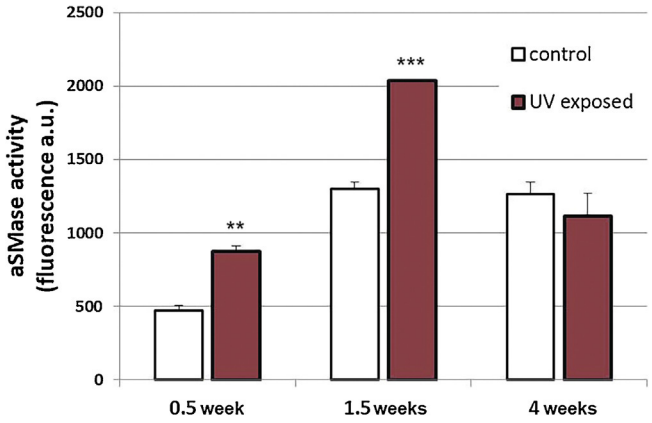

Fig. 4. Assessment of acid SMase activity in irradiated keratinocytes at 0.5, 1.5 and 4 weeks irradiation endpoints. Bar diagram of fluorescence intensity (arbitrary units). Results represented the mean ± SE of three independent experiments (n = 3) performed in triplicate. * $p < 0.05$, *** $p < 0.005$.

3.2. Lipidomic study of UV exposed keratinocytes

Next, the effects on the lipid composition of keratinocytes under UV exposure were explored. Two kinds of lipid extraction were performed, total lipids and sphingolipids, on UV-irradiated and non-irradiated keratinocytes. The samples generated were analysed through full scan UPLC-MS in positive and negative ionization mode. The data generated were analysed by the means ROIMCR methodology, as detailed in the methodology section. Data corresponding to the same endpoint (control and irradiated) were analysed together. The areas of the resolved components were subjected to a PLS-DA analysis in order to investigate if UV-irradiated samples could be differentiated from controls in the two endpoints investigated. The PLS-DA plots of acute and chronic exposures are depicted in Fig. 2. For acute exposure samples, 78.5% of the Y-variance was explained by cumulative X-variance of two latent variables (65.1%). For chronic exposure, 98.2% of the Y-variance was explained by the X-variance of two latent variables (81.1%). The Matthews Correlation Coefficients (MCC) of the cross-validated models were 0.6 and 1.0 for the acute and chronic exposures groups of samples, respectively, indicating that the lipidomic profile of the samples enabled a good discrimination between UV-irradiated and non-irradiated keratinocytes, especially in the case of chronic exposure irradiation. PLS-DA Variable Importance Projection (VIP) scores [37] were calculated to highlight what were the most relevant lipids that discriminated between UV-irradiated and control samples. Only the lipids with VIP values higher than one (*i.e.*, discriminating more than the average) were considered for further analysis and data interpretation. In order to visualize the lipidomics results, in Fig. 3 the most important lipids are represented, together with their VIP values and fold changes. The detailed information about the individual species, *m/z* values, retention times, fold changes and VIP scores values are given in the Supplementary Table S1.

Under acute exposure, the observed changes related to sphingolipids were a slight decrease (0.8 fold) of three sphingomyelin (SM) species concentration and a 1.5 fold increase of glucosylceramide (GluCer) (24:0). Regarding phospholipids, the most relevant changes under acute UV exposure were the increase of phosphatidylcholine (PC) species ((36:2) and (34:0) with fold changes of 4.3 and 5.2, respectively), phosphatidylethanolamine plasmalogen (PE-P) compounds ((30:1), (34:1) and (42:1), with fold changes that range from 2 to 3.7) and phosphatidylglycerol (PG) (36:1) with an increase of 3.9 fold. In contrast, the concentration of five different phosphatidylinositol (PI) species slightly decreased, around 0.8 fold. Concerning neutral lipids, an increase of 3.4 fold was observed for triacylglyceride (TAG) (48:5).

On the other hand, keratinocytes under chronic UV irradiation presented an increase of long-chain ceramide (Cer) species (24:0 Cer and 26:0 Cer with 2.9 and 2.7 fold changes, respectively), and a 0.5 fold decrease of SM (24:1). The most remarkable change among phospholipids was the increase of several Lyso PC species with fold changes between 2.5 to 5.6. Also, the PG(36:0) concentration was found increased (3-fold) as well as two PI species (34:1, and 38:4), with an augmentation of 3 and 4 fold, respectively. Although an important augmentation of PE-P(30:0) concentration was observed, PC and PE species did not present a clear change tendency under chronic UV irradiation. Finally, in the neutral lipids family, two diacylglycerol (DAG) species and one TAG species showed high fold concentration changes from 5.3 to 7.1.

3.3. Acid SMase activity

The reduction of SM levels (in acute and chronic exposure) and the concomitant increase of Cers observed after chronic exposure suggested the activation of acid sphingomyelinase (aSMase) enzymatic activity. This enzyme is responsible for the SM hydrolysis in the cellular membrane leading to ceramide production, which in turn triggers cascade signals involved in different cellular processes such as apoptosis. In order to explore a potential aSMase activation upon UV irradiation in our conditions, aSMase activity was measured. For this study, an intermediate additional irradiation endpoint at 1.5 weeks (meaning a total of 3 UV exposures) was added to better follow the time-course progress of aSMase activity. As a result of these measures, aSMase activity was considerably increased at acute exposure and 1.5 weeks (Fig. 4), whereas at the more chronic exposure, aSMase activity levels were not significantly different between irradiated and non-irradiated keratinocytes.

3.4. Effects of UV exposure on keratinocyte differentiation

Previous studies demonstrated that UV radiation induces keratinocyte differentiation. This process, consisting in a progressive cellular conversion to corneocytes as cells migrate to more superficial layers of the skin [39], is characterized by cytoskeleton changes, the increase of involucrin protein and autophagy induction, among others [40–42]. In order to assess the potential induction of the keratinocyte differentiation process in our primary cultures under UV irradiation, we investigated the presence of involucrin and the induction of autophagy at the three endpoints studied (acute exposure (0.5 weeks), 1.5 weeks and chronic exposure (4 weeks)). First, involucrin presence was analysed in keratinocytes by immunofluorescence. As a result, involucrin levels were higher in irradiated keratinocytes at 1.5 W, and the increase was more prominent at 4 weeks (see Fig. 5A). Second, autophagy was assessed by LC3 immunoblotting detection. LC3 is a central protein in autophagy with a key role in autophagosome biogenesis. When autophagy is induced, the cytosolic form of LC3 (LC3-I) is conjugated to PE to form an LC3-PE conjugate (LC3-II), which is recruited to autophagosomal membranes. In this work, the increase of LC3-II levels is used as a marker of autophagy induction. The results showed a slight decrease of LC3-II in irradiated cells under acute exposure to UV (Fig. 5B). However, at 1.5 weeks and 4 weeks, UV irradiated cells presented a progressive increase of LC3-II protein. This augmentation is especially huge at 4 weeks (Fig. 5B), indicating an enhancement in autophagy levels upon chronic exposure to UV. Altogether, the increase of involucrin levels and LC3-II protein after

N. Dalmau et al. / Journal of Dermatological Science 92 (2018) 97–105

repeated UV doses suggested a differentiation phenotype in irradiated keratinocytes.

4. Discussion

The aim of the study was to reveal the impact of acute and chronic UV irradiation on the phenotype and lipidomic profile of keratinocytes, in order to establish a functional role of the lipid changes observed in the acquisition of a characteristic phenotype, *e.g.* keratinocyte differentiation. To perform this study, a solar unit simulator was used to imitate the UVA/UVB sunlight irradiation ratio, and primary cultures of keratinocytes were used to work with a more realistic model than stable cultured cell lines.

Using a single dose of UV irradiation (acute exposure), ROS were generated and cell viability was not affected. In the context of lipids, the most remarkable changes were found in phospholipids, specifically an increase of PC, PE-P and PG species. These observations are in agreement with previous studies using a single UV irradiation dose on HaCaT keratinocytes in which several species of PC and PE-P presented a considerable rise [39]. Among the sphingolipid changes observed, the increase of GluCer (24:0) agreed with the results of Takagi et al., in which the hydrolytic

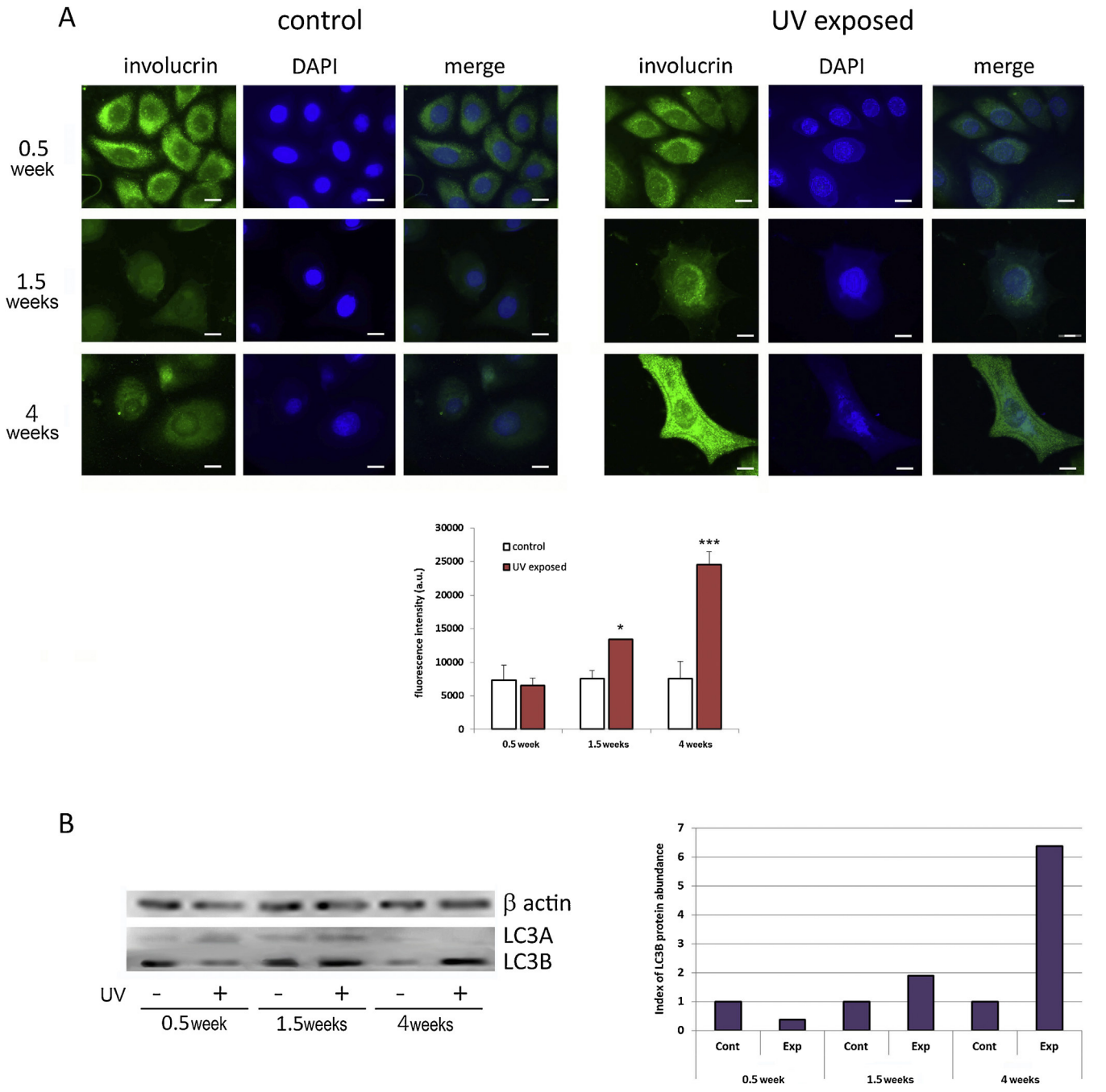

Fig. 5. Assessment of changes in involucrin levels and autophagy in keratinocytes at 0.5 (acute), 1.5 and 4 (chronic) weeks irradiation endpoints. A) Involucrin immunofluorescence assay in keratinocytes 24 h after each irradiation endpoint. Representative pictures of involucrin immunolabelling observed under microscopy. Bar diagram showing the quantification of fluorescence intensity corresponding to involucrin immunolabelling. The results are representative of three independent measurements. B) Western blot bands and relative quantification corresponding to LC3-II. Western blot image is representative of three independent experiments. ** $p < 0.01$, *** $p < 0.005$.

activity of glucocerebrosidase was significantly suppressed in a dose-dependent manner in murine epidermis after UVB irradiation [14]. Also, the slight reduction of SM levels observed correlated to the increased aSMase activity measured at this irradiation endpoint. In this sense, Magnoni et al. have previously reported that both neutral and acidic sphingomyelinases are activated in human keratinocytes upon UVB radiation [10]. Concerning keratinocyte differentiation, since neither an increase of involucrin or LC3-II autophagy marker were observed, it seems that under our conditions differentiation is not induced under one single exposure to UV radiation.

When repeated UV irradiations were applied to keratinocytes (chronic exposure), the phenotype of cells was completely different. First, cell viability decreased dramatically and important alterations in cell morphology were observed. It has previously been reported that repeated exposures to UVB are able to induce keratinocyte differentiation [43]. In the present study, chronic exposure of keratinocytes to UV irradiation has resulted in the increase of involucrin levels and the activation of autophagy, which are both hallmarks of the keratinocyte differentiation process [42,44]. Another characteristic feature of differentiation are changes in the cytoskeleton [40], which may be related to the morphology changes observed in irradiated cells. These observations are in agreement with previous studies in which these differentiation hallmarks have been reported in HaCaT keratinocytes [39] and buccal mucosa keratinocytes from healthy individuals under UV exposure [45].

This differentiation phenotype observed at the end of the chronic exposure under UV was accompanied by changes in the lipid composition. The most remarkable lipid changes were the increase of long-chain Cers, LysoPC and glycerolipid species, whereas phospholipids such as PC and PE were not following a clear increasing/decreasing pattern.

The most significant change at the sphingolipid level was a notable increase of long-chain Cers (24:0 and 26:0) concomitant with a decrease of SM. Although in most tissues Cers chain lengths range from 16 to 24 carbons, in epidermal tissues, long and very long chain Cers (from 24 to 32 carbons) are more abundant and unique to these tissues. When the activity of aSMase was evaluated, no significant differences were found at chronic exposure in UV irradiated keratinocytes compared to controls, suggesting that Cers were produced through an alternative biosynthetic pathway. In this sense, ceramide synthases (CerS) are key enzymes in the *de novo* biosynthesis of ceramides. Mizutani et al. have reported that the expression of CerS3 is increased upon differentiation [46]. Since CerS3 is the most predominantly CerS expressed in keratinocytes and it shows long-chain fatty acyl-CoA preferences (C20–C26), one hypothesis could be that the overexpression of CerS3 is involved in the increase of long-chain Cers observed under UV irradiation.

The most important function of the epidermal barrier is to prevent the excess water loss. Among the lipids that enable this permeability barrier, Cers are major lipid class by weight within the epidermal membrane structure [47]. Wefers et al., based in their work in which UV radiation increased Cers abundance in human stratum corneum, suggested that the rise of Cers could be associated with the beneficial effects of phototherapy in skin diseases such as atopic dermatitis [48].

Another important lipid change observed is the increase of several LysoPC species. LysoPC is a polar phospholipid produced by the action of phospholipase A2 (PLA_2) on membrane phospholipids. Among its intracellular messenger functions, Ryborg et al. have reported that LysoPC is able to induce keratinocyte differentiation through the activation of protein kinase C (PKC) [49] by increasing the expression of important proteins in this process, such as transglutaminase-1 (TG-1) [50]. This suggests that the augmented LysoPC concentrations observed could be involved in the maintenance of the keratinocyte differentiation process.

Also, the increase of PG(36:0) observed under chronic UV irradiation is in accordance to the work of Qin et al. in which the authors demonstrated that PG functions as a signalling molecule able to mediate early epidermal keratinocyte differentiation [51]. In this context, Xie et al. have also reported that exogenously added PG species inhibit the proliferation and promote the differentiation of rapidly dividing keratinocytes [52].

Concerning neutral lipids, two diacylglycerol species were found increased, as well as one TAG compound. Carsberg et al. have demonstrated that UV radiation stimulates sustained DAG formation in cultured human keratinocytes [53], and Punnonen et al. observed that UV irradiation induced a dose-dependent increase in the keratinocyte levels of DAG, which was accompanied by changes in the activity of diacylglycerol kinase [54]. DAGs are known to regulate protein kinase C (PKC), also the isoform PKC delta, which is a regulator of keratinocyte differentiation that increases the expression of differentiation-associated genes, including involucrin [44]. This suggests that higher levels of DAG, could be tightly related to the induction of the differentiation process, as happened for LysoPC, since both are activators of PKC [49].

Overall, despite the low doses of UV irradiation used in the present work, lipid changes were detected in both acute and chronic exposures. Under a single dose, the changes observed might be part of the cell survival response to the UV irradiation. Repeated doses induced a differentiation phenotype in primary cultures of keratinocytes, indicating that UV is able to alter the normal pattern of the process. The untargeted lipidomic analysis performed enabled the identification of the most relevant lipid changes that occurred in keratinocytes under acute and chronic UV irradiation.

5. Conclusion

The present work describes the effects of simulated solar UV radiation on the phenotype and lipid composition of primary cultured keratinocytes. Under acute irradiation, changes in the lipid composition involve a general increase of PE and PC species. Conversely, repeated doses of UV irradiation induced a differentiation phenotype that was accompanied by characteristic lipid changes, *i.e.* increase of long-chain ceramides, LysoPC, DAG and TAG species, among others. These specific changes could be considered as a lipid fingerprint of the differentiation phenotype in primary cultured keratinocytes upon UV irradiation. This information may represent a useful tool in the research of skin diseases that involve alterations in this differentiation process, such as atopic dermatitis.

Conflicts of interest

The authors have no conflict of interest to declare.

Acknowledgments

The research leading to these results has received funding from the European Research Council under the European Union's Seventh Framework Programme (FP/2007-2013)/ERC Grant Agreement no. 320737. We thank Dr. Thierry Levade (Toulouse, France) for critical reading and discussion.

Appendix A. Supplementary data

Supplementary material related to this article can be found, in the online version, at doi:https://doi.org/10.1016/j.jdermsci.2018.07.002.

References

[1] S. Grether-Beck, R. Buettner, J. Krutmann, Ultraviolet A radiation-induced expression of human genes: molecular and photobiological mechanisms, Biol. Chem. 378 (11) (1997) 1231–1236.
[2] W.A. Bruls, H. Slaper, J.C. van der Leun, L. Berrens, Transmission of human epidermis and stratum corneum as a function of thickness in the ultraviolet and visible wavelengths, Photochem. Photobiol. 40 (4) (1984) 485–494.
[3] D.L. Bissett, D.P. Hannon, T.V. Orr, Wavelength dependence of histological, physical, and visible changes in chronically UV-irradiated hairless mouse skin, Photochem. Photobiol. 50 (6) (1989) 763–769.
[4] F. Aubin, Mechanisms involved in ultraviolet light-induced immunosuppression, Eur. J. Dermatol. 13 (6) (2003) 515–523.
[5] R.L. Eckert, J.F. Crish, N.A. Robinson, The epidermal keratinocyte as a model for the study of gene regulation and cell differentiation, Physiol. Rev. 77 (2) (1997) 397–424.
[6] F. Elsholz, C. Harteneck, W. Muller, K. Friedland, Calcium–a central regulator of keratinocyte differentiation in health and disease, Eur. J. Dermatol. 24 (6) (2014) 650–661.
[7] L.J. Löwenau, C. Zoschke, R. Brodwolf, P. Volz, C. Hausmann, S. Wattanapitayakul, A. Boreham, U. Alexiev, M. Schäfer-Korting, Increased permeability of reconstructed human epidermis from UVB-irradiated keratinocytes, Eur. J. Pharm. Biopharm. 116 (2017) 149–154.
[8] E. Proksch, J.M. Brandner, J.M. Jensen, The skin: an indispensable barrier, Exp. Dermatol. 17 (12) (2008) 1063–1072.
[9] Q. Dai, J. Liu, J. Chen, D. Durrant, T.M. McIntyre, R.M. Lee, Mitochondrial ceramide increases in UV-irradiated HeLa cells and is mainly derived from hydrolysis of sphingomyelin, Oncogene 23 (20) (2004) 3650–3658.
[10] C. Magnoni, E. Euclidi, L. Benassi, G. Bertazzoni, A. Cossarizza, S. Seidenari, A. Giannetti, Ultraviolet B radiation induces activation of neutral and acidic sphingomyelinases and ceramide generation in cultured normal human keratinocytes, Toxicol. In Vitro 16 (4) (2002) 349–355.
[11] A. Reich, D. Schwudke, M. Meurer, B. Lehmann, A. Shevchenko, Lipidome of narrow-band ultraviolet B irradiated keratinocytes shows apoptotic hallmarks, Exp. Dermatol. 19 (8) (2010) e103–10.
[12] F.J. Christiaens, A. Chardon, A. Fourtanier, J.E. Frederick, Standard Ultraviolet Daylight for Nonextreme Exposure Conditions, Photochem. Photobiol. 81 (4) (2005) 874–878.
[13] C.S. Wu, C.L. Yu, C.S. Wu, C.C. Lan, H.S. Yu, Narrow-band ultraviolet-B stimulates proliferation and migration of cultured melanocytes, Exp. Dermatol. 13 (12) (2004) 755–763.
[14] Y. Takagi, H. Nakagawa, T. Yaginuma, Y. Takema, G. Imokawa, An accumulation of glucosylceramide in the stratum corneum due to attenuated activity of beta-glucocerebrosidase is associated with the early phase of UVB-induced alteration in cutaneous barrier function, Arch. Dermatol. Res. 297 (1) (2005) 18–25.
[15] P. Waster, I. Rosdahl, B.F. Gilmore, O. Seifert, Ultraviolet exposure of melanoma cells induces fibroblast activation protein-alpha in fibroblasts: implications for melanoma invasion, Int. J. Oncol. 39 (1) (2011) 193–202.
[16] N. Dalmau, J. Jaumot, R. Tauler, C. Bedia, Epithelial-to-mesenchymal transition involves triacylglycerol accumulation in DU145 prostate cancer cells, Mol. Biosyst. 11 (12) (2015) 397–406.
[17] R. Stolt, R.J. Torgrip, J. Lindberg, L. Csenki, J. Kolmert, I. Schuppe-Koistinen, S.P. Jacobsson, Second-order peak detection for multicomponent high-resolution LC/MS data, Anal. Chem. 78 (4) (2006) 975–983.
[18] R. Tauler, Multivariate curve resolution applied to second order data, Chemom. Intell. Lab. Syst. 30 (1) (1995) 133–146.
[19] M. Navarro-Reig, J. Jaumot, A. Baglai, G. Vivó-Truyols, P.J. Schoenmakers, R. Tauler, Untargeted comprehensive two-dimensional liquid chromatography coupled with high-resolution mass spectrometry analysis of rice metabolome using multivariate curve resolution, Anal. Chem. 89 (14) (2017) 7675–7683.
[20] E. Ortiz-Villanueva, F. Benavente, B. Piña, V. Sanz-Nebot, R. Tauler, J. Jaumot, Knowledge integration strategies for untargeted metabolomics based on MCR-ALS analysis of CE-MS and LC-MS data, Anal. Chim. Acta 978 (2017) 10–23.
[21] C. Gómez-Canela, E. Prats, B. Piña, R. Tauler, Assessment of chlorpyrifos toxic effects in zebrafish (Danio rerio) metabolism, Environ. Pollut. 220 (2017) 1231–1243.
[22] A.S. Marques, C. Bedia, K.M.G. Lima, R. Tauler, Assessment of the effects of As (III) treatment on cyanobacteria lipidomic profiles by LC-MS and MCR-ALS, Anal. Bioanal.Chem. 408 (21) (2016) 5829–5841.
[23] E. Gorrochategui, J. Jaumot, S. Lacorte, R. Tauler, Data analysis strategies for targeted and untargeted LC-MS metabolomic studies: Overview and workflow, TrAC Trends Anal. Chem. 82 (2016) 425–442.
[24] R.S. Tauler, A.K, B.R. Kowalski, Multivariate curve resolution applied to second order data, Chemom. Intell. Lab. Syst. (1995) 9.
[25] E. Pere-Trepat, S. Lacorte, R. Tauler, Solving liquid chromatography mass spectrometry coelution problems in the analysis of environmental samples by multivariate curve resolution, J. Chromatogr. A 1096 (1-2) (2005) 111–122.
[26] M. Navarro-Reig, J. Jaumot, A. Garcia-Reiriz, R. Tauler, Evaluation of changes induced in rice metabolome by Cd and Cu exposure using LC-MS with XCMS and MCR-ALS data analysis strategies, Anal. Bioanal. Chem. 407 (29) (2015) 8835–8847.
[27] M. Farres, B. Pina, R. Tauler, Chemometric evaluation of Saccharomyces cerevisiae metabolic profiles using LC-MS, Metabolomics 11 (2015) 210–224.
[28] C. Bedia, N. Dalmau, J. Jaumot, R. Tauler, Phenotypic malignant changes and untargeted lipidomic analysis of long-term exposed prostate cancer cells to endocrine disruptors, Environ. Res. 140 (2015) 18–31.
[29] C. Gomez-Canela, E. Prats, B. Pina, R. Tauler, Assessment of chlorpyrifos toxic effects in zebrafish (Danio rerio) metabolism, Environ. Pollut. 220 (Pt B) (2017) 1231–1243.
[30] M. Navarro-Reig, J. Jaumot, A. Baglai, G. Vivo-Truyols, P.J. Schoenmakers, R. Tauler, Untargeted comprehensive two-dimensional liquid chromatography coupled with high-resolution mass spectrometry analysis of rice metabolome using multivariate curve resolution, Anal. Chem. 89 (14) (2017) 7675–7683.
[31] E. Ortiz-Villanueva, F. Benavente, B. Pina, V. Sanz-Nebot, R. Tauler, J. Jaumot, Knowledge integration strategies for untargeted metabolomics based on MCR-ALS analysis of CE-MS and LC-MS data, Anal. Chim. Acta 978 (2017) 10–23.
[32] A.S. Marques, C. Bedia, K.M. Lima, R. Tauler, Assessment of the effects of As(III) treatment on cyanobacteria lipidomic profiles by LC-MS and MCR-ALS, Anal. Bioanal. Chem. 408 (21) (2016) 5829–5841.
[33] W. Windig, D.A. Stephenson, Self-modeling mixture analysis of second-derivative near-infrared spectral data using the simplisma approach, Anal. Chem. 64 (22) (1992) 2735–2742.
[34] R.M. Tauler, A. de Juan, Multiset Data Analysis: Extended Multivaried Curve Resolution, vol. 2, Elsevier, 2010, pp. 473–505.
[35] D.S. Wishart, T. Jewison, A.C. Guo, M. Wilson, C. Knox, Y. Liu, Y. Djoumbou, R. Mandal, F. Aziat, E. Dong, S. Bouatra, I. Sinelnikov, D. Arndt, J. Xia, P. Liu, F. Yallou, T. Bjorndahl, R. Perez-Pineiro, R. Eisner, F. Allen, V. Neveu, R. Greiner, A. Scalbert, HMDB 3.0—the human metabolome database in 2013, Nucleic Acids Res. 41 (Database issue) (2013) D801–D807.
[36] B.W. Matthews, Comparison of the predicted and observed secondary structure of T4 phage lysozyme, Biochim. Biophys. Acta 405 (2) (1975) 442–451.
[37] S. Wold, M. Sjöström, L. Eriksson, PLS-regression: a basic tool of chemometrics, Chemom. Intell. Lab. Syst. 58 (2) (2001) 109–130.
[38] J. Jaumot, R. Tauler, Potential use of multivariate curve resolution for the analysis of mass spectrometry images, Analyst 140 (3) (2015) 837–846.
[39] E. Olivier, M. Dutot, A. Regazzetti, D. Dargere, N. Auzeil, O. Laprevote, P. Rat, Lipid deregulation in UV irradiated skin cells: Role of 25-hydroxycholesterol in keratinocyte differentiation during photoaging, J. Steroid Biochem. Mol. Biol. 169 (2017) 189–197.
[40] I. Amelio, A.M. Lena, G. Viticchie, R. Shalom-Feuerstein, A. Terrinoni, D. Dinsdale, G. Russo, C. Fortunato, E. Bonanno, L.G. Spagnoli, D. Aberdam, R.A. Knight, E. Candi, G. Melino, miR-24 triggers epidermal differentiation by controlling actin adhesion and cell migration, J. Cell Biol. 199 (2) (2012) 347–363.
[41] R.L. Eckert, J.F. Crish, T. Efimova, S.R. Dashti, A. Deucher, F. Bone, G. Adhikary, G. Huang, R. Gopalakrishnan, S. Balasubramanian, Regulation of involucrin gene expression, J. Invest. Dermatol. 123 (1) (2004) 13–22.
[42] E. Aymard, V. Barruche, T. Naves, S. Bordes, B. Closs, M. Verdier, M.H. Ratinaud, Autophagy in human keratinocytes: an early step of the differentiation? Exp. Dermatol. 20 (3) (2011) 263–268.
[43] J.H. Lee, H.T. An, J.H. Chung, K.H. Kim, H.C. Eun, K.H. Cho, Acute effects of UVB radiation on the proliferation and differentiation of keratinocytes, Photodermatol. Photoimmunol. Photomed. 18 (5) (2002) 253–261.
[44] R.L. Eckert, J.F. Crish, T. Efimova, S.R. Dashti, A. Deucher, F. Bone, G. Adhikary, G. Huang, R. Gopalakrishnan, S. Balasubramanian, Regulation of Involucrin Gene Expression, J. Invest. Dermatol. 123 (1) (2004) 13–22.
[45] M. Misovic, D. Milenkovic, T. Martinovic, D. Ciric, V. Bumbasirevic, T. Kravic-Stevovic, Short-term exposure to UV-A, UV-B, and UV-C irradiation induces alteration in cytoskeleton and autophagy in human keratinocytes, Ultrastruct. Pathol. 37 (4) (2013) 241–248.
[46] Y. Mizutani, A. Kihara, H. Chiba, H. Tojo, Y. Igarashi, 2-Hydroxy-ceramide synthesis by ceramide synthase family: enzymatic basis for the preference of FA chain length, J. Lipid Res. 49 (11) (2008) 2356–2364.
[47] Y. Mizutani, S. Mitsutake, K. Tsuji, A. Kihara, Y. Igarashi, Ceramide biosynthesis in keratinocyte and its role in skin function, Biochimie 91 (6) (2009) 784–790.
[48] H. Wefers, B.C. Melnik, M. Flür, C. Bluhm, P. Lehmann, G. Plewig, Influence of UV Irradiation on the Composition of Human Stratum Corneum Lipids, J. Invest. Dermatol. 96 (6) (1990) 959–962.
[49] S. Jung, Y. Lee, S. Han, Y. Kim, T. Nam, D. Ahn, Lysophosphatidylcholine Increases Ca Current via Activation of Protein Kinase C in Rabbit Portal Vein Smooth Muscle Cells, Korean J. Physiol. Pharmacol. 12 (1) (2008) 31–35.
[50] A.K. Ryborg, C. Johansen, L. Iversen, K. Kragballe, Lysophosphatidylcholine induces keratinocyte differentiation and upregulation of AP-1- and NF-kappaB DNA-binding activity, Acta Derm. Venereol. 84 (6) (2004) 433–438.
[51] H. Qin, X. Zheng, X. Zhong, A.K. Shetty, P.M. Elias, W.B. Bollag, Aquaporin-3 in keratinocytes and skin: its role and interaction with phospholipase D2, Arch. Biochem. Biophys. 508 (2) (2011) 138–143.
[52] D. Xie, M. Seremwe, J.G. Edwards, R. Podolsky, W.B. Bollag, Distinct Effects of Different Phosphatidylglycerol Species on Mouse Keratinocyte Proliferation, PLOS One 9 (9) (2014)e107119.
[53] C.J. Carsberg, J. Ohanian, P.S. Friedmann, Ultraviolet radiation stimulates a biphasic pattern of 1,2-diacylglycerol formation in cultured human melanocytes and keratinocytes by activation of phospholipases C and D, Biochem. J 305 (Pt 2) (1995) 471–477.
[54] K. Punnonen, S.H. Yuspa, Ultraviolet light irradiation increases cellular diacylglycerol and induces translocation of diacylglycerol kinase in murine keratinocytes, J. Invest. Dermatol. 99 (2) (1992) 221–226.

Informació Suplementària a la Publicació V

Phenotypic and lipidomic characterization of primary human epidermal keratinocytes exposed to simulated solar UV radiation

N. Dalmau, N. Andrieu-Abadie, R.Tauler, C. Bedia

J Dermatol Sci **2018**, 92(1), 97-105

Supplementary Table 1. Detailed information about the individual lipid species, retention times, *m/z* values, mass error, fold changes and VIP values of the resolved lipids used for the lipidomics results representation of Figure 4.

0.5W

Identified compound	Rt (min)	m/z measured	Adduct	m/z calculated	Mass error (ppm)	Fold change	VIP value	Database ID
Glucosylceramide (d18:1/2	11.65	856.6860	M+FA-H	856.6883	3	1.55	3.41	HMDB0004978
SM(d18:1/22:1)	9.91	829.6449	M+FA-H	829.644	1	0.92	1.14	HMDB0012104
SM(d18:1/24:0)	12.06	859.6905	M+FA-H	859.691	1	0.90	1.00	HMDB0012095
SM(d18:1/24:1)	11.06	857.6812	M+FA-H	857.6753	7	0.93	1.12	HMDB0012107
LysoPC(14:1)	3.50	464.2876	M-H	464.2783	20	1.18	1.94	HMDB0010380
LysoPC(16:1)	3.78	492.3114	M-H	492.3096	4	0.84	1.53	HMDB0010383
LysoPE(18:0)	2.76	526.3480	M+FA-H	526.315	23	1.34	1.35	HMDB0011130
PC(34:0)	8.47	762.5939	M+H	762.6007	9	2.68	4.30	HMDB0007878
PC(36:2)	8.81	786.6141	M+H	786.6007	17	3.18	5.23	HMDB0000593
PC(36:3)	7.93	784.5891	M+H	784.5851	5	1.14	1.14	HMDB0008136
PC-P(30:1)	7.38	705.5824	M+NH4	705.5541	40	1.44	4.04	HMDB0011204
PC-P(34:1)	8.84	744.5749	M+H	744.5902	21	0.62	11.68	HMDB0011305
PE(36:1)	9.30	746.5851	M+H	746.5694	21	1.18	1.46	HMDB0009253
PE-P(30:1)	9.15	663.4660	M+NH4	663.5072	12	1.50	3.72	HMDB0008883
PE-P(34:1)	9.37	702.5287	M+H	702.5432	21	1.13	1.00	HMDB0009048
PE-P(42:1)	10.05	814.6638	M+H	814.6684	6	1.67	3.51	HMDB0009775
PG(36:1)	6.27	775.5320	M-H	775.5495	23	2.72	3.89	HMDB0010604
PI(34:2)	7.70	833.5194	M-H	833.5186	1	0.80	2.78	HMDB0009846
PI(36:2)	9.01	861.5506	M-H	861.5499	1	0.88	1.00	HMDB0009786
PI(38:2)	10.25	889.5827	M-H	889.5812	2	0.85	1.40	HMDB0009791
PI(38:3)	10.01	887.5677	M-H	887.5655	3	0.83	1.94	HMDB0009907
PI(38:4)	9.20	885.5503	M-H	885.5499	0	0.82	2.61	HMDB0009914
PS(36:1)	9.69	788.5478	M-H	788.5447	4	0.83	2.36	HMDB0010163
DG(44:2)	8.70	777.7044	M+FA-H	777.6614	15	0.84	1.22	HMDB0007413
TG(48:5)	11.01	814.6977	M+NH4	814.6919	7	2.01	3.45	HMDB0042841

4W

Identified compound	Rt (min)	m/z measured	Adduct	m/z calculated	Mass error (ppm)	Fold change	VIP value	Database ID
Ceramide (d18:1/24:0)	11.97	694.6212	M+FA-H	694.6355	21	2.85	2.23	HMDB0004956
Ceramide(d18:1/26:0)	12.97	722.6668	M+FA-H	722.6668	0	2.65	1.75	HMDB0004955
SM(d18:1/24:1)	10.40	813.6889	M+H	813.6844	6	0.50	2.16	HMDB0012095
LysoPC(14:1)	1.97	464.2781	M-H	464.2783	0	4.51	2.16	HMDB0010380
LysoPC(16:0)	2.07	540.3283	M+FA-H	540.3307	4	2.48	1.36	HMDB0010382
LysoPC(18:4)	1.67	496.2791	M-H20-H	496.2828	7	5.57	2.43	HMDB0010389
PC(34:0)	7.72	806.5822	M+FA-H	806.5917	12	0.52	1.70	HMDB0007878
PC(32:0)	7.29	778.5577	M+FA-H	778.5604	3	1.79	1.63	HMDB0000564
PC-P(34:0)	8.63	746.5900	M+H	746.6058	21	0.54	2.15	HMDB0011208
PC-P(42:0)	16.49	875.7919	M+NH4	875.7576	39	3.78	1.10	HMDB0011263
PE(38:3)	8.14	787.6076	M+NH4	787.596	15	0.74	1.06	HMDB0009551
PE-P(30:0)	4.45	648.5178	M+H	648.4963	33	6.06	2.29	HMDB0008850
PG(36:0)	6.35	777.5516	M-H	777.5651	17	2.80	1.33	HMDB0010602
PI(34:1)	5.76	835.5283	M-H	835.5342	7	2.80	1.64	HMDB0009782
PI(38:4)	6.04	885.5482	M-H	885.5499	2	4.31	1.96	HMDB0009914
DG(44:1)	5.85	779.7167	M+FA-H	779.677	11	5.58	2.49	HMDB0007384
DG(32:1)	10.59	584.5611	M+NH4	584.5248	12	7.15	1.36	HMDB0007014
TG(46:2)	15.06	792.7152	M+NH4	792.7076	10	5.31	1.33	HMDB0010419

5.4. Discussió del capítol

5.4.1. Efectes de l'exposició a la radiació UV sobre melanòcits i queratinòcits

Per tal de poder descobrir les alteracions causades per la radiació UV en les cèl·lules de l'epidermis, s'han investigat diferents temps d'exposició a la radiació UV en dos tipus de cèl·lules, melanòcits i queratinòcits. Anomenarem aguda a una única exposició (0.5 setmanes): mentre que considerarem l'exposició repetida durant 1.5 i 3 setmanes com a exposició crònica.

La identificació dels canvis fenotípics produïts com a resposta a la radiació UV són de gran importància alhora d'avaluar el risc dels potencials canvis malignes. L'estudi dels efectes de la irradiació UV es va centrar en l'avaluació de la viabilitat cel·lular i la possible adquisició de certes propietats malignes com poden ser la proliferació o migració cel·lular, la inducció de la EMT o l'aparició de canvis morfològics.

En el cas dels **melanòcits**, es va detectar una disminució en el nombre de cèl·lules a mesura que augmentaven el nombre d'irradiacions UV en aquestes, fet que indicava una reducció de la viabilitat cel·lular en els melanòcits exposats de forma crònica. Amb l'acumulació d'irradiacions UV es van anar observant canvis morfològics significatius com la formació de dendrites, una estructura cel·lular especialitzada en el transport de melanosomes per transferir-los als queratinòcits del seu voltant. Les prolongacions dendrítiques atorguen una aparença similar a les neurones i es donada per una estimulació hormonal per part dels queratinòcits, però també pot aparèixer com efecte directe de la radiació UV en absència dels queratinòcits, com mostra l'estudi de Friedmann *et al.*, en el que uns cultius de melanòcits exposats de forma consecutiva a set exposicions de raciació solar van presentar formació de dendrites.[6] A més a més, es va estudiar el cicle cel·lular i es va detectar una aturada del cicle cel·lular en la fase G1/S i la M (per acumulació de Cdk2 pTyr15) tant en la irradiació aguda com a 1.5 setmanes. A part, es va detectar una disminució dels nivells de E-caderina, una proteïna responsable de l'adhesió entre melanòcits i queratinòcits, a més d'un reconegut supressor de la invasió tumoral.[7] Aquests resultats estan d'acord amb estudis anteriors en els quals s'havia observat que les irradiacions UV poden induir una reducció de la E-caderina en melanòcits i cèl·lules de melanoma.[8] Tant l'aturada del

cicle cel·lular com la disminució de la E-caderina també són detectats a 1.5 setmanes de irradiació UV però en menor mesura. Després de tres setmanes d'irradiació no es detecten canvis significatius respecte els controls. Aquests resultats suggereixen que els melanòcits irradiats són capaços d'adaptar-se a ambients adversos i retornar als paràmetres originals de cicle cel·lular i d'expressió de E-caderina. Per altra banda, tot i aquests canvis, els melanòcits irradiats amb llum solar UV no van presentar cap alteració en la proliferació ni migració cel·lular als diferents temps d'exposició a radiació UV. La Taula 5.1 mostra els canvis soferts en els melanòcits a causa de la radiació UV.

Taula 5.1. Canvis morfològics detectats en els melanòcits.

Assaig	0.5 setmanes	1.5 setmanes	3 setmanes
Viabilitat cel·lular	No es produeixen canvis		Reducció del nivell de proteïnes
Morfologia	No es produeixen canvis		Formació dendrites
ROS (especies reactives d'oxigen)	No es produeixen canvis		Producció de ROS
Cicle cel·lular, (cdk2 ptyr15)	Aturada en fase G1/S i M		Nivells inicials
EMT	↓ E-caderina	↓ E-caderina	Nivells inicials
Proliferació cel·lular	No es produeixen canvis		
Migració cel·lular	No es produeixen canvis		

Respecte els **queratinòcits**, aquests mostren una evolució continua al llarg de les exposicions UV i mostren una progressiva inducció de la diferenciació cel·lular (veure la Taula 5.2). La diferenciació dels queratinòcits consisteix en una progressiva conversió d'aquestes cèl·lules cap a corneòcits, les cèl·lules presents a les capes més superficials de la pell.[9] La diferenciació es caracteritza per canvis en el citoesquelet, augment del nivell de la proteïna involucrin i la inducció de l'autofàgia.[10] Tots aquests paràmetres van ser estudiats en els cultius primaris de queratinòcits irradiats. Després d'una exposició aguda, els queratinòcits no mostren autofàgia, ni augment en els nivells d'involucrin o diferencies en el citoesquelet. En canvi, els queratinòcits irradiats de forma crònica presenten augments significatius en els nivells de LC3-II (indicador d'autofàgia) i d'involucrin. A més a més, es van observar deformacions a la membrana i una disminució dràstica de la viabilitat dels queratinòcits (els nivells de proteïna

disminueixen quatre vegades respecte els control). Tots aquests elements indicaven que s'estava produint una progressiva diferenciació cel·lular dels queratinòcits estimulada per les repetides irradiacions UV.

A part de tots aquests canvis que suggereixen una inducció de la diferenciació cel·lular per la irradiació UV, la viabilitat cel·lular també es va veure afectada i es van generar espècies reactives d'oxigen (ROS), capaces d'induir l'estrès oxidatiu cel·lular i danys en l'ADN. La principal acció de la radiació UVA és la generació d'espècies reactives d'oxigen (ROS)[11] que no representa únicament un dany biològic macromolecular (ADN, carbohidrats, lípids i proteïnes); també és capaç d'esgotar les activitats antioxidants d'enzims com superòxid dismutassa (SOD) i glutatió peroxidasa (GPx).[12-13] L'increment de l'activitat ROS degrada els àcids poliinsaturats de la membrana cel·lular provocant la peroxidació de lípids de la membrana.[14] La peroxidació de lípids és un esdeveniment fisiopatològic crucial en moltes malalties com el càncer, la diabetis, l'envelliment, malalties cardiovasculars o l'artritis reumatoide.[15-16] Una elevada producció de ROS pot produir una degradació del col·lagen i l'elastina, ambdós amb un rol crucial en l'envelliment de la pell.[17]

Taula 5.2. Canvis morfològics detectats en els queratinòcits

Assaig	0.5 setmanes	1.5 setmanes	3 setmanes
Viabilitat cel·lular	No es produeixen canvis		Reducció del nivell de proteïnes
Morfologia	No es produeixen canvis		Deformació de la membrana
ROS (especies reactives d'oxigen)	No es produeixen canvis		Producció de ROS
Autofàgia (LC3-II)	Lleu ↓	↑	↑↑
Involucrin	Nivell control	↑	↑↑

Com a resum inicial en aquest punt, podem concloure que la radiació UV afecta tant a melanòcits com a queratinòcits però la resposta és diferent. D'una banda els melanòcits tenen una reacció de resistència a les condicions adverses externes en el transcurs de les irradiacions i s'observa la formació de dendrites, essencials per vehicular els melanosomes cap als queratinòcits. D'altra banda, els queratinòcits no tendeixen al retorn a les condicions inicials, sinó que s'aprecia una afectació més severa de la viabilitat cel·lular en les irradiacions UV cròniques i els seus canvis

morfològics apunten a un procés de diferenciació cel·lular, recolzat per l'augment dels nivells de la proteïna involucrin i LC3-II autofàgia.

5.4.2. Efectes de l'exposició a la radiació UV en el lipidoma

Els lípids són essencials en un gran nombre de funcions intra i inter-cel·lulars com mantenir la permeabilitat de la membrana, la producció i l'emmagatzematge d'energia, l'organització de membrana o la senyalització cel·lular, entre d'altres.[18-19] A més a més, concretament en la pell, els lípids tenen funcions estructurals, ja que li confereixen protecció enfront factors mediambientals i prevenen la pèrdua d'aigua a través de l'epidermis.[20] Aquesta importància dels lípids en la pell justifica la recerca sobre els possibles efectes de l'exposició a la irradiació UV en melanòcits i queratinòcits, ja sigui després d'una exposició aguda o crònica. A més, cal destacar que en aquest estudi es va realitzar l'anàlisi no dirigit de les dades de lipidòmica, per tal d'abraçar un major nombre de lípids i poder detectar canvis no observats amb anterioritat en estudis d'exposició a radiació UV dirigits a l'anàlisi de lípids específics.[21-24]

5.4.2.1. Esfingolípids (SLs)

Els esfingolípids són una subfamília de lípids que juguen un paper crucial en la senyalització cel·lular, resposta inflamatòria, supervivència i diferenciació cel·lular.[25] En el cas dels **melanòcits**, es van veure canvis significatius en els esfingolípids com a resposta a la irradiació UV. Les alteracions més importants es van observar en les esfingomielines (SMs) de llargades de 14:0 a 26:0, les quals mostraven una progressiva reducció a mesura que augmentaven el nombre d'irradiacions. Juntament amb aquesta disminució cal mencionar l'increment de les ceramides (Cer) 24:0 i 24:1 en els melanòcits irradiats crònicament, el que suggereix que les ceramides podrien induir la mort cel·lular programada o apoptosi, el que estaria relacionat amb la reducció de la viabilitat dels melanòcits. Per altra banda, cal destacar que els gangliòsids presenten una disminució en els melanòcits irradiats respecte els control. Els gangliòsids són un tipus d'esfingolípid complex que es caracteritza per presentar un o més àcids siàlic a la seva estructura. A més, es troben en la membrana cel·lular i juguen un rol important en l'adhesió cel·lular, la proliferació i en processos de reconeixement.[26] En els

melanòcits, els GM3 són els gangliòsids més abundants, un 90% aproximadament, i el seu corresponent derivat disialo GD3 representa el component minoritari (2-6%). No obstant això, els GD3 són els gangliòsids més abundants en les cèl·lules de melanoma.[27] Per això estudis anteriors s'han centrat en l' anàlisis de la relació GM3/GD3 com a índex de classificació per a pacients de melanoma. La progressiva reducció detectada de la relació GM3/GD3 es relaciona amb una supervivència més baixa entre els pacients.[28]

Tant l'esfingomielina com els gangliòsids són components importants dels *lipid rafts*, unes estructures lipídiques organitzades presents en la membrana plasmàtica. Els *lipid rafts* estan presents en la capa exterior de la membrana plasmàtica i són capaços de canviar la seva composició en resposta a estímuls intra- o extracel·lulars, com la irradiació UV, afavorint interaccions proteïna-proteïna específiques i l'activació de cascades de senyalització.[29] En el present estudi, la continua reducció de SMs i gangliòsids GM3 podria estar relacionat amb alteracions en els processos de transducció de senyals.

En l'aspecte dels esfingolípids, els **queratinòcits** segueixen una camí diferent als melanòcits. En els queratinòcits no s'han detectat canvis significatius en els gangliòsids, però s'aprecia una disminució de les SMs com en els melanòcits, tot i que ara combinat amb un increment notable de les ceramides de cadenes llargues, específicament les de 24:0 i les de 26:0, en exposicions cròniques a la radiació UV. Encara que en la majoria de teixits la llargada de les ceramides més comuns sigui de 16 a 24 carbonis; en els teixits epidèrmics, les llargades més habituals són de 24 a 32. Per tant, és normal que les ceramides que veiem més afectades en aquest estudi siguin de cadenes llargues. A partir d'aquests resultats, es va pensar que la disminució de SMs i l'augment de ceramides podria estar causat per un augment de l'activitat esfingomielinasa àcida (aSMase), present a la membrana plasmàtica. No obstant, no es van trobar diferencies significatives d'activitat aSMase en els queratinòcits irradiats de manera crònica respecte els controls. L'absència de canvis en l'activitat aSMase suggeria que les ceramides eren produïdes per una via alternativa. Una possibilitat seria l'activació de les ceramides sintases (CerS) que són enzims clau en la biosíntesis *de novo* de les ceramides. En aquest sentit, Mitzutani *et al.* van descriure que de les sis

CerS existents, la CerS3 és la predominant en queratinòcits, la qual mostra especificitat per àcids grassos de cadena llarga (C20-C26) i seria responsable de la síntesi d'aquest tipus de ceramida. A més a més, els autors van observar que l'expressió de CerS es troba augmentada en el procés de diferenciació [23], el que estaria d'acord amb les nostres observacions. Entre els lípids que caracteritzen la permeabilitat de l'epidermis, les ceramides són els lípids més importants en la prevenció de pèrdua d'aigua.[30] En aquest sentit, un estudi previ de Wefers *et al.* demostra que la radiació UV incrementa el nivells de ceramides en la capa còrnia, el que suggereix que la fototeràpia en les malalties de la pell com la dermatitis atòpica podria resultar beneficiós aquest increment de ceramides.[31]

5.4.2.2. Fosfolípids (PLs)

Els fosfolípids (PLs) són un grup de lípids que contribueix en gran part a la composició de les membranes cel·lulars. Les especies més abundants dins d'aquest grup són les fosfatidilcolines (PCs) i les fosfatidiletanolamines (PEs), components clau en la bicapa lipídica de la membrana i que també participen en d'altres funcions biològiques. En el nostre estudi, l'efecte general de la radiació UV en els **melanòcits** és una disminució progressiva en els nivells de PCs i PEs, amb l'excepció de l'exposició aguda on s'han observat increments significatius de certs PCs. Aquest aspecte és similar al que succeïa en l'anàlisi del cicle cel·lular i l'expressió de E-caderina, on l'exposició aguda mostrava unes alteracions i la crònica unes altres. Per això diem que l'exposició aguda UV presenta un perfil lipídic diferent al dels altres punts de recollida, especialment en els fosfolípids com PC, PC-P i lysoPC. En les irradiacions agudes els PC-P (plasmalògens) mostren un increment general i quatre espècies de lysoPC que disminueixen. Aquesta tendència dels PC-P i els lysoPC també es va observar a les 1.5 setmanes, encara que amb un menor nombre d'espècies involucrades, indicant així una situació intermèdia entre l'exposició UV aguda i la crònica.

La progressiva reducció de PCs i PEs pot ser que reflecteixi els canvis estructurals soferts en els melanòcits a causa de la radiació UV. Aquest balanç lipídic en les membranes dels melanòcits pot influir en la fluïdesa i la morfologia de la membrana,

fent possible d'aquesta manera la formació de les dendrites esmentades anteriorment. Els PCs i PEs, a part de tenir un paper essencial en l'estructura de la membrana, també participen en la transducció de senyals cel·lulars. Per exemple, els PCs són reserves de segons missatgers com els àcids grassos, els diglicèrids (DAG), lysoPC i àcid fosfatídic (PA). Estudis previs han demostrat que els lysoPC són capaços d'estimular la formació de dendrites en els melanòcits[32], i aquest procés és mediat pel seu metabòlit lysoPA, que es produeix a partir de lysoPC per acció de les lysofosfolipases D (lysoPD).[33] En aquest context, una explicació per la reducció dels diferents nivells de lysoPC detectats en 0.5 i 1.5 setmanes d'irradiació podria ser un increment de la transformació de lysoPC a lysoPA, per tal de modificar la morfologia de la cèl·lula i promoure la formació de dendrites.

Altres fosfolípids afectats durant la irradiació UV en melanòcits són els fosfatidilinositols (PIs) i els fosfatidilglicerols (PGs), que presenten una important reducció a mesura que augmenta el temps d'exposició. La família dels PGs juga un paper crucial en la fisiologia cel·lular, principalment involucrada en la resposta de l'estrès. PG és constituent de la membrana i actua com un intermediari essencial en la biosíntesi de nombrosos lípids, especialment cardiolipines (també presenten una disminució a 1.5 setmanes), que estan localitzades en l'interior de la membrana mitocondrial i són requerides pel correcte funcionament dels enzims involucrats en la fosforilació oxidativa.[34] D'altra banda, els PIs són precursors dels PI fosfat (PIP, PIP_2 i PIP_3), que tenen un rol específic en les cascades de senyalització cel·lular i en el tràfic de la membrana intracel·lular. En el nostre estudi, dos dels PIs més abundants en la cèl·lula (38:3 i 38:4) mostren una disminució dels seus nivells, el que podria reflectir un increment en la producció de PIPs. Si aquest fos el cas, suposaria que algunes funcions regulades pels PIPs, com el trànsit de membrana, la selecció de proteïnes, la supervivència cel·lular, la proliferació o la reordenació del citoesquelet[35-36], podrien trobar-se alterades en certa mesura. Bellono *et al.* va demostrar que la radiació UV incrementava la producció de melanina mitjançant l'activació de la cascada de senyalització $G\alpha_{q/11}$ en melanòcits humans que hidrolitzen PI4,5-bifosfat (PIP2) per alliberar DAG i inositol trifosfat.[37] Aquesta activació ha estat reportada amb

anterioritat com a resultat d'un ràpid increment del Ca^{2+} intracel·lular i l'increment del contingut de melanina.[38]

En el cas dels **queratinòcits** irradiats, la tendència en els fosfolípids és un increment general de les espècies PC, PE-P i PG en la irradiació UV aguda . En canvi, la irradiació crònica no mostra un clar patró per PC i PE, tot i que sí que s'observa un increment dels lysoPC, que podria estar més relacionat amb la inducció del procés de diferenciació, i un augment de PG(36:0). L'increment de PC, PE-P i PG degut a la irradiació UV aguda està en concordança amb estudis previs en els que queratinòcits HaCaT, exposats a una sola dosis de irradiació UV, presenten un increment considerable en molts PC i PE-P.[9] Tal com s'ha comentat anteriorment, lysoPC és un grup de fosfolípids polars produïts per l'acció de la fosfolipasa A2 (PLA_2). L'augment de lysoPC pot estar involucrat en el manteniment del procés de diferenciació cel·lular en els queratinòcits ja que, mitjançant l'activació de la proteïna kynasa C (PKC), incrementa l'expressió d'importants proteïnes en aquest procés, com la transglutaminase-1 (TG-1).[39] Pel que fa l'augment de PG(36:0), en tant que transductor de senyals, podria estar involucrat en la diferenciació epidermal prematura dels queratinòcits.[40] En aquest context, l'estudi de Xie *et al.* també ha descrit que l'addició de PG a cultius de queratinòcits inhibeix la proliferació i promociona la diferenciació cel·lular.[41]

5.4.2.3. Lípids neutres

Per últim, la subfamília dels lípids neutres presenta canvis similars tant en **melanòcits** com **queratinòcits** UV-irradiats. La tendència general és un increment en el nivell de triacilglicerols (TAG) amb cadenes acil de 46 a 56 carbonis. L'acumulació de TAG pot ser interpretada com un mecanisme de supervivència ja que aquests lípids suposen una font d'energia, i també de precursors moleculars de components de membrana i transductors de senyals, el que resulta essencial per la supervivència i el manteniment de l'homeòstasi de les cèl·lules en un medi advers com la irradiació UV crònica. Aquest increment de TAG s'ha detectat prèviament en estudis de cèl·lules exposades a estressants ambientals, com en el cas de cèl·lules de placenta exposades de forma

aguda a tributil estany (TBT)[42] o el cas de l'exposició crònica de cèl·lules de càncer de pròstata a disruptors endocrins (Publicació del Capítol 4).

En el cas dels **queratinòcits** també s'observa un increment dels diacilglicerols (DAG), fet que ja ha estat observat en estudis precedents.[43] Els DAG són coneguts per regular la proteïna kinasa C (PKC), també la seva isoforma delta, implicada en la diferenciació dels queratinòcits i en l'expressió de proteïnes específiques com l'involucrin.[44] Tot això suggereix que elevats nivells de DAG poden estar estretament relacionats amb la inducció del procés de diferenciació, com ja s'ha observat en els lysoPC, ja que els dos són activadors de la PKC.[45]

5.4.3. Observacions finals

Publicacions anteriors sobre els efectes de les radiacions UV s'havien centrat en l'estudi de rutes lipídiques o enzimàtiques específiques mitjançant una aproximació analítica dirigida. Per exemple, el treball de Magnoni *et al.* es centra en l'activació d'esfingomielinases en queratinòcits[21], i un altre estudi, Gegotek *et al.* observen l'efecte temps-dependent dels nivells de fosfolípids en fibroblasts exposats a diferents tipus d'irradiació[46]. Malgrat la varietat d'estudis realitzats dins el camp de la radiació UV i les seves afectacions en la pell, mai fins ara s'havia realitzat un estudi lipidòmic no dirigit de cèl·lules de la pell exposades a la radiació solar simulada.

En aquests dos treballs del capítol s'ha realitzat una aproximació no dirigida utilitzant la nova **metodologia ROIMCR**, descrita en el Capítol 3, per a l'anàlisi no dirigit de les dades LC-MS. A diferència del mètode emprat en els primers articles (Capítol 4), l'estratègia ROIMCR no requereix la divisió dels cromatogrames en diferents finestres (*time-windowing*). L'aplicació de ROIMCR ens ha permès conèixer la petjada lipídica tant en melanòcits com queratinòcits exposats a la radiació UV amb un menor temps de tractament de dades i sense pèrdua de resolució espectral.

Com a resum es podria dir que ambdós models de cèl·lules de l'epidermis humana, melanòcits i queratinòcits, presenten patrons fenotípics i una composició de lípids característics que responen a diferents estratègies de supervivència. L'adaptació als

efectes de la radiació UV és diferent per cada tipus de cèl·lules. Els **melanòcits** exposats de forma aguda mostren canvis en el cicle cel·lular i els nivells de E-caderina que disminueixen, així com variacions en el seu lipidoma. El més rellevant en el cas dels melanòcits és que amb el pas de les irradiacions (exposició crònica), aquests tendeixen a adquirir els valors previs a les irradiacions, com és el cas del cicle cel·lular o d'algunes espècies de lípids. En canvi, els **queratinòcits** mostren les modificacions progressivament, fent-se més significatives amb l'augment del nombre d'irradiacions UV. L'exposició aguda afecta principalment als fosfolípids, especialment els PE i PC. En el cas de les dosis repetides de raciació UV, s'observa com s'indueix la diferenciació cel·lular. Aquest fet indica que la radiació UV és capaç d'alterar l'homeòstasi dels queratinòcits per fer-los evolucionar cap a corneòcits.

Els melanòcits són reconeguts per la seva funció de síntesis de la melanina en els melanosomes. També són considerats una barrera protectora contra la radiació UV i l'estrès oxidatiu gràcies a la producció de melanina. En aquest treball hem vist com la radiació UV crònica pot ocasionar la formació de dendrites per iniciar el procés de pigmentació de la pell. Els canvis lipídics descrits per aquestes cèl·lules durant el procés de formació de dendrites podrien ser útils per entendre millor, des del punt de vista dels lípids, els processos patològics relacionats amb la despigmentació, com ara el vitiligo, els èczemes o la psoriasis.[47-49]

En el cas dels **queratinòcits**, en aquest estudi s'ha descrit l'empremta lipídica característica de la diferenciació dels queratinòcits a corneòcits induïda per la radiació UV. Aquest procés és essencial en la pell per mantenir la funcionalitat de l'epidermis. Sabent que els processos de diferenciació aberrants dels queratinòcits es poden associar amb malalties de la pell, com la psoriasis o la dermatitis atòpica,[50-51] els nostres resultats podrien contribuir a un millor coneixement del procés de la diferenciació cel·lular, des del punt de vista dels lípids. Publicacions anteriors ja havien mencionat l'augment en les ceramides a causa de la radiació UV com a efecte fotoprotector de l'epidermis.[30-31] En el nostre cas, en realitzar un estudi lipidòmic no-dirigit, a part de detectar l'augment de ceramides de cadenes llargues (24:0 – 26:0) i la disminució de les esfingomielines, hem detectat altres alteracions lipídiques que podrien ser de gran interès per investigacions futures. Aquest seria el cas dels lysoPC i

els DAGs, mencionats anteriorment, l'increment dels quals suggereix una possible implicació d'aquestes espècies en el manteniment del procés de diferenciació cel·lular dels queratinòcits mitjançant l'activació de la PKC.[45] Tota aquesta informació pot representar una eina molt útil per la recerca de malalties de la pell associades a alteracions en el procés de la diferenciació cel·lular.

Com a punt final d'aquest capítol podríem concloure que la radiació UV produeix canvis fenotípics i lipídics significatius, tant en cultius primaris de melanòcits com de queratinòcits. Aquests resultats s'han de tenir en compte en el context de l'exposició general de la població a la llum solar, la qual s'ha relacionat amb l'aparició de malalties com el melanoma[15, 52] i la dermatitis atòpica.[53-55] Els resultats de les nostres investigacions poden ajudar a entendre millor, des del punt de vista dels lípids, els processos de pigmentació de la pell i de diferenciació cel·lular, així com servir de base per l'estudi de les malalties derivades de la seva alteració.

5.5. Referències

1. de Laat, A.; van der Leun, J. C.; de Gruijl, F. R., Carcinogenesis induced by UVA (365-nm) radiation: the dose-time dependence of tumor formation in hairless mice. *Carcinogenesis* **1997,** *18* (5), 1013-20.
2. Kelfkens, G.; de Gruijl, F. R.; van der Leun, J. C., Tumorigenesis by short-wave ultraviolet A: papillomas versus squamous cell carcinomas. *Carcinogenesis* **1991,** *12* (8), 1377-82.
3. Afaq, F.; Adhami, V. M.; Mukhtar, H., Photochemoprevention of ultraviolet B signaling and photocarcinogenesis. *Mutat Res* **2005,** *571* (1-2), 153-73.
4. Henriksen, T.; Dahlback, A.; Larsen, S. H.; Moan, J., Ultraviolet-radiation and skin cancer. Effect of an ozone layer depletion. *Photochem Photobiol* **1990,** *51* (5), 579-82.
5. Lucas, R. M.; Yazar, S.; Young, A. R.; Norval, M.; de Gruijl, F. R.; Takizawa, Y.; Rhodes, L. E.; Sinclair, C. A.; Neale, R. E., Human health in relation to exposure to solar ultraviolet radiation under changing stratospheric ozone and climate. *Photochem Photobiol Sci* **2019,** *18* (3), 641-680.
6. Friedmann, P. S.; Gilchrest, B. A., Ultraviolet radiation directly induces pigment production by cultured human melanocytes. *J Cell Physiol* **1987,** *133* (1), 88-94.
7. Hsu, M. Y.; Meier, F. E.; Nesbit, M.; Hsu, J. Y.; Van Belle, P.; Elder, D. E.; Herlyn, M., E-cadherin expression in melanoma cells restores keratinocyte-mediated growth control and down-regulates expression of invasion-related adhesion receptors. *Am J Pathol* **2000,** *156* (5), 1515-25.
8. Jamal, S.; Schneider, R. J., UV-induction of keratinocyte endothelin-1 downregulates E-cadherin in melanocytes and melanoma cells. *J Clin Invest* **2002,** *110* (4), 443-52.
9. Olivier, E.; Dutot, M.; Regazzetti, A.; Dargere, D.; Auzeil, N.; Laprevote, O.; Rat, P., Lipid deregulation in UV irradiated skin cells: Role of 25-hydroxycholesterol in keratinocyte differentiation during photoaging. *J Steroid Biochem Mol Biol* **2017,** *169*, 189-197.

10. Amelio, I.; Lena, A. M.; Viticchie, G.; Shalom-Feuerstein, R.; Terrinoni, A.; Dinsdale, D.; Russo, G.; Fortunato, C.; Bonanno, E.; Spagnoli, L. G.; Aberdam, D.; Knight, R. A.; Candi, E.; Melino, G., miR-24 triggers epidermal differentiation by controlling actin adhesion and cell migration. *J Cell Biol* **2012,** *199* (2), 347-63.
11. Tyrrell, R. M.; Keyse, S. M., New trends in photobiology. The interaction of UVA radiation with cultured cells. *J Photochem Photobiol B* **1990,** *4* (4), 349-61.
12. Kong, S. Z.; Shi, X. G.; Feng, X. X.; Li, W. J.; Liu, W. H.; Chen, Z. W.; Xie, J. H.; Lai, X. P.; Zhang, S. X.; Zhang, X. J.; Su, Z. R., Inhibitory effect of hydroxysafflor yellow a on mouse skin photoaging induced by ultraviolet irradiation. *Rejuvenation Res* **2013,** *16* (5), 404-13.
13. Scharffetter-Kochanek, K.; Brenneisen, P.; Wenk, J.; Herrmann, G.; Ma, W.; Kuhr, L.; Meewes, C.; Wlaschek, M., Photoaging of the skin from phenotype to mechanisms. *Exp Gerontol* **2000,** *35* (3), 307-16.
14. Akinyemi, A. J.; Ademiluyi, A. O.; Oboh, G., Aqueous extracts of two varieties of ginger (Zingiber officinale) inhibit angiotensin I-converting enzyme, iron(II), and sodium nitroprusside-induced lipid peroxidation in the rat heart in vitro. *J Med Food* **2013,** *16* (7), 641-6.
15. Bastian, B. C., The molecular pathology of melanoma: an integrated taxonomy of melanocytic neoplasia. *Annu Rev Pathol* **2014,** *9*, 239-71.
16. Aziz, M. H.; Afaq, F.; Ahmad, N., Prevention of ultraviolet-B radiation damage by resveratrol in mouse skin is mediated via modulation in survivin. *Photochem Photobiol* **2005,** *81* (1), 25-31.
17. Uitto, J.; Fazio, M. J.; Olsen, D. R., Molecular mechanisms of cutaneous aging. Age-associated connective tissue alterations in the dermis. *J Am Acad Dermatol* **1989,** *21* (3 Pt 2), 614-22.
18. Fahy, E.; Subramaniam, S.; Murphy, R. C.; Nishijima, M.; Raetz, C. R.; Shimizu, T.; Spener, F.; van Meer, G.; Wakelam, M. J.; Dennis, E. A., Update of the LIPID MAPS comprehensive classification system for lipids. *J Lipid Res* **2009,** *50 Suppl*, S9-14.
19. Subramaniam, S.; Fahy, E.; Gupta, S.; Sud, M.; Byrnes, R. W.; Cotter, D.; Dinasarapu, A. R.; Maurya, M. R., Bioinformatics and systems biology of the lipidome. *Chem Rev* **2011,** *111* (10), 6452-90.
20. Elias, P. M., Skin barrier function. *Curr Allergy Asthma Rep* **2008,** *8* (4), 299-305.
21. Magnoni, C.; Euclidi, E.; Benassi, L.; Bertazzoni, G.; Cossarizza, A.; Seidenari, S.; Giannetti, A., Ultraviolet B radiation induces activation of neutral and acidic sphingomyelinases and ceramide generation in cultured normal human keratinocytes. *Toxicol In Vitro* **2002,** *16* (4), 349-55.
22. Wang, W.; Chapman, N. M.; Zhang, B.; Li, M.; Fan, M.; Laribee, R. N.; Zaidi, M. R.; Pfeffer, L. M.; Chi, H.; Wu, Z. H., Upregulation of PD-L1 via HMGB1-activated IRF3 and NF-kB contributes to UV radiation-induced immune suppression. *Cancer Res* **2019**.
23. Mizutani, Y.; Kihara, A.; Chiba, H.; Tojo, H.; Igarashi, Y., 2-Hydroxy-ceramide synthesis by ceramide synthase family: enzymatic basis for the preference of FA chain length. *J Lipid Res* **2008,** *49* (11), 2356-64.
24. Reichert, O.; Kolbe, L.; Terstegen, L.; Staeb, F.; Wenck, H.; Schmelz, M.; Genth, H.; Kaever, V.; Roggenkamp, D.; Neufang, G., UV radiation induces CXCL5 expression in human skin. *Exp Dermatol* **2015,** *24* (4), 309-12.
25. Hannun, Y. A.; Obeid, L. M., Principles of bioactive lipid signalling: lessons from sphingolipids. *Nat Rev Mol Cell Biol* **2008,** *9* (2), 139-50.
26. Mocchetti, I., Exogenous gangliosides, neuronal plasticity and repair, and the neurotrophins. *Cell Mol Life Sci* **2005,** *62* (19-20), 2283-94.
27. Carubia, J. M.; Yu, R. K.; Macala, L. J.; Kirkwood, J. M.; Varga, J. M., Gangliosides of normal and neoplastic human melanocytes. *Biochem Biophys Res Commun* **1984,** *120* (2), 500-4.
28. Ravindranath, M. H.; Tsuchida, T.; Morton, D. L.; Irie, R. F., Ganglioside GM3:GD3 ratio as an index for the management of melanoma. *Cancer* **1991,** *67* (12), 3029-35.

29. Simons, K.; Toomre, D., Lipid rafts and signal transduction. *Nat Rev Mol Cell Biol* **2000,** *1* (1), 31-9.
30. Mizutani, Y.; Mitsutake, S.; Tsuji, K.; Kihara, A.; Igarashi, Y., Ceramide biosynthesis in keratinocyte and its role in skin function. *Biochimie* **2009,** *91* (6), 784-90.
31. Wefers, H.; Melnik, B. C.; Flur, M.; Bluhm, C.; Lehmann, P.; Plewig, G., Influence of UV irradiation on the composition of human stratum corneum lipids. *J Invest Dermatol* **1991,** *96* (6), 959-62.
32. Scott, G. A.; Jacobs, S. E.; Pentland, A. P., sPLA2-X stimulates cutaneous melanocyte dendricity and pigmentation through a lysophosphatidylcholine-dependent mechanism. *J Invest Dermatol* **2006,** *126* (4), 855-61.
33. Aoki, J.; Taira, A.; Takanezawa, Y.; Kishi, Y.; Hama, K.; Kishimoto, T.; Mizuno, K.; Saku, K.; Taguchi, R.; Arai, H., Serum lysophosphatidic acid is produced through diverse phospholipase pathways. *J Biol Chem* **2002,** *277* (50), 48737-44.
34. Matsuo, H.; Chevallier, J.; Mayran, N.; Le Blanc, I.; Ferguson, C.; Faure, J.; Blanc, N. S.; Matile, S.; Dubochet, J.; Sadoul, R.; Parton, R. G.; Vilbois, F.; Gruenberg, J., Role of LBPA and Alix in multivesicular liposome formation and endosome organization. *Science* **2004,** *303* (5657), 531-4.
35. van Meer, G.; Sprong, H., Membrane lipids and vesicular traffic. *Curr Opin Cell Biol* **2004,** *16* (4), 373-8.
36. Wenk, M. R.; Lucast, L.; Di Paolo, G.; Romanelli, A. J.; Suchy, S. F.; Nussbaum, R. L.; Cline, G. W.; Shulman, G. I.; McMurray, W.; De Camilli, P., Phosphoinositide profiling in complex lipid mixtures using electrospray ionization mass spectrometry. *Nat Biotechnol* **2003,** *21* (7), 813-7.
37. Bellono, N. W.; Najera, J. A.; Oancea, E., UV light activates a Galphaq/11-coupled phototransduction pathway in human melanocytes. *J Gen Physiol* **2014,** *143* (2), 203-14.
38. Wicks, N. L.; Chan, J. W.; Najera, J. A.; Ciriello, J. M.; Oancea, E., UVA phototransduction drives early melanin synthesis in human melanocytes. *Curr Biol* **2011,** *21* (22), 1906-11.
39. Ryborg, A. K.; Johansen, C.; Iversen, L.; Kragballe, K., Lysophosphatidylcholine induces keratinocyte differentiation and upregulation of AP-1- and NF-kappaB DNA-binding activity. *Acta Derm Venereol* **2004,** *84* (6), 433-8.
40. Qin, H.; Zheng, X.; Zhong, X.; Shetty, A. K.; Elias, P. M.; Bollag, W. B., Aquaporin-3 in keratinocytes and skin: its role and interaction with phospholipase D2. *Arch Biochem Biophys* **2011,** *508* (2), 138-43.
41. Xie, D.; Seremwe, M.; Edwards, J. G.; Podolsky, R.; Bollag, W. B., Distinct effects of different phosphatidylglycerol species on mouse keratinocyte proliferation. *PLoS One* **2014,** *9* (9), e107119.
42. Gorrochategui, E.; Lacorte, S.; Tauler, R.; Martin, F. L., Perfluoroalkylated Substance Effects in Xenopus laevis A6 Kidney Epithelial Cells Determined by ATR-FTIR Spectroscopy and Chemometric Analysis. *Chem Res Toxicol* **2016,** *29* (5), 924-32.
43. Carsberg, C. J.; Ohanian, J.; Friedmann, P. S., Ultraviolet radiation stimulates a biphasic pattern of 1,2-diacylglycerol formation in cultured human melanocytes and keratinocytes by activation of phospholipases C and D. *Biochem J* **1995,** *305 (Pt 2)*, 471-7.
44. Eckert, R. L.; Crish, J. F.; Efimova, T.; Dashti, S. R.; Deucher, A.; Bone, F.; Adhikary, G.; Huang, G.; Gopalakrishnan, R.; Balasubramanian, S., Regulation of involucrin gene expression. *J Invest Dermatol* **2004,** *123* (1), 13-22.
45. Jung, S.; Lee, Y.; Han, S.; Kim, Y.; Nam, T.; Ahn, D., Lysophosphatidylcholine Increases Ca Current via Activation of Protein Kinase C in Rabbit Portal Vein Smooth Muscle Cells. *Korean J Physiol Pharmacol* **2008,** *12* (1), 31-5.
46. Gegotek, A.; Bielawska, K.; Biernacki, M.; Dobrzynska, I.; Skrzydlewska, E., Time-dependent effect of rutin on skin fibroblasts membrane disruption following UV radiation. *Redox Biol* **2017,** *12*, 733-744.

47. Arakawa, A.; Siewert, K.; Stohr, J.; Besgen, P.; Kim, S. M.; Ruhl, G.; Nickel, J.; Vollmer, S.; Thomas, P.; Krebs, S.; Pinkert, S.; Spannagl, M.; Held, K.; Kammerbauer, C.; Besch, R.; Dornmair, K.; Prinz, J. C., Melanocyte antigen triggers autoimmunity in human psoriasis. *J Exp Med* **2015,** *212* (13), 2203-12.
48. Liang, L.; Li, Y.; Tian, X.; Zhou, J.; Zhong, L., Comprehensive lipidomic, metabolomic and proteomic profiling reveals the role of immune system in vitiligo. *Clin Exp Dermatol* **2019**.
49. Zokaei, S.; Farhud, D. D.; Keykhaei, M.; Zarif Yeganeh, M.; Rahimi, H.; Moravvej, H., Cultured Epidermal Melanocyte Transplantation in Vitiligo: A Review Article. *Iran J Public Health* **2019,** *48* (3), 388-399.
50. Boehncke, W. H.; Schon, M. P., Psoriasis. *Lancet* **2015,** *386* (9997), 983-94.
51. Chen, H. L.; Chiang, P. C.; Lo, C. H.; Lo, Y. H.; Hsu, D. K.; Chen, H. Y.; Liu, F. T., Galectin-7 Regulates Keratinocyte Proliferation and Differentiation through JNK-miR-203-p63 Signaling. *J Invest Dermatol* **2016,** *136* (1), 182-191.
52. Lo, J. A.; Fisher, D. E., The melanoma revolution: from UV carcinogenesis to a new era in therapeutics. *Science* **2014,** *346* (6212), 945-9.
53. Kim, Y. M.; Kim, J.; Lee, J. Y.; Kim, M.; Kim, H.; Jung, K.; Eo, S.; Ahn, M.; Ahn, K., Impact of solar ultraviolet radiation on atopic dermatitis symptoms in young children: A longitudinal study. *Pediatr Allergy Immunol* **2017,** *28* (6), 551-556.
54. Kramer, U.; Weidinger, S.; Darsow, U.; Mohrenschlager, M.; Ring, J.; Behrendt, H., Seasonality in symptom severity influenced by temperature or grass pollen: results of a panel study in children with eczema. *J Invest Dermatol* **2005,** *124* (3), 514-23.
55. Sargen, M. R.; Hoffstad, O.; Margolis, D. J., Warm, humid, and high sun exposure climates are associated with poorly controlled eczema: PEER (Pediatric Eczema Elective Registry) cohort, 2004-2012. *J Invest Dermatol* **2014,** *134* (1), 51-57.

Capítol 6.
Conclusions

En aquesta Tesi s'han realitzat estudis de lipidòmica en diferents tipus de cèl·lules exposades a estressants ambientals. Per una banda, s'ha estudiat l'efecte dels disruptors endocrins i el mecanisme d'inducció de la EMT en cèl·lules de càncer de pròstata. Per altra banda, s'han estudiat els efectes de la radiació UV aguda i crònica en cèl·lules de l'epidermis. Tots aquests estudis tenen com a punt en comú la realització d'anàlisi lipidòmics no dirigits, per tal de conèixer el paper dels lípids en els escenaris mencionats. A més a més, acompanyant aquests estudis, també s'ha realitzat la validació de la nova metodologia ROIMCR pel tractament de dades òmiques obtingudes mitjançant LC-MS.

A continuació es resumeixen les conclusions referents als tres blocs de treball presentats i discutits en aquesta Tesi.

6.1. Validació del procediment ROIMCR per l'anàlisi lipidòmica quantitativa no dirigida LC-MS

1) El mètode ROIMCR, consistent en el mètode de compressió de dades ROI combinat amb l'estratègia MCR-ALS, es confirma com una gran eina d'anàlisi de dades LC-MS complexes, en particular en estudis metabolòmics i lipidòmics.
2) La metodologia ROIMCR presenta una significativa reducció d'emmagatzematge i temps d'anàlisi de dades LC-MS adquirides en *full scan* en estudis no dirigits. Aquesta nova estratègia no presenta ni pèrdua de resolució espectral ni d'exactitud de masses. A més, no requereix tractament preliminar com l'alineament de pics ni modelatge de la forma del pic. Tot pot ser analitzat en un únic anàlisi.
3) L'aplicació del mètode ROIMCR és una eina quimiomètrica potent i adequada per a l'anàlisi no-dirigida de dades de LC-MS de manera qualitativa i quantitativa relativa de metabòlits i/o lípids en mostres sintètiques i biològiques.

6.2. Efectes dels disruptors endocrins (Aldrin, Aroclor i Clorpirifòs) i la inducció de la EMT en cèl·lules de càncer de pròstata DU145

4) L'exposició crònica als DE indueixen un fenotip pro-metastàtic en les cèl·lules de càncer de pròstata DU145. L'ús d'eines quimiomètriques en l'estudi lipidòmic no dirigit ha permès la identificació de lípids i possibles rutes lipídiques i metabòliques afectades per l'exposició crònica als disruptors endocrins emprats en aquest estudi. S'ha observat la inducció de la EMT per part de dos dels disruptors endocrins, l'Aldrin i el CPF.
5) L'estudi lipidòmic no dirigit de la inducció de la EMT emprant TNF-α ha revelat un augment significatiu del nivell de TAGs en les cèl·lules de càncer de pròstata. Aquest increment de TAGs es veu acompanyat de la formació de *lipid droplets* i la sobrexpressió del gen FASN; suggerint l'activació de la lipogènesi *de novo* durant el procés de EMT.

   L'increment de TAGs podria ser degut al creixent requeriment d'energia per part de les cèl·lules, de components de membrana i/o de senyalitzadors lipídics per l'increment de la migració cel·lular, la proliferació i d'altres característiques agressives de les cèl·lules metastàtiques.

6.3. Efectes de la radiació UV aguda i crònica en melanòcits i queratinòcits primaris

6) Els estudis fenotípics i lipidòmics no dirigits sobre la radiació UV en cèl·lules de cultiu primari de l'epidermis humana, melanòcits i queratinòcits, presenten perfils lipídics diferents segons la radiació aguda o crònica i segons el tipus de cèl·lula.
7) Els melanòcits irradiats presenten canvis en l'expressió de la E-caderina, el cicle cel·lular i la morfologia de les cèl·lules. D'altra banda, l'anàlisi lipidòmic no dirigit mostra múltiples canvis en els perfils lipídics als diferents punts analitzats. Com a canvis més significatius destaquen: un progressiu descens dels nivells d'esfingolípids (SM i GM3), de dos dels PIs més abundants i de vàries espècies de PC i PE. Per contra, s'observa un augment continuat de TAG

a mesura que augmenta el nombre d'irradiacions UV, el que podria interpretar-se com un mecanisme de supervivència a un ambient hostil.

8) En el cas dels queratinòcits, l'exposició aguda origina canvis en la composició dels lípids que implica un increment d'algunes espècies de PC i PE. En el cas de la radiació crònica, s'observa una diferenciació cel·lular dels queratinòcits cap a corneòcits, caracteritzada per un augment de l'autofàgia i de l'expressió de la proteïna involucrin. Aquesta diferenciació va acompanyada de canvis en el perfil lipídic com l'increment en les ceramides de cadena llarga, LysoPC, DAG i TAG, entre d'altres. Aquests canvis lipídics es poden considerar com una empremta lipídica de la inducció de la diferenciació cel·lular en els queratinòcits per una radiació UV crònica.